EISSN: 2687-4482

ABCResearch

Archives of Basic and Clinical Research

Official Journal of the Erzincan Binali Yıldırım University School of Medicine

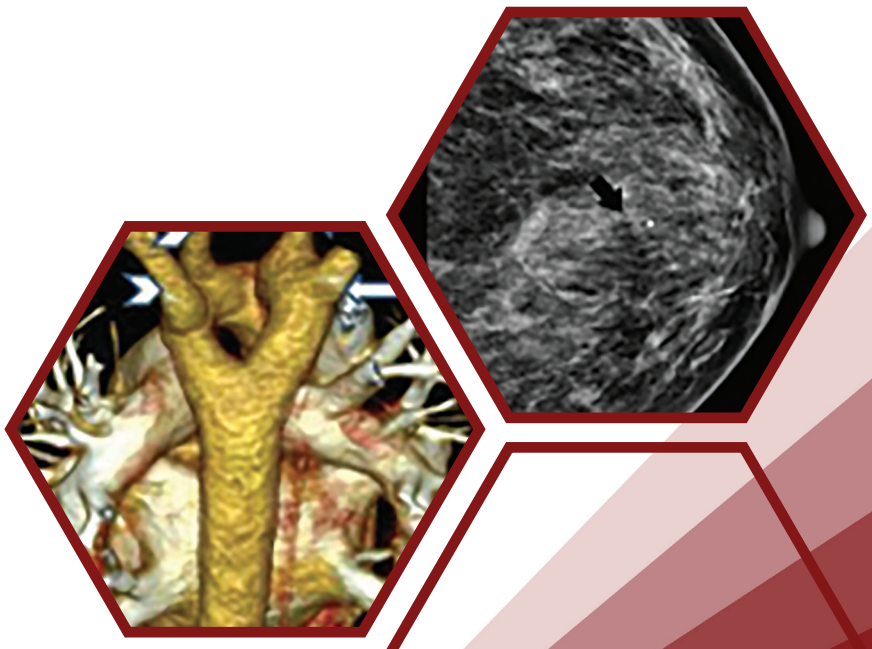

galenos Publishing House

abcresearch.net

Volume 8
Issue 2
May 2026

ABCResearch

Please refer to the journal's webpage (**https://abcresearch.net/**) for "**Journal Policies**" and "**Instructions**".

The editorial and publication process of the Archives of Basic and Clinical Research are shaped in accordance with the guidelines of the **ICMJE, WAME, CSE, COPE, EASE**, and **NISO**. The journal is in conformity with the Principles of Transparency and Best Practice in Scholarly Publishing.

Archives of Basic and Clinical Research is indexed in **CNKI, DOAJ, TUBITAK Ulakbim TR Index, EBSCO**, and **TurkMedline**.

The journal is published online.

Owner: Erzincan Binali Yıldırım University

Responsible Manager: Mecit Kantarcı

Publisher Contact

Address: Molla Gürani Mah. Kaçamak Sk. No: 21/1 34093 İstanbul, Türkiye

Phone: +90 (530) 177 30 97 / +90 (539) 307 32 03

E-mail: info@galenos.com.tr/yayin@galenos.com.tr

Web: www.galenos.com.tr

Publisher Certificate Number: 14521

Publication Date: July 2026

E-ISSN: 2687-448

International scientific journal published quarterly.

Editorial Board

ABCResearch

Contents

Research Articles

ABCResearch

Contents

ABCResearch

Arch Basic Clin Res 2026;8(2):92-99
DOI: 10.4274/ABCR.2026.25384

Research Article

Serum Leptin, Ghrelin, and IGF-1 Levels and Their Association with Bone Mineral Density in Patients with Ulcerative Colitis

Abdulkerim Furkan Tamer[1], Ömer Yılmaz[2]

[1]Department of Internal Medicine and Nephrology, Adnan Menderes University Faculty of Medicine, Aydın, Türkiye
[2]Department of Internal Medicine and Gastroenterology, Atatürk University Faculty of Medicine, Erzurum, Türkiye

Cite this article as: Tamer AF, Yılmaz Ö. Serum leptin, ghrelin, and IGF-1 levels and their association with bone mineral density in patients with ulcerative colitis. *Arch Basic Clin Res*. 2026;8(2):92-99.

ORCID IDs of the authors: A.F.T. 0000-0002-9820-5850, Ö.Y. 0000-0001-7471-4987.

ABSTRACT

Objective: This study aimed to investigate the relationship between serum leptin, ghrelin, and insulin-like growth factor-1 (IGF-1) levels and bone mineral density (BMD) in patients with ulcerative colitis (UC) to elucidate possible mechanisms underlying impaired bone mineralization in UC.

Methods: A total of 38 patients with UC and 38 age- and sex-matched healthy controls were included. Serum levels of leptin, ghrelin, IGF-1, and tumor necrosis factor-alpha (TNF-α) were measured during both the active and remission phases. Bone mineral densitometry was performed using dual-energy X-ray absorptiometry, and vertebral and femoral T- and Z-scores were recorded. The results were compared between disease phases and those of controls.

Results: Among UC patients, 27% had normal BMD, 50% were osteopenic, and 23% were osteoporotic. Mean T- and Z-scores were significantly lower in UC patients than in controls ($P < 0.05$). Serum leptin and IGF-1 levels during the active phase were significantly decreased, while ghrelin and TNF-α levels were significantly elevated, compared with controls ($P < 0.05$). In remission, ghrelin levels remained higher than in controls ($P < 0.05$), whereas leptin, IGF-1, and TNF-α levels were similar. A positive correlation was observed between IGF-1 and femoral neck T-scores in the active phase ($P < 0.05$).

Conclusion: BMD is significantly reduced in UC patients, particularly during active inflammation. Decreased secretion of leptin and IGF-1 and elevated ghrelin levels may contribute to bone loss, highlighting the interplay among inflammation, metabolism, and skeletal health in UC.

Keywords: Ulcerative colitis, leptin, ghrelin, IGF-1, bone mineral density, TNF-α

INTRODUCTION

Ulcerative colitis (UC), although primarily affecting the gastrointestinal tract, is also associated with extraintestinal manifestations and complications, such as decreased bone mineral density (BMD), which may result in osteopenia and osteoporosis. Over the past three decades, studies from different cohorts have reported a prevalence of osteopenia ranging from 22% to 77% and osteoporosis from 17% to 41% among UC patients.[1,2]

The major risk factors for reduced BMD in UC patients include low body weight and body mass index (BMI), chronic inflammation, prolonged corticosteroid therapy, immobilization, and malabsorption of vitamin D, calcium, and vitamin K.[3] Initially, the reduction in BMD was attributed primarily to corticosteroid use; however, the observation that corticosteroids are often used only for remission induction and not for maintenance therapy suggests that additional factors also contribute to decreased BMD.[4]

Corresponding author: Abdulkerim Furkan Tamer, **E-mail:** aftamer@gmail.com

Received: October 14, 2025
Revision Requested: November 17, 2025 **Accepted:** May 25, 2026 **Publication Date:** July, 14, 2026

One possible mechanism involves alterations in the synthesis and secretion of adipokines, such as leptin and ghrelin, by adipose tissue. Anorexia, malnutrition, and cachexia associated with inflammatory bowel disease (IBD) can impair adipose tissue function, leading to alterations in leptin and ghrelin secretion. These disturbances may contribute to the higher prevalence of osteoporosis in UC patients.[3] White adipose tissue, which constitutes the majority of fat in the body, not only regulates energy homeostasis but also plays a critical role in immune and metabolic processes. Cytokines such as interleukin-6 and tumor necrosis factor-alpha (TNF-α), along with adipokines like leptin and ghrelin secreted from adipose tissue, have been shown to influence bone metabolism.[3]

Low circulating leptin levels or leptin resistance, commonly observed in obesity, has been associated with reduced BMD. Leptin replacement has been reported to significantly improve spinal BMD, and the presence of leptin receptors on osteoblasts and chondrocytes indicates direct effects on bone growth and metabolism.[5] Similarly, ghrelin, another adipokine secreted from white adipose tissue, has been implicated in growth hormone secretion, appetite stimulation, gastrointestinal motility, glucose tolerance, and energy homeostasis.[6] Beyond its metabolic effects, ghrelin has also been proposed to play a role in the link between bone mass and adipose tissue.[7]

Several studies have reported elevated ghrelin levels in patients with IBD compared with healthy controls, although findings remain inconsistent.[8,9] Furthermore, increased ghrelin concentrations have been positively correlated with reduced BMD in IBD patients.[7] In line with these findings, we aimed to investigate serum leptin and ghrelin levels in UC patients and their relationships with BMD. To further explore the impact of inflammation and catabolism, we included measurements of serum TNF-α and insulin-like growth factor-1 (IGF-1).

MATERIALS AND METHODS

Study Population

This study included 38 patients who were admitted to the Gastroenterology Clinic of Atatürk University Faculty of Medicine in 2009 and 2010 with complaints of bloody diarrhea, urgency, and abdominal pain, who were diagnosed with UC, and 38 healthy volunteers who served as the control group. The healthy controls were selected to match the UC patients as closely as possible in terms of age and sex. All participants were fully informed about the study, and written informed consent was obtained prior to enrollment.

Clinical Evaluation and Diagnosis

All patients were evaluated through a detailed medical history, physical examination, and laboratory assessments, including blood, urine, and stool analyses. Other gastrointestinal and systemic conditions with similar clinical manifestations were excluded during the differential diagnosis process. The diagnosis of UC was confirmed based on characteristic endoscopic findings and histopathological evaluation of colonic biopsy specimens.

Inclusion and Exclusion Criteria

Patients with renal failure, chronic liver disease, chronic heart disease, systemic infectious diseases, IBDs other than UC, systemic inflammatory or autoimmune disorders, hypertension, diabetes mellitus, or malignancy were excluded from the study.

Assessment of Disease Activity

The disease activity of UC patients was evaluated according to the Truelove-Witts criteria (Table 1).[10] Based on these criteria, patients were categorized as being in either the active phase or remission phase of the disease. Treatment regimens were adjusted for newly diagnosed or relapsed patients during the active phase. After achieving remission, patients were recalled for follow-up visits at intervals ranging from 3 months to 1 year.

Sample Collection and Biochemical Analysis

Before initiation of treatment, a 10 mL venous blood sample was collected from each patient in the morning after an overnight fast during the active phase, and a second 10 mL venous blood sample was collected after remission was achieved. Similarly, fasting venous blood samples were obtained from the control group. Serum leptin, ghrelin, and TNF-α levels were measured by enzyme-linked immunosorbent assay, and IGF-1 was measured by chemiluminescence.

BMD Measurement

BMD was evaluated during both the active and remission phases using dual-energy X-ray absorptiometry (DEXA). Measurements were obtained from the lumbar vertebrae (L1-L4) and femoral neck; BMD (g/cm^2) was calculated, and T and Z scores were derived. Osteopenia was defined as a T-score between -1.0 and -2.5, and osteoporosis as a T-score ≤ -2.5, according to World Health Organization criteria.[11]

Statistical Analysis

All statistical analyses were performed using the Statistical Package for the Social Sciences (SPSS) for Windows, version 18.0 (IBM Corp., Armonk, NY, USA). Data were expressed as mean ± standard deviation.

MAIN POINTS

- In active ulcerative colitis, serum leptin and growth factor-1 (IGF-1) levels were significantly lower, whereas ghrelin and tumor necrosis factor-alpha (TNF-α) levels were elevated.
- Bone mineral density was reduced in Ulcerative colitis (UC) patients compared with controls, and this reduction persisted even during remission.
- A positive correlation was observed between IGF-1 levels and femoral neck T-scores in active UC patients.
- Corticosteroid exposure was associated with higher leptin levels, highlighting treatment-related metabolic effects.
- These findings support the interplay between inflammatory and metabolic pathways in UC pathophysiology.

Table 1. Truelove and Witts Criteria for Assessing Disease Activity in Ulcerative Colitis

Parameter	Mild Disease	Moderate Disease	Severe Disease
Stool frequency	≤ 4 stools/day	4-6 stools/day	≥ 6 bloody stools/day
Blood in stool	Present (occasional)	Frequent	Frequent/continuous
Temperature	Normal	< 37.8 °C	> 37.8 °C
Pulse	Normal	< 90/min	> 90/min
Hemoglobin	Normal	≥ 10.5 g/dL	< 10.5 g/dL
Erythrocyte Sedimentation Rate (ESR)	Normal	20-30 mm/h	> 30 mm/h
General condition	Well	Mild systemic disturbance	Severe systemic disturbance

· The Shapiro-Wilk test was used to assess the normality of data distribution.

· Comparisons between two independent groups were made using the independent samples t-test or the Mann-Whitney U test, as appropriate.

· Categorical variables were compared using the chi-square test.

· Correlations between continuous variables were examined using Pearson's or Spearman's correlation coefficients, depending on their distribution. A *P* value of <0.05 was considered statistically significant.

Ethical Approval

The study protocol was approved by the Ethics Committee of Atatürk University Faculty of Medicine (Department of Internal Medicine, session no: 01, January 13, 2009), the Atatürk University Faculty of Medicine Ethics Committee (session no: 4, May 15, 2009; decision no: 122), and the Internal Medicine Division Council (session no: 4, June 17, 2009; decision no: 48).

RESULTS

Among the 38 patients in the active phase, 10 (27%) had normal BMD, 9 (23%) had osteoporosis, and 19 (50%) had osteopenia. The mean T- and Z-scores of BMD, measured during both the active and remission phases, were significantly lower compared with those of the control group ($P < 0.05$, Tables 2 and 3).

No statistically significant differences were observed in the mean T and Z scores of BMD at the lumbar spine (L1-L4), femoral neck, and total hip between patients in the active and remission phases ($P > 0.05$, Table 4).

Serum leptin and IGF-1 levels were significantly lower in patients with active UC than in the control group ($P < 0.05$). In contrast, serum levels of ghrelin and TNF-α were significantly higher in the active phase than in controls ($P < 0.05$, Table 5).

In the remission phase, serum leptin, IGF-1, and TNF-α levels did not differ significantly from those of the control group ($P > 0.05$, Table 5). However, ghrelin concentrations remained significantly elevated compared with controls ($P < 0.05$; Table 6). This persistent increase in ghrelin, even during clinical remission, may reflect ongoing subclinical inflammation or a compensatory metabolic response to chronic disease burden.

Table 2. Comparison of Mean T and Z Scores of BMD Between Active UC Patients and Controls

Parameter	Active (Mean ± SD)	Control (Mean ± SD)	*P*
L1-L4 T	-1.49 ± 1.26	-0.73 ± 0.94	***P < 0.05***
L1-L4 Z	-1.07 ± 1.11	0.07 ± 1.00	***P < 0.05***
F. Neck T	-0.88 ± 1.03	-0.23 ± 0.72	***P < 0.05***
F. Neck Z	0.02 ± 1.12	0.96 ± 1.04	***P < 0.05***
Total Hip T	-0.78 ± 1.02	-0.04 ± 0.62	***P < 0.05***
Total Hip Z	-0.30 ± 0.99	0.76 ± 0.77	***P < 0.05***

F.: Femur.

Table 3. Comparison of Mean T and Z Scores of BMD Between UC Patients in Remission and Controls

Parameter	Remission (Mean ± SD)	Control (Mean ± SD)	*P*
L1-L4 T	-1.55 ± 1.14	-0.73 ± 0.94	***P < 0.05***
L1-L4 Z	-1.13 ± 1.01	0.07 ± 1.00	***P < 0.05***
F. Neck T+	-0.73 ± 1.15	-0.23 ± 0.72	***P < 0.05***
F. Neck Z	0.11 ± 1.01	0.96 ± 1.04	***P < 0.05***
Total Hip T	-0.69 ± 1.02	-0.04 ± 0.62	***P < 0.05***
Total Hip Z	-0.25 ± 0.92	0.76 ± 0.77	***P < 0.05***

F.: Femur.

Table 4. Comparison of Mean T and Z Scores of BMD Between Active and Remission UC Patients

Parameter	Active (Mean ± SD)	Remission (Mean ± SD)	*P*
L1-L4 T	-1.49 ± 1.26	-1.55 ± 1.14	*P* > 0.05
L1-L4 Z	-1.07 ± 1.11	-1.13 ± 1.01	*P* > 0.05
F. Neck T	-0.88 ± 1.03	-0.73 ± 1.15	*P* > 0.05
F. Neck Z	0.02 ± 1.12	0.11 ± 1.01	*P* > 0.05
Total Hip T	-0.78 ± 1.02	-0.69 ± 1.02	*P* > 0.05
Total Hip Z	-0.30 ± 0.99	-0.25 ± 0.92	*P* > 0.05

F.: Femur; BMD, bone mineral density; UC, ulcerative colitis.

Table 5. Comparison of Serum Leptin, Ghrelin, IGF-1, and TNF-α Between Active UC Patients and Controls

Parameter	Active (Mean ± SD)	Control (Mean ± SD)	*P*
Leptin	5.10 ± 6.67 ng/dL	14.30 ± 1.80 ng/dL	***P < 0.05***
Ghrelin	91.23 ± 62.00 pg/mL	13.40 ± 1.78 pg/mL	***P < 0.05***
IGF-1	103.66 ± 46.38 ng/mL	189.0 ± 12.0 ng/mL	***P < 0.05***
TNF-α	10.93 ± 12.36 pg/mL	2.41 ± 0.18 pg/mL	***P < 0.05***

IGF-1, insulin-like growth factor-1; TNF-α, tumor necrosis factor-alpha.

Table 6. Comparison of Serum Leptin, Ghrelin, IGF-1, and TNF-α Between UC Patients in Remission and Controls

Parameter	Remission (Mean ± SD)	Control (Mean ± SD)	*P*
Leptin	15.67 ± 16.62 ng/dl	14.30 ± 1.80 ng/dl	***P > 0.05***
Ghrelin	65.24 ± 46.89 pg/ml	13.40 ± 1.78 pg/ml	***P < 0.05***
IGF-1	170.08 ± 68.43 ng/ml	189.0 ± 12.0 ng/ml	***P > 0.05***
TNF-α	4.19 ± 7.35 pg/ml	2.41 ± 0.18 pg/ml	***P > 0.05***

IGF-1, insulin-like growth factor-1; TNF-α, tumor necrosis factor-alpha; UC, ulcerative colitis.

Table 7. Comparison of Serum Leptin, Ghrelin, IGF-1, and TNF-α Between Active and Remission UC Patients

Parameter	Active (Mean ± SD)	Remission (Mean ± SD)	*P*
Leptin	5.10 ± 6.67 ng/dL	15.67 ± 16.62 ng/dL	***P < 0.05***
Ghrelin	91.23 ± 62.00 pg/mL	65.24 ± 46.89 pg/mL	***P > 0.05***
IGF-1	103.66 ± 46.38 ng/mL	170.08 ± 68.43 ng/mL	***P < 0.05***
TNF-α	10.93 ± 12.36 pg/mL	4.19 ± 7.35 pg/mL	***P < 0.05***

IGF-1, insulin-like growth factor-1; TNF-α, tumor necrosis factor-alpha; SD, standard deviation; UC, ulcerative colitis.

Serum leptin and IGF-1 levels were significantly lower in patients during the active phase compared with those in remission ($P < 0.05$). Although serum ghrelin concentrations were higher in active UC patients than in remission, this difference did not reach statistical significance ($P>0.05$). By contrast, serum TNF-α levels were significantly elevated in the active phase compared with levels during remission ($P < 0.05$, Table 7).

Serum leptin levels were significantly higher in UC patients who received for induction of remission compared with those who did not ($P < 0.05$). No statistically significant differences were observed between steroid-treated and untreated patients in serum concentrations of ghrelin, IGF-1, or TNF-α ($P > 0.05$, Table 8).

No correlations (positive or negative) were observed between serum leptin or ghrelin levels and either serum TNF-α or BMD in patients in both the active and remission phases. However, in patients with active UC, a statistically significant positive correlation was detected between femoral neck T-scores and serum IGF-1 levels (Tables 9 and 10).

DISCUSSION

The most important findings of this study are that, in patients with UC, serum leptin and IGF-1 levels were reduced, ghrelin levels were increased in patients with UC, and BMD was positively associated with IGF-1 but not with leptin or ghrelin.

While numerous factors play a role in this inflammatory process, recent evidence has suggested that adipokines secreted from mesenteric adipose tissue—now increasingly recognized as a novel immune cell compartment—may also contribute to the pathogenesis of UC. These adipokines have been reported to exert both pro-inflammatory and anti-inflammatory effects. Studies have demonstrated conflicting findings regarding serum leptin levels and the presence of IBD, with some reporting negative associations and others reporting statistically significant positive associations. More recent research has highlighted the potential influence of ethnic and racial variation on circulating leptin levels; however, the underlying mechanisms remain to be fully elucidated. Leptin concentrations are generally lower among non-White patients, suggesting that ethnic variation may indeed play an important role in the correlation between leptinemia and IBD.[12]

Under normal conditions, leptin secreted by adipose tissue is thought to enhance anti-inflammatory macrophage populations and thereby exert an inflammation-reducing effect.[13]

Karmiris et al.[8] reported that serum leptin levels measured during the active phase of UC were significantly lower compared with healthy controls, suggesting that reduced circulating leptin may be associated with intestinal inflammation. Similarly, Franchimont et al. demonstrated that in patients with IBD, serum leptin concentrations increased following treatment with infliximab, an anti-TNF-α agent, accompanied by a reduction in intestinal inflammation.[14]

Table 8. Comparison of Serum Leptin, Ghrelin, IGF-1, and TNF-α According to Steroid use in UC Patients

Parameter	Steroid (+) (Mean ± SD)	Steroid (-) (Mean ± SD)	*P*
Leptin	30.33 ± 18.67 ng/dL	10.05 ± 11.99 ng/dL	***P < 0.05***
Ghrelin	85.53 ± 70.00 pg/mL	57.98 ± 34.24 pg/mL	*P* > 0.05
IGF-1	159.90 ± 55.10 ng/mL	173.71 ± 73.16 ng/mL	*P* > 0.05
TNF-α	2.16 ± 2.25 pg/mL	4.91 ± 8.23 pg/mL	*P* > 0.05
Femur Neck T	-0.75 ± 1.03	-0.83 ± 1.15	*P* > 0.05

IGF-1, insulin-like growth factor-1; TNF-α, tumor necrosis factor-alpha.

Table 9. Correlation Analysis of Serum Leptin, Ghrelin, and IGF-1 with TNF-α and BMD T-Scores in Active UC Patients

Parameter	TNF-α	L1-L4 T	Femur Neck T	Total Hip T
Leptin	0.241 (P > 0.05)	0.164 (P > 0.05)	0.185 (P > 0.05)	0.271 (P > 0.05)
Ghrelin	-0.006 (P > 0.05)	0.017 (P > 0.05)	-0.015 (P > 0.05)	-0.029 (P > 0.05)
IGF-1	-0.167 (P > 0.05)	0.166 (P > 0.05)	0.373 (P < 0.05)	0.316 (P > 0.05)

IGF-1, insulin-like growth factor-1.

Table 10. Correlation Analysis of Serum Leptin, Ghrelin, and IGF-1 with TNF-α and BMD T-scores in Remission UC Patients

Parameter	TNF-α	L1-L4 T	Femur Neck T	Total Hip T
Leptin	0.096 (*P* > 0.05)	0.008 (*P* > 0.05)	-0.090 (*P* > 0.05)	-0.024 (*P* > 0.05)
Ghrelin	-0.188 (*P* > 0.05)	-0.118 (*P* > 0.05)	-0.180 (*P* > 0.05)	-0.195 (*P* > 0.05)
IGF-1	-0.100 (*P* > 0.05)	0.192 (*P* > 0.05)	0.187 (*P* > 0.05)	0.064 (*P* > 0.05)

BMD, bone mineral density; DEXA, dual-energy X-ray absorptiometry; TNF-α, tumor necrosis factor-alpha; IGF-1, insulin-like growth factor-1.

Reduced leptin concentrations appear to contribute to impaired anti-inflammatory regulation in UC. During the active phase, serum leptin levels are significantly lower than those observed in both the remission and control groups (Tables 5 and 7). Notably, leptin concentrations remain decreased even during remission compared with healthy controls, suggesting the persistence of subclinical inflammation (Table 6). Given leptin's anorexigenic properties, the marked reduction in its levels during active disease may represent a compensatory mechanism aimed at mitigating malnutrition, which either precedes or arises as a consequence of intestinal inflammation. In light of leptin's established anti-inflammatory functions, persistently reduced concentrations—both during active disease and relative to controls—support the hypothesis that insufficient leptin-mediated immunoregulatory activity may contribute to the perpetuation of intestinal inflammation in UC.

In UC patients receiving steroids, serum leptin levels measured during remission were significantly higher than in those not receiving steroids. This finding suggests that steroid therapy enhances anti-inflammatory activity, leading to higher leptin concentrations in these patients than in non-users. In other words, serum leptin levels increased in parallel with a reduction in inflammation (Table 8).

Leptin is also believed to have important effects on bone metabolism, promoting bone mineralization and enhancing osteoblastic activity. Consistent with this, our study demonstrated reduced leptin levels in patients with UC. However, correlation analysis did not reveal any statistically significant positive or negative association between leptin concentrations and BMD measurements (Tables 9-10).[15]

In a study by Karmiris et al.[8] that included 100 patients (46 with UC and 54 with Crohn's disease) and 60 healthy controls, serum ghrelin levels were higher in IBD patients than in healthy controls. Moreover, when IBD patients were compared with controls, elevated ghrelin levels were correlated with reduced leptin concentrations. The authors concluded that ghrelin levels positively correlate with the severity of inflammation in IBD and that impaired secretion of adipose tissue-derived proteins may play a role in IBD pathogenesis. Consistent with these findings, our study also demonstrated higher serum ghrelin levels and lower leptin levels in patients with active UC compared with healthy controls.[8]

Ates et al.[16] reported that serum ghrelin levels measured during the active phase were significantly higher than those measured during remission. The same study demonstrated negative correlations between serum ghrelin levels and both serum IGF-1 concentrations and BMI. Consequently, the authors concluded that elevated ghrelin levels correlate positively with disease severity and may serve as a useful marker in assessing both disease activity and nutritional status in UC. In our study, however, no statistically significant difference was observed between ghrelin levels in the active and remission phases. Nevertheless, the borderline trend toward higher ghrelin levels during active disease suggests results consistent with those of Ates et al.[16]

In a study conducted by Konturek et al.[17], colonic mucosal biopsy specimens from 15 UC patients were compared with those from 15 healthy controls, revealing increased mucosal mRNA expression of ghrelin in the UC group. The authors suggested that this elevated colonic mucosal expression of ghrelin may represent a protective response triggered by the heightened mucosal inflammation.[17]

In our study, serum ghrelin levels in active UC patients were marginally higher than in patients in remission, although the difference was not statistically significant. The absence of a significant difference may be explained by the multitude of factors influencing ghrelin secretion, and by its active involvement in numerous metabolic and inflammatory processes. However, ghrelin levels in active UC patients were significantly higher than those in healthy controls. This finding suggests that increased ghrelin secretion occurs during inflammatory processes and that this increase—ghrelin being known for its pro-inflammatory effects— may itself contribute to intestinal inflammation. During remission, serum ghrelin levels in UC patients remained significantly higher than in healthy controls, indicating that, despite clinical remission, the effects of chronic inflammation persist in UC patients for an extended period.

Although Peracchi et al.[18] reported a positive correlation between ghrelin and TNF-α levels, no such association was observed in our study. In both the active and remission phases, ghrelin levels showed no correlation with TNF-α concentrations or BMD. Furthermore, there was no significant difference in ghrelin levels between patients who received steroids for remission induction and those who did not. Taken together, our findings suggest that the dysregulated secretion of ghrelin—known to possess pro-inflammatory properties—may contribute to intestinal inflammation. Alternatively, the increased ghrelin secretion may represent a compensatory protective response of the organism to inflammation. Elevated ghrelin levels could also be interpreted as a response to malnutrition developing during intestinal inflammation, serving to preserve energy stores and counteract cachexia by promoting fat accumulation and appetite stimulation.[18]

In IBD, dysfunction of the growth hormone/IGF-1 axis has been demonstrated. IGF-1, synthesized in the liver, exerts anabolic effects in multiple tissues and plays a crucial role in the regulation of growth and metabolism. During inflammatory processes, hepatic synthesis of IGF-1 is reduced, resulting in decreased serum IGF-1 levels. Growth retardation has frequently been reported in children with UC and Crohn's disease. IGF-1 also plays an important role in bone metabolism and calcium balance, and has been shown to correlate positively with bone mineralization.[19]

In a cohort study including 1,004 individuals, Pöykkö et al.[20] reported a negative correlation between serum ghrelin levels and IGF-1 concentrations. They suggested that this relationship may play an important role in regulating energy metabolism, although further studies are needed to clarify the underlying mechanisms. In our study, while serum ghrelin levels were higher in patients compared with the control group, serum IGF-1 levels were lower than those of healthy controls.[20]

In an experimental study by Haris et al.[21] using colitis-induced mice, BMD and serum TNF-α and IGF-1 levels were evaluated during both the active and remission phases of IBD. They observed that elevated TNF-α and reduced IGF-1 levels during active disease paralleled the reduction in BMD. With disease remission, TNF-α levels decreased, IGF-1 levels increased, and BMD improved. Similarly, our study found a positive correlation between IGF-1 concentrations and BMD in active UC patients. However, no significant correlation was detected between IGF-1 and TNF-α levels during activity. Consistent with the findings of Haris et al.[21], we also observed that IGF-1 levels were lower during the active phase compared with remission. Furthermore, IGF-1 values increased once patients achieved remission. Given its well-known anabolic effects in multiple tissues, as well as its role in enhancing bone mineralization and osteoblastic activity, the observed reduction in IGF-1 levels and the associated correlation with decreased BMD in our study are consistent with previous reports. The observation that IGF-1 concentrations in patients with active UC were lower than in patients in remission and in healthy controls suggests that the IGF-1 axis is disrupted in UC. This impairment may result from altered secretion of adipokines (e.g., leptin and ghrelin) by adipose tissue, as well as from other inflammatory processes upregulated in UC. Ultimately, this disturbance of the IGF-1 axis and reduced serum IGF-1 levels may help explain the increased catabolic state observed in these patients.[21]

TNF-α plays a key role in the pathogenesis of UC, as it does in many other inflammatory diseases, and is an important therapeutic target in UC. Inhibition of TNF-α with monoclonal antibodies such as infliximab and adalimumab has emerged as an effective therapeutic strategy for the management of the most treatment-resistant cases of chronic UC.[22]

Komatsu et al.[23] reported that serum TNF-α levels in UC patients were up to 380 times higher than those in healthy individuals. In their study, TNF-α concentrations were significantly higher during the active phase compared with remission, highlighting the central role of TNF-α in the pathophysiology of IBD and underscoring its value as an important biomarker for assessing disease activity.[23]

In our study, serum TNF-α levels were significantly higher in patients during the active phase compared with both the remission and healthy-control groups, confirming the well-established pro-inflammatory role of TNF-α. No statistically significant difference was observed between patients in remission and controls. The decline in TNF-α levels with remission supports the rationale for the successful outcomes achieved with TNF-α inhibitors, which are increasingly being adopted as a cornerstone in the treatment of UC. The changes observed in our study, together with the recent widespread use of TNF-α inhibitors, further emphasize the role of TNF-α as one of the principal cytokines driving intestinal inflammation in UC.

IBD is recognized as a significant risk factor for reduced BMD, leading to osteopenia and osteoporosis. Previous reports have demonstrated a prevalence of osteopenia and osteoporosis among IBD patients ranging from 7% to 56%. In a cohort study by Koutroubakis et al.[7], BMD was evaluated in 118 patients with UC Crohn's disease, revealing that 40 patients (33.9%) had normal BMD, 55 patients (46.6%) were osteopenic, and 23 patients (19.5%) were osteoporotic. Importantly, this study reported that higher circulating ghrelin levels and longer disease duration were significantly associated with lower BMD and increased osteoporosis frequency, whereas no correlation was observed between leptin levels and BMD.[7]

Consistent with these findings, our analysis of 38 patients demonstrated that 10 (27%) had normal BMD, 19 (50%) were osteopenic, and 9 (23%) were osteoporotic. In contrast to the ghrelin association reported in the previous study, we did not identify any significant correlation between BMD and levels of either ghrelin or leptin.

In a cohort study conducted by Ottaviani et al.[24] involving 336 patients with IBD, osteopenia was identified in 115 patients (34%), while osteoporosis was detected in 40 patients (12%). The study found that older age and female sex were significantly associated with lower BMD. Following clinical evaluation, Vitamin D replacement therapy was initiated for 153 patients (45%), and 24 (7%) began treatment specifically for osteoporosis. The findings emphasize the critical importance of a systematic and multidisciplinary assessment regarding bone fragility in this patient population.[24]

Intestinal inflammation accelerates bone loss by increasing osteoclastic activity and decreasing osteoblastic activity through the release of pro-inflammatory cytokines, such as interleukin-6, interleukin-1, and TNF-α.[25] Studies have shown that even in newly diagnosed and untreated patients with IBD, initial BMD values are already low.[26] Furthermore, the long-term use of glucocorticoids, which are frequently employed in IBD treatment, leads to an additional decline in BMD by inhibiting osteoblasts. In addition, the intake and absorption of essential nutrients for bone health, such as Vitamin D and calcium, are lower in IBD patients compared to healthy individuals, further impacting BMD negatively.[25]

In our study, no statistically significant differences were observed between BMD T- and Z-scores of patients during active and remission phases. This finding may be attributed to factors such as the relatively short interval between active and remission periods (ranging from 3 months to 1 year) and the limited sample size. However, BMD T- and Z-scores in patients in the active phase were significantly lower than those in the healthy control group. This suggests that intestinal inflammation in UC and the associated increase in cytokine release may initiate the osteoporotic process in affected patients.

Furthermore, BMD T- and Z-scores measured during the remission phase were significantly lower than those in healthy controls. These findings indicate that the osteoporotic process initiated during the active phase does not regress immediately upon achieving remission. T his highlights the need for a more proactive and potentially aggressive approach to the prevention and treatment of osteoporosis in patients with UC.

Lee SJ et al.[27] demonstrated that approximately one-third of patients with IBD diagnosed before the age of 50 had low BMD at the time of diagnosis. In that study, the similar prevalence of low BMD in the UC and Crohn's disease subgroups suggested that bone loss may begin early in the disease course, independent of disease duration and treatment. These findings indicate that assessment of BMD at diagnosis in young patients with IBD may be clinically meaningful for early risk stratification and the implementation of preventive strategies.[27]

In our study, BMD T- and Z-scores measured during the remission phase were found to be significantly lower in patients who had received corticosteroids for remission induction compared with those who had not. This finding indicates that the pre-existing risk of osteoporosis among patients with UC is further exacerbated by steroid therapy. Therefore, in the management of UC, all potential risk factors for the development of osteopenia or osteoporosis—ranging from lifestyle-related factors to the therapeutic regimens administered—must be carefully considered.

The pathophysiology and etiology of UC remain incompletely understood. It has become increasingly evident that dysregulated secretion of adipose tissue–derived cytokines may play a critical role in the pathogenesis of UC and in the development of its clinical manifestations and complications. Altered levels of cytokines such as leptin, ghrelin, and TNF-α, together with disturbances in the IGF-1 axis, appear to contribute to the osteopenic and osteoporotic processes observed in UC patients. Given the increased prevalence of osteopenia and osteoporosis in this population, particularly among those receiving corticosteroid therapy, the implementation of appropriate preventive strategies and, when necessary, prophylactic treatments should be considered as part of comprehensive patient management.

Study Limitations

This study has certain limitations. The sample size was relatively small and was derived from a single center, which may limit the generalizability of the findings. In addition, the cross-sectional design precludes causal inference between hormonal changes and BMD. Future multicenter longitudinal studies with larger cohorts are needed to validate and expand upon these results.

CONCLUSION

In conclusion, the pathophysiology and etiology of UC have not yet been fully elucidated. It has become increasingly evident that dysregulated secretion of adipose tissue–derived cytokines may play a critical role in the pathogenesis of UC as well as in the development of its clinical manifestations and complications. Altered levels of cytokines such as leptin, ghrelin, and TNF-α, together with disturbances in the IGF-1 axis, appear to contribute to the osteopenic and osteoporotic processes observed in UC patients. Given the increased prevalence of osteopenia and osteoporosis in this population, particularly among those receiving corticosteroid therapy, the implementation of appropriate preventive strategies and, when necessary, prophylactic treatments should be considered as part of comprehensive patient management.

Ethics

Ethics Committee Approval: The study protocol was approved by the Ethics Committee of Atatürk University Faculty of Medicine (decision no: 122, date: 15.05.2009).

Informed Consent: All participants were fully informed about the study, and written informed consent was obtained prior to enrollment.

Footnotes

Author Contributions

Concept Design – Ö.Y.; Data Collection or Processing – A.F.T.; Analysis or Interpretation – A.F.T.; Literature Review – A.F.T.; Writing, Reviewing and Editing – A.F.T.

Declaration of Interest: The authors declared no conflicts of interest.

Funding: The authors declare that this study has received no financial support.

REFERENCES

1. Abadi MMA, Emadian ST, Zaman M, Khalilizad M. Prevalence of osteoporosis in patients with inflammatory bowel disease: a systematic review and meta-analysis. *J Health Popul Nutr*. 2025;44:178. [CrossRef]

2. Vernia F, Ribichini E, Scotti GB, Latella G. Nutritional deficiencies and reduced bone mineralization in ulcerative colitis. *J Clin Med*. 2025;14(9):3202. [CrossRef]
3. Ratajczak-Pawłowska AE, Michalak M, Szymczak-Tomczak A, et al. Is there any association between fat body mass and bone mineral density in patients with Crohn's disease and ulcerative colitis? *Nutrients*.2025;17:466. [CrossRef]
4. Compston J. Osteoporosis in inflammatory bowel disease. Gut. 2003;52:63–64. [CrossRef]
5. Upadhyay J, Farr OM, Mantzoros CS. The role of leptin in regulating bone metabolism. *Metabolism*. 2015;64:105-113. [CrossRef]
6. Khalaji A, Babajani N, Amirsardari Z, et al. Unveiling the ghrelin and obestatin roles in inflammatory bowel diseases: a systematic review and meta-analysis assessing their pathogenic implications and biomarker utility. *Inflamm Bowel Dis*. 2024;30:629-640. [CrossRef]
7. Koutroubakis IE, Zavos C, Damilakis J, et al. Role of ghrelin and insulin-like growth factor binding protein-3 in the development of osteoporosis in inflammatory bowel disease. *J Clin Gastroenterol*. 2011;45:e60–e65. [CrossRef]
8. Karmiris K, Koutroubakis IE, Xidakis C, et al. Circulating levels of leptin, adiponectin, resistin, and ghrelin in inflammatory bowel disease. *Inflamm Bowel Dis*. 2006;12:100-105. [CrossRef]
9. Sun J, Brooks EC, Houshyar Y, et al. Unravelling the Relationship Between Obesity and Inflammatory Bowel Disease. *Inflamm Bowel Dis*. 2025;31(9):2547-2560. [CrossRef]
10. Truelove SC, Witts LJ. Cortisone in ulcerative colitis; final report on a therapeutic trial. Br Med J. 1955; 29: 1041-1048 [CrossRef]
11. Compston JE, McClung M, Leslie W. Osteoporosis. *Lancet*. 2019;393(10169):364-376.[CrossRef]
12. Carvalho LGF, Lima WG, Coelho LGV, Cardoso VN, Fernandes SOA. Circulating leptin levels as a potential biomarker in inflammatory bowel diseases: a systematic review and meta-analysis. *Inflamm Bowel Dis*. 2021;27(2):169-181 [CrossRef]
13. Weidingera C, Hegazya AN, Siegmund B. The role of adipose tissue in inflammatory bowel diseases. Curr Opin Gastroenterol. 2018;34(4):183-186 [CrossRef]
14. Franchimont D, Roland S, Gustot T, et al. Impact of infliximab on serum leptin levels in patients with Crohn's disease. J Clin Endocrinol Metab. 2005; 90: 3510–3516 [CrossRef]
15. Berner HS, Lyngstadaas SP, Spahr A, et al. Adiponectin and its receptors are expressed in bone-forming cells. Bone. 2004; 35: 842-849. [CrossRef]
16. Ates Y, Degertekin B, Erdil A, Yaman H, Dagalp K. Serum ghrelin levels in inflammatory bowel disease with relation to disease activity and nutritional status. *Dig Dis Sci*. 2008; 53: 2215-2221. [CrossRef]
17. Konturek PC, Brzozowskı T, Engel M, et Al. Ghrelin ameliorates colonic inflammation. Role of nitric oxide and sensory nerves. *J Physiol Pharmacol*. 2009; 60: 41-47. [CrossRef]
18. Peracchi M, Bardella MT, Caprioli F, Massironi S, Conte D. Circulating ghrelin levels in patients with inflammatory bowel disease. *Gut*. 2006; 55: 432–436. [CrossRef]
19. Tvarijonaviciutea A, Eralp O, Kocaturk M, Yilmaz Z, Cerona JJ. Adiponectin and IGF-1 are negative acute phase proteins in a dog model of acute endotoxaemia. *Vet Immunol Immunopathol*. 2011; 140: 147-151. [CrossRef]
20. Pöykkö SM, Ukkola O, Kauma H, Kellokoski E, Hörkkö S, Kesäniemi YA. The negative association between plasma ghrelin and IGF-I is modified by obesity, insulin resistance and type 2 diabetes. *Diabetologia*. 2005; 48: 309-316. [CrossRef]
21. Haris L, Senagore P, Young VB, McCabe LR. Infammatory bowel disease causes reversible suppression of osteoblast and chondrocyte function in mice. *Am J Physiol Gastrointest Liver Physiol*. 2009; 296: 1020-1029. [CrossRef]
22. Song T, Zhuang M, Wong ZYD, et al. Discovery of a deuterated TNF-α small molecule modulator for potential treatment of ulcerative colitis. *Eur J Med Chem*. 2025 Jul 5;291:117616. [CrossRef]
23. Komatsu M, Kobayashi D, Saito K, et al. Tumor necrosis factor-alpha in Serum of patients with inflammatory bowel disease as measured by a highly sensitive immuno-PCR. *Clin Chem*. 2001; 47: 1297-1301. [CrossRef]
24. Ottaviani S, Treton X, Forien M, et al. Screening for osteoporosis in patients with inflammatory bowel diseases: a cross-sectional study. *Clin Rheumatol* . [CrossRef]
25. Chedid VG, Kane SV. Bone health in patients with inflammatory bowel diseases. *J Clin Densitom*. 2020;23(2):182-189. [CrossRef]
26. Even Dar R, Mazor Y, Karban A, Ish-Shalom S, Segal E. 2019 Risk factors for low bone density in inflammatory bowel disease: use of glucocorticoids, low body mass index, and smoking. *Dig Dis.* 37:284-290 [CrossRef]
27. Lee JS, Lee HS, Jang BI, et al. Low bone mineral density in young patients newly diagnosed with inflammatory bowel disease. Dig Dis Sci. 2021;66(2):605-611. [CrossRef]

ABCResearch

Arch Basic Clin Res 2026;8(2):100-105
DOI: 10.4274/ABCR.2026.26438

Research Article

The Relationship Between Non-alcoholic Fatty Liver Disease and Epicardial Adipose Tissue Thickness, Carotid Intima Media Thickness, and Aortic Propagation Velocity

Ersin Öztürk[1], Fatih Özçiçek[1], Muharrem Said Coşkun[2], Serhat Hayme[3], Sonay Aydın[4], Gülay Kızılgün Öztürk[5]

[1]Department of Internal Medicine, Erzincan Binali Yıldırım University Faculty of Medicine, Erzincan, Türkiye
[2]Department of Cardiology, Erzincan Binali Yıldırım University Faculty of Medicine, Erzincan, Türkiye
[3]Department of Biostatistics and Health Informatics, Erzincan Binali Yıldırım University Faculty of Medicine, Erzincan, Türkiye
[4]Department of Radiology, Erzincan Binali Yıldırım University Faculty of Medicine, Erzincan, Türkiye
[5]Family Medicine Specialist, Demirkent Family Health Center, Erzincan, Türkiye

Cite this article as: Öztürk E, Özçiçek F, Coşkun MS, Hayme S, Aydın S, Kızılgün Öztürk G. The relationship between non-alcoholic fatty liver disease and epicardial adipose tissue thickness, carotid intima media thickness, and aortic propagation velocity. *Arch Basic Clin Res*. 2026;8(2):100-105.

ORCID IDs of the authors: E.Ö. 0009-0001-6025-5588, F.Ö. 0000-0001-5088-4893, M.S.C.0000-0003-1042-9954, S.H. 0000-0001-9428-3002, S.A. 0000-0002-3812-6333, G.K.Ö. 0009-0002-0734-1898.

ABSTRACT

Objective: Cardiovascular disease is prevalent among individuals diagnosed with non-alcoholic fatty liver disease (NAFLD). Epicardial adipose tissue (EAT), carotid intima-media thickness (CIMT), and aortic propagation velocity (APV) are associated with atherosclerosis and cardiovascular disease (CVD). The aim of this study is to determine whether NAFLD is associated with EAT, CIMT, and APV.

Methods: Individuals aged ≥18 and <65 years who presented for routine follow-up were included. The study population comprised 75 healthy controls (40 females, 35 males) and 141 patients with NAFLD (68 females, 73 males). Epicardial adipose tissue thickness, carotid intima-media thickness, and aortic propagation velocity were evaluated using transthoracic echocardiography in patients who were diagnosed with hepatosteatosis by ultrasound during routine check-ups at the internal medicine clinic.

Results: NAFLD was positively associated with epicardial adipose tissue thickness and carotid intima–media thickness, and negatively associated with aortic propagation velocity. Patients with NAFLD had significantly higher EAT and CIMT values and lower APV values than controls. Logistic regression analysis identified body mass index (BMI) and EAT as independent predictors of hepatosteatosis. Each unit increase in BMI was associated with a 1.29-fold increase in the risk of hepatosteatosis, whereas each unit increase in EAT was associated with a 5.49-fold increase.

Conclusion: Given the established associations of CIMT, APV, and EAT with atherosclerosis and cardiovascular disease, assessment of patients with NAFLD using these noninvasive parameters may help identify subclinical cardiovascular risk.

Keywords: Non-alcoholic fatty liver disease, epicardial adipose tissue thickness, carotid intima-media thickness, aortic propagation velocity

INTRODUCTION

Non-alcoholic fatty liver disease (NAFLD) is characterized by excessive fat accumulation within hepatocytes, affecting more than 5% of liver cells in individuals without significant alcohol intake or secondary causes of hepatic steatosis such as steatogenic drugs, prior surgery, or other liver disorders.[1] There are insufficient noninvasive parameters demonstrating the association between NAFLD and the risk of atherosclerosis and cardiovascular disease.[2,3] The gold standard for the accurate diagnosis of NAFLD is the pathological evaluation of liver biopsy specimens; however, numerous biomarkers of NAFLD have been investigated to avoid such an invasive

Corresponding author: Ersin Öztürk, **E-mail:** drersinozturk88@gmail.com

Received: April 2, 2026
Revision Requested: May 24, 2026 **Accepted:** June 6, 2026 **Publication Date:** July, 14, 2026

technique.[4,5] Because NAFLD is associated with the risk factors of metabolic syndrome, treatment should primarily focus on the management of hypertension, hyperlipidemia, insulin resistance, and diabetes mellitus.[6]

Epicardial adipose tissue thickness (EAT) and volume have been associated with visceral adiposity, coronary artery disease, subclinical atherosclerosis, insulin resistance, metabolic syndrome, and cardiac structural and functional alterations.[7] EAT thickness is associated with the presence and progression of NAFLD. Individuals with increased EAT may require closer monitoring with regard to NAFLD.[8]

Atherosclerosis is a systemic and chronic disease, characterized by the transendothelial infiltration of low-density lipoprotein cholesterol (LDL-C), its accumulation within the intima, and subsequent oxidative and enzymatic processes.[9] Therefore, the intima–media complex of the arterial wall plays a crucial role in the pathogenesis of atherosclerosis and may reflect different stages of disease development. In the early stages of atherosclerosis, a hypertensive and hypertrophic response of medial cells can be observed, which is assessed by measuring carotid intima–media thickness (CIMT).[10]

Arterial stiffness and atherosclerotic changes within the aorta contribute to vascular wall thickening and reduced elasticity, ultimately increasing vascular resistance. As resistance increases, blood flow propagation within the arterial lumen decreases.[11] In this context, APV has emerged as a practical, reproducible, and non-invasive parameter for assessing arterial stiffness.[12]

The present study aimed to investigate the relationship between NAFLD and atherogenic parameters, including epicardial adipose tissue thickness, CIMT, and APV and to determine which of these parameters is the most valuable predictor of NAFLD.

MATERIAL AND METHODS

This descriptive study included individuals aged 18-64 years who presented to the Internal Medicine outpatient clinic of Erzincan Binali Yıldırım University Mengücek Gazi Training and Research Hospital for routine follow-up between October 25, 2022, and April 25, 2023. A total of 75 healthy individuals (40 females, 35 males) and 141 individuals with NAFLD (68 females, 73 males) were enrolled in the study. Among participants whose stage of hepatic steatosis was determined by ultrasonography, anthropometric measurements and hematological and biochemical tests (including liver and renal function tests, lipid profile, etc.) were evaluated.

Venous blood samples were collected following a fasting period of 10-12 hours.

After excluding, by ultrasonography, liver pathologies that could affect the study outcomes (such as malignancy, cholestasis, and liver cirrhosis), hepatic steatosis was classified into four stages: normal liver, stage 1 (mild),stage 2 (moderate), and stage 3 (severe).

Epicardial adipose tissue thickness measurements were performed by a cardiology specialist using transthoracic echocardiography (Philips EPIQ 7C) with an S4-2 transducer (2-4 MHz).

For CIMT evaluation, participants were examined in the supine position with slight neck extension, achieved by placing a pillow beneath the neck. Bilateral common carotid arteries were visualized using a Philips EPIQ 7C ultrasonography device with a 7.5 MHz linear probe. Three separate measurements were obtained from each side, and the average value was recorded.

For the assessment of APV, participants were positioned supine, and M-mode recordings were obtained by a cardiology specialist using a Philips EPIQ 7C echocardiography system with a 3.0 MHz transducer. The mean of at least three measurements was recorded as the APV value.

Statistical Analysis

Statistical analyses were performed using the Statistical Package for the Social Sciences (SPSS) version 22.0 (IBM Corp., Armonk, NY, USA). The normality of data distribution was assessed using the Kolmogorov-Smirnov test. Descriptive statistics are presented as mean (standard deviation) in the results and in the tables. Comparisons between two groups were performed using the Student's t-test for normally distributed variables and the Mann-Whitney U test for non-normally distributed variables. For comparisons among more than two groups, one-way analysis of variance was used for normally distributed data, while the Kruskal–Wallis test was applied for non-normally distributed data. Categorical variables were compared using the chi-square test.

Logistic regression analysis was conducted to identify factors affecting the risk of hepatic steatosis, including variables found to be significant in univariate analysis. Age and sex were included in the model as biological variables using the enter method; subsequently, significant variables were identified using the forward likelihood ratio method. Results were expressed as odds ratios with 95% confidence intervals.

A P value of <0.05 was considered statistically significant.

RESULTS

Among the 216 individuals included in the study, NAFLD was detected in 141 (65.3%); the remaining 75 individuals (34.7%) comprised the control group.

The study population consisted of 108 women (50%) and 108 men (50%). NAFLD was identified in 68 women (63.0%) and 73 men (67.6%). No statistically significant difference in sex distribution was observed between individuals with and without NAFLD (P = 0.47).

The mean epicardial adipose tissue thickness was 3.9 ± 0.8 mm in individuals without NAFLD and 5.1 ± 0.7 mm in those with NAFLD, demonstrating a statistically significant difference between the groups (P <0.001). The mean carotid intima–media thickness (CIMT) was 0.82 ± 0.12 mm in participants without NAFLD and 1.01 ± 0.12 mm in those with NAFLD (P < 0.001). The mean APV was 56.4 ± 7.9 cm/s in individuals without NAFLD and 43.8 ± 7.9 cm/s in those with NAFLD, with the difference being statistically significant (P < 0.001).

Comparison of laboratory parameters between individuals with and without NAFLD revealed statistically significant differences in the levels of glucose, total cholesterol, high-density lipoprotein cholesterol (HDL-C), LDL-C, triglycerides, alanine aminotransferase (ALT), aspartate aminotransferase (AST), gamma-glutamyl transferase (GGT), and body mass index (BMI) (Table 1).

When demographic, clinical, and laboratory characteristics were compared across levels of hepatic steatosis severity, significant differences were observed in BMI, EAT, CIMT, APV, triglycerides, fasting plasma glucose, ALT, and AST (Table 2).

To identify factors associated with hepatic fat accumulation, logistic regression analysis was performed using variables that were significant in the univariate analysis; age and sex were retained in the model as biological covariates. According to the regression analysis, BMI and EAT were found to be significant independent predictors of NAFLD. Each unit increase in BMI was associated with a 1.29-fold increase in the risk of NAFLD, whereas each unit increase in EAT was associated with a 5.49-fold increase in the risk of NAFLD (Table 3).

DISCUSSION

In this study, laboratory parameters, radiological imaging findings, and anthropometric measurements possibly associated with nonalcoholic fatty liver disease (NAFLD) were evaluated.

When individuals with and without NAFLD were compared, statistically significant associations were observed between NAFLD status and body mass index (BMI), epicardial adipose tissue thickness (EAT), carotid intima–media thickness (CIMT), APV, total cholesterol, high-density lipoprotein cholesterol (HDL-C), low-density lipoprotein cholesterol (LDL-C), triglycerides, fasting plasma glucose, ALT, AST, and GGT.

When data were analyzed according to the degree of hepatosteatosis, statistically significant relationships were found between steatosis severity and BMI, APV, EAT, CIMT, triglycerides, fasting plasma glucose, AST, and ALT.

MAIN POINTS

- Patients with Non-alcoholic fatty liver disease (NAFLD) have significantly increased epicardial adipose tissue (EAT) thickness and carotid intima-media thickness (CIMT), and reduced aortic propagation velocity (APV).
- The severity of hepatic steatosis is associated with progressive increases in EAT and CIMT and a progressive decrease in APV.
- Noninvasive cardiovascular imaging markers, particularly EAT, may facilitate early identification of subclinical cardiovascular risk in patients with NAFLD.
- Routine assessment of EAT together with CIMT and APV may improve cardiovascular risk stratification and support earlier preventive interventions in patients with NAFLD.

Several mechanisms have been proposed to explain the link among NAFLD, various stages of the atherosclerotic process, and alterations in cardiac structure and function. These mechanisms include endothelial dysfunction, atherogenic dyslipidemia, insulin resistance, and impaired cardiac mechanics.[13,14]

An association between obesity and NAFLD has been well established.[15] In a study by Almeida et al. involving 3,841 participants, the prevalence of NAFLD was shown to increase

Table 1. Demographic, Clinical, and Laboratory Characteristics of the Groups

		Control group (n=75)	Study group (n=141)	*P* value
Sex	Female	40 (53.3)	68 (48.2)	0.47
	Male	35 (46.7)	73 (51.8)	
Age (year)*		42.8 (13.2)	46 (11)	0.11
Body mass index (kg/m^2)*		25.9 (3.9)	31.7 (5.4)	**<0.001**
Waist circumference (cm)**		91.3 (12.4)	106 (12.7)	**<0.001**
Hip circumference (cm)*		103.5 (9.7)	113.5 (11.8)	**<0.001**
NAFLD Fibrosis Score**		-2.42 (1.04)	-1.83 (1.38)	**0.001**
Epicardial adipose tissue thickness (mm)*		3.9 (0.8)	5.1 (0.7)	**<0.001**
Carotid intima media thickness (mm)*		0.82 (0.12)	1.01 (0.12)	**<0.001**
Aortic propagation velocity (cm/sn)*		56.4 (7.9)	43.8 (7.9)	**<0.001**
Total Cholesterol (mg/dL)**		189.1(40.9)	203.6 (38.6)	**0.011**
HDL Cholesterol (mg/dL)**		48.4 (10.3)	45.2 (8.8)	**0.019**
LDL Cholesterol (mg/dL)**		126.9 (33.1)	140.1 (29.9)	**0.003**
Triglycerides (mg/dL)*		127.2 (66.3)	188.7 (106.5)	**<0.001**
Fasting Plasma Glucose (mg/dL)*		90.3 (9.7)	110.7 (42.4)	**<0.001**
ALT (U/L)*		21.7 (15)	35.8 (24.6)	**<0.001**
AST (U/L)*		22.7 (9.2)	27.6 (12.4)	**<0.001**
GGT (U/L)*		23.8 (17.1)	37.5 (22.6)	**<0.001**
Creatinine (mg/dL)**		0.85 (0.15)	0.85 (0.14)	0.94
Albumin (g/dL)**		43.7 (2.5)	43.2 (2.7)	0.26
TSH (µU/mL)*		1.84 (1.04)	1.89 (1.06)	0.62
Uric Acid (mg/dL)**		4.5 (1.2)	5.1 (1.4)	**0.001**
Platelet count (10^3/µL)**		244.6 (51.6)	250.6 (53.7)	0.43

*Mann-Whitney U test was applied. ** Student's t-test was applied. *** Chi-square test was applied. (The data in the table are presented as mean (standard deviation) values.)
NAFLD, non-alcoholic fatty liver disease; HDL, high-density lipoprotein; LDL, low-density lipoprotein; ALT, alanine aminotransferase; AST, aspartate aminotransferase; GGT, gamma-glutamyl transferase; TSH, thyroid-stimulating hormone.

with rising BMI, indicating that hepatic steatosis is primarily related to excess adiposity (higher BMI).[16] In a meta-analysis conducted by Yuan et al.[17], an increase in BMI was associated with a 1.33-fold increase in the risk of NAFLD. In the present study, the mean BMI was 25.9 ± 3.9 kg/m^2 in individuals without NAFLD and 31.7 ± 5.4 kg/m^2 in those with NAFLD. Moreover, the severity of NAFLD increased in parallel with BMI. Logistic regression analysis demonstrated that BMI was associated with a 1.29-fold increased risk of NAFLD. These findings are consistent with previous reports.

Epicardial adipose tissue thickness is an easily measurable marker of visceral adiposity. Epicardial adipocytes secrete

Table 2. Comparison of Demographic, Clinical, and Laboratory Data of Groups According to the Degree of Hepatosteatosis

		Grade 1	Grade 2	Grade 3	*P*
Age (year)*		44.5(11.1)	47.1(10.6)	46.7(11.4)	0.43
Sex	Female	26 (50.9)	27 (50)	15 (44.1)	0.85
	Male	27 (49.1)	27 (50)	19 (55.9)	
BMI (kg/m^2) **		29.9 (4.3)^a	31.5 (5.9)^a	34.7 (4.7)^b	**<0.001**
Waist circumference (cm)*		101.8 (12.2)^a	105.2 (11.1)^a	113.8 (12.4)^b	**<0.001**
Hip circumference (cm)*		109.6 (10.7)^a	113.2 (10.8)^a	120.1 (12.4)^b	**<0.001**
NAFLD Fibrosis Score*		-2.25 (1.21)^a	-1.77 (1.31)	-1.26 (1.57)^b	**0.004**
Epicardial adipose tissue thickness (mm)**		4.7(0.5) ^{a}	5.2 (0.75)^b	5.7 (0.6)^c	**<0.001**
Carotid intima media thickness (mm)**		0.94 (0.09)^a	1.02 (0.13)^b	1.09 (0.1)^c	**<0.001**
Aortic propagation velocity (cm^2 .dyn^{-1}X10^{-6})**		49 (5.3)^a	42.6 (7.8)^b	37.5(5.7)^c	**<0.001**
Left ventricular ejection fraction (%)**		56.2 (4.4)	56.6 (4.2)	57.1 (4.3)	0.65
Total Cholesterol (mg/dL)*		199.8 (34.9)	206.9 (38.4)	204.2 (44.6)	0.63
HDL Cholesterol (mg/dL)*		44.1 (8.7)	46.7 (8.9)	44.5 (8.4)	0.27
LDL Cholesterol*		138.2 (28.6)	141.2 (29.9)	141.2 (32.6)	0.85
Triglycerides (mg/dL)**		160.3 (101.1)^a	196.9 (106)	219.7 (107.3)^b	**0.005**
Fasting Plasma Glucose (mg/dL)**		96.7 (19.4)^a	115 (49.5)	125.8 (50.4)^b	**0.009**
ALT (U/L) **		26.5 (15.3)^a	38.2 (24.3)^b	46.7 (31.3)^b	**<0.001**
AST (U/L)*		22.6 (6.6)^a	28.5 (12.7)^b	33.8 (15.7)^b	**<0.001**
GGT (U/L) **		32.4 (18.1)	37.2 (19.9)	45.6 (30.1)	0.08
Kreatinin (mg/dL) *		0.84 (0.14)	0.85 (0.14)	0.86 (0.14)	0.77
Albümin (g/dL) *		43 (2.7)	43.8 (2.8)	42.7 (2.7)	0.12
TSH (µU/mL) *		1.98 (1.1)	2 (1.07)	1.58 (0.92)	0.14
Uric Acid (mg/dL)**		4.8 (1.2)^a	5.1 (1.4)	5.7 (1.3)^b	**0.011**
Platelet count (10^3/µL)*		257.7 (49.7)	246 (55)	246.8 (57.8)	0.48

*One Way ANOVA test was used. **Kruskal Wallis test was used. *** Chi-square test was applied. a,b,c: Groups marked with the same letter are statistically similar, and there is a statistically significant difference at the level of <0.05 between groups with different letters.
BMI, body mass index; NAFLD, non-alcoholic fatty liver disease; HDL, high-density lipoprotein; LDL, low-density lipoprotein; ALT, alanine aminotransferase; AST, aspartate aminotransferase; gamma-glutamyl transferase; TSH, thyroid-stimulating hormone.

Table 3. The Results of the Logistic Regression Analysis Conducted to Determine the risk Factors Affecting Liver Steatosis

	P value	OR	95% CI for OR	
			Lower limit	Upper limit
Gender*	0.96	0.978	0.439	2.175
Age*	0.62	0.966	0.932	1.002
BMI	**<0.001**	1.294	1.152	1.453
EAT	**<0.001**	5.492	3.121	9.664
APV	0.37	1.101	0.893	1.357
CIMT	0.98	1.011	0.374	2.732

*Gender and age were kept constant in the model as biological factors. OR: Odds-ratio; CI: Confidence interval; BMI, body mass index; EAT, epicardial adipose tissue thickness; APV, aortic propagation velocity; CIMT; carotid intima-media thickness.

numerous cytokines and vasoactive peptides, all of which may independently contribute to increased cardiovascular risk.[18] In a study by Oğuz et al.[19] including 78 participants, mean EAT was 5.1 ± 2.5 mm in individuals with NAFLD, compared with 2.9 ± 0.9 mm in healthy controls. In a large multivariate logistic regression analysis conducted by Meng et al.[2] in 2,238 individuals, a significant association between NAFLD and EAT was demonstrated. Participants with higher EAT were older and exhibited greater waist and hip circumferences, lower HDL-C levels, higher body weight and BMI, elevated blood pressure, higher LDL-C, fasting plasma glucose, triglyceride levels, increased CIMT, and poorer overall cardiovascular health.[2] In the present study, the mean EAT was 3.9 ± 0.8 mm in individuals without NAFLD and 5.1 ± 0.7 mm in those with NAFLD, and EAT increased in parallel with the severity of steatosis. Regression analysis revealed that EAT increased the risk of NAFLD by 5.49-fold. EAT was identified as the parameter most strongly associated with NAFLD and therefore may serve as a valuable imaging marker to predict hepatic steatosis.

CIMT is a widely used and reliable method for the assessment of subclinical atherosclerosis.[20] Increased CIMT has been shown to be associated with established atherosclerotic risk factors, including age, sex, BMI, systolic blood pressure, HbA1c, and hyperlipidemia.[21] In a study by Kumari et al.[22] involving 80 participants, CIMT was 0.52 mm in individuals without NAFLD and 0.86 mm in those with NAFLD, and a statistically significant relationship between NAFLD and CIMT was reported. Furthermore, a meta-analysis by Sookoian et al. including 3,497 participants demonstrated a 13% increase in CIMT among individuals with NAFLD compared with those without.[23] In the present study, the mean CIMT was 0.82 ± 0.12 mm in individuals without NAFLD and 1.01 ± 0.12 mm in those with NAFLD. This difference was statistically significant, and CIMT values also differed significantly across steatosis severity groups. However, CIMT was not identified as an independent predictor of NAFLD in the regression analysis.

APV, a parameter reflecting aortic stiffness and arterial resistance, has been shown to be associated with coronary artery disease.[24] In the study by Oğuz et al.,[19] patients with NAFLD exhibited significantly lower APV values and significantly higher epicardial adipose tissue thickness compared with controls.[19] Similarly, Gunes et al.[11] demonstrated that APV, a simple, practical, and non-invasive measure of arterial resistance, was associated with coronary atherosclerosis and significantly lower in individuals with NAFLD than in controls. Additionally, APV was found to decrease in individuals with increased waist circumference, higher BMI, and elevated fasting plasma glucose levels.[11] In our study, the mean APV was 56.4 ± 7.9 cm/s in individuals without NAFLD and 43.7 ± 7.9 cm/s in those with NAFLD. Although APV differed significantly between individuals with and without NAFLD and across steatosis severity groups, it was not identified as an independent predictor of NAFLD in the regression analysis.

Study limitations

This study has several limitations. First, due to its single-center, descriptive design, establishing causal relationships based on the findings is challenging. Second, participants could not be followed longitudinally after the diagnosis of NAFLD; therefore, the duration required for the development of cardiovascular risk could not be determined.

CONCLUSION

Our findings demonstrate significant associations between NAFLD and atherogenic parameters, including EAT, CIMT, and APV. Among these, BMI and EAT were identified as independent predictors of NAFLD. Given the increased cardiovascular risk associated with NAFLD, incorporating noninvasive vascular assessments such as EAT, CIMT, and APV into routine evaluation may facilitate early detection of subclinical cardiovascular disease.

Further multicenter studies with larger cohorts are required to validate these findings and clarify the clinical utility of these parameters.

Acknowledgments

The authors thank those who assisted with data collection.

Ethics

Ethics Committee Approval: The study was approved by the Erzincan Binali Yıldırım University Clinical Research Ethics Committee (approval no.: 02/08, dated: 29.09.2022).

Informed Consent: Written informed consent was obtained from all participats.

Footnotes

Author Contributions

Concept Design – E.Ö., F.Ö.; Data Collection or Processing – E.Ö., M.S.C., S.A., G.K.Ö.; Analysis or Interpretation – E.Ö., F.Ö., S.H., G.K.Ö.; Literature Review - E.Ö., F.Ö., S.A.; Writing, Reviewing and Editing – E.Ö., F.Ö.

Declaration of Interests: The authors declare no conflicts of interest related to the publication of this paper.

Funding: The authors declare no financial support or funding

REFERENCES

1. Schaffner F, Thaler H. Nonalcoholic fatty liver disease. *Prog Liver Dis*. 1986;8:283-298. [CrossRef]
2. Meng X, Wang W, Zhang K, et al. Epicardial adipose tissue volume is associated with non-alcoholic fatty liver disease and cardiovascular risk factors in the general population. *Ther Clin Risk Manag*. 2018;14:1499-1506. [CrossRef]
3. Mladenova IL, Tan EF, Ng JY, Sharma P. Non-alcoholic fatty liver disease(NAFLD)and its association to cardiovascular disease: a comprehensive meta-analysis. JRSM cardiovascular disease. 2025;14:20480040251325929. [CrossRef]
4. Balci IC, Haciagaoglu N, Oner C, Cetin H, Simsek EE. Non-invasive screening of metabolic associated fatty liver disease and affecting factors in primary care. *J Coll of Physicians Surg Pak*. 2023;33(4):390-395. [CrossRef]

5. Saponaro C, Sabatini S. Adipose tissue dysfunction and visceral fat are associated with hepatic insulin resistance and severity of NASH even in lean individuals. *Liver Int*. 2022;42(11):2418-2427. [CrossRef]
6. Rinella ME, Neuschwander-Tetri BA. AASLD practice guidance on the clinical assessment and management of nonalcoholic fatty liver disease. *Hepatology*. 2023;77(5):1797-835. [CrossRef]
7. Jiang H, Zhou Y, Nabavi SM, et al. Mechanisms of oxidized LDL-mediated endothelial dysfunction and ıts consequences for the development of atherosclerosis. *Front Cardiovasc Med*. 2022;9:925923. [CrossRef]
8. Emamat H, Tangestani H, Behrad Nasab M, Ghalandari H, Hekmatdoost A. The association between epicardial adipose tissue and non-alcoholic fatty liver disease: a systematic review of existing human studies. *EXCLI J*. 2021;20:1096-1105. [CrossRef]
9. Jebari-Benslaiman S, Galicia-García U, Larrea-Sebal A, et al. Pathophysiology of atherosclerosis. Int *J Mol Sci*. 2022;23(6):3346. [CrossRef]
10. Choi HI, Kim YT. Segment-specific analysis of carotid ıntima-media thickness and its association with cardiovascular risk factors in a large healthy cohort. *J Clin Med*. 2025;14(6):1918. [CrossRef]
11. Gunes Y, Tuncer M, Guntekin U, et al. The relation between the color M-mode propagation velocity of the descending aorta and coronary and carotid atherosclerosis and flow-mediated dilatation. *Echocardiography*. 2010;27(3):300-305. [CrossRef]
12. Tosun V, Güntekin Ü, Şimşek H, Kandemir YB. Aortic-flow propagation velocity is associated with proteinuria and left ventricular hypertrophy in newly diagnosed hypertensive patients. *Echocardiography*.2019;36(2):328-335. [CrossRef]
13. Lim Y, Jeong S, Hong M, Han HW. Non-alcoholic fatty liver disease, atherosclerosis, and cardiovascular disease in Asia. *Rev in Cardiovas Med*. 2023;24(6):173. [CrossRef]
14. Kosekli MA, Kurtkulagii O, Kahveci G, et al. The association between serum uric acid to high density lipoprotein-cholesterol ratio and non-alcoholic fatty liver disease: the abund study. *Rev Assoc Med Bras (1992)*.2021;67(4):549-554. [CrossRef]
15. Teng ML, Ng CH, Huang DQ, et al. Global incidence and prevalence of nonalcoholic fatty liver disease. *Clin and Mol Hepatol*. 2023;29(Suppl):S32-s42. [CrossRef]
16. Almeida NS, Rocha R. Anthropometric clinical indicators of visceral adiposity as predictors of nonalcoholic fatty liver disease. *Rev Assoc Med Bras (1992)*. 2021;67(11):1544-1549. [CrossRef]
17. Yuan S, Chen J, Li X, et al. Lifestyle and metabolic factors for nonalcoholic fatty liver disease: Mendelian randomization study. *Eur J Epidemiol*. 2022;37(7):723-733. [CrossRef]
18. Malavazos AE, Iacobellis G. Human epicardial adipose tissue expresses glucose-dependent insulinotropic polypeptide, glucagon, and glucagon-like peptide-1 receptors as potential targets of pleiotropic therapies. *Eur J Prev Cardiol*. 2023;30(8):680-693. [CrossRef]
19. Oğuz D, Ünal H, Eroğlu H, Gülmez Ö, Çevik H, Altun A. Aortic flow propagation velocity, epicardial fat thickness, and osteoprotegerin level to predict subclinical atherosclerosis in patients with nonalcoholic fatty liver disease. *Anatol J Cardiol*. 2016;16(12):974-979. [CrossRef]
20. Fernández-Alvarez V, Linares Sánchez M, López Alvarez F. Evaluation of ıntima-media thickness and arterial stiffness as early ultrasound biomarkers of carotid artery atherosclerosis. *Cardiol Therapy*. 2022;11(2):231-247. [CrossRef]
21. Takase M, Nakaya N, Nakamura T, et al. Carotid ıntima media thickness and risk factor for atherosclerosis: tohoku medical megabank community-based cohort study. *J Atheroscler Thromb*.2023;30(10):1471-1482. [CrossRef]
22. Kumari S, Porwal YC, Gupta R. Correlation between carotid ıntima media thickness and non-alcoholic fatty liver disease. *J Assoc Physicians India*. 2022;70(4):11-12. [CrossRef]
23. Sookoian S, Pirola CJ. Non-alcoholic fatty liver disease is strongly associated with carotid atherosclerosis: a systematic review. *J Hepatol*. 2008;49(4):600-607. [CrossRef]
24. Ghaderi F, Samim H, Keihanian F. The predictive role of aortic propagation velocity for coronary artery disease. *BMC Cardiovasc Disorders*. 2018;18(1):121. [CrossRef]

ABCResearch

Arch Basic Clin Res 2026;8(2):106-111
DOI: 10.4274/ABCR.2026.26419

Research Article

Prognostic Value of Eosinophil-Derived Hematological Indices in Acute Decompensated Heart Failure

Burak Kardeşler[1], Fikriye Kalkan[2]

[1]Clinic of Cardiology, Ankara Bilkent City Hospital, Ankara, Türkiye
[2]Clinic of Allergy and Immunology, Ankara Bilkent City Hospital, Ankara, Türkiye

Cite this article as: Kardeşler B, Kalkan E. Prognostic value of eosinophil-derived hematological indices in acute decompensated heart failure. *Arch Basic Clin Res*. 2026;8(2):106-111

ORCID IDs of the authors: B.K. 0000-0003-4576-5798, F.K. 0000-0002-7199-436X.

ABSTRACT

Objective: Eosinophil-derived hematological indices have been proposed as potential prognostic markers for cardiovascular disease; however, their clinical value in acute decompensated heart failure (ADHF) remains unclear. This study aimed to comprehensively evaluate the prognostic significance of eosinophil-based hematological indices, particularly the neutrophil-to-eosinophil ratio (NER), in hospitalized patients with ADHF.

Methods: This single-center, retrospective observational study included 245 consecutive adult patients hospitalized for ADHF between January 2023 and January 2024. Patients with conditions known to influence eosinophil counts, including allergic diseases, recent systemic corticosteroid use, active infection, malignancy, chronic inflammatory disorders, end-stage renal failure, and severe liver disease, were excluded. Hematological indices calculated from blood samples obtained within the first 24 h of admission included NER, eosinophil-to-lymphocyte ratio (ELR), eosinophil-to-monocyte ratio (EMR), eosinophil percentage, neutrophil-to-lymphocyte ratio (NLR), and systemic immune-inflammation index (SII). The primary outcome was all-cause mortality during the one-year follow-up period.

Results: During the follow-up period, 93 (38.0%) patients died. Non-survivors were significantly older and exhibited a higher inflammatory burden, with increased C-reactive protein levels, NLR, and SII values. Eosinophil counts, eosinophil percentages, and EMR values were significantly lower in non-survivors, whereas the NER and ELR did not differ between the groups. Receiver operating characteristic analysis demonstrated poor discriminative performance for eosinophil-derived indices, with area under the curve values of ≤ 0.55. In the multivariate logistic regression analysis, only age was an independent predictor of mortality.

Conclusion: Eosinophil-based hematological indices have limited prognostic value for mortality in patients hospitalized with ADHF. Although eosinophil suppression is associated with adverse outcomes, these indices do not provide independent prognostic information beyond age.

Keywords: Acute decompensated heart failure, Eosinophils, Eosinophil-derived hematological indices, inflammation, mortality, prognosis

INTRODUCTION

Acute decompensated heart failure (ADHF) continues to be one of the leading causes of hospitalization among adults worldwide.[1,2] It is also associated with significant morbidity, prolonged hospitalization, and increased healthcare utilization. Inflammation plays an important role in both the development and progression of heart failure.[3,4]. Numerous hematological indices derived from hemogram parameters have emerged as practical and cost-effective biomarkers for risk stratification in cardiovascular disease and are currently used as auxiliary techniques in clinical practice.[5,6]

Among these markers, eosinophils are valuable because of their role in immune regulation, cytokine response formation, and tissue-level inflammatory responses.[7,8] Although traditionally associated with parasitic infections and allergic diseases, eosinophils also participate in cardiovascular inflammation and stress responses through mechanisms involving interleukin-5 (IL-5), IL-4, and IL-13.[3,9] Importantly, eosinophil levels may

Corresponding author: Burak Kardeşler, **E-mail:** burak_kardesler@hotmail.com

Received: 17 February, 2026
Revision Requested: 27 March, 2026 **Accepted:** 3 June, 2026 **Publication Date:** July, 14, 2026

be significantly affected by allergic disorders such as asthma, atopic dermatitis, and allergic rhinitis, which promote type-2 immune activation and eosinophil proliferation.[10,11]

Various eosinophil-derived hematological indices, including the neutrophil-to-eosinophil ratio (NER), eosinophil-to-monocyte ratio (EMR), and eosinophil-to-lymphocyte ratio (ELR), have been investigated as potential prognostic markers for cardiovascular disease.[12-14] Previous studies have suggested that excessive eosinopenia or high ratios may reflect increased physiological stress or systemic inflammation and may potentially be associated with adverse outcomes, such as death or rehospitalization.[15,16] However, the prognostic value of these indices has been inconsistent across studies, and their independent contributions beyond traditional clinical predictors remain uncertain.

Further studies are needed to clarify the prognostic importance of eosinophil-derived indices in heart failure. In this context, the study aimed to investigate the relationship between eosinophil-based hematological indices, specifically the NER, and mortality in patients hospitalized with ADHF.

MATERIAL AND METHODS

This single-center, retrospective, observational study included consecutive adult patients hospitalized with a diagnosis of ADHF between January 2023 and January 2024. This study was approved by the Ankara Bilkent City Hospital Medical Research Scientific and Ethical Evaluation Board (decision number: TABED 2-26-1823, date: 07.01.2026). The diagnosis of ADHF was established according to the current European Society of Cardiology guidelines based on compatible clinical symptoms, physical examination findings, laboratory results, and echocardiographic assessments.[17] Only the first hospitalization of each patient during the study period was considered for the analysis. A one-year period after hospital admission was used as the basis for mortality assessment.

Patients aged 18 years or older who had a complete blood count obtained within the first 24 h of hospitalization were considered eligible for the study. To minimize factors affecting eosinophil levels, patients with active infection at admission; hematological malignancies or active solid tumors; chronic inflammatory or autoimmune diseases; allergic diseases known to alter eosinophil counts, including asthma, atopic dermatitis, and allergic rhinitis; systemic corticosteroid use within the last 30 days; end-stage renal failure requiring dialysis; severe liver failure; or missing or incomplete laboratory or clinical data required for analysis were excluded from the study. After applying these criteria, 245 patients were included in the final study.

MAIN POINTS

- Among patients hospitalized with acute decompensated heart failure, eosinophil counts and some eosinophil-derived indices were lower in non-survivors; however, their overall prognostic performance was poor.
- Classical inflammatory markers such as C-reactive protein, neutrophil-to-lymphocyte ratio, and systemic immune-inflammation index showed stronger univariate associations with mortality; however, none remained independent predictors after multivariable adjustment.
- Age emerged as the only independent determinant of all-cause mortality, indicating that eosinophil-based hematological indices provide limited incremental prognostic value beyond established clinical predictors.

Demographic characteristics, comorbidities, clinical findings, medication history, laboratory parameters, echocardiographic measurements, and follow-up outcomes were obtained from electronic medical records. Cardiac function was assessed using transthoracic echocardiography, and the left ventricular ejection fraction (LVEF) was recorded.

Blood parameters were used to calculate the following ratios: neutrophil-to-lymphocyte ratio (NLR) = neutrophil/lymphocyte, NER = neutrophil/eosinophil, ELR = eosinophil/lymphocyte, EMR = eosinophil/monocyte, eosinophil percentage (EOS percent) = (eosinophil/white blood cell) × 100, and systemic immune-inflammation index (SII) = (platelet × neutrophil)/lymphocyte.[18] All hematological indices were calculated using the earliest laboratory values obtained within the first 24 hours of hospitalization. NER could not be calculated in 38 patients because the eosinophil count, used as the denominator, was zero. These patients were excluded only from NER-related analyses; other hematological indices were calculated when the required parameters were available.

The primary outcome of the study was all-cause mortality, defined as death from any cause during the follow-up. Mortality status was available for all patients included in the study. Mortality data were obtained from hospital records and national death registry data, and no patient was lost to follow-up for the primary endpoint. Secondary descriptive outcomes included hematological and inflammatory differences between survivors and non-survivors.

Statistical Analysis

Statistical analyses were performed using SPSS (version 26). Continuous variables were evaluated for normality using the Kolmogorov-Smirnov test and presented as medians and interquartile ranges. Categorical variables are expressed as numbers and percentages. Differences between survivors and non-survivors were compared using the Mann-Whitney U test for continuous variables or the chi-square test for categorical variables.

The diagnostic performance of hematological indices in predicting mortality was evaluated using receiver operating characteristic (ROC) curve analysis, and the area under the curve (AUC) was calculated (Figure 1). Optimal cut-off values were determined using the Youden index. Variables deemed clinically relevant or demonstrating significance in the univariate analysis were included in a multivariate logistic regression model to identify independent determinants of all-cause mortality. Because exact time-to-event data were not consistently available, all-cause mortality was analyzed as a binary outcome, and multivariable logistic regression was used instead of Cox proportional hazards regression. In addition,

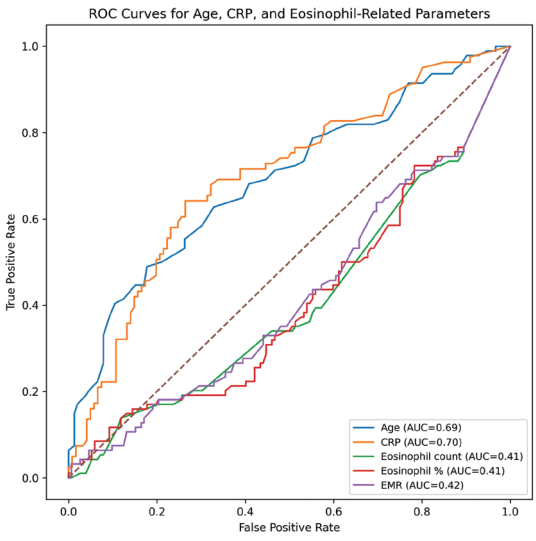

Figure 1. ROC curves for age, CRP, and Eosinophil-Related Parameters

ROC, receiver operating characteristic; AUC, area under curve; CRP, c-reactive protein; EMR, eosinophil-to-monocyte ratio.

renal function and major comorbidities, including hypertension, chronic obstructive pulmonary disease, and atrial fibrillation, were incorporated into the model when sufficient data were available. Odds ratios with 95 percent confidence intervals are reported. A two-sided *P* value of less than 0.05 was considered statistically significant.

RESULTS

In total, 245 patients were included in this study. In the study population, 152 patients (62.0 percent) survived, while 93 patients (38.0 percent) died during the one-year follow-up. The baseline clinical, laboratory, and inflammatory characteristics of survivors and non-survivors are summarized in Table 1. Patients who died were significantly older than survivors ($P < 0.001$). The mean LVEF was slightly higher in non-survivors than in survivors ($P = 0.009$).

Inflammatory burden differed significantly between the groups. C-reactive protein (CRP) levels were markedly higher in non-survivors than in survivors ($P < 0.001$). Lymphocyte counts were significantly lower in the mortality group ($P < 0.001$), whereas neutrophil counts were similar between groups. Eosinophil counts ($P = 0.016$) and eosinophil percentages ($P = 0.015$) were significantly lower in patients who died. The EMR was also reduced in non-survivors ($P = 0.029$). In contrast, the NER did not differ significantly between survivors and non-survivors ($P = 0.28$). Similarly, the ELR did not differ significantly between groups ($P = 0.15$).

Classical inflammation-based markers were more strongly associated with mortality than eosinophil-derived markers. The NLR was significantly higher in the mortality group ($P = 0.0015$). The SII was also higher among the non-survivors ($P = 0.013$).

Variables with clinical significance in the univariate analysis were included in the multivariable logistic regression model: age, LVEF, CRP, NLR, NER, eosinophil percentage, renal function,

Table 1. Baseline Demographic, Clinical, and Laboratory Characteristics of Survivors and Non-Survivors

Variable	Survivors (n=152)	Non-survivors (n=93)	*P* value
Age (years)	58 (48.8-67)	67 (56-78)	**< 0.001**
Male sex, n (%)	96 (62.7)	60 (64.5)	0.78
LVEF (%)	25 (20-30)	28 (21-35)	**0.009**
CRP (mg/L)	3.85 (0.58-19.0)	20.9 (3.2-65.0)	**< 0.001**
WBC (10^3/μL)	8.30 (6.65-10.3)	8.50 (6.6-11.5)	0.69
Neutrophils (10^3/μL)	5.45 (4.1-7.3)	5.50 (3.8-7.5)	0.31
Lymphocytes (10^3/μL)	1.90 (1.3-2.6)	1.40 (0.90-2.20)	**< 0.001**
Eosinophils (10^3/μL)	0.165 (0.10-0.26)	0.10 (0.04-0.20)	**0.016**
NLR	2.86 (1.91-4.53)	4.22 (2.40-6.46)	**0.001**
NER	28.4 (15-60)	36.9 (15-89)	0.28
EMR	0.20 (0.11-0.35)	0.17 (0.07-0.29)	**0.029**
Eosinophil %	1.94 (1.09-3.04)	1.23 (0.55-2.38)	**0.015**
SII	619 (392-1081)	874 (493-1399)	**0.013**
DM, n(%)	56 (36.8)	35 (37.2)	1.000
HT, n(%)	86 (56.6)	70 (74.5)	**0.007**
HL, n(%)	33 (21.7)	29 (30.9)	0.146
CAD, n(%)	71 (46.7)	53 (56.4)	0.179
COPD, n(%)	26 (17.1)	29 (30.9)	**0.018**
AF, n(%)	35 (23.0)	42 (44.7)	**0.001**

LVEF, left ventricular ejection fraction; CRP, C-reactive protein; WBC, white blood count; NLR, neutrophil-to-lymphocyte ratio; NER, neutrophil-to-eosinophil Ratio, EMR, eosinophil-to-monocyte ratio; SII, systemic immune-inflammation index; DM, diabetes mellitus; HT, hypertension, HL, hyperlipidemia; CAD, coronary artery disease; COPD, chronic obstructive pulmonary disease; AF: atrial fibrillation.

hypertension, chronic obstructive pulmonary disease (COPD), and atrial fibrillation (Table 2). In this model, only age remained an independent predictor of all-cause mortality. Other variables, including LVEF, CRP, NLR, NER, eosinophil percentage, renal function, hypertension, COPD, and atrial fibrillation, were not independently associated with mortality. SII was evaluated in the ROC analysis and was presented in Table 3, but it was not included in the final multivariable logistic regression model.

The discriminative performance of the hematological indices in predicting all-cause mortality is summarized in Table 3. Overall, age and CRP levels exhibited the highest discriminative ability, whereas eosinophil-derived indices showed poor predictive performance, with AUC values approximately 0.55 or lower.

DISCUSSION

In our study, we evaluated the prognostic value of eosinophil-derived hematological indices, particularly the NER, for predicting all-cause mortality among patients hospitalized for heart failure. Non-survivors had significantly lower eosinophil counts, eosinophil percentages, and EMR values than survivors. Classical inflammatory markers such as CRP, NLR, and SII were more strongly associated with mortality. The NER did not differ significantly between survivors and non-survivors, and was a poor predictor in the ROC analysis. In the multivariate regression analysis, only age remained an independent predictor of all-cause mortality, whereas eosinophil-based indices failed to maintain statistical significance. By systematically assessing all commonly used eosinophil-derived hematological indices, this study provides a comprehensive overview of their prognostic relevance in ADHF.

Table 2. Multivariable Logistic Regression for All-Cause Mortality

Variable	OR	95% CI	*P* value
Age (per 1 year increase)	1.05	1.01-1.09	**0.007**
LVEF (%)	1.00	0.95-1.05	0.98
Creatinine	1.18	0.87-1.60	0.28
Hypertension	1.42	0.74-2.73	0.29
COPD	1.51	0.75-3.06	0.24
Atrial fibrillation	1.93	0.94-3.98	0.071
CRP	1.10	0.90-1.35	0.31
NLR	1.02	0.91-1.14	0.68
NER	1.00	0.98-1.02	0.89
Eosinophil %	1.04	0.80-1.36	0.77

LVEF, left ventricular ejection fraction; COPD, chronic obstructive pulmonary disease; CRP, C-reactive protein; NLR, neutrophil-to-lymphocyte ratio; NER, neutrophil-to-eosinophil ratio; OR, odds ratio; CI, confidence interval.

Table 3. ROC Curve Analysis for Predicting All-Cause Mortality

Variables	AUC	95% CI	Optimal cut-off values
Age	0.686	0.619-0.761	≥ 69 years
CRP	0.683	0.623-0.771	≥ 10.7 mg/L
NLR	0.621	0.550-0.696	≥ 4.06
SII	0.595	0.514-0.661	≥ 749.9
EF	0.599	0.525-0.669	≥ 25%
NER	0.545	0.469-0.633	≥ 23.48
Eosinophil count	0.409	0.334-0.476	≤ 0.13
Eosinophil %	0.407	0.332-0.478	≤ 2.40
EMR	0.417	0.344-0.490	≤ 0.176

CI, confidence interval; AUC, area under curve; CRP, c-reactive protein; NLR, neutrophil-to-lymphocyte ratio; SII, systemic immune-inflammation index; LVEF, left ventricular ejection fraction; NER, neutrophil-to-eosinophil ratio, EMR, eosinophil-to-monocyte ratio; ROC, receiver operating characteristic.

In our study, the LVEF was slightly higher in non-survivors than in survivors. This unexpected finding may be related to older age and a higher comorbidity burden in these patients, particularly atrial fibrillation, hypertension, and chronic obstructive pulmonary disease. Therefore, mortality may have been influenced more by age, rhythm disorders, and systemic comorbidities than by systolic dysfunction alone.

These findings partially overlap with previous studies demonstrating an association between eosinophil-related indices and adverse outcomes in heart failure.[12,19] Some reports have suggested that high NER or low eosinophil counts may be linked to an increased risk of death or major adverse cardiovascular events, possibly reflecting heightened systemic stress responses and dysregulated inflammation.[20,21] However, the prognostic power of eosinophil-derived indices has varied significantly between studies, and many did not adjust for important clinical confounders, particularly age.[20,22] Our results show that although eosinophil parameters differed between survivors and non-survivors in univariate analysis, their predictive value diminished after adjustment, suggesting that eosinophil dynamics may reflect overall disease severity rather than provide incremental prognostic information.

The biological rationale for eosinopenia in critically ill or decompensated patients is well recognized.[23,24] Acute physiological stress, adrenergic activation, and elevated endogenous corticosteroids suppress eosinophil function and accelerate apoptosis, leading to low circulating eosinophil levels.[25,26] Similarly, allergic diseases, type-2 immune activation, and exogenous corticosteroid use may significantly alter eosinophil kinetics. These mechanisms highlight the complexity of interpreting eosinophil-related indices in heterogeneous clinical populations such as patients with heart failure.[10,27] In our study, eosinophil counts and EMR were significantly lower in non-survivors; however, these markers did not provide prognostic information beyond age and broader inflammatory markers. This reinforces the concept that eosinophil suppression may be a non-specific indicator of physiological stress, rather than a heart failure-specific predictor.[28]

In contrast, CRP, NLR, and SII were moderately associated with mortality consistent with substantial evidence linking systemic inflammation and adverse outcomes in heart failure. However, these indices did not remain independent predictors after accounting for age and LVEF. This underscores the dominant prognostic role of age, which has consistently emerged as a strong predictor of mortality in heart failure cohorts. The lack of independent prognostic value for NER and related indices in our

study suggests that their utility may be limited in populations with wide age variability or in settings where stronger clinical predictors overshadow the inflammatory indices.

Study Limitations

This study had several strengths, including detailed hematological profiling and comprehensive adjustment for multiple inflammatory variables. However, this study has some limitations. This retrospective single-center design may limit the generalizability of our results. Eosinophil counts may be affected by unmeasured confounding factors, including subclinical infections, undocumented allergic conditions, or undocumented corticosteroid exposure. Although our dataset included a substantial number of patients, certain eosinophil-derived indices (particularly NER) could not be calculated for patients with zero eosinophil counts, reducing statistical power. Another limitation was that exact time-to-event data were not uniformly available; therefore, Cox proportional hazards regression could not be performed, and mortality was analyzed as a binary outcome at one-year. Because of the retrospective design, BNP/NT-proBNP levels and admission blood pressure values were not uniformly available; therefore, they could not be included in the multivariable model. We did not perform subgroup analyses by heart failure phenotype (e.g., HFrEF vs. HFpEF), which may have provided additional insights. Finally, we did not include long-term cardiovascular outcomes beyond all-cause mortality, which may have provided additional insights.

CONCLUSION

This study evaluated the relationship between eosinophil-based hematological indices and all-cause mortality in patients with acute heart failure and demonstrated that these indices had limited value in predicting all-cause mortality. Although low eosinophil levels were observed in patients who died, ROC analysis and multivariate statistical models revealed that eosinophil-derived indices were not independent prognostic markers. In contrast, age was identified as the strongest and only independent determinant of mortality. These findings indicate that eosinophil-based indices may assist in risk stratification for acute heart failure, but they are not appropriate for stand-alone use in clinical decision-making.

Ethics

Ethics Committee Approval: Ankara Bilkent City Hospital Medical Research Scientific and Ethical Evaluation Board (decision number: TABED 2-26-1823, date: 07.01.2026).

Informed Consent: Retrospective study. Permission was obtained from hospital management to collect study data from the Information Management System.

Footnotes

Author Contributions

Concept Design – B.K. F.K.; Data Collection or Processing – B.K. F.K.; Analysis or Interpretation – B.K. F.K.; Literature Review – B.K. F.K.; Writing, Reviewing and Editing – B.K. F.K.

Declaration of Interests: The authors have no conflict of interest to declare.

Funding: No funding.

REFERENCES

1. Sheehan M, Sokoloff L, Reza N. Acute heart failure: from the emergency department to the intensive care unit. *Cardiol Clin*. 2024;42(2):165-186. [CrossRef]
2. López-Díez MP, Alquézar-Arbé A, Jacob J, et al, en representación del grupo ICA-SEMES. Hospital development of heart failure follow-up units and short-term prognosis after acute decompensation in Spain. *Int J Cardiol*. 2023;378:64-70. [CrossRef]
3. Amara M, Stoler O, Birati EY.The role of inflammation in the pathophysiology of heart failure. *Cells*. 2025;14(14):1117. [CrossRef]
4. Pah AM, Serban S, Mateescu DM, et al. A systemic inflammatory biomarkers (ınterleukin-6, high-sensitivity c-reactive protein, and neutrophil-to-lymphocyte ratio) and prognosis in heart failure: a meta-analysis of prospective cohort studies. *J Clin Med*. 2025;14(23):8610. [CrossRef]
5. Monteiro Júnior JGM, de Oliveira Cipriano Torres D, Filho DCS. Hematological parameters as prognostic biomarkers in patients with cardiovascular diseases. *Curr Cardiol Rev*. 2019;15(4):274-282. [CrossRef]
6. Ramos TMB, Monteiro Júnior JGM, Furtado VC, Sobral Filho DC. The relationship between hematological parameters and coronary angiographic lesions. *Front Cardiovasc Med*. 2025;12:1589121. [CrossRef]
7. Lombardi C, Berti A, Cottini M. The emerging roles of eosinophils: implications for the targeted treatment of eosinophilic-associated inflammatory conditions. *Curr Res Immunol*. 2022;3:42-53. [CrossRef]
8. Broide D. Targeting eosinophils in asthmatic inflammation: benefits and drawbacks. *J Inflamm Res*. 2025;18:12421-12445. [CrossRef]
9. Landolina NA, Levi-Schaffer F. Eosinophils as a pharmacological target for the treatment of allergic diseases. *Curr Opin Pharmacol*. 2014;17:71-80. [CrossRef]
10. Ogulur I, Mitamura Y, Yazici D, et al. Type 2 immunity in allergic diseases. *Cell Mol Immunol*. 2025;22(3):211-242. [CrossRef]
11. Gao YD, Wang ZJ, Ogulur I, et al. The evolution, immunopathogenesis and biomarkers of type 2 inflammation in common allergic disorders. *Allergy*. 2025;80(7):1848-1877. [CrossRef]
12. Vural A, Aydın E. The predictive value of eosinophil indices for major cardiovascular events in patients with acute decompensated HFrEF. *Medicina (Kaunas)*. 2022;58(10):1455. [CrossRef]
13. Schmitt A, Schupp T, Reinhardt M, et al. Prognostic impact of acute decompensated heart failure in patients with heart failure with mildly reduced ejection fraction. *Eur Heart J Acute Cardiovasc Care*. 2024;13(2):225-241. [CrossRef]
14. Liu D, Hu K, Schregelmann L, et al. Determinants of ejection fraction improvement in heart failure patients with reduced ejection fraction. *ESC Heart Fail*. 2023;10(2):1358-1371. [CrossRef]
15. Farah W, Wang Z, Gajic O, Odeyemi YE. Eosinopenia as a predictor of clinical outcomes in hospitalized patients with community-acquired pneumonia: a retrospective cohort study. *PLoS One*.2025;20(3):e0314336. [CrossRef]
16. Mao Y, Qian Y, Sun X, Li N, Huang H. Eosinopenia predicting long-term mortality in hospitalized acute exacerbation of COPD patients with community-acquired pneumonia-a retrospective analysis. *Int J Chron Obstruct Pulmon Dis*. 2021;16:3551-3559. [CrossRef]

17. McDonagh TA, Metra M, Adamo M, et al; ESC Scientific Document Group. 2021 ESC guidelines for the diagnosis and treatment of acute and chronic heart failure. *Eur Heart J*. 2021;42(36):3599-3726. [CrossRef] Erratum in: *Eur Heart J*. 2021;42(48):4901. [CrossRef]
18. Kalkan K, Tunca C, Ozan Tanik V. Association of controlling nutritional status score and long-term mortality in acute pulmonary embolism. *Biomed Pap Med Fac Univ Palacky Olomouc Czech Repub*. 2025;169(3):188-195. [CrossRef]
19. Zhang R, Chang R, Qi X, et al. Eosinophil counts predict 3-year risk of major adverse cardiovascular and cerebrovascular events in carotid artery stenosis patients. *Sci Rep*. 2025;15(1):20939. [CrossRef]
20. Lin K, Luo M, Gu X, et al. Changes in blood eosinophil counts predict the death of patients with myocardial infarction after hospital discharge. *J Am Heart Assoc*. 2025;14(1):e035383. [CrossRef]
21. Alkhalil M, Kearney A, Hegarty M, Eosinopenia as an adverse marker of clinical outcomes in patients presenting with acute myocardial Infarction. Am J Med. 2019;132(12):e827-e834. [CrossRef]
22. Guan C, Wang K, Gong A, et al. Association between blood eosinophil levels and prognosis in critically ill patients with different heart failure phenotypes. *Sci Rep*. 2025;15(1):6008. [CrossRef]
23. Abidi K, Belayachi J, Derras Y, et al. Eosinopenia, an early marker of increased mortality in critically ill medical patients. *Intensive Care Med*. 2011;37(7):1136-1142. [CrossRef]
24. Ata A, Anıl M, Helvacı M. The role of eosinopenia in the diagnosis of bacterial infection in children. *Pamukkale Medical Journal*. 2022;15:467-473. [CrossRef]
25. Mei Z, Khalil MA, Guo Y, et al. Stress-induced eosinophil activation contributes to postoperative morbidity and mortality after lung resection. *Sci Transl Med*. 2024;16(761):eadl4222. [CrossRef]
26. Kanamori A, Tanaka F, Ominami M, et al. Psychological stress exacerbates inflammation of the ileum via the corticotropin-releasing hormone-mast cell axis in a mouse model of eosinophilic enteritis. *Int J Mol Sci*. 2022;23(15):8538. [CrossRef]
27. Marra AM, Rossi CM, Piga MA, Moroncini G, Bilò MB. Eosinophil-associated diseases: the allergist's and clinical immunologist's perspective. *Eur Ann Allergy Clin Immunol*. 2024;56(5):195-209. [CrossRef]
28. Bozkuş F, Samur A, Yazıcı O. Can blood eosinophil count be used as a predictive marker for the severity of COPD and concomitant cardiovascular disease? The relationship with the 2023 version of the global initiative for chronic obstructive lung disease staging. *Eur Rev Med Pharmacol Sci*. 2024;28(7):2777-2787. [CrossRef]

ABCResearch

Arch Basic Clin Res 2026;8(2):112-119
DOI: 10.4274/ABCR.2026.26429

Research Article

Comprehensive *MEFV* Variant Spectrum in Pediatric Patients with Suspected Familial Mediterranean Fever: A Whole-Gene Sequencing Study

Bahtınur Yeter[1], Abdussamed Yasin Demir[2], Murat Günay[3]

[1]Department of Pediatrics, Erzincan Binali Yıldırım University Faculty of Medicine, Erzincan, Türkiye
[2]Department of Medical Genetics, Erzincan Binali Yıldırım University Faculty of Medicine, Erzincan, Türkiye
[3]Department of Biochemistry, Erzincan Binali Yıldırım University Faculty of Medicine, Erzincan, Türkiye

Cite this article as: Yeter B, Demir AY, Günay M. Comprehensive MEFV variant spectrum in pediatric patients with suspected familial mediterranean fever: a whole-gene sequencing study. *Arch Basic Clin Res*. 2026;8(2):112-119

ORCID IDs of the authors: B.Y. 0000-0003-0336-8161, A.Y.D. 0000-0002-0420-5017, M.G. 0000-0002-2079-6654.

ABSTRACT

Objective: To determine the *Mediterranean Fever (MEFV)* variant spectrum using whole-gene next-generation sequencing (NGS) in pediatric cases with suspected Familial Mediterranean Fever (FMF).

Methods: This retrospective cross-sectional study included 471 pediatric cases referred for *MEFV* analysis. All exons were analyzed using NGS, and variants were classified according to American College of Medical Genetics and Genomics criteria.

Results: At least one *MEFV* variant was detected in 59.4% of cases. A total of 23 variants were identified, predominantly in exon 10 (43.5%) and exon 2 (34.8%). The most frequent variants were R202Q (43.3%), E148Q (16.3%), and M694V (13.7%). A low-frequency variants of uncertain significance, G150R, was detected in one case. Heterozygous genotypes were the most common (59.6%).

Conclusion: Whole-gene sequencing enables the detection of both common and rare *MEFV* variants that may be missed by limited mutation panels. However, frequently detected variants, such as R202Q, require careful interpretation because of their high population frequency and controversial pathogenicity.

Keywords: Familial Mediterranean Fever, *MEFV*, pediatric, next-generation sequencing, variant spectrum, whole-gene sequencing

INTRODUCTION

Familial Mediterranean Fever (FMF) (OMIM #249100) is one of the most common monogenic autoinflammatory diseases and is characterized by recurrent fever attacks and inflammatory findings such as peritonitis, pleuritis, arthritis, and erysipelas-like erythema.[1,2,3] The disease is particularly common in populations living in the Mediterranean basin; Türkiye is among the countries with a high prevalence of FMF.[4,5] In cases that begin in childhood, early diagnosis is important for initiating appropriate treatment and preventing long-term complications.[6,7]

FMF is mainly associated with variants in the *Mediterranean Fever (MEFV)* gene, which is located on the short arm of chromosome 16 and encodes the pyrin protein.[2,4] Although numerous variants have been identified in the *MEFV gene*, commonly observed variants such as M694V, V726A, M680I, M694I, and E148Q are detected in a significant proportion of cases.[1,5] However, when examinations are performed with standard panels, no diagnostic result can be reached in some cases, suggesting that rare or out-of-panel variants, in particular, may be overlooked.[1,3] In an FMF-specific study, broader next-generation sequencing (NGS)-based analysis of patients with negative or single-heterozygous results after traditional 16-variant screening identified clinically relevant variants in 34% of cases and detected previously missed *MEFV* variants in 54 patients.[8] This indicates that traditional

Corresponding author: Bahtınur Yeter, **E-mail:** byeter@erzincan.edu.tr

Received: April 8, 2026
Revision Requested: April 29, 2026 **Accepted:** June 11,2026 **Publication Date:** July, 14, 2026

genetic screening approaches focusing only on certain exons may remain limited in the diagnostic evaluation of cases with atypical clinical features or rare variants.

In the pediatric population, the diagnosis of FMF is of particular importance because symptoms often begin in the first decade of life and serious complications, such as amyloidosis, can be prevented.[6,7] In the literature, a substantial proportion of studies focusing on the pediatric age group, both in Türkiye and in other populations, have been conducted using limited variant panels, whereas NGS-based studies covering all exons of the *MEFV* gene remain limited.[1,2] Whole-gene analysis may expand the scope of genetic evaluation by enabling the detection of rare or previously undescribed variants that may be missed in standard tests.[2,3]

Given the limited number of studies that analyze all exons of the *MEFV* gene in pediatric cases evaluated with a preliminary diagnosis of FMF in Türkiye, this study is expected to fill an important gap. This study aimed to determine, using NGS, the distribution of variants across all exons of the *MEFV* gene in pediatric cases referred for genetic evaluation with a preliminary diagnosis of FMF in our region. Thus, it aimed to comprehensively reveal the regional variant spectrum, to more accurately evaluate the frequency of variants that may be overlooked in limited panels, and to provide a data infrastructure that will form the basis for future genotype-phenotype correlation studies.

MATERIALS AND METHODS

Design and Case Group

This was a retrospective, cross-sectional, descriptive study. The study included 471 pediatric cases who were evaluated with a preliminary diagnosis of FMF according to the Tel-Hashomer criteria and who were requested to undergo *MEFV* gene analysis at Erzincan Binali Yıldırım University-Mengücek Gazi Training and Research Hospital between 01.01.2024 and 31.12.2024. The cases had been referred from pediatric outpatient clinics for genetic evaluation because of clinical findings compatible with FMF, such as recurrent fever, abdominal pain, chest pain, arthralgia, and/or erysipelas-like erythema. Cases younger than 18 years and those who underwent NGS of all exons of the *MEFV* gene were included in the study. Cases with completed genetic data were included in the study. This study was conducted in accordance with the World Medical Association's Declaration of Helsinki, and ethics committee approval was obtained from the Erzincan Binali Yıldırım University Non-Interventional Clinical Research Ethics Committee (decision number: 2026-04/12, date: 19.02.2026).

MAIN POINTS

- Whole-gene next-generation sequencing identified *MEFV* variants in 59.4% of pediatric cases referred for suspected Familial Mediterranean Fever.
- A total of 23 distinct *MEFV* variants were detected, most located in exons 2 and 10.
- R202Q was the most frequently detected variant; however, its clinical significance remains controversial and requires cautious interpretation.
- Whole-gene analysis contributed to the detection of low-frequency and potentially panel-excluded variants, including G150R, I259V, and C355S.
- The findings support the use of whole-gene sequencing for broader variant detection and more comprehensive characterization of the regional *MEFV* variant spectrum.

Data Collection

Demographic data and genetic analysis results of the cases were retrospectively obtained from the hospital information system and laboratory records. In this study, age, sex, detected *MEFV* variants, zygosity status, and the distribution of variants across exons were evaluated.

Whole-gene Sequencing of the *MEFV* Gene

For *MEFV* gene analysis, 2 mL of peripheral venous blood was obtained from each case and placed into tubes containing ethylenediaminetetraacetic acid. Genomic DNA was isolated using an automated DNA isolation system. The concentration and purity of the obtained DNA samples were evaluated using a spectrophotometric method, and samples of suitable quality for analysis were included in the study.

NGS was used for genetic analysis. For this purpose, library preparation and target region enrichment were performed to capture all coding regions of the *MEFV* gene and exon-intron junctions. Sequencing was performed on the Illumina MiSeq platform. The obtained sequencing data were analyzed using the Genomize bioinformatics platform and compared with the reference genome. NM_000243.3 was used as the reference transcript for *MEFV* gene analysis. Quality control and variant calling were performed according to the workflow of the Genomize platform. Variant calls were reviewed considering read depth, variant allele fraction, and overall call quality. Only variants located within the targeted coding regions and exon-intron junctions and that were considered reportable by the software were included in the final analysis. Low-quality calls, insufficiently covered regions, and variants outside the targeted regions were excluded from interpretation.

Variant Classification

Detected *MEFV* variants were evaluated according to the criteria of the American College of Medical Genetics and Genomics (ACMG).[9] The variants were classified as pathogenic, likely pathogenic, of uncertain significance (VUS), or benign. In cases where different clinical interpretations were present among databases or literature sources, the variants were additionally indicated as ''variants with conflicting classifications'' In addition, ClinVar, INFEVERS, and the Human Gene Mutation Database were used to evaluate the variants.

Statistical Analysis

Statistical analyses were performed using SPSS (Statistical Package for the Social Sciences) version 22.0. Continuous variables were expressed as mean ± standard deviation and median (minimum-maximum), whereas categorical variables

were expressed as number and percentage. Descriptive statistical methods were used to evaluate demographic data, the distribution of detected *MEFV* variants, zygosity status, and allele frequencies.

RESULTS

Demographic Characteristics and Overall Variant Distribution

A total of 471 pediatric patients who had a preliminary diagnosis of FMF and underwent *MEFV* gene analysis were included in the study. Of these, 259 (55.0%) were female and 212 (45.0%) were male, with a female-to-male ratio of 1.2:1. The mean age was 7.3 ± 4.1 years. At least one *MEFV* variant was detected in 280 cases (59.4%), whereas no variant was identified in 191 cases (40.6%) (Table 1).

Whole-gene *MEFV* Analysis Findings

Analysis of all exons of the *MEFV* gene detected 23 variants. Of these variants, 8 (34.8%) were localized in exon 2, 4 (17.4%) in exon 3, 1 (4.3%) in exon 9, and 10 (43.5%) in exon 10. Based on ACMG criteria, 6 variants were classified as pathogenic, 1 as likely pathogenic, 9 as variants of uncertain significance (VUS), 5 as benign, and 2 as having conflicting classifications (Table 2). Among the low-frequency variants, G150R was detected in one case in the heterozygous state and

Table 1. Demographic Characteristics of The Study Cohort and *MEFV* Variant Status

Total cases, n	**471**
Gender, n (%)	
Female	259 (55)
Male	212 (45)
Age (years), mean ± SD	7.3 ± 4.1
Variant status, n (%)	
Positive	280 (59.4)
Negative	191 (40.6)

Table 2. *MEFV* Variants Detected in the Study Cohort (n=23)

Exon	Coding change (HGVS, c.)	Protein change (HGVS, p.)	Protein change (short)	ACMG classification
2	c.329T > C	p.Leu110Pro	L110P	B
2	c.442G > C	p.Glu148Gln	E148Q	B
2	c.443A > T	p.Glu148Val	E148V	VUS
2	c.448G > A	p.Gly150Arg	G150R	VUS
2	c.605G > A	p.Arg202Gln	R202Q	B
2	c.688G > A	p.Glu230Lys	E230K	VUS
2	c.775A > G	p.Ile259Val	I259V	Conflicting (VUS/B)
2	c.866C > T	p.Ala289Val	A289V	VUS
3	c.1016C > T	p.Ser339Phe	S339F	VUS
3	c.1063T > A	p.Cys355Ser	C355S	B
3	c.1105C > T	p.Pro369Ser	P369S	VUS
3	c.1223G > A	p.Arg408Gln	R408Q	VUS
9	c.1772T > C	p.Ile591Thr	I591T	B
10	c.1958G > A	p.Arg653His	R653H	Conflicting (VUS/P)
10	c.2040G > C	p.Met680Ile	M680I	P
10	c.2060G > A	p.Gly687Asp	G687D	LP
10	c.2082G > A	p.Met694Ile	M694I	P
10	c.2080A > G	p.Met694Val	M694V	P
10	c.2084A > G	p.Lys695Arg	K695R	P
10	c.2110G > A	p.Val704Ile	V704I	VUS
10	c.2177T > C	p.Val726Ala	V726A	P
10	c.2230G > T	p.Ala744Ser	A744S	VUS
10	c.2282G > A	p.Arg761His	R761H	P

*P, pathogenic; LP, likely pathogenic; VUS, variant of uncertain significance; ACMG, American College of Medical Genetics and Genomics; B, benign; Conflicting, variants with discordant clinical classifications across databases/sources.

was classified as VUS.

When the genotype distribution was evaluated among 280 cases in which *MEFV* variants were detected, the most common genotype was heterozygous, observed in 167 cases (59.6%). This was followed by compound heterozygous genotypes in 64 cases (22.9%), complex genotypes in 33 cases (11.8%), and homozygous genotypes in 16 cases (5.7%) (Table 3a and 3b).

In the heterozygous group, the most frequently observed genotype was R202Q/- (n=75, 26.8%), followed by E148Q/- (n=42, 15.0%) and M680I/- (n=13, 4.6%). A total of 15 heterozygous genotypes were identified. In the homozygous group, the most frequently observed genotype was R202Q/R202Q (n=12, 4.3%); this was followed by V726A/V726A (n=3, 1.1%) and E148Q/E148Q (n=1, 0.4%) (Table 3a).

Among genotypes classified as compound heterozygous, the most frequent combination was R202Q/M694V (n=30, 10.7%). This was followed by R202Q/E148Q (n=6, 2.1%) and R202Q/V726A (n=4, 1.4%). A total of 19 different genotypes were identified in this group. In the complex genotype group, the most frequent combinations were those containing R202Q/M694V (n=11, 3.9%); these were followed by R202Q/E148Q/M694V (n=5, 1.8%) and R202Q/P369S/R408Q (n=4, 1.4%). A total of 12 complex genotypes were identified, including one case carrying four variants (Table 3b).

Table 3a. Distribution of Heterozygous and Homozygous Genotypes Among Variant-Positive Cases

Genotype Type	Genotype	n (%)
Heterozygous	R202Q/-	75 (26.8)
	E148Q/-	42 (15.0)
	M680I/-	13 (4.6)
	V726A/-	12 (4.3)
	R761H/-	6 (2.1)
	M694V/-	5 (1.8)
	E148V/-	4 (1.4)
	A744S/-	2 (0.7)
	K695R/-	2 (0.7)
	G150R/-	1 (0.4)
	G687D/-	1 (0.4)
	I259V/-	1 (0.4)
	I591T/-	1 (0.4)
	M694I/-	1 (0.4)
	S339F/-	1 (0.4)
Subtotal		**167 (59.6)**
Homozygous	R202Q/R202Q	12 (4.3)
	V726A/V726A	3 (1.1)
	E148Q/E148Q	1 (0.4)
Subtotal		**16 (5.7)**
Total		**183 (65.3)**

A total of 430 variant alleles were identified in 280 cases with detected variants. Among 23 variants, the five most frequently detected accounted for 85.1% of all variant alleles. R202Q was the most frequently detected variant (n=186, 43.3%), followed by E148Q (n=70, 16.3%), M694V (n=59, 13.7%), V726A (n=28, 6.5%), and M680I (n=23, 5.3%) (Table 4).

Table 3b. Distribution of Compound Heterozygous and Complex Genotypes Among Variant-Positive Cases

Genotype Type	Genotype	n (%)
Compound Heterozygous	R202Q/M694V	30 (10.7)
	R202Q/E148Q	6 (2.1)
	R202Q/V726A	4 (1.4)
	E148Q/M680I	3 (1.1)
	P369S/R408Q	3 (1.1)
	A744S/M680I	2 (0.7)
	R202Q/M680I	2 (0.7)
	E148Q/V726A	2 (0.7)
	E148V/V726A	2 (0.7)
	A289V/R202Q	1 (0.4)
	A744S/R202Q	1 (0.4)
	R202Q/R761H	1 (0.4)
	R202Q/C355S	1 (0.4)
	R202Q/E230K	1 (0.4)
	E148Q/E148V	1 (0.4)
	E148Q/L110P	1 (0.4)
	E148Q/M694V	1 (0.4)
	M680I/R761H	1 (0.4)
	S339F/V726A	1 (0.4)
Subtotal		**64 (22.9)**
Complex Genotype	R202Q/M694V*	11 (3.9)
	R202Q/E148Q/M694V	5 (1.8)
	R202Q/P369S/R408Q	4 (1.4)
	E148Q/P369S/R408Q	4 (1.4)
	R202Q/M680I/M694V	2 (0.7)
	R202Q/E148Q/P369S/R408Q	1 (0.4)
	R202Q/E148Q/R653H	1 (0.4)
	R202Q/E148Q/L110P	1 (0.4)
	R202Q/M694V/K695R	1 (0.4)
	R202Q/M694V/V726A	1 (0.4)
	R202Q/V704I*	1 (0.4)
	E230K/P369S/R408Q	1 (0.4)
Subtotal		**33 (11.8)**
Total		**97 (34.7)**

*Genotypes containing a variant also observed in the homozygous state in this cohort.

Table 4. Allele Distribution of Detected *MEFV* variants (n=430 variant alleles)

Variant	n	%	Variant	n	%
R202Q	186	43.3	S339F	2	0.5
E148Q	70	16.3	E230K	2	0.5
M694V	59	13.7	A289V	1	0.2
V726A	28	6.5	G150R	1	0.2
M680I	23	5.3	C355S	1	0.2
P369S	13	3.0	G687D	1	0.2
R408Q	13	3.0	I259V	1	0.2
R761H	8	1.9	I591T	1	0.2
E148V	7	1.6	M694I	1	0.2
A744S	5	1.2	R653H	1	0.2
K695R	3	0.7	V704I	1	0.2
L110P	2	0.5			
			Total	**430**	**100**

DISCUSSION

In this study, analysis of all exons of the *MEFV* gene by NGS in 471 pediatric cases referred for genetic evaluation with a preliminary diagnosis of FMF revealed a comprehensive profile of regional variant distribution. Detection of at least one *MEFV* variant in 59.4% of cases shows that genetic evaluation plays an important role in the pediatric referral population. This rate is generally consistent with data reported in large Turkish NGS-based series. Kırnaz et al.[2] reported a variant positivity rate of 56.9% in their series of 3230 cases, whereas Düzkale Teker and Öz[10] similarly showed that variants were detected at a rate of approximately 59%. In contrast, this rate may vary across studies with different panel coverage or referral populations. This suggests that variant positivity rates are influenced not only by population characteristics but also by the scope of the genetic method used.

In our study, the most frequently detected variants, R202Q, E148Q, M694V, V726A, and M680I, are largely consistent with the general distribution reported in the Turkish population. However, the relative ranking and frequencies of these variants may differ among studies. In particular, R202Q ranking first with an allele frequency of 43.3% is consistent with the high rates reported by Kırnaz et al.[2] and Aksoy et al.[5] In the previous study conducted in the same region using a limited panel, R202Q was not evaluated, and M694V was reported as the most frequently detected variant, clearly demonstrating the effect of test coverage on variant distribution.[11] From this perspective, whole-gene analysis appears to reveal the regional variant spectrum more broadly.

Although the R202Q variant was detected at high frequency in our cohort, its clinical significance remains controversial. Although this variant is classified as benign or of low clinical effect in some databases, studies such as Kandur et al.[11] and Dundar et al.[12] have reported it either alone or together with other *MEFV* variants in symptomatic cases. Nevertheless, in several international recommendations and variant interpretation frameworks, R202Q is regarded primarily as a polymorphism or a low-penetrance (modifier) allele rather as a primary disease-causing variant when present alone. Therefore, R202Q should not be interpreted as a standalone diagnostic marker in the absence of typical Tel-Hashomer clinical features; its clinical relevance should be assessed in conjunction with *MEFV* variants and possible complex haplotypes.

E148Q was identified as the second most frequent variant in our study, with an allele frequency of 16.3%. This rate is consistent with the rates of 17.49% reported by Kırnaz et al.[2] and 11.5% reported by Aksoy et al.[5] and is lower than the rate of 32.5% reported by Binici et al.[13] in Southeastern Anatolia. The clinical significance of E148Q has long been controversial in the literature; in some studies it has been associated with incomplete attack forms and a relatively mild clinical phenotype, whereas in others it has been regarded as a change close to the benign boundary.[15,16] Therefore, although the frequent detection of E148Q in our study is noteworthy, direct interpretation of its clinical effect is not appropriate. Taken together, our findings suggest that although NGS may increase the detection of R202Q and E148Q, these variants should be interpreted as low-penetrance or modifier alleles rather than primary diagnostic markers in the absence of typical Tel-Hashomer clinical features.

In our study, M694V was the third most frequent variant detected, with an allele frequency of 13.7%. This rate is markedly lower than that reported in many studies of the Turkish population. Coşkunpınar et al.[16] reported an M694V frequency of 48.3%, Demir and Admış[10] 48.3%, Düzkale Teker and Öz[10] 46.6%, Çilingir et al.[17] 40.13%, Bayrak et al.[18] 34.9%, and Barış et al.[4] 30.2%. The main reason for this marked difference in frequency is that all exons, including R202Q, were screened in our study, resulting in a decreased relative proportion of M694V as the total number of alleles increased. Indeed, in the studies by Aksoy et al.[5] and Kırnaz et al.[2], which included R202Q in their panels, the frequency of M694V was reported as 25.1% and 16.84%, respectively, which is consistent with our findings. Although genotype-phenotype correlation could not be performed in our study, M694V is the variant in the *MEFV*

gene most strongly associated in the literature with the most severe phenotype and, particularly in the homozygous form, it is characterized by severe attacks of peritonitis, pleuritis, and arthritis and is accepted as the most important genetic risk factor for the development of secondary amyloidosis.[20,21] Beshlawy et al.[7] reported in their Egyptian pediatric cohort that the homozygous M694V genotype was associated with a severe phenotype at a rate of 65.2%. Because clinical findings, attack severity, and treatment response were not evaluated in our study, this relationship could not be demonstrated directly in cases carrying the M694V mutation.

V726A (6.5%) and M680I (5.3%) were the fourth and fifth most frequent variants, respectively, in our study. These rates are consistent with those for V726A (5.30%) and M680I (5.12%) reported by Kırnaz et al.[2] However, Düzkale Teker and Öz[10] reported V726A and M680I frequencies of 14.5% and 14.0%, respectively, whereas Taşdemir[21] reported an M680I rate of 9.85% in the Konya region. These differences indicate that the distribution of *MEFV* gene variants is heterogeneous across the geographical regions of Türkiye. Bayrak et al.[18] also emphasized that the frequency of *MEFV* mutation types may vary from region to region and from population to population. According to literature data, the V726A mutation is generally associated with a moderate disease phenotype, and Beshlawy et al.[7] reported a moderate clinical picture in 50% of heterozygous V726A carriers. The M680I variant is associated, particularly in the homozygous form, with a severe clinical course and risk of amyloidosis.[23,24] Detection of these two variants at relatively low rates in our study reflects regional genetic heterogeneity, but does not reduce the importance of clinical follow-up of carriers.

The predominance of heterozygosity observed in the genotypic distribution is consistent with other Turkish studies. Kırnaz et al.[2] reported heterozygous, compound heterozygous, complex genotype, and homozygous rates of 57.8%, 22.3%, 12.9%, and 7.0%, respectively. Demir and Admış[10] reported rates of 70.1% heterozygous, 16.8% compound heterozygous, and 13.1% homozygous in the same region. In our study, the higher rates of compound-heterozygous and complex genotypes may be due to whole-gene analysis more effectively revealing carriage of multiple variants. Nevertheless, particularly for heterozygous or complex genotypes, it is inappropriate to infer the clinical effects of variants solely from the genotype. Since penetrance, the presence of accompanying second variants, and the relationship with the clinical phenotype may vary in pediatric cases, the clinical counterparts of genotypes should be evaluated in conjunction with more detailed phenotypic data.

In our study, 12 complex genotypes were identified, and the complex genotype rate was 11.8%; one patient carried four variants (R202Q/E148Q/P369S/R408Q). This rate is similar to the complex genotype finding of 12.9% reported by Kırnaz et al.[2] Aksoy et al.[5], in their larger series, reported a complex genotype (compound homozygous/heterozygous) rate of 19.6%. The high rate of detection of complex genotypes can be explained by the ability of NGS-based whole-gene analysis to identify more than one variant simultaneously. This suggests that the true frequency of complex genotypes may have been underestimated in studies using limited mutation panels. In terms of clinical reflection, the literature reports that cases with complex genotypes carrying more than one pathogenic variant may face earlier age at symptom onset, more frequent and severe attacks, and a higher risk of amyloidosis.[20,25]

Examination of the distribution of the 23 detected variants across exons showed that most changes were concentrated in exon 10 (43.5%) and exon 2 (34.8%). This finding is consistent with studies reporting that *MEFV* variants cluster particularly in these two hotspot regions. Çilingir et al.[17] reported that the most frequent mutations in the Turkish population are concentrated in exon 2 and exon 10 and that these hotspot regions account for 90% of molecular diagnosis. In addition, the detection in our study of 4 variants in exon 3 and 1 variant in exon 9 suggests that testing approaches focusing only on classical hotspot regions may overlook some variants. Sağ et al.[1] also emphasized that including rare mutations in routine genetic panels may significantly affect diagnosis and treatment planning. According to the literature, variants clustered in exon 10 (M694V, M680I, M694I, V726A, K695R, R761H) affect the B30.2 (SPRY) domain of the pyrin protein; mutations in this region are generally associated with a more severe clinical phenotype, higher penetrance, and increased risk of amyloidosis.[15] In contrast, variants in exon 2 (E148Q, R202Q) have been reported to present with relatively mild or variable clinical manifestations.[12,16] In this respect, the study demonstrates that not only common variants, but also changes in less frequently screened regions should be evaluated within the diagnostic framework.

Another relevant finding of our study was the detection of low-frequency and potentially panel-excluded variants, including G150R, I259V, and C355S. G150R and I259V are located in exon 2, whereas C355S is located in exon 3. G150R was classified as a variant of uncertain significance (VUS), I259V was given a conflicting classification (VUS/benign), and C355S was classified as benign. The detection of such variants suggests that whole-gene analysis may reveal not only common *MEFV* variants but also low-frequency and potentially panel-excluded changes. However, further evaluation through detailed phenotype correlations, segregation analyses, and functional studies is required to clarify the clinical significance of variants with uncertain or conflicting interpretations, such as G150R and I259V.

The sex distribution (55% female, 45% male) and mean age (7.3 ± 4.1 years)in our study are generally consistent with other studies in the Turkish population. Elmas et al.[6] reported a female/male ratio of 1.5 and a mean age at presentation of 10.74 ± 4.06 years in pediatric FMF cases in Afyonkarahisar, whereas Beshlawy et al.[7] reported male predominance (54%) in an Egyptian pediatric cohort. Barış et al.[4] reported a female patient rate of 55.18% and a symptom onset age of 4.8 ± 2.3 years in their study. The slight female predominance in our study was a noteworthy finding.

Overall, our study stands out as one of the regional studies in Türkiye that reveal the distribution of *MEFV* variants at the whole-gene level in pediatric cases referred for genetic evaluation with a preliminary diagnosis of FMF. The findings

from our study show that in addition to common variants, low-frequency and out-of-panel changes are present in this referral population at a level that should not be ignored. This suggests that restricting genetic evaluation to the most common variants may not fully capture variant diversity in some cases. Because clinical findings, attack characteristics, treatment response, and complication data were not evaluated in this study, definitive conclusions about the effects of the detected variants on disease severity or clinical course cannot be drawn. Therefore, the genetic findings obtained should be considered not as direct clinical determinants but as molecular data that can form the basis for future genotype-phenotype association studies.

These findings highlight the importance of comprehensive genetic analysis in regions with a high prevalence of FMF, particularly in referral populations. Whole-gene sequencing may provide a broader understanding of variant diversity compared to limited mutation panels.

Study Limitations

Our study has some limitations. First, its retrospective and single-center design may limit the generalizability of the findings to the broader Turkish pediatric population. Second, genotype-phenotype correlation could not be performed because detailed clinical and treatment-response data were unavailable. Third, Sanger confirmation was not performed for all detected variants, particularly low-frequency variants. Fourth, variant phasing was not available; therefore, compound heterozygous and complex genotypes should be interpreted in light of the lack of cis/trans information. Fifth, the clinical significance of variants with uncertain or conflicting interpretations, such as G150R and I259V, could not be clarified because segregation and functional validation analyses were not available. Deep intronic variants and copy-number changes were outside the scope of this study.

CONCLUSION

This study presents a large pediatric series from our region in which all exons of the *MEFV* gene were analyzed using NGS. R202Q was identified as the most frequently detected variant; however, its clinical significance remains controversial and should be interpreted with caution. The identification of 23 different variants, including low-frequency and potentially panel-excluded variants, demonstrates that whole-gene sequencing contributes to broader variant detection and more comprehensive characterization of the regional variant spectrum. Further multicenter studies incorporating detailed clinical data and functional analyses are needed to clarify the clinical significance of the detected variants.

Ethics

Ethics Committee Approval: Approval was obtained from Erzincan Binali Yıldırım University Non-Interventional Clinical Research Ethics Committee (decision number 2026-04/12, date: 19.02.2026).

Informed Consent: This was a retrospective, cross-sectional, descriptive study. Permissions were obtained from the hospital management to collect study data from the hospital information system and laboratory records.

Footnotes

Author Contributions: Concept Design – B.Y., A.Y.D., M.G.; Data Collection or Processing – A.Y.D.; Analysis or Interpretation – A.Y.D.; Literature Review – B.Y., A.Y.D., M.G.; Writing, Reviewing and Editing – B.Y., A.Y.D.

Declaration of Interests: The authors declare no conflict of interest.

Funding: The authors declare no financial support or funding.

References

1. Sağ ŞÖ, Alemdar A, Aliyeva L, Kaya N, Temel ŞG. Frequency and distribution of *MEFV* gene mutation in familial Mediterranean fever cases: a single center experience. *Med J SDU*. 2020;26(1):40-46. [CrossRef]
2. Kırnaz B, Gezgin Y, Berdeli A. *MEFV* gene allele frequency and genotype distribution in 3230 cases' analyses by next generation sequencing methods. *Gene*. 2022;827:146447. [CrossRef]
3. Choi SR, Yoon CJ, Lee JS, Ju YS, Lee EY. Identification of pathogenic *MEFV* variants in Korean cases with familial Mediterranean fever via whole-genome sequencing: a case report. *J Rheum Dis*. 2025;32(4):292-297. [CrossRef]
4. Barış S, Yavaş C, Atan Uzun Ç, et al. Ailesel Akdeniz Ateşi hastalarının *MEFV* gen mutasyon tiplerinin sıklığı ve hastalarda gen mutasyonu ile klinik bulgular arasındaki ilişkilerin değerlendirilmesi. *Dicle Med J*. 2023;50(4):545-552. [CrossRef]
5. Aksoy R, Us E, Farhoomand Aksoy D, Dumlupınar E, Turgay TM. Molecular analyses of *MEFV* gene mutation variants in Turkish population. *Mol Biol Rep*. 2024;51:844. [CrossRef]
6. Elmas E, Bükülmez A, Elmas M, Demircin G. Evaluation of demographic, clinical, laboratory and genetic characteristics of children with familial Mediterranean fever in Afyonkarahisar region. *Kocatepe Tıp Derg*. 2021;22:333-341. [CrossRef]
7. Beshlawy AE, Zekri AER, Ramadan MS, et al. Genotype-phenotype associations in familial Mediterranean fever: a study of 500 Egyptian pediatric cases. *Clin Rheumatol*. 2022;41(5):1511-1521. [CrossRef]
8. Karaer D, Durak T, Aydin LR, et al. Next-generation sequencing reveals genetic heterogeneity in *MEFV*-negative or heterozygous familial Mediterranean fever: a retrospective study. Expert Rev Clin Immunol. 2026;1-11. [CrossRef]
9. Richards S, Aziz N, Bale S, et al. Standards and guidelines for the interpretation of sequence variants: a joint consensus recommendation of the American College of Medical Genetics and Genomics and the Association for Molecular Pathology. *Genet Med*. 2015;17(5):405-424. [CrossRef]
10. Düzkale Teker N, Öz Ö. Analysis of the *MEFV* gene by NGS in cases with familial Mediterranean fever: a single center experience. *Harran Univ Med Fac J*. 2020;17(3):454-459. [CrossRef]
11. Demir AY, Admış Ö. *MEFV* gene mutations in familial Mediterranean fever cases: Erzincan experience. *Erzincan Univ J Sci Technol*. 2024;17(2):377-384. [CrossRef]

12. Kandur Y, Kocakap DBS, Alpcan A, Tursun S. Clinical significance of *MEFV* gene variation R202Q. *Clin Rheumatol*. 2022;41(1):271-274. [CrossRef]
13. Dundar M, Fahrioglu U, Yildiz S, et al. Clinical and molecular evaluation of *MEFV* gene variants in the Turkish population: a study by the National Genetics Consortium. *Funct Integr Genomics*. 2022;22:291-315. [CrossRef]
14. Binici M, Tekeş S, Balkan M, Oral D, Yücel İ, Tunç Ş. Çocuk ailesel Akdeniz ateşi hastalarında *MEFV* mutasyonlarının dağılımı: Türkiye'nin güneydoğusunda tek merkezli çalışma. *Dicle Med J*. 2022;49(2):361-366. [CrossRef]
15. Shinar Y, Obici L, Gattorno M, et al. Guidelines for the genetic diagnosis of hereditary recurrent fevers. *Ann Rheum Dis*. 2012;71(10):1599-1605. [CrossRef]
16. Cekin N, Akyurek ME, Pinarbasi E, Ozen F. *MEFV* mutations and their relation to major clinical symptoms of familial Mediterranean fever. *Gene*. 2017;626:9-13. [CrossRef]
17. Coşkunpınar E, Özvarnalı A, Çefle K, et al. Ailevi Akdeniz Ateşinde moleküler tanı deneyimi: *MEFV* geninde sık görülen mutasyonlar. *Med Bull Haseki*. 2018;56:42-49. [CrossRef]
18. Çilingir O, Akalın T, Artaç A, et al. Ailesel Akdeniz Ateşi tanısı alan olgularda *MEFV* geni mutasyonlarının ve allel frekanslarının dağılımı: tek merkez deneyimi. *Osmangazi Tıp Derg*. 2018;40(2):35-45. [CrossRef]
19. Bayrak M, Çelik HT, Kadıoğlu Yılmaz B, et al. Ailesel Akdeniz Ateşinde *MEFV* mutasyon sıklığı. *KÜ Tıp Fak Derg*. 2019;21(2):254-260. [CrossRef]
20. Yalçınkaya F, Cakar N, Mısırlıoğlu M, et al. Genotype-phenotype correlation in a large group of Turkish cases with familial Mediterranean fever: evidence for mutation-independent amyloidosis. *Rheumatology (Oxford)*. 2000;39(1):67-72. [CrossRef]
21. Kasifoglu T, Bilge SY, Sari I, et al. Amyloidosis and its related factors in Turkish cases with familial Mediterranean fever: a multicentre study. *Rheumatology (Oxford)*. 2014;53(4):741-745. [CrossRef]
22. Taşdemir P. Konya bölgesinde *MEFV* gen mutasyonlarının sıklığı ve dağılımı. *Bozok Tıp Derg*. 2018;8(3):35-39. [CrossRef]
23. Ozalkaya E, Mir S, Sozeri B, et al. Familial Mediterranean fever gene mutation frequencies and genotype-phenotype correlations in the Aegean region of Turkey. *Rheumatol Int*. 2011;31(6):779-784. [CrossRef]
24. Coşkun S, Kurtgöz S, Keskin E, Sönmez F, Bozkurt G. Frequency of mutations in Mediterranean fever gene, with gender and genotype-phenotype correlations in a Turkish population. *J Genet*. 2015;94(4):629-635. [CrossRef]
25. Bodur H, Yıldırım Çetin G, Yılmaz Ö, et al. Familial Mediterranean fever: assessment of clinical manifestations, pregnancy, genetic mutational analyses, and disease severity in a national cohort. *Rheumatol Int*. 2020;40(1):29-40. [CrossRef]

ABCResearch

Arch Basic Clin Res 2026;8(2):120-128
DOI: 10.4274/ABCR.2026.26420

Research Article

Diagnostic Comparison of MRI/Ultrasound Fusion Biopsy and Systematic Biopsy in PI-RADS 4-5 Prostate Lesions

Akın Levent, Önder Durmaz

Department of Radiology, Erzincan Binali Yıldırım University Faculty of Medicine, Erzincan, Türkiye

Cite this article as: Levent A, Durmaz Ö. Diagnostic comparison of MRI/Ultrasound fusion biopsy and systematic biopsy in PI-RADS 4-5 prostate lesions. *Arch Basic Clin Res*. 2026;8(2):120-128

ORCID IDs of the authors: A.L. 0000-0003-0136-4570, Ö.D. 0000-0003-1157-2787.

ABSTRACT

Objective: Multiparametric magnetic resonance imaging (mpMRI) has transformed prostate cancer (PCa) diagnosis by enabling lesion-targeted biopsies. The optimal biopsy approach—systematic biopsy (SB), MRI-ultrasound fusion targeted biopsy (TB), or their combination (CB)—remains debated, especially in patients with high-risk Prostate Imaging-Reporting and Data System (PI-RADS) 4-5 lesions. This study compared these strategies for detecting overall and csPCa.

Methods: This retrospective study included 330 patients who underwent MRI-ultrasound fusion TB with 12-core SB between July 2022 and May 2025. Only lesions classified as PI-RADS v2.1 category 4 or 5 were analyzed. Detection rates of overall PCa and csPCa (Gleason score ≥ 7) were compared among SB, TB, and CB. Subgroup analyses were performed by PI-RADS category and lesion location (anterior, middle, posterior). Logistic regression identified independent predictors of csPCa.

Results: A total of 429 lesions were evaluated. Overall, PCa detection rates were 62% for SB, 70% for TB, and 77% for CB ($P < 0.001$); the corresponding csPCa rates were 47%, 56%, and 63% ($P < 0.001$). TB detected csPCa more effectively than SB (56% vs. 47%, $P < 0.01$). PI-RADS 5 lesions had higher detection rates than PI-RADS 4 lesions across all methods. CB achieved the highest rates in all locations, especially in anterior and middle lesions. Age, positive digital rectal examination, prostate-specific antigen density, prior biopsy, and PI-RADS category 5 were independent predictors of csPCa.

Conclusion: In PI-RADS 4–5 lesions, combined SB and TB provide the highest detection rate for csPCa. While TB improves selective detection, SB remains essential to avoid missing significant disease.

Keywords: Prostate cancer, multiparametric MRI, PI-RADS, MRI-ultrasound fusion biopsy, targeted biopsy, systematic biopsy, clinically significant prostate cancer

INTRODUCTION

Prostate cancer (PCa) is one of the most commonly diagnosed solid malignancies in men and ranks among the leading cancers worldwide in terms of incidence.[1,2] Its frequency increases markedly with age; most cases are diagnosed in men over 65 years.[3,4] With the widespread use of prostate-specific antigen (PSA) screening, an increase in diagnoses has also been observed in younger age groups, particularly for tumors with limited clinical significance.[5,6] PCa exhibits highly heterogeneous biological behavior, ranging from indolent lesions to aggressive, life-threatening forms.[7,8]

For many years, the diagnostic evaluation of patients with suspected PCa has relied on standard extended sextant biopsy performed under transrectal ultrasound (TRUS) guidance.[1] While image-guided biopsies have become an essential component of diagnosis in most other solid-organ tumors, PCa has traditionally been diagnosed by systematic and random sampling of the gland. However, this approach has increasingly been questioned, as it may fail to accurately localize clinically significant tumors and lead to the overdiagnosis of low-risk disease.[2,3]

Corresponding author: Önder Durmaz, **E-mail:** drmzonder2577@gmail.com

Received: 29 March, 2026

Accepted: 03 June, 2026 **Publication Date:** July, 14, 2026

In recent years, mpMRI has entered clinical practice and led to a significant paradigm shift in the diagnostic algorithm for PCa.[4,5] mpMRI provides high diagnostic accuracy, particularly for detecting high-grade and clinically significant prostate cancers (csPCa), and enables imaging-based localization of tumors.[6,7] This development has paved the way for more targeted diagnostic biopsy strategies.[8]

Advances in imaging technologies have led to the development of MRI-ultrasound fusion biopsy systems, which allow electronic co-registration of lesions identified as suspicious on mpMRI with real-time TRUS images.[9] Using these platforms, direct sampling can be performed from areas identified on prostate mpMRI as at risk for clinically significant cancer, thereby improving diagnostic yield.[10,11]

Targeted biopsy performed after mpMRI provides additional diagnostic value in PCa detection beyond that achieved by systematic biopsy alone. The literature demonstrates that this approach detects csPCas with greater accuracy while reducing diagnoses of low-grade tumors.[4,6,10] This selective diagnostic advantage decreases the risk of overdiagnosis and overtreatment, and may also reduce the number of biopsy cores taken and the related complications.[4,10] Studies by Barış Türkbey et al.[11,12] have further shown that mpMRI-guided targeted biopsy offers high diagnostic accuracy, particularly in Prostate Imaging-Reporting and Data System (PI-RADS) 4-5 lesions.

MAIN POINTS

- Superiority of Combined Biopsy: In high-risk Prostate Imaging-Reporting and Data System (PI-RADS) 4-5 lesions, the concurrent use of systematic and multiparametric magnetic resonance imaging-targeted biopsies significantly outperforms either approach alone in detecting both overall and clinically significant prostate cancer (csPCa).
- Selective Accuracy of Targeted Biopsy: Targeted biopsy enables precise detection of clinically significant cancers, especially in high-risk and anterior or mid-gland lesions; however, relying solely on this method may miss a subset of cancers.
- Impact of Lesion Location: Anatomical location critically influences diagnostic performance. In anterior PI-RADS 5 lesions, combined biopsy is essential, whereas in posterior lesions, targeted biopsy alone suffices in most cases, with minimal added value from systematic sampling.
- PI-RADS as a Key Predictor: The PI-RADS category stands out as the strongest independent predictor of csPCa, with PI-RADS 5 lesions conferring a markedly elevated risk regardless of other clinical or biochemical factors.
- Need for Individualized Biopsy Strategies: These findings highlight that prostate biopsy should not follow a one-size-fits-all model; tailoring approaches based on PI-RADS score and lesion location maximizes diagnostic accuracy and clinical impact.

Nevertheless, it has been reported that a strategy based solely on targeted biopsy may miss a proportion of clinically significant tumors that are not visible or cannot be adequately targeted on mpMRI.[5,9,13] For this reason, current European guidelines recommend the combined use of systematic and targeted biopsies to enhance diagnostic safety, while a targeted-only approach is generally reserved for patients with persistently elevated clinical suspicion despite prior negative biopsies.[7]

A substantial proportion of previous studies have been conducted in heterogeneous patient populations including PI-RADS 3 lesions, making it difficult to delineate the diagnostic contribution of different biopsy strategies in high-risk lesion groups. Although PI-RADS 4 and 5 lesions are considered high risk for clinically significant PCa, the superiority of MRI-ultrasound fusion-guided targeted biopsy over systematic biopsy and the additional diagnostic value of a combined approach in this subgroup remain subjects of ongoing debate.[11,12,14]

In a study published in 2024, Thomas in de Braekt and colleagues compared the diagnostic accuracy of MRI-ultrasound fusion-guided targeted biopsy with systematic biopsy. They reported that targeted biopsy provided higher specificity for detecting clinically significant PCa; however, systematic biopsy continued to contribute diagnostically in certain patient subgroups.[15]

The aim of the present study is to evaluate, in patients with PI-RADS 4 and 5 lesions, the performance of MRI-ultrasound fusion-guided targeted biopsy in detecting clinically significant PCa compared with that of standard systematic biopsy and to determine whether the combined application of the two methods provides additional diagnostic accuracy.

MATERIAL AND METHODS

Study Design and Patient Selection

Approval for this retrospective study was obtained from the Institutional Review Board. Due to the retrospective design of the study, the requirement for informed consent was waived by the Erzincan Binali Yıldırım University Ethics Committee (approval number: 2026-01-01; date: 08.01.2026). This retrospective study included patients who underwent MRI-guided targeted prostate biopsy and simultaneous 12-core systematic prostate biopsy at our institution between July 1, 2022, and May 1, 2025. A total of 330 patients were evaluated. Patient data were retrospectively obtained from the institution's electronic medical record system. The planning, conduct, and reporting of the study followed the Standards of Reporting for MRI-targeted Prostate Biopsy Studies.

The study population consisted of men who were either undergoing their first prostate biopsy or had previously undergone a biopsy with benign results. Patients under active surveillance, with a known diagnosis of PCa, with insufficient imaging quality, or with a history of non-prostate malignancy were excluded. The research protocol was approved by the local ethics committee; because of the study's retrospective design, the requirement for informed consent was waived.

Imaging Protocol

All patients underwent mpMRI using a 1.5 Tesla MRI system (Siemens Healthineers, Erlangen, Germany) with a surface body coil. The imaging protocol included high spatial resolution T2-weighted turbo spin-echo sequences acquired in the axial, coronal, and sagittal planes, and axial diffusion-weighted imaging. Diffusion data were acquired using b-values of 0, 50, 800, and 1500 s/mm^2, from which apparent diffusion coefficient maps were generated for quantitative analysis.

Dynamic contrast-enhanced MRI was performed selectively when deemed necessary to support the diagnostic interpretation of the dominant sequence, in accordance with the PI-RADS version 2.1 guidelines. All mpMRI examinations were conducted in accordance with the technical adequacy and image-quality criteria defined by PI-RADS.

Image Evaluation Criteria

Multiparametric prostate MRI examinations were analyzed by radiologists with extensive experience in urogenital imaging, who took into account patients' clinical data and followed the PI-RADS version 2.1 guidelines. Lesions were assessed and classified based on their anatomical location and on morphological and functional features observed in the dominant imaging sequences. Foci classified as PI-RADS 4 or 5 were considered highly suspicious for clinically significant PCa and were designated as targets for biopsy.

Biopsy Protocol

In this retrospective study, experienced urologists performed prostate biopsies with patients positioned in the left lateral decubitus position. The interpreting radiologist uploaded mpMRI images to a software-based MRI-US fusion biopsy system (Hitachi Hi Vision Preirus, Hitachi, Japan). After defining the prostate's anatomical reference structures, the MRI data were co-registered with real-time TRUS images using the software; cognitive fusion techniques were not used.

Following the completion of image fusion, TRUS-guided targeted biopsies were obtained, using a transrectal firing biopsy probe, from lesions identified as suspicious according to PI-RADS version 2.1 criteria. Targeted biopsy specimens were placed in separate containers, preserving lesion localization information, and sent for pathological evaluation without staining.

After targeted biopsies, systematic TRUS-guided biopsies were performed in both lobes, covering the apex, mid-zone, and base of the prostate. Regardless of prostate volume, all patients underwent a standard 12-core systematic biopsy protocol.

Histopathological

Assessment: All biopsy samples were fixed in formalin and embedded in paraffin, following the institution's routine pathology procedures. From each tissue block, at least three sections were prepared and stained with hematoxylin and eosin. Additionally, at least one section per block underwent immunohistochemical staining to evaluate the basal cell layer.

Evaluation of the specimens was conducted by specialized uropathologists, and the detected malignancies were classified according to the Gleason scoring system.

Statistical Analysis

Descriptive statistics were used to summarize patient demographics, imaging findings, and biopsy data. To assess differences between biopsy methods, Cochran's Q test was applied to the entire cohort and within each PI-RADS category. Post hoc comparisons of cancer detection rates between biopsy techniques, including overall and clinically significant PCa, were performed using the McNemar test.

The relationships between clinical and pathological variables and the likelihood of detecting clinically significant cancer were evaluated using logistic regression analysis. All tests were two-sided, and a P value < 0.05 was considered statistically significant. The Holm-Bonferroni method was applied for multiple testing correction. All analyses were conducted using SPSS Statistics for Windows, version 26.0 (IBM Corp., Armonk, NY, USA).

Patient Characteristics

A total of 330 patients were included in this study. The median age of the cohort was 66 years, and the median interval between multiparametric prostate MRI and biopsy was approximately 1.5 months. The median serum PSA level was around 8.5 ng/mL, while the mean prostate volume was approximately 55 cm^2. The median PSA density was 0.15 ng/mL/cm^2. The mean number of suspicious MRI lesions per patient was 1.3, indicating a limited but clinically significant lesion burden.

Only PI-RADS 4 and PI-RADS 5 lesions detected on mpMRI were included in the study. A total of 429 suspicious lesions were identified, of which 279 were PI-RADS 4 and 150 were PI-RADS 5. This distribution indicates a predominance of intermediate- and high-risk prostate lesions in the study population.

Histopathological analysis revealed clinically significant PCa in 198 of the 330 patients. Among patients diagnosed with cancer, the most common pathological subgroup was Gleason score 3+3=6, represented by 78 patients, followed by Gleason score 3+4=7 (52 patients) and Gleason score 4+3=7 (28 patients). High-grade disease (Gleason ≥ 8) was detected in 40 patients. Overall, Gleason ≥ 7 tumors were present in 120 patients, reflecting a cohort with a notable risk profile for clinically significant and intermediate-to-high-risk PCa.

This cohort of 330 patients, with a median age of 66 years and a median MRI-to-biopsy interval of approximately 1.5 months, predominantly consisted of patients with PI-RADS 4-5 lesions. Histopathological findings indicate a substantial representation of intermediate- and high-grade PCa. The mean number of targeted biopsies per patient was 2.5 ± 0 (Table 1).

Representative cases are shown in Figures 1 and 2. A 64-year-old male with a PSA of 7.9 ng/mL and PSA density of 0.14 ng/mL/cm^2 was found to have a PI-RADS 4 lesion, which was confirmed as Gleason 3 + 4 (Grade Group 2) prostate adenocarcinoma on targeted biopsy. Another example is a 69-year-old male with a PSA of 12.4 ng/mL and PSA density of 0.22 ng/mL/cm^2 who

Table 1. Patient Characteristics

Characteristic	First-time biopsy patients	Previously negative biopsy patients	All patients
Age (years), median (IQR)	65 (61-71)	68 (64-73)	66 (62-72)
Digital rectal examination, n (%)			
· Positive	78 (31.2)	32 (40.0)	110 (33.3)
· Negative	172 (68.8)	48 (60.0)	220 (66.7)
PSA level (ng/mL), median (IQR)	8.1 (6.2-11.4)	9.6 (7.4-13.2)	8.5 (6.6-12.1)
Prostate volume (cm^2), median (IQR)	53 (45-62)	58 (48-68)	55 (46-64)
PSA density ($ng/mL/cm^2$), median (IQR)	0.14 (0.10-0.19)	0.17 (0.12-0.22)	0.15 (0.11-0.20)
Interval between MRI and biopsy (days), median (IQR)	42 (30-58)	47 (35-62)	45 (32-60)
Number of MRI lesions (mean ± SD)	1.3 ± 0.5	1.4 ± 0.6	1.3 ± 0.5
Number of targeted biopsies (mean ± SD)	2.5 ± 0.6	2.6 ± 0.7	2.5 ± 0.6
PI-RADS category, n (%)			
· PI-RADS 4	210 (84.0)	69 (86.3)	279 (84.5)
· PI-RADS 5	40 (16.0)	11 (13.7)	51 (15.5)
Gleason score, n (%)			
· 3+3=6	62 (24.8)	16 (20.0)	78 (23.6)
· 3+4=7	40 (16.0)	12 (15.0)	52 (15.8)
· 4+3=7	22 (8.8)	6 (7.5)	28 (8.5)
· ≥ 8	28 (11.2)	12 (15.0)	40 (12.1)
Clinically significant PCa (Gleason ≥ 7), n (%)	90 (36.0)	30 (37.5)	120 (36.4)

PSA, prostate-specific antigen; SD, standard deviation; PCa, prostate cancer; MRI: magnetic resonance ımaging; PI-RADS, prostate ımaging-reporting and data system; IQR, interquartile range.

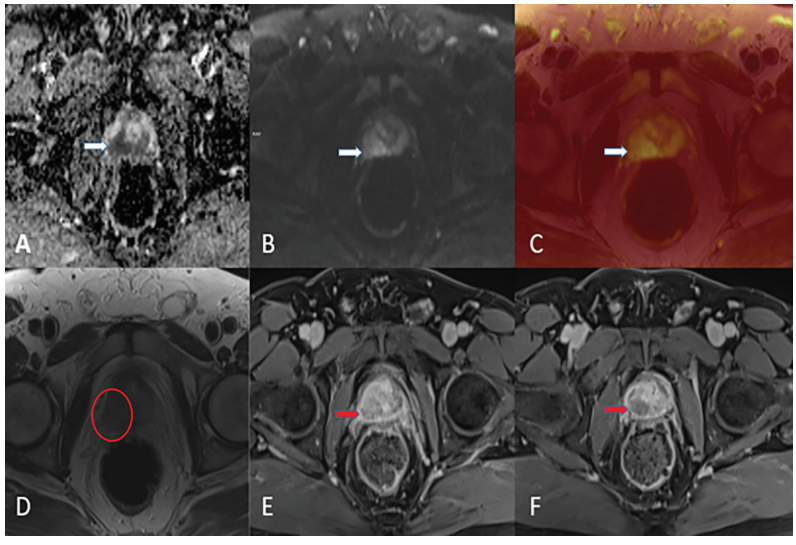

Figure 1. Shows mpMRI of the prostate in a 64-year-old male with elevated PSA, demonstrating a PI-RADS 4 lesion. On axial imaging, a focal lesion is seen in the right peripheral zone at the mid-gland level. The T2-weighted image **A)** demonstrates a moderately hypointense lesion without definite extracapsular extension, whereas the diffusion-weighted image **B)** shows marked hyperintensity of the lesion. The corresponding apparent diffusion coefficient map **C)** confirms restricted diffusion. A T2-weighted image with a red circle **D)** highlights the lesion's exact location. Dynamic contrast-enhanced imaging **E)** reveals early focal enhancement of the lesion compared with the surrounding parenchyma, and the color-coded perfusion map **F)** emphasizes the hypervascularity. The lesion was assigned a PI-RADS 4 score, and targeted MRI-ultrasound fusion biopsy confirmed clinically significant prostate adenocarcinoma (Gleason score 3+4, Grade Group 2).

DCE, dynamic contrast-enhanced; MRI, magnetic resonance imaging; PSA, prostate-specific antigen; PI-RADS, prostate ımaging-reporting and data system.

demonstrated a PI-RADS 5 lesion that was confirmed as high-grade Gleason 4+4 (Grade Group 4) adenocarcinoma. Detailed multiparametric MRI findings for these cases are illustrated in the respective figure legends.

Overall Detection Rate

The detection rates of PCa and clinically significant PCa for all biopsy methods, based on PI-RADS v2.1 classification and considering only PI-RADS 4-5 lesions, are presented in Table 2. The overall PCa detection rate was 62% (267/429) for systematic biopsy alone, 70% (301/429) for targeted biopsy alone, and 77% (331/429) for combined biopsy. Clinically significant PCa detection rates were 47% (203/429), 56% (240/429), and 63% (270/429), respectively. The combined biopsy approach demonstrated significantly higher detection rates for both overall and clinically significant PCa compared with either systematic or targeted biopsy alone ($P < 0.001$ for all comparisons).

When comparing the performance of systematic versus targeted biopsies alone in detecting overall PCa, the targeted biopsy showed a significant advantage (70% vs. 62%, $P < 0.01$). For clinically significant PCa, targeted biopsy achieved a significantly higher detection rate than systematic biopsy (56% vs. 47%, $P < 0.01$).

In the PI-RADS v2.1 subgroup analysis, PI-RADS 5 lesions demonstrated substantially higher detection rates for both overall PCa and clinically significant PCa across all biopsy methods, compared with PI-RADS 4 lesions. This superiority remained significant after correction for multiple testing, with the combined biopsy method showing the highest diagnostic performance in detecting clinically significant PCa in PI-RADS 5 lesions.

Detection Rates According to Lesion Location

For patients with a single suspicious lesion, the detection rates of PCa and csPCa for anterior, middle (mid-gland), and posterior PI-RADS 4/5 lesions are summarized in Table 3. Combined biopsy demonstrated significantly higher detection rates for both overall PCa and csPCa across all anatomical regions than either systematic or targeted biopsy alone (all comparisons, $P < 0.001$).

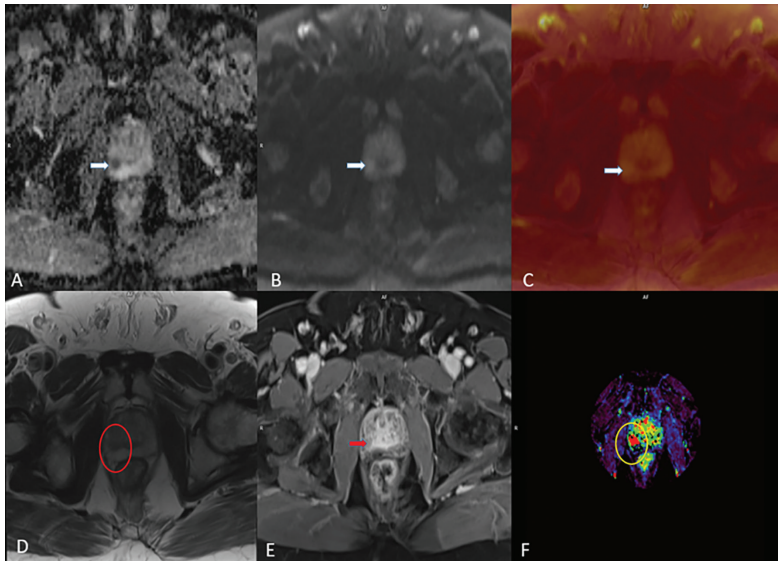

Figure 2. mpMRI of a PI-RADS 5 lesion in a 69-year-old male patient. A) Axial ADC map showing a focal lesion with markedly low signal intensity (white arrow). **B)** High b-value DWI demonstrating pronounced diffusion restriction (white arrow). **C)** Fusion PET/MRI image highlighting hypermetabolic activity corresponding to the lesion (white arrow). **D)** Axial T2-weighted image showing a hypointense lesion in the left peripheral zone (red circle). **E-F)** Axial post-contrast T1-weighted images demonstrate **e**arly enhancement with capsular bulging (red arrows); F additionally shows rapid washout, suggestive of aggressive behavior. Targeted biopsy confirmed clinically significant prostate adenocarcinoma, Gleason 4+4 (Grade Group 4).

DWI,diffusion-weighted imaging; ADC, apparent diffusion coefficien; PI-RADS, prostate ımaging-reporting and data system; MRI, magnetic resonance imaging.

Table 2. (2a and 2b) Detection Rates of Prostate Cancer and Clinically Significant Prostate Cancer According to PI-RADS classification for Systematic Biopsy, Targeted Biopsy, and Combined Biopsy Methods (2a: Total Prostate Cancer, 2b: Clinically Significant Prostate Cancer) -**Table 2a**-

PI-RADS	Total	SB n(%)	FB n(%)	KB n(%)	*P* value
PI-RADS-4	279	155 (%56)	178(%64)	196(%70)	**< 0.001**
PI-RADS 5	150	112 (%75)	123(%82)	135 (%90)	**< 0.001**
Overall total	429	267 (62)	301 (70)	331 (77)	**< 0.001**

SB, systematic biopsy; FB, targeted fusion biopsy; CB, combined biopsy; PI-RADS, prostate imaging-reporting and data system

For anterior lesions, targeted biopsy showed higher detection rates than systematic biopsy for both overall PCa and csPCa. This difference was particularly pronounced in anterior PI-RADS 5 lesions, where systematic biopsy lagged behind targeted biopsy in detecting overall PCa. However, no statistically significant difference was observed between the two methods for detecting csPCa in this subgroup. Additionally, for anterior PI-RADS 5 lesions, no significant advantage in overall PCa detection was observed between targeted and combined biopsies.

For middle (mid-gland) lesions, targeted biopsy yielded higher detection rates than systematic biopsy for both overall PCa and csPCa. Nevertheless, combined biopsy provided the highest detection rates compared to either method alone, highlighting its diagnostic advantage in this region. The superiority of combined biopsy was maintained in PI-RADS 5 middle-segment lesions for both overall and clinically significant cancers.

For posterior lesions, systematic biopsy demonstrated higher overall PCa detection rates than targeted biopsy. However, no significant differences were observed between biopsy methods for csPCa detection. Specifically, in posterior PI-RADS 5 lesions, no statistically significant differences were noted between biopsy techniques in detecting either overall PCa or csPCa.

Associations with and Presence of csPCa

Variables associated with csPCa are summarized in Table 4. In univariable analysis, advanced age, prior biopsy, a positive digital rectal examination (DRE), and elevated PSA density were significantly associated with the detection of csPCa. Among imaging parameters, PI-RADS category emerged as the strongest predictor, with PI-RADS 5 lesions showing a markedly higher likelihood of clinically significant cancer compared to PI-

-**Table 2b**-

PI-RADS	Total	SB n (%)	FB n (%)	KB n (%)	*P value*
PI-RADS-4	279	98 (35)	124 (44)	142 (51)	**< 0.001**
PI-RADS 5	150	105 (70)	116 (77)	128 (85)	**< 0.001**
Overall Total	429	203 (47)	240 (56)	270 (63)	**< 0.001**

SB, systematic biopsy; FB, targeted fusion biopsy; CB, combined biopsy; PI-RADS, prostate ımaging-reporting and data system KB,

Table 3a/3b: Detection Rates of Clinically Significant Prostate Cancer (csPCa) and Overall Prostate Cancer (PCa) Diagnosed by Biopsy Alone, Stratified by Anatomical Location (Anterior, Mid-Gland, and Posterior) of PI-RADS 4-5 Lesions, Using Systematic, Fusion-Targeted, and Combined Biopsy Methods

Anatomic location	PI-RADS	Total (n)	SB kPca (n) (%)	FB kPCa (n) (%)	KB kPCa (n) (%)	*P* value
Anterior	4	92	50 (54)	61(66)	68 (74)	< 0.001
	5	58	43 (74)	48 (83)	52 (90)	< 0.001
	Total	150	93 (62)	109 (73)	120 (80)	**< 0.001**
Orta (middle)	4	84	46 (55)	54 (64)	61 (73)	< 0.001
	5	45	33 (73)	37 (82)	41 (91)	< 0.001
	Total	129	79 (61)	91 (71)	102 (79)	**< 0.001**
Posterior	4	103	59 (57)	63 (61)	67 (65)	0.008
	5	47	36 (77)	38 (81)	42 (89)	< 0.001
	Total	150	95 (63)	101 (67)	109 (73)	**< 0.001**
Anatomic location	**PI-RADS**	**Total (n)**	**SB Pca (n) (%)**	**FB PCa (n) (%)**	**KB PCa (n) (%)**	***P* value**
Anterior	4	92	32 (35)	41 (45)	48 (52)	<0.001
	5	58	40 (69)	45 (78)	49 (84)	<0.001
	Total	150	72 (48)	86 (57)	97 (65)	**<0.001**
Middle	4	84	29 (35)	37 (44)	43 (51)	<0.001
	5	45	31 (69)	35 (78)	39 (87)	<0.001
	Total	129	60 (47)	72 (56)	82 (64)	**<0.001**
Posterior	4	103	37 (36)	46 (45)	51 (50)	<0.001
	5	47	34 (72)	36 (77)	40 (85)	<0.001
	Total	150	71 (47)	82 (55)	91 (61)	**<0.001**

SB, systematic biopsy; FB, targeted fusion biopsy; CB, combined biopsy; PCa, prostate cancer; kPCa, clinically significant prostate cancer; PI-RADS, prostate ımaging-reporting and data system

Note: Data are presented as n(%). P values indicate comparisons between biopsy methods (SB vs. FB, SB vs. CB, and FB vs. CB). For multiple comparisons, Bonferroni correction was applied, and statistical significance was set at $P < 0.0167$. Clinically significant prostate cancer was defined as Gleason score ≥ 7. Only PI-RADS v2.1 lesions scored 4 and 5 were included in the analysis.

Table 4. Single-Variable and Multiple-Variable Regression Analyses for Predicting Significant Prostate Cancer

Variable regressin analysis		Single		Multiple	
Parameter	**Comparison**	**OR (95% CI)**	***P* value**	**OR (95% CI)**	***P* value**
Age (median 66)	≤ 66 vs. > 66	1.48 (1.10-1.98)	**0.009**	1.36 (1.02-1.82)	0.037
DRE	Pos vs. Neg	2.21 (1.45-3.36)	**< 0.001**	1.88 (1.21-2.93)	**0.005**
PSA (Median 8.5 ng/mL	≤ 8.5 vs. > 8.5	1.31 (0.96-1.78)	.086	-	-
Prostate volüme (median 55 cm^2)	≤ 55 vs. > 55	0.71 (0.52-0.98)	.038	-	-
PSA density (median 0.15 bg7mL/cm^2)	≤ 0.15 vs. > 0.15	2.54 (1.88-3.43)	**< 0.001**	2.19 (1.61-2.98)	**< 0.001**
First biopsy	Yes vs. No	0.59 (0.42-0.83)	**0.002**	0.61 (0.43-0.87)	0.006
PI-RADS 4	-	-	-	-	-
PI-RADS 5	According to 4	6.12 (4.02-9.31)	**< 0.001**	5.48 (3.61-8.32)	**< 0.001**

OR, odds ratio; CI, confidence interval; DRE, digital rectal examination; PSA, prostate-specific antigen; MRI, magnetic resonance imaging; PI-RADS, prostate ımaging-reporting and data system

Notes: Clinically significant prostate cancer was defined as Gleason score ≥ 7. Only PI-RADS v2.1 - PI-RADS 4 and 5 lesions were included in the analysis. Variables with $P < 0.10$ in the univariable analysis that were considered clinically relevant were included in the multivariable model. PSA and prostate volume were not included in the multivariable model due to collinearity with PSA densi.

RADS 4 lesions. In contrast, total PSA level and prostate volume were not significantly associated with the presence of csPCa.

In multivariable logistic regression analysis, age, prior biopsy history, positive DRE, PSA density, and higher PI-RADS category remained independent predictors of csPCa. Notably, PI-RADS 5 lesions significantly increased the probability of detecting csPCa, independent of other clinical and biochemical variables.

DISCUSSION

In this retrospective study, the diagnostic contribution of mpMRI-based biopsy strategies for detecting PCa, including clinically significant cases was analyzed in a homogeneous cohort comprising only PI-RADS 4 and 5 lesions. Excluding PI-RADS 3 lesions and earlier PI-RADS versions enhanced the methodological consistency of the study and allowed a clearer assessment of the diagnostic performance specific to high-risk lesions.

The results presented in Table 2 indicate that systematic and targeted biopsies demonstrate comparable overall diagnostic performance when used alone. However, combining these two approaches provides a significant incremental benefit for detecting both overall and csPCa. This finding suggests that in higher PI-RADS categories, intralesional heterogeneity and multifocal tumor architecture may not be fully captured by a single biopsy approach. The superiority of combined biopsy likely reflects not only the increased sampling of lesions but also the capture of tumor foci with distinct biological behaviors.

Targeted biopsy appears to offer an advantage over systematic biopsy in detecting clinically significant cancer. This observation aligns with the ability of mpMRI to localize higher-grade tumors and supports its potential to reduce overdiagnosis of clinically insignificant disease. However, given the additional diagnostic benefit provided by combined biopsy, relying on a single biopsy method may be insufficient, particularly for high-risk patient groups.

Analyses based on lesion location (Table 3) revealed that the diagnostic performance of biopsy strategies anatomical localization significantly influences. In anteriorly located lesions, especially within higher PI-RADS categories, the combined biopsy approach provided the greatest diagnostic yield for clinically significant cancer. This finding reflects the risk that anterior zone lesions are missed due to the posterior sampling bias inherent in systematic biopsy. Nevertheless, targeted biopsy alone was not fully sufficient for anterior lesions, as some clinically significant cancers were detected only through systematic sampling.

For PI-RADS 5 lesions located posteriorly, differences in diagnostic performance among biopsy methods were markedly reduced. This can be explained by the posterior zone being more accessible to both systematic and targeted biopsies. In particular, adding a systematic biopsy when the targeted biopsy is negative may serve as a balanced approach that enhances diagnostic safety. These results strongly support the notion that biopsy strategies should be individualized based on lesion risk and anatomical location rather than adopting a "one-size-fits-all" approach.

The regression analyses presented in Table 4 highlight the central role of imaging-based parameters in the clinical decision-making process. The PI-RADS category emerged as the strongest independent predictor of the presence of csPCa. Notably, PI-RADS 5 lesions significantly increased the risk of clinically significant cancer, independent of other clinical and biochemical variables, thereby reinforcing the indispensable role of mpMRI in risk stratification.

Following PI-RADS, PSA density was identified as the second most powerful predictor. The lack of a significant association with total PSA level or prostate volume further underscores the limited standalone value of these parameters in clinical decision-making. In contrast, PSA density, as a biochemical marker more reflective of tumor burden, serves a complementary role to imaging findings. Additionally, advanced age, prior biopsy history, and positive DRE were independently associated with clinically significant cancer, emphasizing the importance of a multidisciplinary risk assessment approach.

A recent study by Thomas, de Braekt, and colleagues compared the diagnostic accuracy of MRI-ultrasound fusion-guided

targeted biopsy with systematic biopsy, demonstrating the superiority of a combined biopsy approach for detecting both overall and csPCa.[15] These findings align closely with the results of our study, particularly supporting the selective diagnostic advantage of targeted biopsy in high-risk lesions. Both studies emphasize that in posteriorly located PI-RADS 5 lesions, targeted biopsy rarely misses clinically significant cancer, whereas the contribution of systematic biopsy in this subgroup is limited.

The distinguishing feature of our study lies in its exclusive focus on PI-RADS 4 and 5 lesions as defined by PI-RADS v2.1, thereby reducing methodological heterogeneity and systematically analyzing lesion location (anterior-middle-posterior) to provide a more detailed assessment of biopsy strategy performance in an anatomical context. In contrast, the study by in de In de Braekt et al.[15] encompassed a broader PI-RADS spectrum, offering generalizability to routine clinical practice. However, the inclusion of PI-RADS 3 lesions introduces potential issues related to overdiagnosis of clinically insignificant cancer and unnecessary biopsies. In this regard, our study provides a clearer clinical signal specific to high-risk lesions, whereas the comparative study presents a more comprehensive perspective across a wider patient population.

The strengths of this study include its exclusive focus on high-risk PI-RADS categories, adherence to the current PI-RADS v2.1 classification, and detailed subgroup analyses based on lesion location. This approach ensures that the results are both methodologically robust and directly applicable to clinical practice. Additionally, the large patient cohort and the use of real-world data enhance the relevance and generalizability of the findings for routine practice in tertiary care centers.

Study Limitations

However, certain limitations should be acknowledged. The retrospective design cannot completely eliminate the risk of bias related to patient selection and biopsy performance. Furthermore, all biopsies were performed by a single operator familiar with the lesion information, which may have partially enhanced the performance of systematic biopsy. Finally, the use of histopathological thresholds to define clinically significant cancer may not capture the full spectrum of the biological behavior of tumors.

CONCLUSION

This study provides a comprehensive evaluation of mpMRI-based biopsy strategies in a well-defined cohort focused on high-risk lesions. The findings underscore the indispensable role of combined biopsy, particularly in selected patient subgroups, and highlight that tailoring biopsy approaches according to PI-RADS category and lesion location can further optimize diagnostic yield. These insights provide a robust scientific foundation for developing individualized prostate biopsy algorithms.

For the detection of csPCa, the concurrent use of systematic and targeted biopsies emerges as the most reliable strategy. While targeted biopsy allows for more selective sampling of high-risk lesions, relying on it alone may result in missed diagnoses in certain cases. Notably, in posterior PI-RADS 5 lesions, targeted biopsy demonstrates high diagnostic sufficiency, with limited incremental value from systematic biopsy; however, incorporating systematic biopsy when targeted biopsy is negative can enhance overall diagnostic safety.

This evidence emphasizes that an adaptive, lesion-specific approach—rather than a one-size-fits-all method—maximizes both precision and clinical utility in PCa detection.

Ethics

Ethics Committee Approval: Approval for the study was obtained by the Erzincan Binali Yıldırım University Ethics Committee (approval number: 2026-01-01; date: 08.01.2026).

Informed Consent: All imaging data were anonymized, with patients' names and other identifying information removed. Due to the retrospective nature of the study, informed consent was waived.

Footnotes

Author Contributions

Concept – O.D.; Design – O.D., A.L; Supervision – A.L.; Resources – O.D.; Materials – O.D., A.L.; Data Collection and/or Processing – A.L.; Analysis and/or Interpretation – A.L.; Literature Search – O.D., A.L.; Writing Manuscript – O.D.; Critical Review – O.D., A.L.; Other – A.L.

Declaration of Interest: The authors declare that they have no conflicts of interest.

Funding: The authors declare that this study has received no financial support.

REFERENCES

1. Sung H, Ferlay J, Siegel RL, et al. Global cancer statistics 2020: GLOBOCAN estimates of incidence and mortality Worldwide for 36 cancers in 185 countries. *CA Cancer J Clin.* 2021;71(3):209-249. doi: 10.3322/caac.21660. [CrossRef]
2. Siegel RL, Miller KD, Wagle NS, Jemal A. Cancer statistics, 2023. *CA Cancer J Clin.* 2023;73(1):17-48. doi: 10.3322/caac.21763. [CrossRef]
3. Haffner J, Lemaitre L, Puech P, et al. Role of magnetic resonance imaging before initial biopsy: comparison of magnetic resonance imaging-targeted and systematic biopsy for significant prostate cancer detection. *BJU Int.* 2011;108(8 Pt 2):E171-E178. [CrossRef]
4. Ahmed HU, El-Shater Bosaily A, Brown LC, et al; PROMIS study group. Diagnostic accuracy of multi-parametric MRI and TRUS biopsy in prostate cancer (PROMIS): a paired validating confirmatory study. *Lancet.* 2017;389(10071):815-822. [CrossRef]
5. Welch HG, Albertsen PC. Prostate cancer diagnosis and treatment after the introduction of prostate-specific antigen screening: 1986-2005. *J Natl Cancer Inst.* 2009;101(19):1325-1329. [CrossRef]
6. Kasivisvanathan V, Rannikko AS, Borghi M, et al; PRECISION study group collaborators. MRI-targeted or standard biopsy for prostate-cancer diagnosis. *N Engl J Med.* 2018;378(19):1767-1777. [CrossRef]

7. Rouvière O, Puech P, Renard-Penna R, et al; MRI-FIRST investigators. Use of prostate systematic and targeted biopsy on the basis of multiparametric MRI in biopsy-naive patients (MRI-FIRST): a prospective, multicentre, paired diagnostic study. *Lancet Oncol*. 2019;20(1):100-109. [CrossRef]
8. van der Leest M, Cornel E, Israël B, et al. Head-to-head comparison of transrectal ultrasound-guided prostate biopsy versus multiparametric prostate resonance imaging with subsequent magnetic resonance-guided biopsy in biopsy-naïve men with elevated prostate-specific antigen: a large prospective multicenter clinical study. *Eur Urol*. 2019;75(4):570-578. [CrossRef]
9. Siddiqui MM, Rais-Bahrami S, Turkbey B, et al. Comparison of MR/ultrasound fusion-guided biopsy with ultrasound-guided biopsy for the diagnosis of prostate cancer. *JAMA*. 2015;313(4):390-397. [CrossRef]
10. Schoots IG, Roobol MJ, Nieboer D, Bangma CH, Steyerberg EW, Hunink MG. Magnetic resonance imaging-targeted biopsy may enhance the diagnostic accuracy of significant prostate cancer detection compared to standard transrectal ultrasound-guided biopsy: a systematic review and meta-analysis. *Eur Urol*. 2015;68(3):438-450. [CrossRef]
11. Turkbey B, Pinto PA, Mani H, et al. Prostate cancer: value of multiparametric MR imaging at 3 T for detection-histopathologic correlation. *Radiology*. 2010;255(1):89-99. [CrossRef]
12. Hoeks CM, Barentsz JO, Hambrock T, et al. Prostate cancer: multiparametric MR imaging for detection, localization, and staging. *Radiology*. 2011;261(1):46-66. [CrossRef]
13. Cornford P, van den Bergh RCN, Briers E, et al. EAU-EANM-ESTRO-ESUR-ISUP-SIOG guidelines on prostate cancer-2024 update. Part I: screening, diagnosis, and local treatment with curative intent. *Eur Urol*. 2024;86(2):148-163. [CrossRef]
14. Cooperberg MR, Carroll PR. Trends in management for patients with localized prostate cancer, 1990-2013. *JAMA*. 2015;314(1):80-82. [CrossRef]
15. in de Braekt T, van Rooij SBT, Daniels-Gooszen AW, et al. Accuracy of MRI-ultrasound fusion-guided and systematic biopsy of the prostate. *Br J Radiol*. 2024;97(1158):1132-1138. [CrossRef]

ABCResearch

Arch Basic Clin Res 2026;8(2):129-134
DOI: 10.4274/ABCR.2026.26421

Research Article

Diagnostic Performance of Dual-Source CT Angiography Compared with Echocardiography in Pediatric Congenital Heart Disease

Hafize Otçu Temur

Department of Radiology, Bezmialem Vakıf University Faculty of Medicine, İstanbul, Türkiye

Cite this article as: Otçu Temur H. Diagnostic performance of dual-source CT angiography compared with echocardiography in pediatric congenital heart disease. *Arch Basic Clin Res*. 2026;8(2):129-134.

ORCID IDs of the authors: H.O.T. 0000-0003-0849-0705.

ABSTRACT

Objective: The aim of this study was to assess the diagnostic performance and radiation dose of 128-slice dual-source computed tomography (DSCT) angiography in pediatric patients with congenital heart disease (CHD) and to compare its diagnostic accuracy with that of transthoracic echocardiography (TTE).

Methods: Fifty-seven pediatric patients (mean age: 34.1 months; range: 0.5-156 months; 25 males and 32 females; mean body weight: 10.3 kg) who underwent thoracic DSCT angiography and TTE for suspected or confirmed CHD were retrospectively evaluated. Surgical findings conventional catheter angiography, alone or in combination, served as the reference standard. Diagnostic performance metrics, including sensitivity, specificity, positive predictive value (PPV), negative predictive value (NPV), and overall diagnostic accuracy, were calculated. Agreement between imaging techniques and the reference standard was assessed using Cohen's kappa coefficient, and paired comparisons were performed using the McNemar test.

Results: A total of 199 cardiovascular anomalies were confirmed, including 67 intracardiac and 132 extracardiac abnormalities. Computed tomography (CT) angiography detected 193 anomalies (96.9%), whereas TTE detected 179 anomalies (89.9%). For CT angiography, sensitivity, specificity, PPV, NPV, and overall diagnostic accuracy were 96.9%, 99.9%, 99.0%, 99.6%, and 99.5%, respectively. The corresponding values for TTE were 89.9%, 99.6%, 96.8%, 98.8%, and 98.5%. CT angiography demonstrated significantly higher overall detection rates than TTE (P = 0.01). Subgroup analysis showed that TTE had higher sensitivity for intracardiac anomalies, whereas CT angiography demonstrated superior performance in identifying extracardiac vascular abnormalities.

Conclusion: Dual-source CT angiography enables highly accurate anatomical assessment in pediatric CHD while maintaining acceptable radiation exposure levels. Although echocardiography remains the first-line imaging modality, CT angiography represents a valuable complementary technique, particularly for evaluating extracardiac vascular anomalies.

Keywords: Congenital heart disease, CT angiography, low effective dose, pediatric cardiac imaging, radiation dose

Corresponding author: Hafize Otçu Temur, **E-mail:** hotcutemur@bezmialem.edu.tr

Received: 21 April, 2026
Revision Requested: 3 June, 2026 **Accepted:** 11 June, 2026 **Publication Date:** July, 14, 2026

INTRODUCTION

Congenital heart disease (CHD) is among the most frequently encountered congenital anomalies worldwide and continues to represent an important cause of morbidity and mortality in pediatric populations. Precise delineation of cardiac and vascular anatomy is essential for optimal clinical management and surgical planning. Current international guidelines emphasize the importance of multimodality imaging approaches—including echocardiography, computed tomography (CT), and magnetic resonance imaging —for the comprehensive evaluation of congenital cardiovascular anomalies.[1,2]

Transthoracic echocardiography (TTE) is widely regarded as the first-line imaging modality for evaluating CHD because it is readily available, portable, and capable of providing real-time assessment of cardiac structure and hemodynamics without exposure to ionizing radiation.[3] However, echocardiography is highly dependent on operator experience and may be limited by inadequate acoustic windows, particularly when assessing extracardiac vascular structures such as the aortic arch, pulmonary arteries, and pulmonary venous connections.[4]

Historically, cardiac catheterization served as the reference method for detailed anatomical evaluation of congenital cardiovascular abnormalities. Nevertheless, because this technique is invasive and associated with radiation exposure, its role in diagnostic evaluation has gradually decreased in contemporary pediatric practice.[5,6]

Recent developments in multidetector CT, particularly dual-source CT technology, have significantly improved the non-invasive evaluation of congenital cardiovascular anomalies. High spatial resolution and rapid acquisition capabilities allow detailed visualization of complex cardiovascular anatomy even in infants and young children with relatively high heart rates.[6,7] Numerous studies have demonstrated the high diagnostic accuracy of CT angiography in patients with CHD and highlighted its usefulness in detecting extracardiac vascular abnormalities that may not be adequately evaluated by echocardiography alone.[8-11]

MATERIALS AND METHODS

Study Population

This retrospective study included pediatric patients younger than 13 years who underwent thoracic CT angiography for suspected or confirmed CHD. All patients also underwent transthoracic echocardiography. Surgical findings and/or conventional catheter angiography served as the reference standard. The study protocol was approved by the Bezmialem Vakıf University Institutional Ethics Committee (Date: 16.10.2018, Decision No: 19/245), and written informed consent was obtained from the parents or legal guardians of all participants.

CT Angiography Protocol

All CT examinations were performed using a dual-source CT scanner (Somatom Definition Flash, Siemens Healthcare). Imaging was performed with the patient in the supine position. Peripheral intravenous access (20-24 gauge) was established, and iodinated contrast material was administered using an automated injector at 0.5-2 mL/s, with an average dose of 2 mL/kg. Scan timing was determined using bolus tracking, with the region of interest (ROI) placed in the descending aorta. Image acquisition was initiated when attenuation reached 100 Hounsfield Unit (HU). The scan range extended from the thoracic inlet to the diaphragm. Scanning parameters included collimation 128 × 0.6 mm, gantry rotation time 0.28 s, pitch 3, tube voltage 80-100 kVp, and tube current 30-120 mAs, adjusted according to the patient's body size. All imaging data were analyzed on a dedicated workstation (Syngo.via, Siemens Healthcare) using vascular imaging software. All CT angiography examinations were reviewed by an experienced radiologist.

The radiation dose was estimated from the dose-length product values provided by the CT scanner. Because these values were calculated using a 32-cm phantom, they were multiplied by two to convert them to the 16-cm phantom equivalent recommended for pediatric dose estimation. Effective radiation dose was calculated using age-specific conversion factors for thoracic CT examinations.

Statistical Analysis

Statistical analyses were performed using SPSS (version 16.0; SPSS Inc., Chicago, IL, USA). Diagnostic performance metrics, including sensitivity, specificity, positive predictive value, negative predictive value, and overall diagnostic accuracy, were calculated using surgical findings, conventional catheter angiography, or both as the reference standard. Agreement between imaging modalities and the reference standard was assessed using Cohen's kappa coefficient. Diagnostic performance parameters were calculated together with their corresponding 95% confidence intervals (95% confidence intervals). Paired comparisons between CT angiography and TTE for anomaly detection were performed using the McNemar test, and a P value < 0.05 was considered statistically significant.

RESULTS

A total of 57 children were included in the study. The demographic characteristics of the study population are summarized in Table 1.

Following TTE and CT angiography, 22 patients underwent conventional angiography, 28 patients underwent surgery, and 7

MAIN POINTS

- Dual-source computed tomography (CT) angiography demonstrated higher diagnostic sensitivity than transthoracic echocardiography in detecting congenital cardiovascular anomalies.
- CT angiography was superior in identifying extracardiac vascular abnormalities, such as major aortopulmonary collateral arteries, vascular rings, and pulmonary venous anomalies.
- Low-dose CT protocols allow for accurate diagnosis while maintaining acceptable radiation exposure in pediatric patients.

patients underwent both procedures; these procedures served as the reference standard for diagnostic evaluation. A total of 199 cardiovascular anomalies were confirmed by surgery and/or conventional angiography, including 67 intracardiac and 132 extracardiac anomalies.

CT angiography detected more anomalies than TTE, corresponding to detection rates of 96.9% and 89.9%, respectively. The detection rates of both imaging modalities are summarized in Table 2. The diagnostic performance parameters their corresponding 95% confidence intervals for CT angiography and TTE are presented in Table 3. CT angiography demonstrated higher overall sensitivity, specificity, and diagnostic accuracy compared with TTE. A paired comparison using the McNemar test showed that CT angiography detected significantly more anomalies than TTE ($P = 0.01$).

The subgroup analysis showed that TTE had higher sensitivity for intracardiac anomalies, whereas CT angiography had higher sensitivity for extracardiac vascular abnormalities (Table 3).

Table 1. Demographic Characteristics of the Study Population

Variable	*P* value
Number of patients	57
Male/female	25/32
Mean age (months)	34.1 ± 36.8
Age range (months)	0.5-156
Mean body weight (kg)	10.3 ± 7.9
Weight range (kg)	3-38

A representative example of a coronary artery anomaly associated with Tetralogy of Fallot, demonstrated by CT angiography, is shown in Figure 1. Examples of extracardiac vascular anomalies detected by CT angiography are illustrated in Figure 2.

Agreement analysis demonstrated excellent concordance between CT angiography and the reference standard ($\kappa = 0.974$, $P < 0.001$), whereas TTE demonstrated very good agreement ($\kappa = 0.929$, $P < 0.001$).

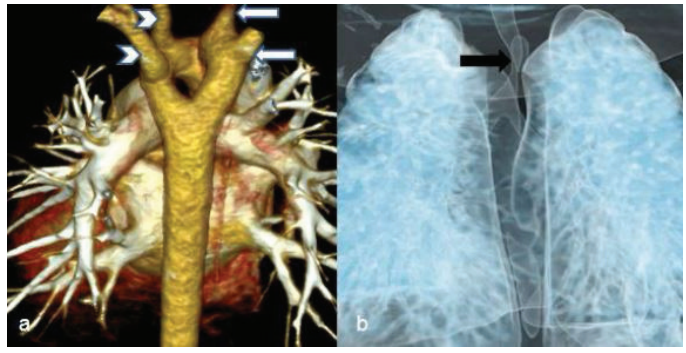

Figure 1. Coronary artery anomaly in a 2-year-old girl with Tetralogy of Fallot. Three-dimensional CT angiography (a) and maximum-intensity projection (MIP) images (b) demonstrate pulmonary artery stenosis (curved arrow) and the origin and proximal segments of the coronary arteries. A single coronary artery originates from the left sinus of Valsalva (black arrow), and the left anterior descending artery crosses the right ventricular outflow tract (white arrow).

CT, computed tomography.

Table 2. Detection of Intracardiac and Extracardiac Anomalies by Imaging Modality

Anomaly type	Total anomalies	Detected by TTE n (%)	Detected by CT angiography n (%)	*P* value
Intracardiac anomalies	67	67 (100)	61 (91.0)	**0.031**
Extracardiac anomalies	132	112 (84.8)	132 (100)	**< 0.001**
Total anomalies	199	179 (90.0)	193 (96.9)	**0.01**

P value < 0.05 was considered statistically significant.
CT, Computed tomography; TTE: Transthoracic echocardiography

Table 3. Diagnostic Performance of CT Angiography and TTE for Intracardiac and Extracardiac Anomalies

Parameter	CT Angiography % (95% CI)	TTE % (95% CI)	*P* value
Intracardiac anomalies			
Sensitivity	91.0 (82.0-96.3)	100 (94.6-100)	**0.031**
Extracardiac anomalies			
Sensitivity	100 (97.2-100)	84.8 (77.5-90.1)	**< 0.001**
Overall diagnostic performance			
Sensitivity	96.9 (93.4-98.8)	89.9 (84.9-93.5)	**0.01**
Specificity	99.9 (99.5-100)	99.6 (99.1-99.9)	-
Positive predictive value	99.0 (96.2-99.9)	96.8 (93.2-98.7)	-
Negative predictive value	99.6 (99.0-99.9)	98.8 (97.6-99.5)	-
Accuracy	99.5 (98.9-99.9)	98.5 (97.5-99.2)	-

P value < 0.05 was considered statistically significant.
CI, Confidence interval; CT, Computed tomography; TTE: Transthoracic echocardiography.

In addition to assessing cardiovascular abnormalities, CT angiography enabled the evaluation of thoracic structures and revealed airway compression caused by vascular anomalies in six patients, as illustrated in Figure 3. Findings consistent with heterotaxy syndrome were also identified in four patients.

Radiation dose parameters are summarized in Table 4. The mean effective radiation dose for CT angiography was 1.46 ± 0.39 mSv.

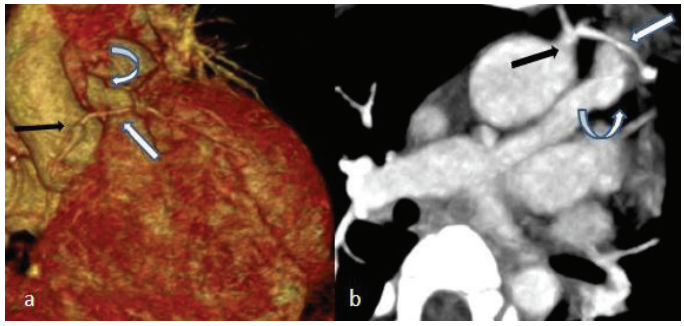

Figure 2. Partial anomalous pulmonary venous return in a 4-month-old girl. Three-dimensional CT angiography (a), a coronal maximum intensity projection (MIP) image (b), and axial CT images (c, d) demonstrate that the right inferior, left superior, and left inferior pulmonary veins drain into the vertical vein (black arrow), whereas the right superior pulmonary vein drains into the superior vena cava (white arrow). An associated atrial septal defect is also present.

LSPV, left superior pulmonary vein; RSPV, right superior pulmonary vein; SVC, superior vena cava; ASD, atrial septal defect; CT, computed tomography.

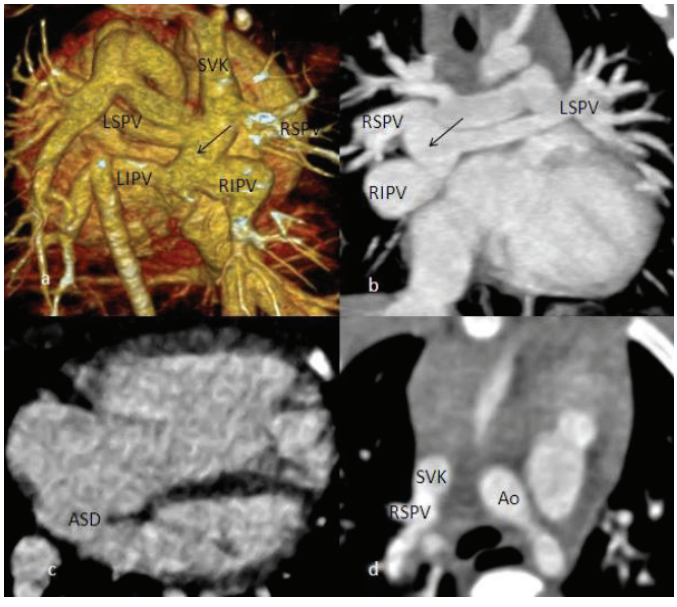

Figure 3. Double aortic arch causing vascular ring in a 1-year-old male patient. Three-dimensional CT angiography demonstrates bilateral aortic arches (a). Airway reconstruction images (b) show tracheal narrowing due to compression by the vascular ring.

CT, computed tomography

Table 4. Radiation Dose Parameters in CT Angiography

Parameter	*P* value
Mean dose-length product (DLP)	32.14 ± 8.97 mGy·cm
Effective dose range	0.88-2.5 mSv
Mean effective dose	1.46 ± 0.39 mSv
Mean effective dose (< 1 year)	1.71 ± 0.36 mSv

CT, Computed tomography.

DISCUSSION

Echocardiography continues to serve as the primary imaging modality for the initial assessment of CHD because it is widely available and enables real-time evaluation of cardiac morphology and hemodynamics without exposure to ionizing radiation.[3] However, previous studies have shown that echocardiography may be limited in the assessment of extracardiac vascular structures due to its dependence on acoustic windows and relatively limited spatial resolution.[4] These limitations are particularly relevant for patients with complex congenital cardiovascular anomalies who require comprehensive anatomical evaluation.

Historically, cardiac catheterization was considered the reference method for detailed anatomical assessment of congenital cardiovascular abnormalities. Nevertheless, because of its invasive nature and associated radiation exposure, its role in routine diagnostic evaluation has decreased in contemporary pediatric practice.[5,6] Consequently, non-invasive cross-sectional imaging techniques have become increasingly important in the diagnostic work-up of CHD.

Advances in multidetector CT technology, particularly the development of dual-source CT systems, have significantly improved the diagnostic capabilities of CT angiography. The combination of high spatial resolution and rapid acquisition enables detailed visualization of complex cardiovascular anatomy even in pediatric patients with elevated heart rates.[6,7] Furthermore, three-dimensional reconstruction techniques provide comprehensive anatomical information that may facilitate surgical planning and clinical decision-making.

Several studies have reported high diagnostic accuracy of CT angiography in patients with CHD. Reported diagnostic accuracy values generally range between approximately 95% and 99% for CT angiography, whereas echocardiography demonstrates diagnostic accuracies between 83% and 93%, particularly for extracardiac vascular anomalies.[8-11] In addition, Kravchenko et al.[12] demonstrated high diagnostic performance of dual-source CT angiography in pediatric patients with CHD, supporting the reliability of modern CT techniques for detailed anatomical assessment of complex cardiovascular anomalies.

The findings of this study are consistent with previous reports and indicate that CT angiography provides higher overall diagnostic accuracy compared with TTE. In our cohort, CT angiography detected more anomalies than TTE, and statistical analysis confirmed that the difference was significant.

A key finding of this study was the superior performance of CT angiography in detecting extracardiac vascular anomalies. Previous studies have consistently demonstrated

that CT angiography is particularly effective in identifying extracardiac abnormalities such as aortic arch anomalies, major aortopulmonary collateral arteries, and anomalous pulmonary venous connections.[8-11] Consistent with these findings, CT angiography detected all extracardiac anomalies in our cohort, whereas TTE failed to identify several clinically significant lesions.

Conversely, TTE demonstrated higher sensitivity for intracardiac abnormalities, particularly small septal defects. Similar observations have been reported in previous comparative studies evaluating CT angiography and echocardiography in CHD.[13-14] The relatively low sensitivity of CT angiography for small intracardiac defects may be related to the absence of electrocardiogram (ECG)-gated acquisition and their small size.

Another important advantage of CT angiography is its ability to simultaneously evaluate thoracic structures beyond the cardiovascular system. In the present study, CT imaging enabled the identification of airway compression caused by vascular anomalies and provided additional information regarding heterotaxy syndrome. Previous reports have also emphasized the value of CT imaging in evaluating thoracic structures outside the cardiovascular system.[15]

Radiation exposure remains an important consideration in pediatric CT imaging. However, recent technological advances, including high-pitch acquisition techniques, automated tube current modulation, and advanced reconstruction algorithms, have significantly reduced radiation doses in pediatric cardiac CT examinations. In previous studies, reported effective radiation doses for pediatric cardiac CT have ranged between approximately 1.0 and 5.0 mSv, depending on scanning protocols and patient characteristics.[15-20] In this study, the mean effective radiation dose was 1.46 mSv, which is within the lower range reported in the literature. These findings indicate that the dual-source CT protocol used in our study provides diagnostically adequate image quality while maintaining a relatively low radiation exposure compared with those reported in previously published studies.

Study Limitations

This study has several limitations. First, the relatively small sample size may limit the generalizability of the findings. In addition, the retrospective design and the wide age distribution of the study population may have influenced image quality and diagnostic performance. Image interpretation was performed by a single experienced radiologist; therefore, interobserver variability was not assessed. The absence of automatic tube current modulation and prospective ECG-gating may have limited further dose reduction and the optimal visualization of coronary artery anatomy. Future multicenter studies, including larger patient populations and optimized low-dose CT protocols, are needed to provide a more comprehensive assessment of the diagnostic role of CT angiography in pediatric CHD.[21]

CONCLUSION

Dual-source CT angiography provides highly accurate anatomical evaluation with acceptable radiation exposure in pediatric patients with CHD. While TTE remains the first-line imaging modality for intracardiac assessment, CT angiography offers superior visualization of extracardiac vascular anomalies. Therefore, CT angiography represents an effective complementary imaging technique, particularly in patients with complex congenital cardiovascular anomalies or inconclusive echocardiographic findings.

Ethics

Ethics Committee Approval: The study protocol was approved by the Bezmialem Vakıf University Institutional Ethics Committee (Date: 16.10.2018, Decision No: 19/245)

Informed Consent: Written informed consent was obtained from the parents or legal guardians of all participants.

Footnes

Declaration of Interests: The authors declared no conflicts of interest.

Funding: No funding.

REFERENCES

1. Baumgartner H, De Backer J, Babu-Narayan SV, et al; ESC Scientific Document Group. 2020 ESC guidelines for the management of adult congenital heart disease. *Eur Heart J*. 2021;42(6):563-645. [CrossRef]
2. Stout KK, Daniels CJ, Aboulhosn JA, et al. 2018 AHA/ACC guideline for the management of adults with congenital heart disease: a report of the American College of Cardiology/American Heart Association task force on clinical practice guidelines. *Circulation*. 2019;139(14):e698-e800. [CrossRef] Erratum in: *Circulation.* 2019 Apr 2;139(14):e833-e834. [CrossRef]
3. Han BK, Rigsby CK, Hlavacek AM, et al. Computed tomography imaging in patients with congenital heart disease: indications, imaging technique, and clinical applications. J Cardiovasc Comput Tomogr. 2019;13(3):152-164.
4. Freire G, Miller MS. Echocardiographic evaluation of coronary arteries in congenital heart disease. *Cardiol Young.* 2015;25(8):1504-1511. [CrossRef]
5. Raimondi F, Warin-Fresse K. Computed tomography imaging in children with congenital heart disease: Indications and radiation dose optimization. *Arch Cardiovasc Dis.* 2016;109(2):150-157. [CrossRef]
6. Han BK, Rigsby CK, Hlavacek A, et al; Society of cardiovascular computed tomography; society of pediatric radiology; North American society of cardiac imaging. Computed tomography imaging in patients with congenital heart disease part 1: rationale and utility. An expert consensus document of the society of cardiovascular computed tomography (SCCT): endorsed by the society of pediatric radiology (SPR) and the North American Society of cardiac ımaging (NASCI). *J Cardiovasc Comput Tomogr.* 2015;9(6):475-492. [CrossRef]
7. DiGeorge NW, El-Ali AM, White AM, Harris MA, Biko DM. Pediatric cardiac CT and MRI: considerations for the general radiologist. *AJR Am J Roentgenol.* 2020;215(6):1464-1473. [CrossRef]
8. Cheng Z, Wang X, Duan Y, et al. Low-dose prospective ECG-triggering dual-source CT angiography in infants and children with

complex congenital heart disease: first experience. *Eur Radiol.* 2010;20(10):2503-2511. [CrossRef]

9. Huang MP, Liang CH, Zhao ZJ et al. Evaluation of image quality and radiation dose at prospective ECG-triggered axial 256-slice multi-detector CT in infants with congenital heart disease. *Pediatr Radiol.* 2011;41(7):858-866. [CrossRef]
10. Nie P, Yang G, Wang X, et al. Application of prospective ECG-gated high-pitch 128-slice dual-source CT angiography in the diagnosis of congenital extracardiac vascular anomalies in infants and children. *PLoS One.* 2014;9(12):e115793. [CrossRef]
11. Ruan W, Yang ZG, Li Y, et al. Diagnostic accuracy of CT angiography versus echocardiography in congenital heart disease. *Eur J Radiol.* 2020;131:109241. [CrossRef]
12. Kravchenko D, Hart C, Garbe S, et al. Diagnostic performance of dual-source CT angiography in pediatric congenital heart disease**.** *Sci Rep.* 2022;12:21495. [CrossRef]
13. Koplay M, Sivri M, Erdogan H, et al. Prospective ECG-gated high-pitch dual-source CT angiography in congenital cardiovascular abnormalities. *Diagn Interv Imaging***.** 2016;97(5):543-550. [CrossRef]
14. Liu Y, Chen S, Zühlke L, et al. Image quality and radiation dose of dual-source CT cardiac angiography in pediatric congenital heart disease. *Int J Cardiovasc Imaging.* 2016;32(2):287-294. [CrossRef]
15. Warin-Fresse K, Isornii MA, Dacher JN, et al. Pediatric cardiac computed tomography angiography: Expert consensus from the filiale de cardiologie pédiatrique et congénitale (FCPC) and the société française d'imagerie cardiaque et vasculaire diagnostique et interventionnelle (SFICV). *Diagn Interv Imaging.* 2020;101(6):335-345. [CrossRef]
16. Rigsby CK, McKenney SE, Hill KD, et al. Radiation dose management for pediatric cardiac computed tomography: a report from the image gently ''Have-A-Heart'' campaign. *Pediatr Radiol.* 2018;48(1):5-20. [CrossRef]
17. Goo HW. Image quality and radiation dose of high-pitch dual-source spiral cardiothoracic computed tomography in young children with congenital heart disease: comparison of non-electrocardiography synchronization and prospective electrocardiography triggering. *Korean J Radiol.* 2018;19(6):1031-1041. [CrossRef]
18. Hong SH, Goo HW, Maeda E, Choo KS, Tsai IC; Asian society of cardiovascular imaging congenital heart disease study group. User-friendly vendor-specific guideline for pediatric cardiothoracic computed tomography provided by the asian society of cardiovascular imaging congenital heart disease study group: part 1. imaging techniques. *Korean J Radiol.* 2019;20(2):190-204. [CrossRef]
19. Malone LJ, Morin CE, Browne LP. Coronary computed tomography angiography in children. *Pediatr Radiol.* 2022;52(13):2498-2509. [CrossRef]
20. Francone M, Gimelli A, Budde RPJ, et al. Radiation safety for cardiovascular computed tomography imaging in paediatric cardiology: a joint expert consensus document of the EACVI, ESCR, AEPC, and ESPR. *Eur Heart J Cardiovasc Imaging.* 2022;23(8):e279-e289. [CrossRef] Erratum in: *Eur Heart J Cardiovasc Imaging.* 2022;23(8):e306. [CrossRef]
21. Fogel MA, Fratz S, Cohen MS, et al. Multimodality imaging in congenital heart disease. J Cardiovasc Magn Reson. 2022;24(1):37. [CrossRef]

ABCResearch

Arch Basic Clin Res 2026;8(2):135-142
DOI: 10.4274/ABCR.2026.26424

Research Article

Association of Infrapatellar Fat Pad Morphology and Signal Changes with Patellar Chondromalacia

Ece Zengin, Behlül Atalay, İhsaniye Süer Doğan

Clinic of Radiology, University of Health Sciences Türkiye, Ankara Etlik City Hospital, Ankara, Türkiye

Cite this article as: Zengin E, Atalay B, Süer Doğan İ. Association of infrapatellar fat pad morphology and signal changes with patellar chondromalacia. *Arch Basic Clin Res.* 2026;8(2):135-142.

ORCID IDs of the authors: E.Z., 0009-0005-1488-6820 B.A., 0000-0002-8179-2753 İ.S.D. 0000-0002-7586-0537.

ABSTRACT

Objective: To evaluate the association between infrapatellar fat pad (IPFP) maximal area, depth, and signal intensity alterations and the presence and severity of patellar chondromalacia on magnetic resonance imaging (MRI).

Methods: In this single-center retrospective study, 172 knee MRI examinations with patellar chondromalacia and 78 control examinations were analyzed between January 1, 2024, and January 1, 2025. MRI scans were acquired without contrast using a 1.5-Tesla system (Ingenia Evolution, Philips Medical System, Best, the Netherlands). Alterations in IPFP maximal area, depth, and signal intensity (graded 0-3) were measured on fat-suppressed proton density-weighted images. Chondromalacia was staged using the MRI-adapted Outerbridge classification. Demographic characteristics, medial subcutaneous fat thickness, and IPFP measurements were compared between groups. Correlation analyses were performed to assess associations between IPFP metrics and chondromalacia severity. Parametric and nonparametric tests were applied; $P < 0$ .05 was considered statistically significant.

Results: Patients with chondromalacia were older than controls (50.8 ± 10.1 vs. 38.7 ± 12.7 years; $P < 0.001$) and included a higher proportion of females ($P = 0.009$). Medial subcutaneous fat thickness was greater in the chondromalacia group ($P < 0.001$). Male sex was correlated with larger maximal IPFP area and depth ($P < 0.001$). No significant correlation was observed between medial subcutaneous fat thickness and IPFP size. The IPFP signal intensity score was positively correlated with age (r = 0.50) and with chondromalacia grade (r = 0.377; $P < 0.001$ for both). IPFP maximal area and depth showed no significant association with chondromalacia grade, lesion location, or signal intensity score.

Conclusion: MRI signal intensity alterations of the IPFP are strongly associated with patellar chondromalacia severity. In contrast, dimensional measurements alone (area or depth) do not reflect disease severity, highlighting the superior diagnostic value of qualitative signal assessment.

Keywords: Patellar chondromalacia, infrapatellar fat pad, knee magnetic resonance imaging, signal intensity alteration, cartilage degeneration

INTRODUCTION

Hoffa's fat pad, also known as the infrapatellar fat pad (IPFP), is an intracapsular, yet extrasynovial structure located beneath the patella within the knee joint. Anteriorly, it is bordered by the patellar tendon; posteriorly, by the synovium-lined knee joint. Superiorly, it attaches to the inferior pole of the patella; inferiorly, it extends to the periosteum of the tibia.[1]

Structurally, the IPFP shares characteristics with subcutaneous adipose tissue, yet it also serves important biomechanical functions such as absorbing mechanical loads transmitted through the knee and attenuating shock. In addition, it has been shown to play a role in joint metabolic and inflammatory processes. The IPFP is known to be involved in the production of adipokines such as interleukin-6, tumor necrosis factor-α, and leptin, thereby influencing the biological environment of the knee joint.

Magnetic resonance imagin (MRI) studies conducted in patients with osteoarthritis (OA) have demonstrated that the IPFP exhibits increased signal intensity, suggesting that it may serve as a biomarker in knee OA.[2-4] Therefore, standardized,

Corresponding author: Behlül Atalay,, **E-mail:** atalaybehlul@gmail.com

Received: March 25, 2026

Accepted: June 22, 2026 **Publication Date:** July, 14, 2026

reproducible measurements of IPFP dimensions are important for evaluating metabolic and degenerative joint disorders.[1]

MRI studies in patients with OA have shown increased signal intensity of the IPFP, suggesting its potential as a biomarker for knee OA.[4] Alterations within the IPFP—such as inflammation or fibrosis—can be visualized on sagittal MRI sections by characteristic variations in signal intensity.[5]

Patellar chondromalacia is characterized by anterior knee pain and softening of the articular cartilage on the patellar surface, often accompanied by fibrillation or ulceration.[6] In addition to patient history and physical examination, radiological imaging methods are widely used in the diagnostic process. MRI is considered one of the most valuable imaging modalities for evaluating patellar chondromalacia and other cartilage pathologies.[7] Several studies have suggested that IPFP dimensions may be associated with patellar chondromalacia, implying that changes in IPFP size could alter the mechanical load distribution across the patellofemoral joint (PFJ), thereby contributing to cartilage degeneration.[5]

In this study, we aimed to investigate the association of maximal IPFP area, depth, and signal intensity alterations with the presence of patellar chondromalacia, considering the close anatomical relationship between the IPFP, patella, and PFJ.

MATERIAL AND METHODS

Study Approval

This retrospective study was approved by the Clinical Research Ethics Committee of the Ministry of Health University of Health Sciences Türkiye, Ankara Etlik City Hospital (approval no: 2025/0231, date: 26.02 2025). In this retrospective study, the requirement for informed consent was waived. The study was conducted in accordance with the principles of the Declaration of Helsinki.

Study Population

This retrospective study evaluated patients who underwent non-contrast knee MRI between January 1, 2024, and January 1, 2025. The inclusion criteria were as follows:

1. Age ≥18 years

2. Availability of knee MRI examinations in our radiology database

The exclusion criteria were:

1. History of trauma to the knee

2. Prior open or arthroscopic knee surgery

3. Presence of rheumatologic disease or synovitis

4. Anatomical variants of the patella (e.g., bipartite patella)

5. Evidence of significant joint effusion and/or hemarthrosis

6. Presence of any intra-articular space-occupying lesion

7. Poor image quality preventing adequate evaluation

The study included 172 knee MRI examinations from 150 patients who met the inclusion criteria and had been diagnosed with patellar chondromalacia. The control group included 78 knee MRI examinations from 68 patients without patellar chondromalacia. In total, 250 knee MRI examinations were analyzed.

The study included 172 knee MRI examinations obtained from 150 patients who met the inclusion criteria and were diagnosed with patellar chondromalacia. The control group comprised 78 knee MRI examinations from 68 patients without patellar chondromalacia. In total, 250 knee MRI examinations were analyzed.

Anthropometric Measurements

Body weight and height were measured in kilograms and centimeters, respectively. Body mass index (BMI) was calculated using the following formula:

BMI = kg/m^2, where kg represents the patient's body weight and m^2 represents the square of the patient's height.

Magnetic Resonance Imaging Assessment

All knee MRI examinations were performed on a 1.5-Tesla MR system (Ingenia Evolution, Philips Medical System, Best, the Netherlands) using a standard knee protocol. Coronal T1-weighted images were acquired with TR 622 ms, TE 8 ms, FOV 18 cm, slice thickness 3 mm, and a matrix of 360×204 pixels. Sagittal proton density SPAIR (PD SPAIR) images were obtained with TR 3466 ms, TE 30 ms, FOV 18 cm, slice thickness 3 mm, and a matrix of 292×272 pixels. Axial PD SPAIR images were acquired with TR 3333 ms, TE 30 ms, FOV 18 cm, slice thickness 3 mm, and a matrix of 360×263 pixels, while coronal PD SPAIR images were obtained with TR 622 ms, TE 8 ms, FOV 18 cm, slice thickness 3 mm, and a matrix of 360×304 pixels.

IPFP Measurements

The maximal cross-sectional area of the IPFP was calculated on sagittal T2-weighted MR images using our institutional workstation (IntelliSpace Portal v12.1, Philips, Best, the Netherlands) after manually delineating its borders. IPFP depth was defined as the distance from the anterior to the posterior surface, measured along a line perpendicular to the patellar tendon (Figure 1).

Medial Subcutaneous Fat Thickness

Medial subcutaneous fat (SCF) thickness of the knee joint region was measured as an indicator of body adiposity. The measurement was performed on axial PD-weighted images and extended from the skin surface to the posteromedial aspect of the femoral condyle cortex, as illustrated in Figure 2.

MAIN POINTS

- Infrapatellar fat pad (IPFP) signal changes on magnetic resonance imaging (MRI) strongly reflect the severity of patellar chondromalacia.
- IPFP size (area or depth) does not correlate with lesion severity or location.
- Qualitative MRI assessment of the IPFP has greater diagnostic value than dimensional measures.

Patellar Chondromalacia Assessment

Patellar chondromalacia was graded from 0 to 4 on fat-suppressed proton density-weighted axial MRI images according to the MRI-adapted Outerbridge classification.

Assessment of IPFP Signal Intensity Changes

Changes in IPFP signal intensity were evaluated on sagittal fat-suppressed proton density-weighted images (Figure 3). The sagittal plane demonstrating the most prominent signal increase was selected, and edema was defined as areas of high signal on the fat-suppressed sequence. Signal intensity alterations of the IPFP were classified as follows: grade 0 = no change; grade 1 = ≤ 10% of the area; grade 2 = 10-20% of the area; grade 3 = ≥ 20% of the area. Two observers (EZ, BA) independently performed the assessments, and a random cross-check method was used to compare the observers' assessments. Intra-observer reliability, assessed using the intraclass correlation coefficient, was 0.90, while inter-observer reliability was 0.88.

RESULTS

A total of 250 knee MRI examinations were analyzed, including 78 in the control group and 172 in the patellar chondromalacia group. The mean age of the control group was 38.74 ± 12.72 years, whereas that of the patellar chondromalacia group was 50.83 ± 10.09 years, a difference that was statistically significant (P < 0.001). In the control group, 48.5% (n=33) were female and 51.5% (n=35) were male; in the patient group, 72.7% (n=109) were female and 27.3% (n=41) were male (P = 0.009). Medial SCF thickness was significantly higher in the patient group (23.57 ± 10.36 mm) compared to the control group (17.55 ± 7.31 mm; P < 0.001). Baseline characteristics, including sex, weight, and BMI, are presented in Table 1.

Correlation analysis revealed a significant relationship between sex and both the maximal IPFP cross-sectional area (r =-0.364; P < 0.001) and the IPFP depth (r = -0.338; P < 0.001), indicating that males had significantly greater maximal IPFP area and depth than females. Subgroup analyses supported this finding, showing that males had a significantly greater maximal IPFP area (667.78 ± 134.59 mm^2 vs. 533.02 ± 109.79 mm^2, P < 0.001) and depth (29.50 ± 3.49 mm vs. 25.78 ± 3.44 mm, P < 0.001) than females (Tables 2, 3).

Medial SCF thickness was not significantly correlated with IPFP area or depth. The IPFP signal intensity score demonstrated a significant positive correlation with age (r = 0.50; P < 0.001) and chondromalacia grade (r = 0.377; P < 0.001), indicating that increases in age and chondromalacia severity were associated with higher IPFP signal intensity scores. No significant correlations were observed with other variables (P > 0.05; Table 2).

The maximal IPFP cross-sectional area was significantly greater in males (667.78 ± 134.59 mm^2) than in females (533.02 ± 109.79 mm^2; P < 0.001). Comparisons according to chondromalacia grade revealed no significant differences (Grade 1: 558.66 ± 110.73 mm^2, Grade 2: 574.72 ± 129.33 mm^2,

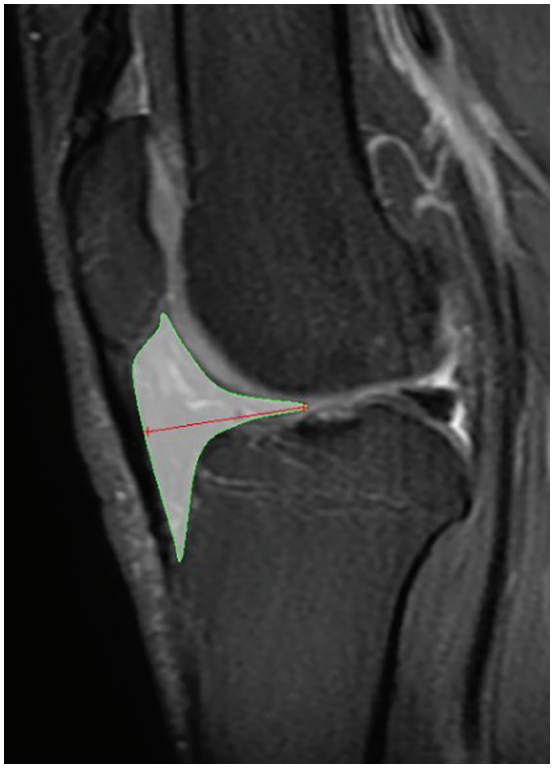

Figure 1. Sagittal T2-weighted MRI demonstrating the maximal cross-sectional area and depth of the infrapatellar fat pad (IPFP). The white shaded region represents the maximal cross-sectional area of the IPFP. The red line, drawn perpendicular to the patellar tendon from the anterior to the posterior surface, indicates the IPFP depth

MRI: Magnetic resonance imaging

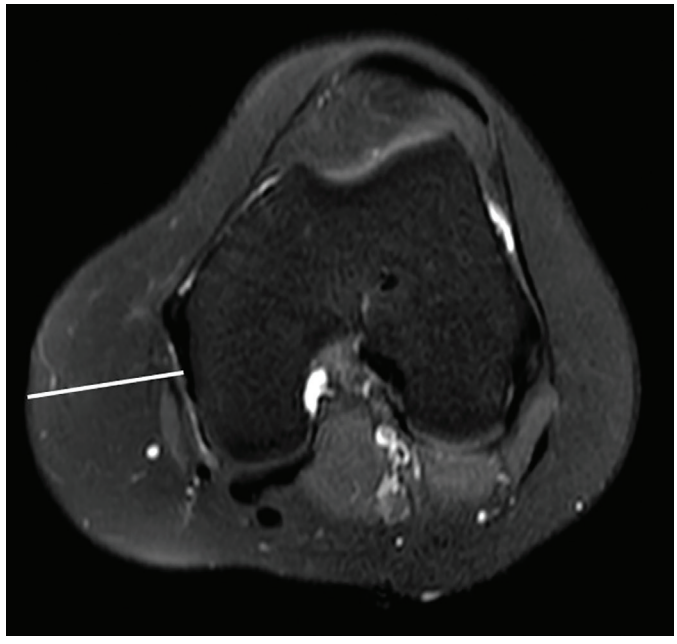

Figure 2. Measurement of subcutaneous fat thickness. Axial T2-weighted MRI of the knee demonstrating measurement of the subcutaneous fat thickness on the medial aspect of the knee joint at the level of the medial femoral condyle

MRI: Magnetic resonance imaging

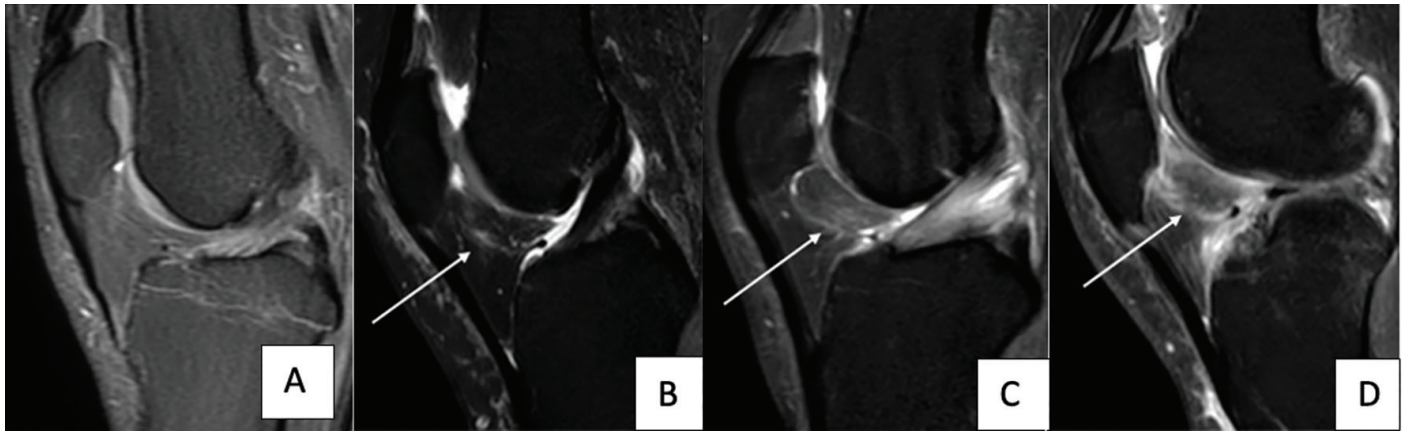

Figure 3. Classification of infrapatellar fat pad (IPFP) signal intensity alterations on MRI. The white arrows indicate regions of increased signal intensity within the IPFP. Each grade represents the percentage of IPFP involvement: Grade 0, no alteration; Grade 1, ≤ 10%; Grade 2, 10-20%; Grade 3, ≥ 20%

A) – IPFP Grade 0: No signal alteration, B) – IPFP Grade 1: Involvement of ≤10% of the IPFP area (white arrow indicates region of increased signal), C) – IPFP Grade 2: Involvement of 10-20% of the IPFP area (white arrow indicates region of increased signal), D) – IPFP Grade 3: Involvement of ≥20% of the IPFP area (white arrow indicates region of increased signal)

MRI: Magnetic resonance imaging

Grade 3: 580.00±132.66 mm^2, Grade 4: 559.91 ± 122.11 mm^2; *P* = 0.595). Similarly, no significant differences were observed in maximal IPFP area based on chondromalacia location (medial: 575.48 ± 110.15 mm^2, lateral: 553.34±152.01 mm^2, central: 602.33 ± 161.06 mm^2; *P* = 0.537) (Table 3). Regarding IPFP depth, males (29.50 ± 3.49 mm) had significantly greater values than females (25.78 ± 3.44 mm; *P* < 0.001). However, IPFP depth did not differ significantly according to chondromalacia grade (Grade 1: 27.00 ± 3.16 mm, Grade 2: 26.00 ± 3.66 mm, Grade 3: 27.45 ± 3.82 mm, Grade 4: 27.10 ± 4.14 mm; *P* = 0.512),chondromalacia location (medial: 26.83 ± 3.83 mm, lateral: 26.43 ± 3.84 mm, central: 28.00 ± 3.77 mm; *P* = 0.399), or IPFP signal intensity score (Grade 0: 26.08 ± 3.72 mm, Grade 1: 26.84 ± 4.19 mm, Grade 2: 27.47 ± 3.82 mm, Grade 3: 27.40 ± 3.15 mm; *P*=0.793) (Table 3).

DISCUSSION

Knee OA is the most common degenerative joint disease among middle-aged and elderly individuals, characterized by joint swelling, pain, and limited range of motion.[8] Depending on the location of the lesion, OA can be classified as tibiofemoral joint OA or patellofemoral joint osteoarthritis (PFOA). Studies have shown that approximately 60% of patients with symptomatic knee OA exhibit PFJ abnormalities.[9]

Several risk factors have been identified for OA, with advanced age recognized as a major contributor.[10] In the present study, PFJ degeneration was found to increase with age. This phenomenon may be attributed to the natural aging process of the PFJ and, potentially, to the effects of osteoporosis.[11] Recent studies suggest that the inflammatory milieu created by senescence-associated secretory phenotype factors associated with aging contributes to cartilage degeneration and subchondral bone remodeling, ultimately leading to cartilage loss and progression of OA.[12] In our study, we observed a moderate positive correlation between changes in IPFP signal intensity and age, indicating that IPFP alterations are closely associated with the aging process.

Consistent with previous findings, our study demonstrated a higher incidence of PFOA in females than in males.[13] Many researchers attribute this difference to estrogen levels in women. While some studies suggest that estrogen plays a protective role in OA, others report that it may contribute to the pathogenesis of the disease. This indicates that sex differences cannot be explained solely by estrogen and that other factors, such as muscle strength, lifestyle habits, and bone density, may also play important roles.[2]

Additionally, Wang and He reported that obesity is one of the most influential and modifiable risk factors for OA. In our study, patients with PFOA had a higher BMI than those in the control group. The increased load associated with overweight and obesity accelerates the progression of PFOA and induces abnormal changes in PFJ mechanics.[15] The relationship between obesity and joint degeneration is not only biomechanical but also involves adipose tissue, which can activate inflammatory processes. The IPFP plays a role in the initiation and progression of OA through the release and activation of pro-inflammatory mediators. Due to its anatomical location, the IPFP can directly influence the composition of synovial fluid, which in turn may affect other joint structures. Proinflammatory cytokines activate substance P-containing nerve fibers, which mediate anterior knee pain. These cytokines, in conjunction with adipose tissue, immune cells, and the nervous system, directly contribute to the production of chemokines, other cytokines, and growth factors. Collectively, these effects influence the metabolism and function of the synovial membrane and articular cartilage.[16]

In our study, a weak positive correlation was observed between BMI and changes in IPFP signal intensity (r=0.22; *P* < 0.02).

Table 1. Comparison of Demographic Characteristics and Infrapatellar Fat Pad (IPFP) Measurements Between Control and Patient Groups

		Control	Patient		
Variables		**Mean ± SD/median (min-max)/N (%)**	**Mean ± SD/median (min-max)/N (%)**	**t/ Z/ X^2**	***P***
Age (years)		38.74 ± 12.72	50.83 ± 10.09	-5.741*	**< 0.001**
Gender	Female	33 (48.5%)	109 (72.7)	6.805‡	**0.009**
	Male	35 (51.5%)	41 (27.3%)		
Side	Right	40 (55.5%)	87 (50.6%)	0.302‡	0.583
	Left	32 (44.5%)	85 (49.4%)		
Height (cm)		164.70 ± 6.44 165 (158-182)	165.66 ± 8.91 166 (150-183)	-0.726†	0.468
Weight (kg)		64.08 ± 9.91 67 (45-85)	82.05 ± 10.49 78 (58-103)	-8.326†	**< 0.001**
BMI (kg/m^2)		23.67 ± 3.52 23.2 (16.5-27.2)	29.99 ± 3.78 29.7 (21-41.6)	-8.077†	**< 0.001**
IPFP maximum CSA (mm^2)		544.49 ± 120.62	569.66 ± 131.03	-1.118*	0.265
IPFP depth (mm)		25.67 ± 3.99	26.79 ± 3.82	-1.637*	0.104
Medial subcutaneous fat thickness (mm)		17.55 ± 7.31 15 (7-41)	23.57 ± 10.36 21 (5-63)	-3,847†	**< 0.001**
Chondromalacia location	Medial	-	93 (54.4%)	-	-
	Lateral	-	63 (36.9%)	-	-
	Medial+lateral	-	16 (8.7%)	-	-
Chondromalacia grade	Grade 1	-	15 (8.8%)	-	-
	Grade 2	-	60 (35%)	-	-
	Grade 3	-	40 (23.2%)	-	-
	Grade 4	-	57 (33%)	-	-
IPFP signal intensity score	Grade 0	-	57 (33.1%)	-	-
	Grade 1	-	58 (33.8%)	-	-
	Grade 2	-	31 (18%)	-	-
	Grade 3	-	26 (15.1%)	-	-

*: t-value: Independent samples t-test, †: Z-value: Mann-Whitney U test, ‡: X^2-value Pearson chi-square test, BMI: Body mass index, IPFP: Infrapatellar fat pad, CSA: Cross-sectional area, IPSS: Infrapatellar fat pad signal intensity, SD: Standart deviation. *P* < 0.05 considered statistically significant (indicated in bold).

Table 2. Correlation Analysis Between İnfrapatellar Fat Pad Maximum Cross-Sectional Area, Depth, Signal Intensity Scores, and Other Variables

Variables	**IPFP maximum CSA**		**IPFP depth**		**IPFP signal intensity score**	
	r	***P***	**r**	***P***	**r**	***P***
Gender	-0.364	**< 0.001**	-0.338	**< 0.001**	0.033	0.738
Age	0.087	0.291	0.135	0.100	0.50	**< 0.001**
Side	0.058	0.481	0.141	0.086	0.03	0.766
Height	0.045	0.582	0.025	0.763	-0.096	0.335
Weight	0.150	0.066	0.158	0.054	0.106	0.287
BMI	0.097	0.237	0.107	0.192	0.229	**0.020**
Med. fat thickness	-0.150	0.067	-0.273	0.058	0.142	0.152
CM grade	-0.029	0.771	0.037	0.711	0.377	**< 0.001**
CM location	-0.052	0.599	-0.016	0.870	0.022	0.826

IPFP: Infrapatellar fat pad, CSA: Cross-sectional area, BMI: Body mass index, CM: Chondromalacia, med: medial, r: Spearman correlation coefficient; p: Significance level from Spearman correlation analysis (p<0.05 considered statistically significant)

Table 3. Comparison of Infrapatellar Fat Pad Maximum Cross-Sectional Area and Depth According to Gender, Chondromalacia Grades, Chondromalacia Locations, and IPFP Signal Intensity Scores

Variables		IPFP maximum CSA (mean ± SD)	*P* value	IPFP depth (mean ± SD)	*P* value
Gender					
	Male	667.78 ± 134.59	**< 0.001***	29.50 ± 3.49	**< 0.001***
	Female	533.02 ± 109.79		25.78 ± 3.44	
Chondromalacia grade					
	1	558.66 ± 110.73	0.595†	27.00 ± 3.16	0.512†
	2	574.72 ± 129.33		26.00 ± 3.66	
	3	580.00 ± 132.66		27.45 ± 3.82	
	4	559.91 ± 122.11		27.10 ± 4.14	
IPFP signal intensity score					
	0	569.32 ± 150.12	0.838‡	26.08 ± 3.72	0.793†
	1	573.80 ± 139.48		26.84 ± 4.19	
	2	583.57 ± 110.55		27.47 ± 3.82	
	3	543.13 ± 89.20		27.40 ± 3.15	
Chondromalacia location					
	Medial	575.48 ± 110.15	0.537‡	26.83 ± 3.83	0.399†
	Lateral	553.34 ± 152.01		26.43 ± 3.84	
	Medial+lateral	602.33 ± 161.06		28.00 ± 3.77	

*: Independent samples t-test; †: Kruskal-Wallis test, ‡: ANOVA test. $P < 0.05$ (considered statistically significant). IPFP: Infrapatellar Fat Pad, CSA: Cross-sectional area. SD: Standart deviation

This correlation suggests that as BMI increases, there may be a corresponding increase in IPFP inflammation or signal intensity. However, given the weakness of this relationship, BMI alone cannot fully explain the changes in IPFP signal, and other factors such as inflammation, mechanical stress, and synovial fluid composition are likely to contribute.

In our study, no significant relationship was found between BMI and IPFP area or depth. Similarly, Han et al.[17] reported no significant association between IPFP area and BMI. Recent studies from the United States and the Netherlands have reported that BMI is not significantly associated with IPFP volume in either the control or the OA groups.[18,19] The lack of a relationship between IPFP volume and obesity or body weight changes may be explained by the IPFP's anatomical location within the joint capsule, thereby isolating it from systemic circulation. Its limited capacity to absorb circulating free fatty acids and, consequently, its inability to increase in volume by accumulating fat have been proposed as potential mechanisms.[20]

BMI does not accurately assess fat distribution around the body and cannot distinguish adipose tissue from non-adipose body mass, which limits its utility. In contrast, measurements of SCF around the knee provide a more localized assessment of periarticular fat, offering additional information beyond BMI regarding the impact of adipose tissue changes on OA progression.[21] In our study, medial SCF thickness was significantly greater in the patient group with patellar chondromalacia than in the control group ($P < 0.001$).

Studies investigating the relationship between IPFP area and SCF thickness are limited. In our study, no significant associations were observed between medial SCF thickness and IPFP area or depth ($P = 0.067$ and $P = 0.058$, respectively). These findings are consistent with previous reports. Ragab and Serag[22] reported a weak negative correlation between SCF thickness and IPFP area ($r = 0.201$, $P < 0.01$, 95% confidence interval), although this association did not reach significance in multivariate analysis ($P = 0.14$). Similarly, Teichtahl et al.[23] found no significant relationship between body fat measures (subcutaneous fat, total body fat) and IPFP size. These findings suggest that the IPFP may be independent of systemic adiposity. Furthermore, Masaki et al.[20] reported that the IPFP is preserved even under fasting conditions. This observation supports the notion that the IPFP may represent a metabolically distinct fat depot with limited direct association with systemic fat accumulation.

In our study, the mean IPFP area for all patients was 5.69 cm^2 [±1.3 (standard deviation) SD], which is lower than the values reported by Ricatti et al.[1], 7.59 cm^2 (± 1.18 SD), and Ragab and Serag[22], 6.9 cm^2 (± 1.6 SD). This discrepancy may be attributable to differences in the demographic characteristics of the patient populations included in these studies.

In our study, males exhibited significantly greater IPFP maximum cross-sectional area ($r = -0.364$; $P < 0.001$) and depth ($r = -0.338$; $P < 0.001$) than females. This finding is consistent with previous literature. Duran et al.[24] reported a significant difference in mean IPFP area between males and females, with males having larger values ($P < 0.05$). Similarly, Han et al.[17] noted

a negative association between increased IPFP area and female sex. Although the underlying mechanisms linking sex and IPFP volume are not fully understood, sex hormones may play a role in this process. Prior studies have shown that sex hormones influence fat distribution across different anatomical regions.[25]

In our study, no significant relationship was observed between IPFP area or depth and patient age (P = 0.291 and P = 0.100, respectively). Ragab et al.[22] reported a negative correlation between IPFP area and age (r = -0.401, P < 0.001), whereas Han et al.[17] found a significant positive association between IPFP volume and age (P < 0.05). These contrasting findings suggest that the effect of age on IPFP measurements may be complex, and age-related changes in periarticular fat may vary according to individual and population-level factors.

The IPFP has long been considered a structural fat pad with minimal or no metabolic response. However, a meta-analysis by Clockaerts et al.[26] suggested that the IPFP is a complex structure containing nerve fibers, adipocytes, and immune cells, and may contribute to the progression of knee OA through the production and release of inflammatory mediators. In this context, a large-volume IPFP may induce pathological outcomes by altering cytokine release from adipocytes and other pro-arthritic mediators, or by affecting the distribution and magnitude of forces within the PFJ. Conversely, the molecular and local mechanical effects of OA developing in the PFJ may alter the local environment, potentially leading to IPFP enlargement.

Cowan et al.[27] reported that individuals with knee OA predominantly affecting the PFJ exhibited larger MRI-measured IPFP volumes compared to asymptomatic individuals, and greater IPFP volume was associated with more severe pain. In contrast, Han et al.[17] observed that individuals with larger IPFP areas had less radiographic evidence of OA. Similarly, Uludağ and Sirik found that increased IPFP dimensions were associated with a lower prevalence of patellar chondromalacia. Pan et al.[3] suggested that the IPFP may exert protective effects against mechanical and inflammatory knee pain, noting that reduction of the IPFP during knee surgery could lead to increased postoperative pain. Consequently, preservation of the normal IPFP during knee surgery has been emphasized.

These divergent findings in the literature suggest that the IPFP may play a physiologically beneficial role due to its biomechanical or anti-catabolic properties, while simultaneously potentially contributing pathologically through its pro-inflammatory or metabolic characteristics.[4]

The maximum cross-sectional area and depth of the IPFP are commonly used to define IPFP size on MRI.[1] In our study, no statistically significant differences in IPFP area or depth were observed between subjects with and without patellar chondromalacia. This finding suggests that assessing the influence of the IPFP on patellar chondromalacia based solely on dimensional parameters may be insufficient, and analysis of IPFP signal intensity changes reflecting inflammatory mediator release should also be considered. Furthermore, IPFP dimensions may be associated with multiple factors, including OA stage, subtype, and genetic predisposition. Therefore, more in-depth studies are warranted to better characterize the role of IPFP volume in OA progression.

In our study, changes in IPFP signal intensity showed a significant positive correlation with the degree of chondromalacia (r = 0.377; P < 0.001). This finding suggests that the IPFP is not merely a structural fat pad but may also be closely associated with degenerative processes in the knee joint. Our results, together with previous findings in the literature[1,28], indicate that changes in IPFP signal intensity could be considered clinically meaningful parameters, relevant not only for the diagnosis of OA but also for guiding treatment planning. The relationship between IPFP signal intensity changes on MRI and circulating inflammatory factor levels remains an important issue to be addressed in future studies.

Study Limitations

This study has several limitations. First, due to its retrospective design, the clinical information and physical examination findings for the patients were incomplete. Additionally, cartilage damage was assessed only qualitatively, which may have introduced some inaccuracies. Therefore, future studies are planned to include quantitative or semi-quantitative analyses. Due to study constraints, pathological evaluation of synovial inflammation could not be performed, potentially resulting in the overlooking of non-OA causes of synovitis.

CONCLUSION

This study demonstrated a significant relationship between IPFP signal intensity changes on MRI and the degree of patellar chondromalacia. However, the lack of a direct association of IPFP area and depth with chondromalacia suggests that the IPFP should not be evaluated solely based on dimensional measurements. Prospective studies, supported by clinical data and incorporating quantitative analyses, will help better understand the role of the IPFP in knee OA.

Ethics

Ethics Committee Approval: This retrospective study was approved by the Clinical Research Ethics Committee of the Ministry of Health University of Health Sciences Türkiye, Ankara Etlik City Hospital (approval no: 2025/0231, date: 26.02 2025).

Informed Consent: The requirement for informed consent was waived due to the retrospective nature of the study.

Footnotes

Author Contributions

Concept Design – E.Z., B.A., İ.S.D., Data Collection or Processing – E.Z., B.A., İ.S.D., Analysis or Interpretation – E.Z., B.A., Literature Review – E.Z., B.A., Writing, Reviewing and Editing – E.Z., B.A.

Declaration of Interests: The authors declare that they have no conflicts of interest.

Funding: The authors declare that this study has received no financial support.

REFERENCES

1. Ricatti G, Veronese N, Gangai I, Paparella M, Testini V, Guglielmi G. Hoffa's fat pad thickness: a measurement method with sagittal MRI sequences. *La Radiol Med.* 2021;126(6):886-893. [CrossRef]
2. Liu Z, Wu J, Xiang W, et al. Correlation between the signal intensity alteration of infrapatellar fat pad and knee osteoarthritis: a retrospective, cross-sectional study. *J Clin Med.*2023; 12(4):1331. [CrossRef]
3. Pan F, Han W, Wang X, et al. A longitudinal study of the association between infrapatellar fat pad maximal area and changes in knee symptoms and structure in older adults. *Ann Rheum Dis.*2015;74:1818-1824. [CrossRef]
4. Han W, Aitken D, Zhu Z, et al. Signal intensity alteration in the infrapatellar fat pad at baseline for the prediction of knee symptoms and structure in older adults: a cohort study. *Ann Rheum Dis* 2016;75:1783-1788. [CrossRef]
5. Uludag A, Sirik M. Effects on patellar chondromalacia of the size of the infrapatellar fat pad. *Medicine.2019;* 8(1):138-142. [CrossRef]
6. Özkoç G.Patellar kondromalazi. *Totbid Derg.*2012.11(4):335-338. [CrossRef]
7. Dejour D, Saggin PRF, Kuhn VC. Disorders of the patellofemoral joint. In: Scott WN (ed) *Insall & Scott Surgery of the Knee*, 5th edn. Philadelphia: Churchill Livingstone,2012: pp 843-844. [CrossRef]
8. Brophy RH, Fillingham YA.AAOS clinical practice guideline summary: management of osteoarthritis of the knee (nonarthroplasty). *J Am Acad Orthop Surg.*2022;30(9):e721-e729. [CrossRef]
9. Duncan RC, Hay EM, Saklatvala J, Croft PR. Prevalence of radiographic osteoarthritis—it all depends on your point of view. *Rheumatology.2006;*45(6):757-760. [CrossRef]
10. Liu Y, Zhang Z, Li T, Xu H, Zhang H. Senescence in osteoarthritis: from mechanism to potential treatment. *Arthritis Res Ther.2022;* 24:174. [CrossRef]
11. Zhao J, Liu J, Han J, et al.Analysis of risk factors on patellofemoral osteoarthritis: distribution characteristics and radiographic parameters of patellofemoral joint. *Orthop Surg.2024;* 16:3151-3161. [CrossRef]
12. Childs BG, Durik M, Baker DJ, Van Deursen JM. Cellular senescence in aging and age-related disease: from mechanisms to therapy. *Nat Med.*2015; 21:1424-1435. [CrossRef]
13. Kobayashi S, Pappas E, Fransen M, Refshauge K, Simic M.The prevalence of patellofemoral osteoarthritis: a systematic review and meta-analysis. *Osteoarthritis Cartilage.2016;*24(10):1697–1707. [CrossRef]
14. Wang T, He C. Pro-inflammatory cytokines: the link between obesity and osteoarthritis. *Cytokine Growth Factor Rev.*2018. 44:38-50. [CrossRef]
15. Tamayo KS, Heckelman LN, Spritzer CE, DeFrate LE, Collins AT. Obesity impacts the mechanical response and biochemical composition of patellofemoral cartilage: an in vivo, MRI-based investigation. *J Biomech.* 2022;134:110991. [CrossRef]
16. Paduszyński W, Jeśkiewicz M, Uchański P, Gackowski S, Radkowski M, Demkow U. Hoffa's fat pad abnormality in the development of knee osteoarthritis. *Curr Concepts Med Res Pract.*2018. 95-102. [CrossRef]
17. Han W, Cai S, Liu Z, et al.Infrapatellar fat pad in the knee: is local fat good or bad for knee osteoarthritis? *Arthritis Res Ther.*2014;16:1-8. [CrossRef]
18. Chuckpaiwong B, Charles HC, Kraus VB, Guilak F, Nunley JA. Age-associated increases in the size of the infrapatellar fat pad in knee osteoarthritis as measured by 3T MRI. *J Orthop Res.*2010;28(9):1149-1154. [CrossRef]
19. de Jong AJ, Klein-Wieringa IR, Andersen SN, et al.Lack of high BMI-related features in adipocytes and inflammatory cells in the infrapatellar fat pad (IFP). *Arthritis Res Ther.*2017; 19:1-12. [CrossRef]
20. Masaki T, Takahashi K, Hashimoto S, et al. Volume change in infrapatellar fat pad is associated not with obesity but with cartilage degeneration. *J Orthop Res.*2019.37(3):593-600. [CrossRef]
21. Joseph GB, Takakusagi M, Arcilla G, et al. Associations between weight change, knee subcutaneous fat and cartilage thickness in overweight and obese individuals: 4-year data from the osteoarthritis initiative. *Osteoarthritis Cartilage.2023;* 31(11):1515-1523. [CrossRef]
22. Ragab E, Serag D. Infrapatellar fat pad area on knee MRI: does it correlate with the extent of knee osteoarthritis? *Egypt J Radiol Nucl Med.2021;* 52:1-9. [CrossRef]
23. Teichtahl AJ, Wulidasari E, Brady SR, et al. A large infrapatellar fat pad protects against knee pain and lateral tibial cartilage volume loss. *Arthritis Res Ther.*2015;17:1-7. [CrossRef]
24. Duran S, Akşahin E, Kocadal O, Aktekin CN, Hapa O, Genctürk ZB. Effects of body mass index, infrapatellar fat pad volume and age on patellar cartilage defect. *Orthop J Sports Med.*2014;2(11_suppl3):2325967114S00159. [CrossRef]
25. Blaak E. Gender differences in fat metabolism. *Curr Opin Clin Nutr Metab Care.*2001;4(6):499-502. [CrossRef]
26. Clockaerts S, Bastiaansen-Jenniskens YM, Runhaar J, et al.The infrapatellar fat pad should be considered as an active osteoarthritic joint tissue: a narrative review. *Osteoarthritis Cartilage.*2010; 18:876-882. [CrossRef]
27. Cowan SM, Hart HF, Warden SJ, Crossley KM.Infrapatellar fat pad volume is greater in individuals with patellofemoral joint osteoarthritis and associated with pain. *Rheumatol Int.2015;* 35:1439-1442. [CrossRef]
28. Zhang Y, Nevitt M, Niu J, et al. Fluctuation of knee pain and changes in bone marrow lesions, effusions, and synovitis on magnetic resonance imaging. *Arthritis Rheum.2011;* 63(3):691-699. [CrossRef]

ABCResearch

Arch Basic Clin Res 2026;8(2):143-149
DOI: 10.4274/ABCR.2026.25402

Research Article

The Relationship Between Mammographic Features of BI-RADS 4 and 5 Calcifications and Pathological Diagnoses

Ayça Seyfettin[1], Emre Utkan Büyükceran[1], Zeynep Eskalen[1], Andelib Babatürk[1], Kemal Buğra Memiş[2], Esin Kaymaz[3], Serap Gültekin[4]

[1]Clinic of Radiology, Private Ankara Güven Hospital, Ankara, Türkiye
[2]Department of Radiology, Erzincan Binali Yıldırım University Faculty of Medicine, Erzincan, Türkiye
[3]Clinic of Pathology, Private Ankara Güven Hospital, Ankara, Türkiye
[4]Department of Radiology, Gazi University Faculty of Medicine, Ankara, Türkiye

Cite this article as: Seyfettin A, Büyükceran EU, Eskalen Z, et al. The relationship between mammographic features of BI-RADS 4 and 5 calcifications and pathological diagnoses. *Arch Basic Clin Res*.2026;8(2):143-149.

ORCID IDs of the authors: A.S. 0000-0002-8540-9432, E.U.B. 0000-0001-6912-7737, Z.E. 0000-0001-7671-5131, A.B. 0000-0002-8406-6159, K.B.M. 0000-0007-6746-3906, E.K. 0000-0003-4127-6559, S.G. 0000-0002-4973-0624.

ABSTRACT

Objective: To evaluate the relationship between mammographic features of BI-RADS category 4 and 5 breast calcifications and their corresponding pathological diagnoses, and to determine whether specific morphological or distribution patterns are predictive of malignancy.

Methods: This retrospective study included 54 patients who underwent biopsy for suspicious breast calcifications between August 2021 and March 2024. Among these patients, 30 underwent stereotactic vacuum-assisted biopsy, and 24 underwent wire-guided localization followed by excisional biopsy. The mammographic morphology and distribution patterns of the calcifications were assessed using the BI-RADS lexicon, and the corresponding histopathological diagnoses were recorded. The association between mammographic features and pathological outcomes was subsequently analyzed.

Results: Fine pleomorphic calcifications were the most common morphology (40.7%). A grouped distribution was the predominant pattern (61.1%). Benign lesions were mostly categorized as BI-RADS 4A, B3 lesions as BI-RADS 4B, and DCIS cases as BI-RADS 4C (P = 0.03). The Grouped distribution was more frequent among benign and B3 lesions, whereas DCIS exhibited more frequent linear and segmental patterns (P = 0.01). Malignancy rates were highest for fine linear/branching and fine pleomorphic morphologies.

Conclusion: A significant association exists between the mammographic characteristics of BI-RADS 4 and 5 calcifications and their pathological outcomes. In our study, fine pleomorphic morphology and linear or segmental distribution patterns consistently indicated a increased likelihood of malignancy, particularly ductal carcinoma *in situ*, whereas benign and B3 lesions were more commonly associated with grouped distribution patterns. These results highlight that detailed evaluation of calcification morphology and distribution on mammography can improve diagnostic confidence, aid in distinguishing higher-risk lesions, and contribute to more informed biopsy decision-making.

Keywords: BI-RADS, breast calcifications, mammography, breast malignancy, pathology correlation

Corresponding author: Ayça Seyfettin, **E-mail:** aycaseyfettin@hotmail.com

Received: January 12, 2026
Revision Requested: February 20, 2026 **Accepted:** May 25, 2026 **Publication Date:** July, 14, 2026

This study presented as an oral presentation at the TÜKRAD 2024 Congress.

INTRODUCTION

Breast cancer is the most commonly diagnosed malignancy among women worldwide, and early detection constitutes one of the principal determinants in reducing disease-related mortality.[1] Mammography, as the primary imaging modality for breast cancer screening, plays a pivotal role in the detection of microcalcifications, which may represent one of the earliest radiological manifestations of ductal carcinoma *in situ* (DCIS) and invasive carcinoma.[2] Breast calcifications are among the most frequently encountered findings in mammographic practice and represent one of the most challenging features for radiologists in terms of diagnostic interpretation.[3] The mammographic evaluation of breast calcifications constitutes a well-recognized diagnostic challenge in breast imaging, largely attributable to the substantial overlap in morphological and distributional characteristics between benign entities and malignant lesions.[4]

To address the diagnostic challenges associated with the overlapping mammographic appearances of breast calcifications, the Breast Imaging Reporting and Data System (BI-RADS) was developed to standardize lesion description and stratify malignancy risk based on morphological and distributional criteria.[5]

Despite advances in mammographic interpretation and standardized classification, suspicious breast calcifications often require image-guided tissue sampling, as stereotactic core needle biopsy remains the reference standard for distinguishing benign from malignant findings on mammography.[6]

The aim of this study is to systematically evaluate the association between the morphological and distributional mammographic characteristics of non-mass-associated BI-RADS category 4 and 5 breast calcifications and their corresponding histopathological diagnoses, and to assess the diagnostic value of specific mammographic patterns for predicting malignancy, with particular emphasis on early-stage breast cancer. Through a detailed analysis of the correlation between mammographic findings and pathological outcomes in cases with isolated calcifications, this study aims to facilitate earlier detection of malignancy while minimizing unnecessary invasive procedures.

MAIN POINTS

- A significant association was identified between the mammographic morphology and distribution patterns of BI-RADS 4-5 calcifications and their corresponding pathological diagnoses.
- Fine pleomorphic and fine linear/branching calcifications were associated with the highest malignancy rates and were strong predictors of malignancy, particularly of ductal carcinoma *in situ*.
- Linear and segmental distribution patterns were observed more frequently in malignant lesions, whereas benign and B3 lesions predominantly demonstrated grouped distributions.
- Detailed assessment of calcification morphology and distribution improves the accuracy of malignancy risk estimation and strengthens biopsy decision-making.

MATERIAL AND METHODS

In this retrospective study, 54 patients who underwent interventional procedures for non-mass-associated suspicious breast calcifications detected on mammography at the Ankara Güven Hospital Breast Unit between August 2021 and March 2024 were evaluated. Of these patients, 30 underwent stereotactic vacuum-assisted biopsy, while 24 underwent wire-guided excisional biopsy. The mammographic features and corresponding histopathological diagnoses of all cases were reviewed retrospectively. Ethical approval for this study was obtained from the Erzincan Binali Yıldırım University Non-Interventional Clinical Research Ethics Committee (approval date: 18.09.2025, decision no: 2025-16/08).

All mammographic examinations were retrospectively evaluated by two breast radiologists with 20 and 3 years' experience, respectively. The senior radiologist reviewed all cases, and consensus-based final assessments were established. Both radiologists were blinded to histopathological outcomes. Interobserver agreement analysis was not performed; final assessments were based on consensus between the two radiologists. Breast calcifications were evaluated in accordance with the criteria defined in the American College of Radiology (ACR) BI-RADS® Atlas, Fifth Edition. Standard mammographic views were reviewed, and magnification views were used when available to allow detailed evaluation of calcification morphology. Calcifications were classified based on their morphological characteristics as amorphous, coarse heterogeneous, fine pleomorphic, fine linear, fine linear branching, and punctate. In addition, the distribution patterns of calcifications were assessed and categorized as diffuse, regional, grouped, linear, or segmental.[7]

Suspicious breast calcifications were assigned BI-RADS assessment categories based on a combined evaluation of calcification morphology and distribution patterns, in accordance with the ACR BI-RADS® Atlas, Fifth Edition. Subcategorization of BI-RADS category 4 lesions (4A, 4B, and 4C) was performed using established criteria integrating morphologic descriptors and distribution characteristics, as previously described in the literature. Amorphous calcifications with a regional or grouped distribution were categorized as BI-RADS 4A, whereas those with a linear or segmental distribution were classified as BI-RADS 4B. Coarse heterogeneous calcifications were categorized as BI-RADS 4B regardless of their distribution pattern. Fine pleomorphic calcifications with grouped distribution were classified as BI-RADS 4B, while those exhibiting linear or segmental distribution were assigned BI-RADS 4C. Calcifications with fine linear or fine-linear branching morphology were categorized as BI-RADS 4C when grouped, and as BI-RADS 5 when associated with a linear or segmental distribution, particularly when newly developed. Additionally, punctate calcifications demonstrating interval increase and clustering on follow-up mammography were categorized as BI-RADS 4A.[8]

Stereotactic vacuum-assisted biopsies were performed in the mammography unit with the patient seated upright, using a full-field digital mammography system (MAMMOMAT Revelation, Siemens Healthineers, Erlangen, Germany). Prior to the procedure, the skin overlying the target area was cleansed with an antiseptic solution, and the procedure was carried out under sterile conditions. Local anesthesia was administered using 1% lidocaine to ensure adequate analgesia.

After target localization under mammographic guidance and breast compression, tissue sampling was performed using a 10-gauge vacuum-assisted biopsy system (EnCor, USA). During the procedure, an initial 360° probe rotation was performed and multiple tissue samples were obtained. Specimen radiography was subsequently performed, and the retrieved samples were evaluated to confirm that they adequately represented the target calcifications. If the lesion was not considered sufficiently represented, an additional 360° rotation of the probe was performed.

Histopathological evaluation of biopsy or surgical excision specimens was performed by an experienced breast pathologist with 10 years' experience, and diagnoses were categorized according to the 2019 World Health Organization Classification of Tumours of the Breast. Pathological outcomes were classified as benign lesions, B3 lesions, DCIS, and invasive breast carcinoma. B3 lesions include atypical ductal hyperplasia, flat epithelial atypia, classic lobular intraepithelial neoplasia, radial scar, complex sclerosing lesion, papillary lesions, and benign or borderline phyllodes tumors.[9]

Statistical Analysis

Statistical analyses were performed using the Statistical Package for the Social Sciences for Windows (SPSS), version 25.0 (IBM Corp., Armonk, NY, USA). Continuous variables were summarized as mean ± standard deviation or median (minimum-maximum), as appropriate, while categorical variables were expressed as frequencies and percentages. Associations between mammographic characteristics of breast calcifications, including morphological features and distribution patterns, and histopathological outcomes were evaluated using the chi-square test. Comparisons were primarily conducted between benign and malignant pathological groups to assess the diagnostic significance of specific mammographic patterns. A two-tailed *P* value of less than 0.05 was considered statistically significant.

RESULTS

The mammographic characteristics of calcifications in the 54 included cases are summarized in Table 1. With respect to morphology, the most frequently observed calcification type was fine pleomorphic, which was identified in 22 cases (40.7%). This was followed by amorphous calcifications in 12 cases (22.2%) and punctate calcifications in 10 cases (18.5%). Coarse heterogeneous calcifications were observed in 8 cases (14.8%), whereas fine linear calcifications were identified in 2 cases (3.7%). The majority of calcifications demonstrated a grouped distribution (33 cases, 61.1%). Regional distribution was observed in 11 cases (20.4%), while linear and segmental distributions were each identified in 5 cases (9.3%). According to BI-RADS assessment categories, 45% of cases were classified as BI-RADS 4A, 33% as BI-RADS 4B, 20% as BI-RADS 4C, and 2% as BI-RADS 5.

Among the 54 cases included in the study, histopathological examination revealed DCIS in 20 cases (37%), benign lesions in 18 cases (33%), and B3 lesions in 15 cases (28%). Invasive carcinoma was identified in 1 case (2%). In patients who underwent subsequent surgical excision following stereotactic vacuum-assisted biopsy, no histopathological diagnostic upgrade was observed. Because only one patient was diagnosed with invasive carcinoma, this subgroup was not included in the statistical analysis owing to the insufficient sample size.

Benign and B3 lesions more frequently showed grouped distributions, whereas DCIS lesions were more commonly associated with linear and segmental distributions; this difference was statistically significant (P = 0.01). When distribution patterns were ranked by malignancy rate, the highest rate occurred in the segmental distribution, followed by the linear, grouped, and regional distributions.

Although differences in calcification morphology among pathological diagnosis groups did not reach statistical significance, malignancy rates decreased in the following order: fine linear or fine linear branching, fine pleomorphic, coarse heterogeneous, amorphous, and punctate calcifications. Detailed results regarding morphology and distribution patterns are presented in Table 2.

Independent of these findings, benign lesions were most frequently classified as BI-RADS 4A; B3 lesions were predominantly categorized as BI-RADS 4B; and DCIS cases were most commonly assigned to BI-RADS 4C. This distribution demonstrated a statistically significant association between BI-RADS assessment categories and histopathological diagnoses (P = 0.03).

Representative Cases

Case 1

A screening mammography examination demonstrated grouped amorphous calcifications in the retroareolar region of the left breast. Based on the morphological appearance and

Table 1. Mammographic Morphological and Distributional Characteristics of Breast Calcifications

	N	%
Morphology		
Amorphous	12	22.2
Fine linear	2	3.7
Fine pleomorphic	22	40.7
Coarse heterogeneous	8	14.8
Punctate	10	18.5
Distribution		
Regional	11	20.4
Grouped	33	61.1
Linear	5	9.3
Segmental	5	9.3

distribution pattern, the findings were categorized as BI-RADS 4A. The Craniocaudal mammographic view demonstrated the calcifications (Figure 1a), and subsequent magnification views were obtained to further characterize their morphology (Figure 1b). Stereotactic vacuum-assisted biopsy was subsequently performed, and radiographic images acquired during the biopsy procedure demonstrated accurate targeting of the calcifications (Figure 1c). Specimen radiography confirmed adequate sampling of the calcifications (Figure 1d). Histopathological examination revealed columnar cell change without atypia accompanied by apocrine metaplasia, consistent with a benign diagnosis.

Case 2

Mammography revealed grouped fine pleomorphic calcifications in the retroareolar region of the left breast, which were assessed as BI-RADS 4B. The craniocaudal mammographic view demonstrated the clustered calcifications (Figure 2a). Stereotactic vacuum-assisted biopsy was subsequently performed, and the scout image obtained during the biopsy procedure confirmed accurate localization of the target area (Figure 2b). Specimen radiography verified successful retrieval of the calcifications (Figure 2c). Histopathological examination revealed atypical lobular hyperplasia, consistent with a B3 lesion.

Case 3

Mammographic evaluation, performed in the setting of bloody nipple discharge, revealed newly developed, segmental, fine linear, and pleomorphic calcifications in the lower inner quadrant of the right breast, raising high suspicion for malignancy. The findings were categorized as BI-RADS 5. The c raniocaudal mammographic view demonstrated a segmental distribution of calcifications (Figure 3a), and magnification views further delineated the calcifications' fine linear and pleomorphic morphology (Figure 3b). Stereotactic vacuum-assisted biopsy was subsequently performed, and images obtained during the procedure confirmed accurate targeting of the calcifications (Figure 3c). Specimen radiography demonstrated successful retrieval of the calcifications (Figure 3d). Histopathological examination confirmed the diagnosis of DCIS, which was consistent with the highly suspicious imaging features.

Table 2. Association of Calcification Morphology, Distribution Patterns, and BI-RADS Assessment Categories with Histopathological Diagnosis in Non-Mass-Associated Suspicious Breast Calcifications

Category	Subgroup	Benign n (%)	B3 n (%)	DCIS n (%)	*P* value
Morphology	Amorphous	4 (22.2)	5 (33.3)	3 (15.0)	0.29
	Fine linear	0 (0.0)	0 (0.0)	2 (10.0)	
	Fine pleomorphic	3 (16.7)	7 (46.7)	11 (55.0)	
	Coarse heterogeneous	3 (16.7)	3 (20.0)	2 (10.0)	
	Punctate	8 (44.4)	0 (0.0)	2 (10.0)	
Distribution	Regional	4 (22.2)	3 (20.0)	3 (15.0)	**0.01**
	Grouped	14 (77.8)	10 (66.7)	9 (45.0)	
	Linear	0 (0.0)	2 (13.3)	3 (15.0)	
	Segmental	0 (0.0)	0 (0.0)	5 (25.0)	
BI-RADS	4A	18 (100.0)	2 (13.3)	4 (20.0)	**0.03**
	4B	0 (0.0)	10 (66.7)	7 (35.0)	
	4C	0 (0.0)	3 (20.0)	8 (40.0)	
	5	0 (0.0)	0 (0.0)	1 (5.0)	

DCIS, ductal carcinoma in situ; BI-RADS, Breast Imaging Reporting and Data System. The invasive carcinoma subgroup (n=1) was excluded from the statistical analysis because only one case was identified.

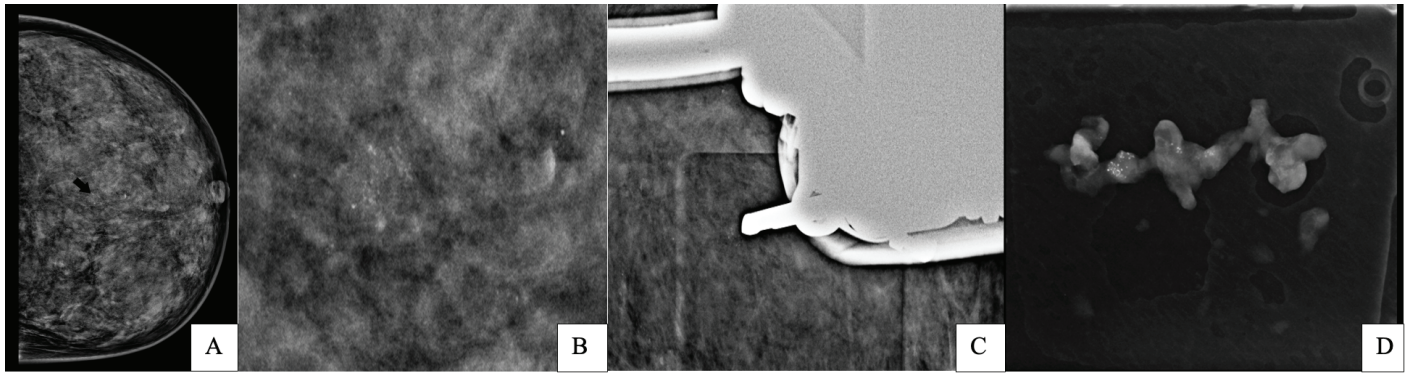

Figure 1. BI-RADS 4A calcifications. (a) Craniocaudal mammographic view shows grouped amorphous calcifications in the retroareolar region of the left breast (arrow). (b) Magnification view further characterizes the amorphous morphology. (c) Stereotactic vacuum-assisted biopsy image confirms accurate targeting. (d) Specimen radiograph demonstrates retrieval of calcifications.

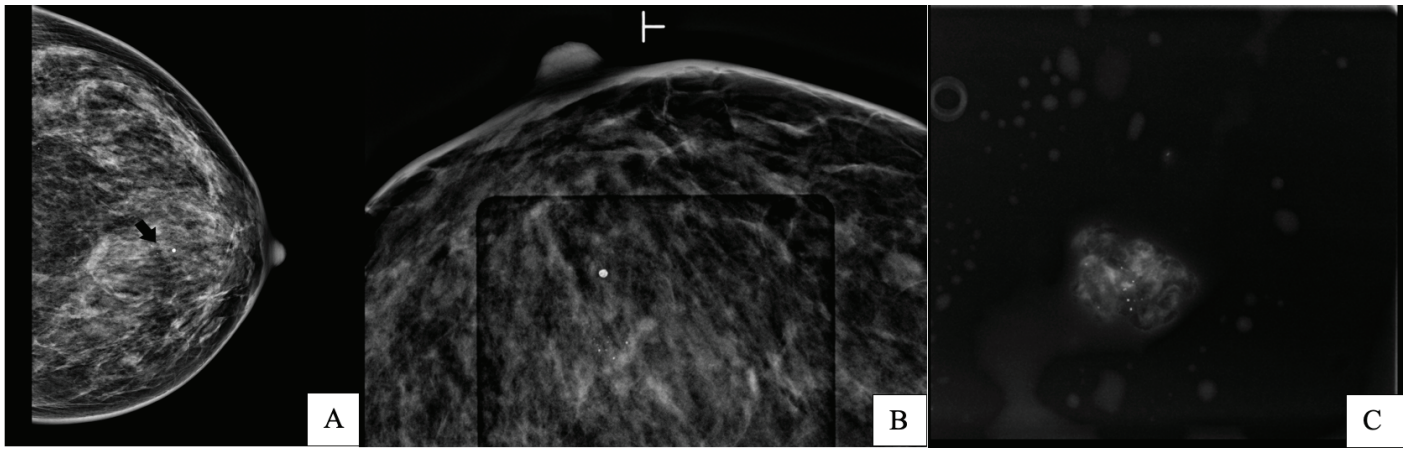

Figure 2. BI-RADS 4B calcifications. (a) Craniocaudal mammographic view demonstrates grouped fine pleomorphic calcifications in the retroareolar region of the left breast (arrow). (b) Scout image obtained during stereotactic vacuum-assisted biopsy confirms accurate localization. (c) Specimen radiograph demonstrates retrieval of calcifications.

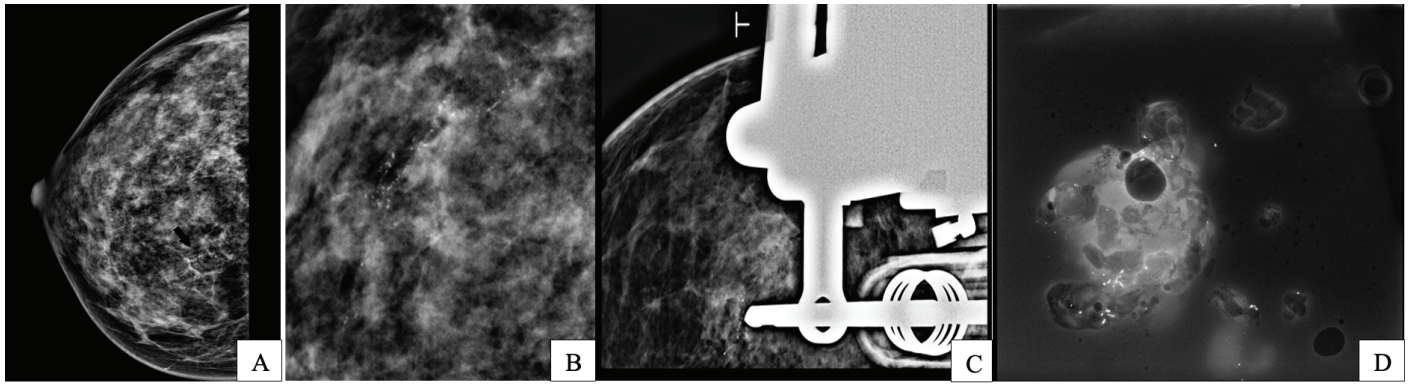

Figure 3. BI-RADS 5 calcifications. (a) Craniocaudal mammographic view demonstrates newly developed segmental fine linear and pleomorphic calcifications in the lower inner quadrant of the right breast (arrow). (b) Magnification view highlights the fine linear and pleomorphic morphology. (c) Stereotactic vacuum-assisted biopsy image confirms accurate targeting. (d) Specimen radiograph demonstrates retrieval of calcifications.

DISCUSSION

In this study, the relationship between mammographic features of non-mass-associated suspicious breast calcifications and histopathological diagnoses was evaluated. The findings demonstrated that calcification distribution patterns and BI-RADS assessment categories were significantly associated with pathological outcomes, whereas morphological characteristics alone were not sufficiently discriminative. In particular, grouped distribution patterns were more frequently observed in benign and B3 lesions, while linear and segmental distribution patterns were more strongly associated with DCIS. These results underscore the importance of calcification distribution patterns and BI-RADS classification in evaluating suspicious breast calcifications and guiding clinical decision-making.

Distribution patterns of calcification were significantly associated with histopathological diagnoses. The higher frequency of grouped distribution in benign and B3 lesions suggests that this pattern predominantly reflects localized and limited proliferative processes. In contrast, the stronger association of linear and segmental distribution patterns with DCIS may be explained by these patterns, which represent pathological processes that extend along the ductal system. Consistent with previous reports, linear and segmental distributions of calcifications, indicative of ductal spread, are associated with a higher risk of malignancy, particularly DCIS.[8,10-12] In this context, the assessment of distribution patterns emerges as an independent and robust indicator for the differential diagnosis of non–mass-associated suspicious breast calcifications.

Analysis of calcification morphology revealed no statistically significant association with histopathological diagnoses, although there was a trend toward higher malignancy rates in certain suspicious morphological subtypes. This finding may be attributed to the well-documented overlap in the mammographic morphologies of calcifications between benign and malignant lesions. Although fine linear, fine linear branching, and fine pleomorphic calcifications have traditionally been associated with an increased risk of malignancy, these morphologic patterns may also be encountered in benign or borderline lesions, thereby limiting their specificity in differential diagnosis.[13] Accordingly, calcification morphology, while informative, appears insufficient as a standalone predictor

of malignancy and should be interpreted in conjunction with distribution patterns and the overall imaging context, particularly in cases of suspicious, non-mass-associated breast calcifications.

Evaluation of BI-RADS assessment categories revealed a significant correlation between the categories and histopathological outcomes in this cohort. The predominance of benign lesions within the BI-RADS 4A category is consistent with prior reports describing this subgroup as comprising findings with a relatively low probability of malignancy.[14,15] In contrast, B3 lesions were more frequently classified as BI-RADS 4B, reflecting their intermediate and uncertain malignant potential. DCIS was most commonly associated with BI-RADS 4C, highlighting the ability of BI-RADS subcategorization to capture progressively increasing malignancy risk. Previous studies have demonstrated that subdivision of BI-RADS category 4 into 4A, 4B, and 4C facilitates more homogeneous risk stratification and supports clinical decision-making by balancing the avoidance of unnecessary invasive procedures with the early detection of breast cancer.[16-20] Nevertheless, given the broad range of malignancy probabilities encompassed by BI-RADS category 4, imaging findings alone remain insufficient for a definitive diagnosis, particularly for calcification-based lesions. Accordingly, histopathological confirmation remains essential for the management of non–mass-associated suspicious breast calcifications classified as BI-RADS 4 and 5.

Study Limitations

This study has several limitations that should be acknowledged. First, the retrospective design may be associated with inherent selection bias and limited control over imaging acquisition parameters and follow-up protocols. Second, the relatively small sample size may have reduced the statistical power of the analyses and limited the generalizability of the findings. Because only one patient in the cohort was diagnosed with invasive carcinoma, the invasive carcinoma subgroup could not be included in the statistical analyses, precluding a comprehensive evaluation of invasive malignancies. Furthermore, the limited number of cases in specific subgroups restricted detailed statistical analyses of combined morphology-distribution patterns and their associations with histopathological diagnoses, particularly for less frequent combinations such as segmental amorphous or regional fine pleomorphic calcifications.

CONCLUSION

Subcategorization of suspicious breast calcifications based on distribution patterns and BI-RADS assessment categories contributes to more accurate estimation of malignancy risk and more appropriate clinical management. Our findings emphasize that integrating distribution patterns with standardized BI-RADS subcategories improves risk stratification beyond morphologic assessment alone, thereby helping to balance avoidance of unnecessary invasive procedures with timely detection of early breast cancer. Nevertheless, given the inherent limitations of retrospective analyses and the complexity of calcification-based lesions, further prospective studies with larger patient cohorts are warranted. Future research incorporating additional imaging parameters, such as contrast-enhanced mammography and artificial intelligence-based decision support systems, may further refine diagnostic accuracy and optimize management strategies for non-mass-associated suspicious breast calcifications.

Ethics

Ethics Committee Approval: Ethical approval for this study was obtained from the Erzincan Binali Yıldırım University Non-Interventional Clinical Research Ethics Committee (approval date: 18.09.2025, decision no: 2025-16/08).

Informed Consent: Due to the nature of the retrospective study, written informed consent form was waived.

Footnotes

Author Contributions

Concept Design – A.S., E.U.B., Z.E., A.B., K.B.M., E.K., S.G.; Data Collection or Processing – A.S., A.B.; Analysis or Interpretation – A.S., S.G.; Literature Review – Z.E., K.B.M.; Writing, Reviewing and Editing – A.S., E.U.B., Z.E., A.B., K.B.M., E.K., S.G.

Declaration of Interest: The authors declared no conflicts of interest.

Funding: The authors declare that this study has received no financial support.

REFERENCES

1. Łukasiewicz S, Czeczelewski M, Forma A, Baj J, Sitarz R, Stanisławek A. Breast cancer-epidemiology, risk factors, classification, prognostic markers, and current treatment strategies-an updated review. *Cancers(Basel)*. 2021;13(17).4287. [CrossRef]
2. Azam S, Eriksson M, Sjölander A, et al. Mammographic microcalcifications and risk of breast cancer. *British Journal of Cancer*. 2021;125(5):759-765. [CrossRef]
3. Logullo AF, Prigenzi KCK, Nimir C, Franco AFV, Campos M. Breast microcalcifications: Past, present and future (Review). *Mol Clin Oncol*. 2022;16(4):81. [CrossRef]
4. Yamada T, Mori N, Watanabe M, et al. Radiologic-pathologic correlation of ductal carcinoma in situ. *Radiographics*. 2010;30(5):1183-1198. [CrossRef]
5. Narayan AK, Keating DM, Morris EA, Mango VL. Calling all calcifications: a retrospective case control study. *Clinical Imaging*.2019;53:151-154. [CrossRef]
6. Itani M, Griffin AT, Whitman GJ. Mammography of breast calcifications. *Imaging in Medicine*. 2013;5:63-74. [CrossRef]
7. Spak DA, Plaxco JS, Santiago L, Dryden MJ, Dogan BE. BI-RADS(®) fifth edition: a summary of changes. *Diagn Interv Imaging*.2017;98(3):179-190. [CrossRef]
8. Kim SY, Kim HY, Kim EK, Kim MJ, Moon HJ, Yoon JH. Evaluation of malignancy risk stratification of microcalcifications detected on mammography: a study based on the 5th edition of BI-RADS. *Ann Surg Oncol*.2015;22(9):2895-2901. [CrossRef]
9. Tan PH, Ellis I, Allison K, et al. The 2019 World Health Organization classification of tumours of the breast. *Histopathology*. 2020;77(2):181-185. [CrossRef]

10. Bent CK, Bassett LW, D'Orsi CJ, Sayre JW. The positive predictive value of BI-RADS microcalcification descriptors and final assessment categories. *AJR Am J Roentgenol*.2010;194(5):1378-1383. [CrossRef]

11. Choi WJ, Han K, Shin HJ, Lee J, Kim EK, Yoon JH. Calcifications with suspicious morphology at mammography: should they all be considered with the same clinical significance? *Eur Radiol*.2021;31(4):2529-2538. [CrossRef]

12. Oligane HC, Berg WA, Bandos AI, et al. Grouped amorphous calcifications at mammography: frequently atypical but rarely associated with aggressive malignancy. *Radiology*.2018;288(3):671-679. [CrossRef]

13. Kaltenbach B, Brandenbusch V, Möbus V, et al. A matrix of morphology and distribution of calcifications in the breast: Analysis of 849 vacuum-assisted biopsies. *Eur J Radiol*.2017;86:221-226. [CrossRef]

14. Kim J, Kim EK, Kim MJ, Moon HJ, Yoon JH. "Category 4A" microcalcifications: how should this subcategory be applied to microcalcifications seen on mammography? *Acta Radiol*. 2018;59(2):147-153. [CrossRef]

15. Wang H, Hu Y, Lu Y, Zhou J, Guo Y. The uncertainty of boundary can improve the classification accuracy of BI-RADS 4A ultrasound image. *Med Phys*. 2022;49(5):3314-3324. [CrossRef]

16. Mohapatra SK, Mishra A, Sahoo TK, Nayak RB, Das PK, Nayak B. The positive predictive values of the breast imaging reporting and data system (BI-RADS) 4 Lesions and its Mammographic Morphological Features. *Indian J Surg Oncol*. 2021;12(1):182-189. [CrossRef]

17. Li J, Zheng H, Cai W, Wang Y, Zhang H, Liao M. Subclassification of BI-RADS 4 Magnetic Resonance Lesions: A Systematic Review and Meta-Analysis. *J Comput Assist Tomogr*. 2020;44(6):914-920. [CrossRef]

18. Yoon JH, Kim MJ, Moon HJ, Kwak JY, Kim EK. Subcategorization of ultrasonographic BI-RADS category 4: positive predictive value and clinical factors affecting it. *Ultrasound Med Biol*. 2011;37(5):693-639. [CrossRef]

19. Strigel RM, Burnside ES, Elezaby M, et al. Utility of BI-RADS Assessment Category 4 Subdivisions for Screening Breast MRI. *American Journal of Roentgenology*.2017;208(6):1392-1399. [CrossRef]

20. Elverici E, Barça AN, Aktaş H, et al. Nonpalpable BI-RADS 4 breast lesions: sonographic findings and pathology correlation. *Diagn Interv Radiol*.2015;21(3):189-94. [CrossRef]

ABCResearch

Arch Basic Clin Res 2026;8(2):150-156
DOI: 10.4274/ABCR.2026.26450

Research Article

Evaluation of Aortic and Pulmonary Artery Diameters Using Computed Tomography Angiography

Halime Kabalcı[1], Ali Osman Gülmez[2]

[1]Department of Anatomy, Kahramanmaraş Sütçü İmam University Faculty of Medicine, Kahramanmaraş, Türkiye
[2]Department of Radiology, Erzincan Binali Yıldırım University Faculty of Medicine, Erzincan, Türkiye

Cite this article as: Kabalcı H, Gülmez AO. Evaluation of aortic and pulmonary artery diameters using computed tomography angiography. *Arch Basic Clin Res*. 2026;8(2):150-156.

ORCID IDs of the authors: H.K. 0009-0009-2027-1653, A.O.G. 0000-0001-7050-1765.

ABSTRACT

Objective: The truncus pulmonalis, the main pulmonary artery (MPA), originates from the right ventricle at the level of the upper edge of the left third rib cartilage and carries blood to both lungs. After a short course, it branches into two arteries beneath the aortic arch: the right pulmonary artery (RPA) and the left pulmonary artery (LPA). The aorta, the main artery that carries blood to the body, originates from the left ventricle. It is divided into three sections: the ascending aorta (AA), the aortic arch, and the descending aorta.

Methods: Between January and December 2023, the files of adult patients who were suspected of having pulmonary embolism and who underwent thoracic CT angiography (CTA) at the Erzincan Mengücek Gazi Training and Research Hospital Emergency Department were reviewed. The patients' DICOM-format images were exported. These images were uploaded to the 3D-Slicer (version 5.10.0 for Windows) and the MPA, RPA, LPA, and AA diameters were measured in the axial plane. The MPA-to-AA diameter ratio was calculated for each patient and designated PA:A.

Results: This study included 52 men and 50 women, for a total of 102 patients. The patients' average age was 67. No significant difference in vessel diameters was observed between genders. AA, MPA, RPA, and LPA diameters were higher in the >67 age group than in the ≤67 age group. There was no significant difference in the PA:A ratio between age groups. A positive, moderate, and statistically significant correlation was found between age and the diameters of AA, MPA, RPA, and LPA. No significant correlation was found between age and the pulmonary artery-to-aorta (PA:A) ratio. A strong, positive, and statistically significant correlation was found between MPA diameter and the diameters of RPA and LPA. A positive, moderately significant correlation was found between MPA diameter and AA diameter. A strong, significant positive correlation was found between RPA diameter and LPA diameter.

Conclusion: Aortic and pulmonary artery diameters have been evaluated using various methods in previous studies. To better understand the clinical importance of aortic and pulmonary artery diameters in cardiopulmonary diseases, it is necessary to know their normal reference values. The Framingham Heart Study reported an average MPA diameter of 25.1 mm and an average PA:A ratio of 0.77. In our study of the Turkish population, the mean AA, MPA, RPA, and LPA diameters were 34.1 mm, 25.9 mm, 21.1 mm, and 20.2 mm, respectively, and the PA:A ratio was 0.78. Further studies in larger populations are needed to establish reference values for aortic and pulmonary artery diameters in healthy individuals.

Keywords: Pulmonary artery, Pulmonary hypertension, Computed tomography angiography

Corresponding author: Ali Osman Gülmez, **E-mail:** aliosmangulmez.2@gmail.com

Received: June 2, 2026
Revision Requested: June 11, 2026 **Accepted:** June 22, 2026 **Publication Date:** July, 14, 2026

INTRODUCTION

The pulmonary trunk, or main pulmonary artery (MPA), originates from the right ventricle at the level of the upper edge of the left third rib cartilage and carries blood to both lungs. It is approximately 5 cm long and 3 cm.[1] After a short course, the pulmonary trunk divides, just below the aortic arch, into two branches: the right pulmonary artery (RPA) and the left pulmonary artery (LPA). The aorta is the main vessel that originates from the left ventricle and carries blood to the body. In adults, it has an average diameter of 3 cm and a wall thickness of approximately 1.5 mm.[1,2] The aorta is examined in three sections: the ascending aorta (AA), the aortic arch, and the descending aorta. The pars descendens aorta consists of two parts: the pars thoracica aorta and the pars abdominalis aorta.[2]

Pulmonary hypertension (PH) is characterized by increased mean pulmonary artery pressure and can result from various causes such as left heart failure, chronic lung disease, and chronic thromboembolic PH. Its prevalence is estimated at 1% worldwide across all age groups and 10% in the over-65 age group. Given the estimated non-transplant survival rate among all PH patients, widely available tools that enable early diagnosis and rapid initiation of treatment are needed.

Computed Tomography Angiography (CTA) is an imaging technique that uses X-rays and is performed after the intravenous administration of iodinated contrast medium. It is the primary diagnostic method of choice and widely used in the diagnosis of pulmonary embolism.[3] Although right heart catheterization is the gold-standard examination for the diagnosis of PH, this method is invasive and carries potential complications. Therefore, CTA has become an important imaging method in the diagnosis and prognosis of PH.[4] CTA provides valuable information for visualizing the heart, pulmonary vascular tree, and lung parenchyma. An Increased MPA diameter and an elevated PA:A ratio are the best-known CTA signs of PH. Traditionally, an MPA diameter greater than 29 mm is considered an important indicator in the diagnosis of PH, and this has been used as a threshold by most clinicians.[5] A recent study showed that an MPA diameter of ≥30 mm had 83.1% sensitivity and 90.4% specificity in predicting PH.[6] Some studies have suggested that the ratio of MPA diameter to AA diameter (PA:A) could be used as a more specific marker in PH diagnosis.[7] However, such measurements have limited sensitivity and specificity due to single-point assessment and inter-observer variability.

MAIN POINTS

- Computed tomography angiography provides reliable measurements of thoracic arterial diameters.
- Ascending aortic and pulmonary artery diameters increase significantly with advancing age.
- No significant sex-related differences were observed in thoracic arterial diameters.
- The reported reference values may support the radiological assessment of pulmonary hypertension in the Turkish population.

The aim of this study is to determine the mean diameters of the pulmonary arteries (MPA, RPA, and LPA) and the AA diameter in healthy Turkish individuals and to prepare a database for future studies on pulmonary hypertension by calculating the PA:A ratio.

MATERIAL AND METHODS

The Erzincan Binali Yıldırım University Clinical Research Ethics Committee unanimously decided, via its decision dated 21.04.2026 and numbered 541720, that the study complies with legal regulations regarding scientific research and publication ethics. Due to the retrospective nature of our study, the ethics committee waived the requirement of obtaining informed consent from patients.

In this study, the files of all adult patients who presented to the Emergency Department of Erzincan Binali Yıldırım University Mengücek Gazi Training and Research Hospital between January 2023 and December 2023 and who underwent thoracic CT scans due to suspected pulmonary embolism were reviewed in the e-archive. Patients without findings of pulmonary embolism on their CT scans and in their reports were identified. The images of these patients were retrospectively evaluated by a radiologist. Two patients were excluded from the study due to intrathoracic masses, two due to pleural effusion, one due to a combination of pleural effusion and intrathoracic mass, and one due to pneumothorax. In addition, the CT scans of 9 patients that could not be clearly evaluated due to movement or other technical artifacts were excluded. The images of the remaining 102 patients were exported in DICOM format. These images were loaded into 3D-Slicer (version 5.10.0 for Windows), open-source software, and converted into sections in the three planes—sagittal, coronal, and axial—using multiplanar reconstruction (MPR).

All thoracic CTA scans were performed on a 128-detector, multislice computed tomography scanner (Somatom Definition Flash, Siemens Healthcare, Forchheim, Germany) with patients in the supine position during breath holding. The scan coverage was adjusted from the apex to the base of the lungs. The imaging parameters were as follows: slice area, 256 × 0.625 mm; tube voltage, 80/140 kVp; auto-tube current, 60 mAs; return time, 0.28 s; slice thickness, 1 mm. During the examination, 60 to 90 mL of intravenous iodinated contrast medium was administered at a rate of 4 to 6 mL/s. This was followed by 50 mL of saline solution. Neither nitroglycerin nor beta-blockers were used. During imaging, the coronary arteries were primarily opacified, while homogeneous contrast enhancement occurred in the pulmonary arteries. To evaluate the maximum-density projection of the aorta, coronary, and pulmonary arteries, curved-planar and volumetric reconstructions were obtained; the findings were then translated into axial CT images.

Images in DICOM format were imported into 3D-Slicer software and examined in cross-sections. All measurements were taken in

the axial plane. The MPA diameter was measured perpendicular to the long axis of the vessel at the pulmonary artery bifurcation level, similar to previous studies (Figure 1).[4] The diameters of the RPA and LPA were measured perpendicular to the long axis of each vessel, 1.5 cm distal to the bifurcation (Figure 2 and 3). The AA diameter was measured perpendicular to the long axis of the vessel at the pulmonary artery bifurcation level (Figure 4).[8] Findings were recorded in millimeters. Then, the ratio of MPA diameter to AA diameter was calculated for each patient; this ratio was designated PA:A and recorded.

Statistical Analysis

Statistical analysis was performed using SPSS v.22.0 (Statistical Package For Social Sciences, IBM, Chicago, IL, USA). The normality of the data distribution was assessed using the Kolmogorov-Smirnov test and visual methods (histograms and probability plots). Categorical variables were summarized as frequencies and percentages. Quantitative variables were presented as mean ± standard deviation (SD), median (Q1-Q3), and min-max. For comparisons between two independent groups, the independent-samples t-test was used when the data were normally distributed, and the Mann-Whitney U test was used when they were not.

The relationship between two numerical variables was examined using Spearman correlation analysis. Correlation values were classified as follows: r = 0.00-0.05 (very low), r = 0.05-0.30 (low), r = 0.30-0.40 (low-moderate), r = 0.40-0.60 (moderate), r = 0.60-0.70 (good), r = 0.70-0.75 (very good), and r = 0.75-1.00 (excellent). All analyses were performed at a 95% confidence level; a p-value < 0.05 was considered statistically significant.

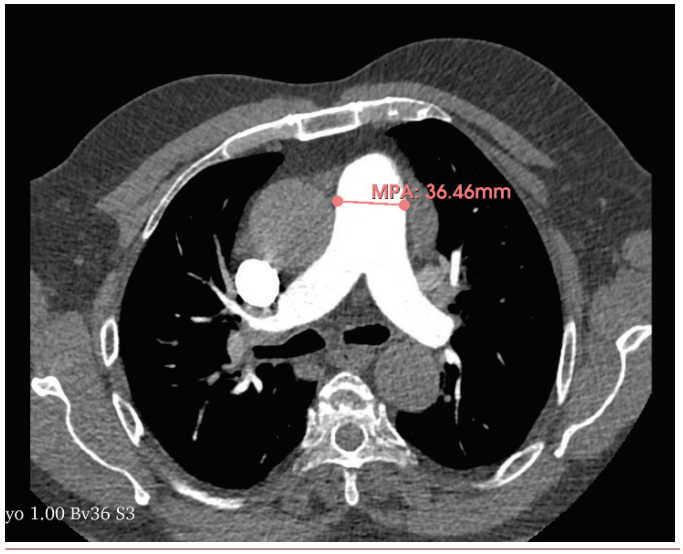

Figure 1. Measurement of the mean pulmonary artery branch on axial sections.

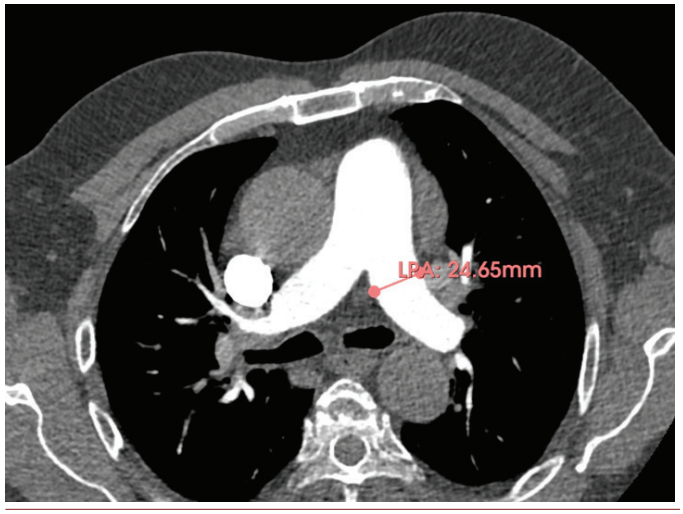

Figure 2. Measurement of the left pulmonary artery branch on axial sections.

RESULTS

The study included 102 patients. Of the patients, 51% were male and 49% were female. The mean age of the patients was 67.67 ± 18.45 years. Demographic data and mean artery diameters of the patients are given in Table 1.

No statistically significant differences were found between genders in age and vascular parameters ($P > 0.05$). The findings are shown in Table 2.

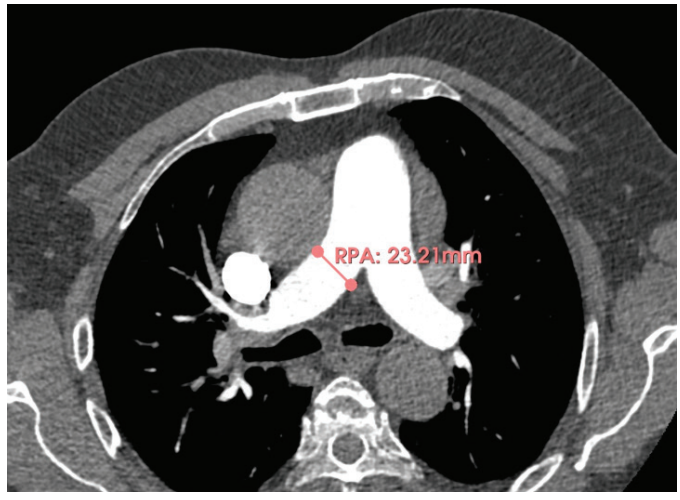

Figure 3. Measurement of the right pulmonary artery branch on axial sections.

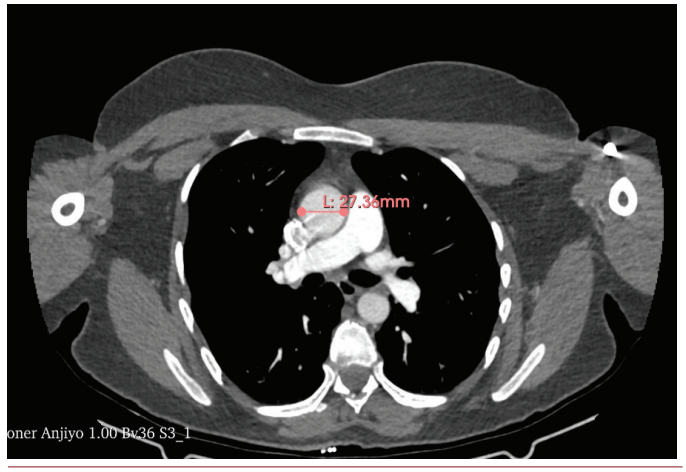

Figure 4. Measurement of the ascending aorta on axial sections.

The mean age of the patients was 67.67 ± 18.45, and statistical comparisons were made based on age, dividing them into two groups: those below and those above the mean age. When comparing age and vascular parameters between patients aged 67 and under (≤67 years) and those aged 67 and over (>67 years), a statistically significant difference was found between the two groups ($P > 0.001$).

Pulmonary artery measurements revealed that MPA, RPA, and LPA values were significantly higher in the >67 age group compared to the ≤67 age group ($P < 0.001$; $P < 0.001$; $P < 0.001$, respectively). This finding suggests that pulmonary artery diameters increase with age. The aortic diameter was also found to be significantly higher in the older age group ($P < 0.001$).

Table 1. Demographic Data and Mean Artery Diameters of Patients

Variables	n/average ± SS	%/ hydrangea (Q1-Q3)	Min-max
Gender			
Female	50	49	
Male	52	51	
Age (years)	67.67 ± 18.45	72.00	21.00-99,00
MPA (mm)	25.93 ± 5.13	25.97	17.36-46.44
RPA (mm)	21.07 ± 3.75	20.74	12.03-33.73
LPA (mm)	20.19 ± 3.70	19.68	12.79-28.35
AA (mm)	34.13 ± 5.22	33.82	21.57-47.67
PA:A	0.78 ± 0.11	0.78	0.58-1.13

MPA, main pulmonary artery; RPA, right pulmonary artery; LPA, left pulmonary artery; AA, ascending aorta; PA:A, pulmonary artery-to-aorta ratio.

There was no statistically significant difference in the PA:A ratio between the two groups ($P = 0.522$). The findings are shown in Table 3.

A moderate positive correlation was observed between age and MPA diameter ($P < 0.001$). A moderate, statistically significant positive correlation was found between age and RPA diameter ($P < 0.001$). A moderate, statistically significant positive correlation was found between age and LPA ($P<0.001$). A moderate positive correlation was found between age and AA diameter ($P < 0.001$). No statistically significant correlation was found between age and PA:A ratio ($P = 0.423$).

A highly significant positive correlation was found between MPA diameter and RPA diameter ($P < 0.001$). A highly significant positive correlation was found between MPA diameter and LPA diameter ($P < 0.001$). A moderately strong positive correlation was found between MPA diameter and AA diameter ($P < 0.001$). A statistically significant moderate positive correlation was found between MPA diameter and PA:A ratio ($P < 0.001$).

A highly significant positive correlation was found between RPA and LPA diameters ($P < 0.001$). A strong positive correlation was observed between RPA diameter and AA diameter ($P < 0.001$). A strong positive correlation was found between LPA diameter and AA diameter ($P < 0.001$). A negative, non-significant correlation was found between AA diameter and PA:A ratio ($P < 0.005$). The findings are shown in Table 4.

Table 2. Comparison of Age and Vascular Parameters by Gender

Variables	Male (n=52)	Female (n=50)	*P*
Age (years)	71.50 (55.25-82.00)	7300 (56.00-82.00)	0.846[2]
MPA (mm)	25.85 (23.58-29.17)	26.00 (23.20-29.55)	0.920[2]
RPA (mm)	21.18 (19.49-23.16)	20.50 (17.69-22.39)	0.078[2]
LPA (mm)	20.56 (17.66-23.16)	18.99 (16.90-23.05)	0.119[2]
AA (mm)	34.80 ± 5.42	33.42 ± 4.96	0.183[1]
PA:A	0.77 ± 0.11	0.80 ± 0.11	0.186[1]

MPA, main pulmonary artery; RPA, right pulmonary artery; LPA, left pulmonary artery; AA, ascending aorta; PA:A, pulmonary artery-to-aorta ratio.

Table 3. Comparison of Vascular Parameters by Age Groups

Variables	≤ 67 (n=43)	> 67 (n=59)	*P*
Age (years)	55.00 (42.00-61.00)	80.00 (75.00-84.00)	**< 0.001**
MPA (mm)	24.69 (22.12-26.25)	27.96 (23.99-32.31)	**< 0.001**
RPA (mm)	18.65 (16.88-20.57)	21.86 (20.57-24.65)	**< 0.001**
LPA (mm)	17.63 (16.48-20.51)	21.40 (18.99-24.39)	**< 0.001**
AA (mm)	31.54 ± 4.97	36.01 ± 4.59	**< 0.001**
PA:A	0.78 ± 0.10	0.79 ± 0.12	0.522[1]

MPA, main pulmonary artery; RPA, right pulmonary artery; LPA, left pulmonary artery; AA, ascending aorta; PA:A, pulmonary artery-to-aorta ratio.

Table 4. Correlation of Patients' Age and Vascular Parameters

Variables		Age	MPA	RPA	LPA	AA	PA:A
Age (years)	r	1	0.426	0.592	0.533	0.438	0.080
	p	.	**< 0.001**	**< 0.001**	**< 0.001**	**< 0.001**	0.423
MPA (mm)	r		1	0.730	0.717	0.581	0.550
	p		.	< 0.001	< 0.001	**< 0.001**	**< 0.001**
RPA (mm)	r			1	0.829	0.700	0.158
	p			.	< 0.001	**< 0.001**	0.112
LPA (mm)	r				1	0.673	0.185
	p				.	**< 0.001**	0.063
AA (mm)	r					1	-0.279
	p					.	**0.005**
PA:A	r						1
	p						.

MPA, main pulmonary artery; RPA, right pulmonary artery; LPA, left pulmonary artery; AA, ascending aorta; PA:A, pulmonary artery-to-aorta ratio.

DISCUSSION

Diameters of the pulmonary artery and the aorta have been evaluated using various methods in previous studies. Radiological examinations such as CT, CTA, multislice CT, echocardiography, and cardiac magnetic resonance imaging have been used for vessel diameter measurement.[9] Some of these studies were conducted in healthy individuals, while others were performed in patient groups with conditions such as PH, sarcoidosis, and COVID-19. The importance of MPA diameter and the PA:A ratio in the diagnosis of PH is particularly emphasized. The mean MPA determined by thoracic CT is a reliable predictor of PH, defined as a resting mean pulmonary artery pressure ≥ 25 mmHg measured by right heart catheterization.[10] Recently, Nakanishi et al.[11] in the study by 2013, it was reported that a PA:A ratio greater than 0.9, independent of coronary artery disease, was associated with a significant increase in the risk of all-cause mortality. Therefore, the PA:A ratio can provide clinicians with information about the risk and current status of various underlying diseases and patient prognosis. However, to better determine the clinical significance of these values in cardiopulmonary diseases, knowledge of normal reference values is necessary. Vessel diameters can vary with race, age, and gender. Therefore, it is essential to determine the normal ranges of pulmonary artery and aortic diameters in the Turkish population.

The average MPA diameter varies among studies conducted on healthy groups. Data from the Framingham Heart Study, which has the largest patient population in the literature (3171 patients), revealed an average MPA diameter of 25.1 mm.[12] In a study conducted with CT in the Turkish population, the average MPA diameter was reported as 23.3 mm, 22.4 mm in women and 24.1 mm in men.[13] In a study conducted with BTA, the average MPA diameter was reported as 32.0 mm; 31.2 mm in women and 32.2 mm in men.[14] In a study conducted with CT, the average MPA diameter was 25.9 mm, 26.5 mm in men and 25.8 mm in women.[9] A study using CT in the Turkish population reported an average MPA diameter of 26.6 mm, 25.9 mm in women and 27.0 mm in men.[15] Kuriyama et al.[16] measured the average MPA as 24.2 mm in their CT study. In this study, the average MPA diameter was 25.9 mm overall (25.9 mm in women and 26.0 mm in men). These findings are consistent with the literature.

A review of the literature reveals a limited number of studies measuring the diameters of the right and left pulmonary arteries. A recent study conducted in Türkiye reported an average RPA diameter of 17.3 mm (16.4 mm in women and 18.0 mm in men). In the same study, the average LPA diameter was reported as 17.6 mm; 16.9 mm in women and 18.2 mm in men.[13] Another study reported an average RPA diameter of 25.2 mm (24.9 mm in women and 25.2 mm in men). The same study reported an average LPA diameter of 24.9 mm; 24.8 mm in women and 25.0 mm in men.[14] In our study, the average RPA diameter was 21.1 mm overall (20.1 mm in women and 21.2 mm in men), and the average LPA diameter was 20.2 mm overall (19.0 mm in women). It has been calculated to be 20.6 mm in men.

Studies conducted in healthy populations show that the average AA diameter ranges from 28.5 to 34.0 mm. In the Turkish population, the average AA diameter has been reported as 28.5 mm, 26.9 mm in women, and 30.0 mm in men.[13] In the study by Berger et al.[14], the average AA diameter was reported as 34.0 mm; 32.8 mm in women and 34.3 mm in men. In one study, the average AA diameter was 30.0 mm.[9] In another study, the average AA diameter was reported as 34.1 mm in men and 31.9 mm in women.[17] In yet another study, the average AA diameter was reported as 33.6 mm in men and 31.1 mm in women.[18] In this study, the average AA diameter was 34.1 mm, similar to previous studies (33.4 mm in women and 34.8 mm in men). AA diameter is affected by diseases such as heart failure, valvular anomalies, and hypertension, as well as by the use of medications such as beta-blockers and digoxin.[19,20] However, previous studies have shown that AA diameter is associated with mortality in patients with heart failure.[21]

Studies in healthy individuals show that the average PA:A ratio is less than 0.9. This ratio (0.9) was accepted as the threshold

value for PH in the Framingham Heart Study. The average PA:A ratio reported in the Framingham Heart Study was 0.77.[12] In the study by Lee et al. [9], the PA/A ratio was 0.87. In this study, the average PA:A ratio was 0.78.

Many studies have shown that the average arterial diameters are larger in male patients than in female patients. In the study by Tekcan Şanlı et al.[13], it was found that all vessel diameters (AA, MPA, RPA, and LPA) were significantly higher in men than in women. Li et al. [22], reported that the AA and MPA diameters were significantly larger in men. Similarly, in the study by Karazincir et al.[15], it was stated that the MPA diameter was significantly higher in men than in women. However, no significant differences were found between genders in any of the measured parameters in this study.

While a significant relationship between age and AA diameter is generally found in the literature, the relationship between age and MPA is debatable.[15,12,21] In the study by Tekcan Şanlı et al.,[13] it was observed that the AA diameter was larger in individuals ≥ 40 compared to those < 40. In our study, it was determined that the MPA, RPA, LPA, and AA diameters increased with age, and these values were significantly higher in the > 67 age group than in the ≤67 age group.

This study had several limitations that should be acknowledged. First, the study was retrospective and single-center, which may limit the generalizability of the findings to the Turkish population. Regional demographic differences, environmental factors, and variations in imaging protocols between institutions may influence vascular measurements. Second, detailed clinical histories of the participants were unavailable. Therefore, potential confounding factors such as undiagnosed cardiovascular or pulmonary diseases, smoking history, body mass index, hypertension, diabetes mellitus, or medication use could not be evaluated. Although individuals with evident pulmonary pathology on CT were excluded, the presence of subclinical conditions that might affect vascular diameters could not be completely ruled out.

Another important limitation was the uneven age distribution of the study population, as most participants were middle-aged or elderly. Consequently, younger age groups were underrepresented, which may have affected the assessment of age-related vascular changes and normal reference values across all age categories. In addition, the cross-sectional design of the study precluded longitudinal evaluation of changes in vascular diameter. Therefore, causal relationships between age and vascular measurements could not be established.

Furthermore, pulmonary artery pressures were not confirmed by right heart catheterization or echocardiographic evaluation, which are considered standard methods for the diagnosis of pulmonary hypertension. The classification of participants as healthy was based primarily on CT findings and the absence of known pulmonary disease. Finally, measurements were performed using CT imaging, and despite standardized measurement techniques, interobserver and intraobserver variability may still have influenced the results.

Future multicenter studies including larger sample sizes, balanced age groups, comprehensive clinical data, and prospective follow-up are needed to establish more reliable reference values for pulmonary artery and aortic diameters in the Turkish population.

CONCLUSION

This retrospective study evaluated the diameters of the ascending aorta (AA), main pulmonary artery (MPA), right pulmonary artery (RPA), left pulmonary artery (LPA), and the PA:A ratio in individuals with no known history of pulmonary hypertension and no pulmonary pathology detected on CT examinations who were therefore considered healthy. The mean diameters were 34.1 mm for the AA, 25.9 mm for the MPA, 21.1 mm for the RPA, and 20.2 mm for the LPA; the mean PA:A ratio was 0.78. No significant gender-related differences were observed in the vascular measurements. A positive correlation was identified between age and the diameters of the AA, MPA, RPA, and LPA. In contrast, no significant correlation was found between age and the PA:A ratio.

Ethics

Ethics Committee Approval: The study was approved by the

Erzincan Binali Yıldırım University Clinical Research Ethics Committee (decision numbered:541720, date: 21.04.2026).

Informed Consent: Retrospective study.

Footnotes

Author Contributions

Concept Design – H.K., Data Collection or Processing – A.O.G., Analysis or Interpretation – H.K., Literature Review – A.O.G., Writing, Reviewing and Editing – H.K.

Declaration of Interests: The authors declare that they have no conflicts of interest.

Funding: The authors declare that this study has received no financial support.

REFERENCES

1. Ozan H. Ozan Anatomi. 3rd ed. Ankara: Klinisyen Tıp Kitabevleri, 2014. [CrossRef]
2. Arıncı K, Elhan A. Anatomi. 7th, Ankara; Güneş Kitabevleri 2020. [CrossRef]
3. Karakuş H, Poyraz N. Pulmonary angiography with low dose contrast media in 64-Slice CT: a feasibility study. *Selcuk Med J*.2021;37(1): 64-69. [CrossRef]
4. Zhao W, Guo J, Dong N, Hei H, Duan X, Shen C. Diagnostic value of 3D volume measurement of central pulmonary artery based on CTPA images in the pulmonary hypertension. *BMC Med Imaging*. 2023;13; 23(1):211. [CrossRef]
5. Lewis G, Hoey ET, Reynolds JH, Ganeshan A, Ment J. Multi-detector CT assessment in pulmonary Hypertension: techniques, systematic approach to interpretation and key findings. *Quant Imaging Med Surg*. 2015;5(3):423-432. [CrossRef]

6. Liu A, Xu W, Xi L, Deng M, Yang H, Huang Q, et al. Cardiovascular metrics on CT pulmonary angiography in patients with pulmonary hypertension–re-evaluation under the updated guidelines of pulmonary hypertension. *Insights Imaging*. 2023;14:179. [CrossRef]
7. Shen Y, Wan C, Tian P, et al. CT-base pulmonary artery measurement in the detection of pulmonary hypertension: a meta-analysis and systematic review. *Medicine (Baltimore*). 2014; 93(27): e256. [CrossRef]
8. Couch TJ, Beck GJ, Berman-Rosenzweig E, Carr JJ, Erzurum SC, Frantz RP et al. Pulmonary artery size on computed tomography associates with mean pulmonary artery pressure and mortality. *Annals of the American Thoracic Society*. 2026; 23(4):494-505. [CrossRef]
9. Lee SH, Kim YJ, Lee HJ, Kim HY, Kang YA, Park MS, et al. Comparison of CT-Determined Pulmonary Artery Diameter, Aortic Diameter, and Their Ratio in Healthy and Diverse Clinical Conditions. *PLoS One*. 2015;10(5):e0126646. [CrossRef]
10. Lange TJ, Dornia C, Stiefel J, Stroszczynski C, Arzt M, Pfeifer M, et al. Increased pulmonary artery diameter on chest computed tomography can predict borderline pulmonary hypertension. *Pulm Circ* 2013; 3:363-368. [CrossRef]
11. Nakanishi R, Rana JS, Shalev A, et al. Mortality risk as a function of the ratio of pulmonary trunk to ascending aorta diameter in patients with suspected coronary artery disease. *Am J Cardiol*. 2013; 111:1259-1263. [CrossRef]
12. Truong QA, Massaro JM, Rogers IS, et al. Reference values for normal pulmonary artery dimensions by noncontrast cardiac computed tomography: the Framingham Heart Study. *Circ Cardiovasc Imaging*. 2012;5:147-154. [CrossRef]
13. Tekcan Sanli DE, Sanli AN, Yildirim O, Erginoz E, Yildirim D. Normative reference values of major thoracic arterial vasculature in Turkiye. *North Clin Istanb*. 2023;17;10(2):263-270. [CrossRef]
14. Berger T, Siepe M, Simon B, et al. Pulmonary artery diameter: means and normal limit-assessment by computed tomography angiography, *Interactive CardioVascular and Thorac Surg*. 2022;34:637-644.
15. Karazincir S, Balcı A, Seyfeli E, et al. CT assessment of main pulmonary artery diameter. *Diagn Interv Radiol*. 2008; 14:72-74. [CrossRef]
16. Kuriyama K, Gamsu G, Stern RG, Cann CE, Herfkens RJ, Brundage BH. CT-determined pulmonary artery diameters in predicting pulmonary hypertension. *Invest Radiol*. 1984; 19:16-22.
17. Rogers R. Digital Methods. Cambridge, MA: MIT Press;2013. [CrossRef]
18. Mao Y, Yuan J, Zhong J. Density functional calculation of transition metal adatom adsorption on graphene. *J Phys Condens Matter*. 2008;19;20(11):115209. [CrossRef]
19. Canadas V, Vilacosta I, Bruna I, Fuster V. Marfan syndrome. Part: 2. treatment and management of patients. *Nat Rev Cardiol*. 2010; 7:266-76. [CrossRef]
20. Srimannarayana I, Varma RS, Satheesh S, Anilkumar R, Balachander J. Supravalvular aortic stenosis and coronary ostial stenosis in homozygous familial hypercholesterolemia. *Indian Heart J*. 2004; 56:152-4. [CrossRef]
21. Kamimura D, Uchino K, Ogawa H, Shimizu M, Shigemasa T, Morita Y, et al. Small proximal aortic diameter is associated with higher central pulse pressure and poor outcome in patients with congestive heart failure. *Hypertens Res*. 2014;37:57-63. [CrossRef]
22. Li S, Zhuang B, Yin G, Yang X, Zhao S, Lu M. Reference values of thoracic aorta and pulmonary artery diameters by age and gender in healthy Chinese adults assessed by cardiac magnetic resonance imaging: data from national center for cardiovascular diseases of China. *Int J Cardiovasc Imaging*. 2021;37(4):1423-1431. [CrossRef]

ABCResearch

Arch Basic Clin Res 2026;8(2):157-163
DOI: 10.4274/ABCR.2026.26436

Research Article

Investigation of Nailfold Capillary Structures Using Digital Dermatoscopy in Rheumatological Diseases

Haticetül Kübra Sarı[1], Şevki Özdemir[2]

[1]Department of Dermatology, Private Dermatology Practice, Erzincan, Türkiye
[2]Department of Dermatology, Erzincan Binali Yıldırım University Faculty of Medicine, Erzincan, Türkiye

Cite this article as: Sarı HK, Özdemir Ş. Investigation of nailfold capillary structures using digital dermatoscopy in rheumatological diseases. *Arch Basic Clin Res*. 2026;8(2):157-163.

ORCID IDs of the authors: H.K.S. 0000-0003-1885-973X, Ş.Ö. 0000-0003-3423-6209.

ABSTRACT

Objective: Evaluating the microvascular structure in rheumatological diseases provides important information for understanding the pathogenesis and clinical management of these diseases. Nail capillaroscopy is a reliable method that allows non-invasive examination of these changes. This study aimed to evaluate nail capillary findings in rheumatological diseases using digital dermoscopy and to compare capillary patterns in different disease groups.

Methods: The study included 200 patients diagnosed with rheumatological diseases and 50 healthy volunteers. The nail bed capillaries of all participants were evaluated using a digital dermatoscope. Capillary examination assessed the presence of edema, tortuous, elongated, dilated, and brush-like capillaries, microhemorrhages, and avascular areas. Statistical analyses were performed using appropriate parametric and non-parametric tests, and a P value < 0.05 was considered statistically significant.

Results: The frequency of capillary abnormalities was significantly higher in the patient group than in the control group. The most frequently observed findings were edema and tortuous, elongated capillaries. Capillary patterns differed by disease group, with more specific findings particularly prominent in patients with systemic sclerosis.

Conclusion: Nail capillaroscopy is an effective, easily applicable, and non-invasive method for evaluating microvascular changes in rheumatological diseases. Capillary patterns observed in different disease groups can provide clinically valuable information for diagnosis and disease monitoring.

Keywords: Capillaroscopy, nail capillaroscopy, rheumatological diseases, digital dermatoscopy, microvascular changes, systemic sclerosis.

INTRODUCTION

Rheumatological diseases constitute a group of chronic, multisystemic disorders affecting connective tissue and vascular structures. In these diseases, microvascular involvement plays a crucial role in pathogenesis and may directly influence clinical outcomes. In particular, microcirculatory alterations in autoimmune connective tissue diseases can be detected early and may provide valuable information for diagnosis and prognosis.[1,2]

Nailfold capillaroscopy is a non-invasive, easily applicable, and reproducible method that allows *in vivo* evaluation of the microcirculation.[2, 3]. It enables detailed assessment of capillary morphology and identification of disease-specific patterns. The "scleroderma pattern," particularly observed in systemic sclerosis (SSc), is one of the most characteristic examples demonstrating the diagnostic value of capillaroscopy.[1] However, varying degrees of capillary abnormalities may also be observed in other rheumatological diseases such as systemic lupus erythematosus (SLE), rheumatoid arthritis (RA), and ankylosing spondylitis (AS).[4]

Recent technological advancements, particularly digital dermoscopy, have increased the accessibility and standardization of capillary evaluation.[3,5,6] These developments have facilitated the assessment of microvascular changes in larger patient populations and contributed to the expansion of

Corresponding author: Haticetül Kübra Sarı, **E-mail:** drhksari@gmail.com

Received: 1 June, 2026
Revision Requested: 11 June, 2026 **Accepted:** 22 June, 2026 **Publication Date:** July, 14, 2026

clinical data in this field. However, studies that directly compare capillary findings across different rheumatological disease groups remain limited.

The aim of this study was to evaluate nailfold capillary findings in patients with rheumatological diseases using digital dermoscopy and to compare capillary patterns among different disease groups.

Capillaroscopy

Nailfold capillaroscopy is a valuable method for evaluating microcirculation and blood supply *in vivo* (Figure 1). It is a non-invasive, cost-effective, and easily repeatable technique. The capillaries in the nail bed consist of arterial and venous limbs connected by an apical loop, which runs parallel to the skin surface, allowing direct visualization.[2] Normal nailfold capillaries are regularly arranged, hairpin-shaped, and homogeneously distributed.[7] (Figure 2).

Capillaroscopic examination has been used for over two decades in the evaluation of autoimmune connective tissue diseases.[2] Many connective tissue diseases, such as SSc, dermatomyositis, and mixed connective tissue disease, exhibit characteristic capillary abnormalities.[5,6] Among rheumatological diseases, SSc exhibits the most specific capillary pattern. Microcirculatory impairment is a central feature of the disease process in SSc.[1]

The most common capillaroscopic findings in SSc include giant capillaries, microhemorrhages, and avascular areas.[7,8] In addition, tortuous (Figure 3), elongated, and dilated capillaries may also be observed in diseases such as dermatomyositis, mixed connective tissue disease, and SLE.[5,6,9]

Capillaroscopy is a convenient technique that can provide reliable information about disease severity and differentiate primary from secondary Raynaud's phenomenon (RP) in patients. It has also been reported that it can be a useful device in evaluating follow-up in RF associated with coronary heart disease (CHD).[10,11]

Procedure

Morphological evaluation of cutaneous capillaries is usually performed at the nail bed because the main axis of the capillaries is parallel to the skin surface (in other areas the capillaries are perpendicular) and the nail bed is easily accessible for sampling. All patients should wait in the test room for at least 15 minutes before evaluation. The ideal room temperature for the procedure is 20-22 °C. Traumatized fingers are not evaluated. The nail bed capillaries of the fourth and fifth fingers of the non-dominant hand are the most suitable sites for evaluation because the skin of these fingers is more transparent than that of other fingers. Before performing nail bed videocapillaroscopy, immersion oil is applied to the nail bed, and the capillaries are evaluated at 100x or 200x magnification with minimal pressure.

Early capillary changes seen in autoimmune connective tissue diseases include large and prominent capillaries,

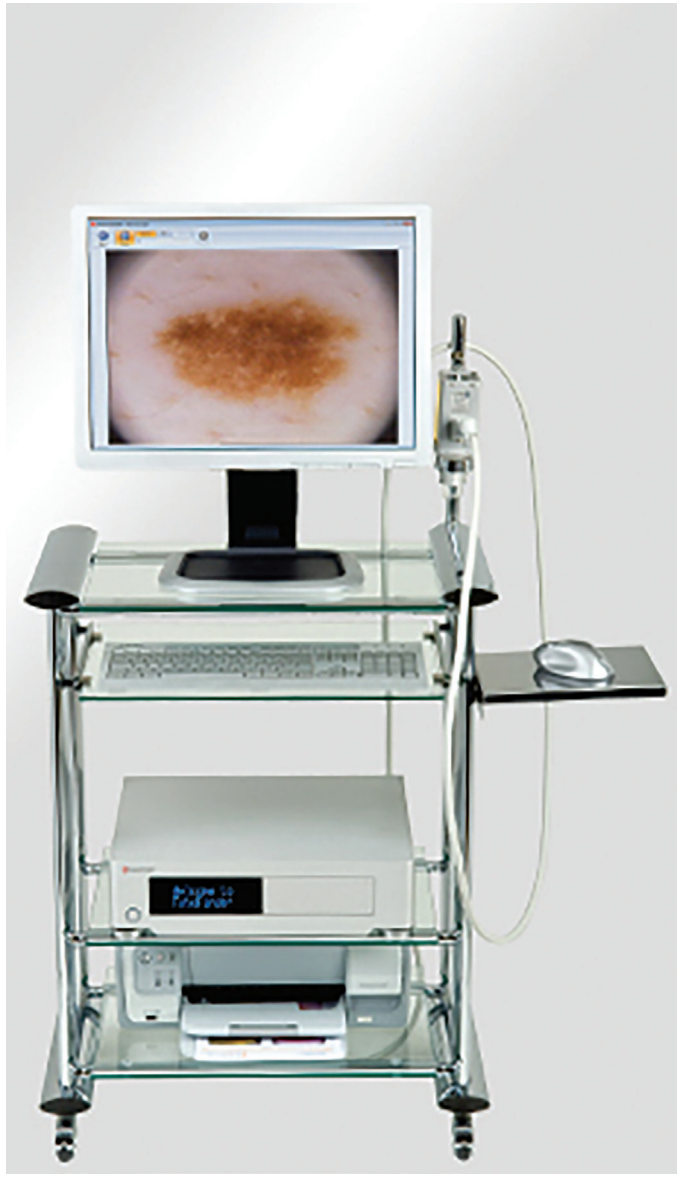

Figure 1. Due to the cumbersome equipment required for photographic documentation, in vivo nail bed capillaroscopy has not yet been integrated into clinical practice as a standard bedside routine in rheumatology and dermatology clinics. Recent studies have suggested that the hand dermatoscope can be used as a capillary-scopic device for this purpose.

MAIN POINTS

- Digital dermoscopy detected significantly more nailfold capillary abnormalities in patients with rheumatological diseases than in healthy controls.
- Distinct capillary patterns were identified among different rheumatological diseases, particularly in systemic sclerosis
- Nailfold capillaroscopy is a practical, non-invasive, and accessible method for evaluating microvascular involvement.
- Capillaroscopic findings may support the diagnosis and clinical follow-up of patients with rheumatological diseases.

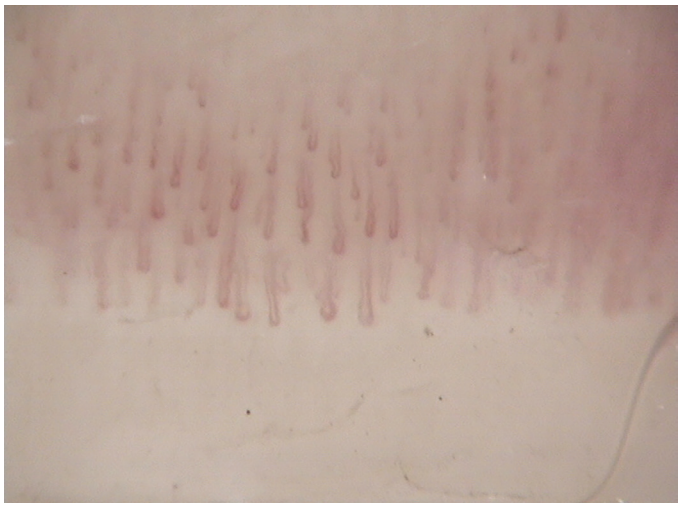

Figure 2. Many instruments have been used in the evaluation and characterization of nail bed capillary morphologies. The most commonly used capillary microscope consists of an optical microscope connected to a camera and a light source with external cooling. 30X and 50X magnification is usually sufficient to evaluate the morphological structure of the nail bed capillary plexus. Monitor-connected video capillaroscopes can provide 100X, 200X magnification, enabling storage and display with the help of a specific program.

Figure 3. Torsional capillaries. Patients with increased torsion in the descending and ascending limbs of capillary loops were classified as having torsional capillaries.

microhemorrhages, capillary loss, edema (Figure 4), branched-brush capillaries (angiogenesis) (Figure 5), irregularities in the vascular sequence, capillary loss and/or avascular areas(Figure 6), and irregularities in the vascular periphery.[12]

MATERIAL AND METHODS

Ethical approval for this study was obtained from the Atatürk University Faculty of Medicine Ethics Committee (approval date: 03.12.2015, decision number: 25). The study was conducted in accordance with the Declaration of Helsinki. Informed consent was obtained from all participants prior to inclusion in the study.

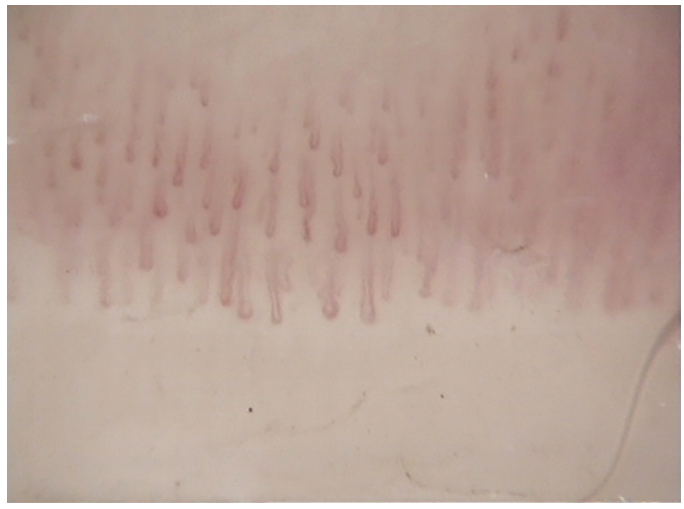

Figure 4. Edema. Edema was considered present if the capillary image appeared cloudy due to damaged vessels or if the dermal papilla appeared empty due to increased synthesis of extracellular matrix proteins.

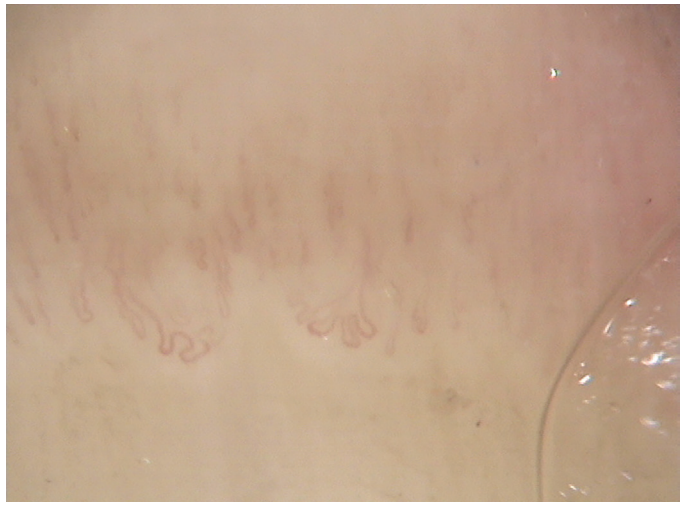

Figure 5. Ramified/bushy capillaries (angiogenesis). Excessively convoluted and branched capillary arch clusters are characteristic of angiogenesis findings. Patients with ramified capillary clusters consisting of thin and thick capillaries showing significant heterogeneity, which is the main morphological feature of angiogenesis, were classified as having branched/brushed capillaries.

Between July 2015 and December 2015, 268 patients with a history of rheumatic disease were evaluated; these patients had presented to the rheumatology outpatient clinic and were referred to the dermatology outpatient clinic at Atatürk University Faculty of Medicine Research Hospital. Comorbidities, smoking, and the use of vasoconstrictive agents were considered exclusion criteria. 200 patients with a diagnosis of rheumatic disease who did not meet the exclusion criteria and 50 volunteers forming the control group were included in the study. In our study, the patients' file numbers, ages, genders, and rheumatic disease diagnoses were recorded.

Figure 6. Capillary loss and/or avascular areas. Patients with extensive avascular areas (5 mm < 30 loops in the distal row of the nail bed) resulting from widespread capillary loss in the nail bed were classified as avascular.

Patients were acclimatized in the test room at approximately 20-22°C for at least 15 minutes before capillaroscopy. The procedure was not performed on fingers with local trauma. The capillaries of the fourth and fifth nail beds of the non-dominant finger were evaluated first. The capillaroscope (FotoFinder® dermoscope, FotoFinder Systems GmbH, Bad Birnbach, Germany) was applied with very little pressure. The presence of homogeneously dilated, giant, irregularly dilated, brush-like, and tortuous capillaries, microhemorrhages, edema, and avascular areas was investigated and noted.

Normal Pattern

Patients with capillary loss in the nail fold (30 capillaries linearly in 5 mm) and with homogeneous capillary distribution without morphological changes were considered normal.

Statistical Analysis

Statistical analysis was performed using SPSS Statistics 22.0 (IBM Corp., Armonk, NY, USA). Descriptive data were presented as mean ± standard deviation, median (min-max), and frequency (%). The normality of the distribution was assessed using the Kolmogorov-Smirnov test. For comparisons between groups, the Student's t-test or Mann-Whitney U test was used for continuous variables, and the Chi-square test or Fisher's exact test was used for categorical variables. A *P* value < 0.05 was considered statistically significant.

RESULTS

The nail beds of 200 patients with a history of rheumatic disease and of 50 healthy volunteers with no history of disease were evaluated by capillaroscopy.

All patients underwent capillaroscopy to assess nail bed edema, convoluted capillaries (Figure 7), elongated capillaries, dilated giant capillaries (Figure 8), microhemorrhages (Figure 9), and avascular areas.

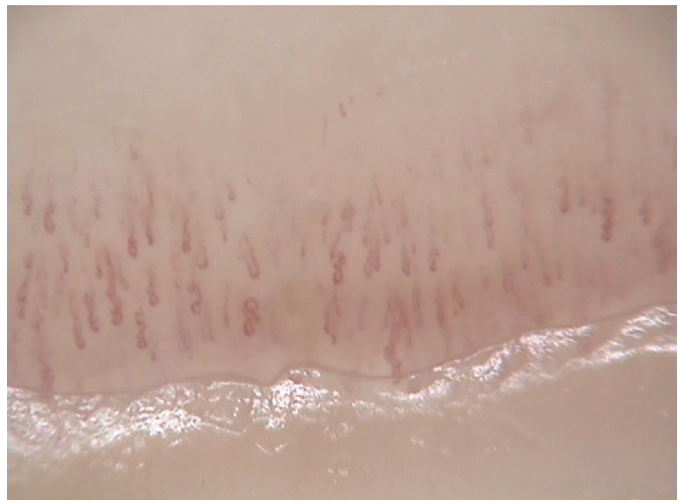

Figure 7. Convoluted capillaries.

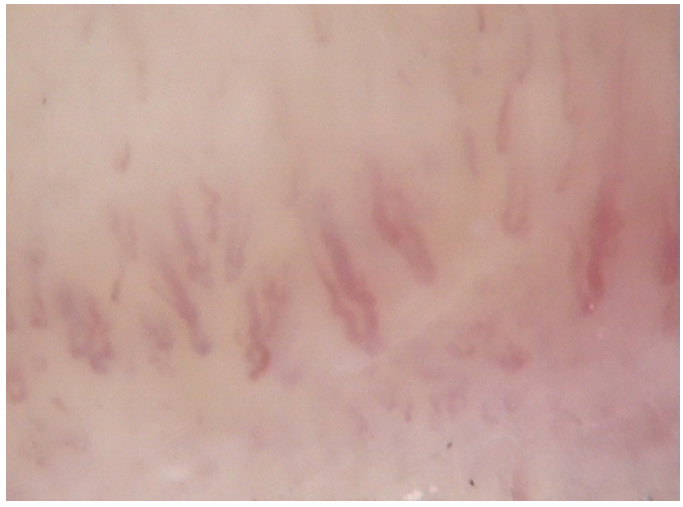

Figure 8. Enlarged capillaries (giant capillaries). Patients with symmetrical giant enlargements (> 50 µm enlargement) in the capillaries were classified as having enlarged capillaries.

In the patient group, 56 participants (28%) were male and 144(72%) were female, with a mean age of 43.01 ± 12.6 years. In the control group, 24 participants (48%) were male and 26 (52%) were female, with a mean age of 29.56 ± 8.8 years (Table 10).

Among the patients included in the study, 50% were diagnosed with RA, 23% with AS, 21% with SLE, and 6% with SSc (Figure 10).

In the capillaroscopic evaluation of patients with SLE (n=42), the most frequently observed abnormalities were tortuous capillaries, followed by edema and bushy (branched) capillaries.

Among patients with RA (n=101), edema was the most common finding, followed by tortuous and elongated capillaries.

In patients with AS (n=46), the most frequent abnormalities were edema, avascular areas, tortuous, elongated capillaries.

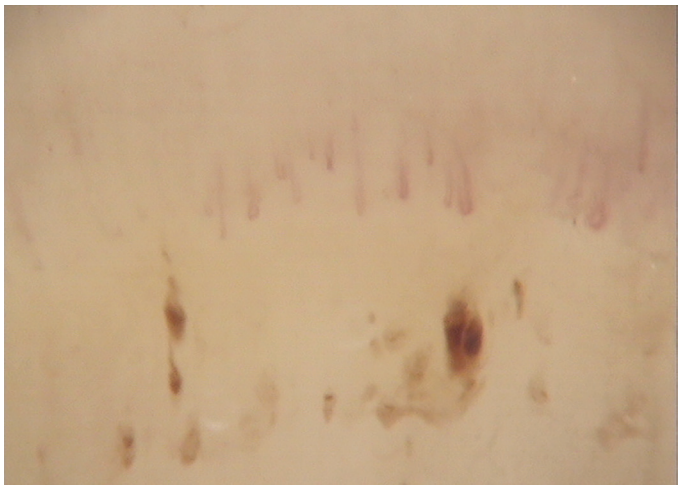

Figure 9. Microhemorrhage. Microhemorrhages may be found around the capillaries, either as pinpoint or linear formations. (More than two punctate hemorrhages or converging hemorrhage areas per finger). Microhemorrhages occur after extravasation of red blood cells following damage to the vessel wall. Patients exhibiting these findings were classified as having microhemorrhages.

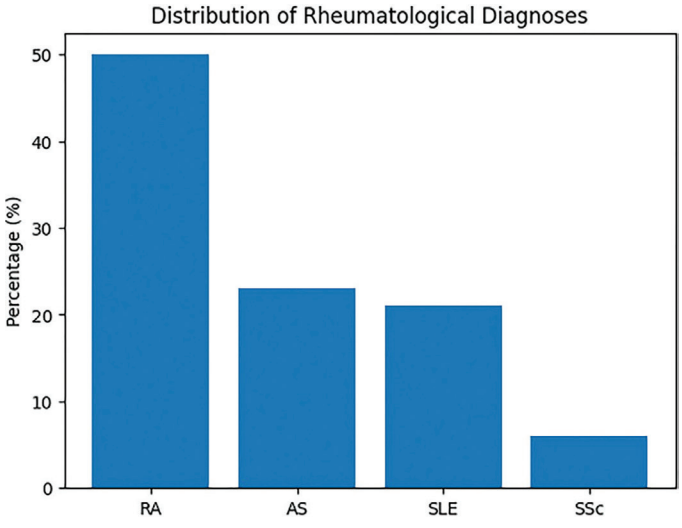

Figure 10. igure 10. Distribution of rheumatological diagnoses among study participants[3]

[3]Data are presented as percentages. RA, rheumatoid arthritis; AS, ankylosing spondylitis; SLE, systemic lupus erythematosus; SSc, systemic sclerosis.

Table 1. Gender Distribution of the Study and Control Groups*

Gender	Patient Group (n=200) n (%)	Control Group (n=50) n (%)
Male	56 (28.0)	24 (48.0)
Female	144 (72.0)	26 (52.0)

*Data are presented as n (%).

In SSc patients (n=11), the predominant finding was dilated capillaries, followed by bushy capillaries (Table 2).

Capillaroscopic evaluation of the nailfold revealed a significantly higher overall frequency of abnormalities, including edema, tortuous, elongated, and bushy capillaries, and microhemorrhages, in the patient group than in the control group (Table 3).

DISCUSSION

Nail bed capillaroscopy is an inexpensive, simple, and non-invasive technique used to evaluate the blood supply and microcirculation of the nail bed.

Many instruments have been used to characterize nail-bed capillary morphology. The most commonly used capillaroscopic device consists of an optical microscope connected to a camera and to a light source with external cooling. 30X and 50X magnification are usually sufficient to evaluate the morphological structure of the nail bed capillary plexus. Monitor-connected video capillaroscopes can provide 100X and 200X magnification, enabling storage and display with the help of a specific program.[2]

Microscopic *in vivo* examination of the nail bed vascular plexus in patients with autoimmune connective tissue diseases has been performed for over 25 years. Many connective tissue diseases (CTDs), such as scleroderma and mixed connective tissue disease (MCTD), frequently exhibit characteristic capillary abnormalities. Among rheumatological diseases, the most important specific capillary pattern is that associated with SSc.

Although the factors triggering vasculopathy, the initial stage of SSc, are not clearly known, it is thought that cytomegalovirus (CMV), whose epitopes resemble endothelial cell surface molecules, anti-endothelial cell antibodies, or free oxygen radicals cause endothelial cell damage, leading to apoptosis in endothelial cells.[13,14] A low number or impaired function of endothelial progenitor cells is also considered a cause of vasculogenesis disorders.[15] Capillary examination can demonstrate microvascular damage in almost all patients. Microcirculation is the main center of the pathological process in SSc.[1] The most frequent changes in SSc are dilated capillaries[7], hemorrhage[8], and avascular areas. Torsional, elongated, and dilated capillaries can also be found in DM, MKDH, and SLE.[5,6,9]

In our study, the nail beds of 11 SSc patients were examined capillaroscopically; dilated capillaries were observed in 6 patients and brush-like capillaries in 3 patients. Edema was observed in 1 patient, and avascular areas were observed in 2 patients. Contrary to the literature, microhemorrhages were not detected in any of the patients.

Dilated, giant capillaries, hemorrhage areas, and avascular areas seen in SSc are much rarer in SLE.[3,6] According to some researchers, capillaroscopic findings are mostly non-specific. The specific nail-bed changes most frequently described in SLE patients include capillary tortuosity or convolution, increased capillary length or diameter, transformation of loops into bizarre forms, and prominence of the subpapillary plexus.

Table 2. Comparison of Capillaroscopic Findings Among Diagnostic Groups[1]

Disease	n	Normal n (%)	Edema n (%)	Tortuous capillaries n (%)	Elongated capillaries n (%)	Dilated capillaries n (%)	Bushy capillaries n (%)	Microhemorrhage n (%)	Avascular areas n (%)
SLE	42	9 (21.4)	6 (14.3)	11 (26.2)	2 (4.8)	3 (7.1)	6 (14.3)	3 (7.1)	2 (4.8)
RA	101	29 (28.7)	32 (31.7)	21 (20.8)	10 (9.9)	3 (3.0)	1 (1.0)	4 (4.0)	1 (1.0)
AS	46	7 (15.2)	21 (45.7)	3 (6.5)	3 (6.5)	0 (0)	1 (2.2)	1 (2.2)	10 (21.7)
SSc	11	0 (0)	1 (9.1)	0 (0)	0 (0)	6 (54.5)	3 (27.3)	0 (0)	1 (9.1)

[1]Data are presented as n(%).

Table 3. Comparison of Capillaroscopic Findings Between Patient and Control Groups[2]

Finding	Patient Group (n=200) Present n (%)	Control Group (n=50) Present n (%)	*P* value
Normal	44 (22.0)	41 (82.0)	**<0.001**
Edema	63 (31.5)	3 (6.0)	**<0.001**
Tortuous capillaries	52 (26.0)	5 (10.0)	**0.02**
Elongated capillaries	15 (7.5)	0 (0)	**0.04**
Dilated (giant) capillaries	12 (6.0)	1 (2.0)	0.47
Bushy capillaries	18 (9.0)	0 (0)	**0.03**
Microhemorrhages	16 (8.0)	0 (0)	**0.04**
Avascular areas	18 (9.0)	1 (2.0)	0.13

[2]Data are presented as n (%). Statistical comparisons were performed using the Chi-square or Fisher's exact test.

In some studies, these SLE-specific changes have been termed the SLE-type capillary pattern (SLE pattern).[3] The SLE pattern is essentially formed by an increase in capillary convolution.[16]

In our study, the most frequently observed pathologies in the capillaroscopic evaluation of 42 patients with SLE were, in order, convoluted capillaries (n=11), edema (n=6), and brush capillaries (n=6). Pathologies were detected in 33 patients, and all types of these pathologies were observed in the nail bed capillaries of SLE patients. In our study, consistent with the literature, convoluted and brush capillaries were the most frequently detected.

Rheumatism, or rheumatic disease, is a term used to describe more than 200 chronic diseases that affect the joints and/or connective tissues and cause pain. Although rheumatic diseases generally begin in the joints, with joint pain as the most common complaint, many exhibit multisystem involvement.

RA is the most common rheumatic disease. Currently, the cause of RA remains unknown, and the lack of a pathognomonic diagnostic method means that diagnosis can only be made through a combination of laboratory, clinical, and imaging methods, thus requiring additional diagnostic techniques.[17]

Although there are insufficient studies evaluating whether nail capillaroscopy in RA patients can aid diagnosis, data in the literature are contradictory. In a study by Redisch et al.[18] involving 31 RA patients, they found elongation of capillaries, increased folds, and prominent subpapillary plexuses. However, none of the RA patients in this study showed a scleroderma pattern.[18]

Our study included 101 patients diagnosed with RA, of whom pathology was detected in the nail bed capillaries of 72 patients. The most common pathologies were edema (n=32), tortuous capillaries (n=21), and elongated capillaries (n=10). In 3 of our patients, an SSc pattern was detected even though no diagnosis of SSc had been made.

AS is a chronic, multisystemic rheumatic disease that primarily affects the sacroiliac joints and spine.18 AS is a spondyloarthropathy. Spondyloarthropathies are related to each other genetically human leukocyte antigen and through a shared pathology (enthesitis). Although there is no specific diagnostic method for AS, diagnosis is based on a combination of inflammatory low back pain and radiological evidence of enthesitis or arthritis.

There are insufficient studies on nail bed capillaroscopy in patients with AS. Wendling et al.,[19] in their study with 32 AS patients, reported that there was more edema and microangiopathy at the nail bed compared to the control group.

Our study included 46 AS patients, and pathology was detected in the nail bed capillaries of 39 of them. The most frequently detected pathologies were edema, avascular areas, tortuous capillaries, and elongated capillaries. No SSc pattern was detected in any of our AS patients.

Study Limitation

This study has several limitations. First, it was conducted at a single center; therefore, the patient population, referral patterns, and clinical characteristics may not fully represent those of other centers, potentially limiting the generalizability of the findings. Second, although the overall sample size was sufficient for the main comparisons, the number of patients in some disease subgroups, particularly systemic sclerosis,

was relatively limited. This may have reduced the statistical power for subgroup analyses and should be considered when interpreting disease-specific capillary findings. Third, interobserver variability was not assessed, which may have affected the evaluation of capillary abnormalities. In addition, capillary findings were evaluated using digital dermoscopy rather than conventional nailfold videocapillaroscopy, which may limit direct comparability with studies using standard nailfold videocapillaroscopy. Finally, the cross-sectional design of the study does not allow assessment of causal relationships, temporal changes, disease progression, or treatment-related changes in capillary structures.

CONCLUSION

Nail bed capillaroscopy can aid in diagnosing the disease, and abnormalities detected by BPC can reflect the extent of microvascular involvement in SLE, thereby informing treatment strategies in cases of systemic organ failure. In one study, severe or moderate pathological changes in nail bed capillaries were also detected in SLE patients with internal organ involvement.[3]

It has been reported that nail bed capillaroscopy can be used in patients with RA when findings suggestive of microangiopathy are detected, to classify the disease into subgroups and/or to monitor for overlap syndrome with other connective tissue diseases.

Ethics

Ethics Committee Approval: Ethical approval for this study was obtained from the Atatürk University Faculty of Medicine Clinical Research Ethics Committee (approval date: 03.12.2015, decision number: 25).

Informed Consent: Informed consent was obtained from all participants prior to inclusion in the study.

Footnotes

Author Contributions:

Concept Design – H.K.S., Ş.Ö.; Data Collection or Processing –H.K.S.; Analysis or Interpretation – H.K.S.; Literature Review – H.K.S., Ş.Ö.; Writing, Reviewing and Editing – H.K.S., Ş.Ö.

Declaration of Interests: The authors declare no conflict of interest regarding the publication of this paper.

Funding: The authors declare no financial support or funding.

REFERENCES

1. Lambova SN, Müller-Ladner U. Capillaroscopic pattern in systemic sclerosis: an association with dynamics of processes of angio- and vasculogenesis. *Microvasc Res.* 2010;80(3):534-539. [CrossRef]
2. Cutolo M, Grassi W, Matucci Cerinic M. Raynaud's phenomenon and the role of capillaroscopy. *Arthritis Rheum.* 2003;48(11):3023-3030. [CrossRef]
3. Bergman R, Sharony L, Schapira D, Nahir MA, Balbir-Gurman A. The handheld dermatoscope as a nail-fold capillaroscopic instrument. *Arch Dermatol.* 2003;139(8):1027-1030. [CrossRef]
4. Sontheimer RD. A portable digital microphotography unit for rapid documentation of periungual nailfold capillary changes in autoimmune connective tissue diseases. *J Rheumatol.* 2004;31(3):539-544. [CrossRef]
5. Hoffman RW, Greidinger EL. Mixed connective tissue disease. *Curr Opin Rheumatol.* 2000;12(5):386-390. [CrossRef]
6. Nagy Z, Czirják L. Nailfold digital capillaroscopy in 447 patients with connective tissue disease and Raynaud's disease. *J Eur Acad Dermatol Venereol.* 2004;18(1):62-68. [CrossRef]
7. Grassi W, Del Medico P, Izzo F, Cervini C. Microvascular involvement in systemic sclerosis: capillaroscopic findings. *Semin Arthritis Rheum.* 2001;30(6):397-402. [CrossRef]
8. Sulli A, Burroni A, Tuccio M, et al. Nailfold videocapillaroscopy in systemic sclerosis: diagnostic and follow-up parameters and correlation with both specific serum autoantibodies and subsets of skin involvement. *Reumatismo.* 2004;56(1):36-45. [CrossRef]
9. Keberle M, Tony HP, Jahns R, Hau M, Haerten R, Jenett M. Assessment of microvascular changes in Raynaud's phenomenon and connective tissue disease using colour Doppler ultrasound. *Rheumatology (Oxford).* 2000;39(11):1206-1213. [CrossRef]
10. Anders HJ, Sigl T, Schattenkirchner M. Differentiation between primary and secondary Raynaud's phenomenon: a prospective study comparing nailfold capillaroscopy using an ophthalmoscope or stereomicroscope. *Ann Rheum Dis.* 2001;60(4):407-409. [CrossRef]
11. Wigley FM. Clinical practice. Raynaud's phenomenon. *N Engl J Med.* 2002;347(13):1001-1008. [CrossRef]
12. Cutolo M, Pizzorni C, Secchi ME, Sulli A. Capillaroscopy. *Best Pract Res Clin Rheumatol.* 2008;22(6):1093-1108. [CrossRef]
13. Sgonc R, Gruschwitz MS, Boeck G, et al. Endothelial cell apoptosis in systemic sclerosis is induced by antibody-dependent cell-mediated cytotoxicity via CD95. *Arthritis Rheum.* 2000;43(11):2550-2562. [CrossRef]
14. Gabrielli A, Svegliati S, Moroncini G, Pomponio G, Santillo M, Avvedimento EV. Oxidative stress and the pathogenesis of scleroderma: the Murrell's hypothesis revisited. *Semin Immunopathol.* 2008;30(3):329-337. [CrossRef]
15. Rabquer BJ, Koch AE. Angiogenesis and vasculopathy in systemic sclerosis: evolving concepts. *Curr Rheumatol Rep.* 2012;14(1):56-63. [CrossRef]
16. Capobianco KG, Xavier RM, Bredemeier M, et al. Nailfold capillaroscopic findings in primary Sjögren's syndrome: clinical and serological correlations. *Clin Exp Rheumatol.* 2005;23(6):789-794. [CrossRef]
17. Aletaha D, Neogi T, Silman AJ, et al. 2010 rheumatoid arthritis classification criteria: an American College of Rheumatology/European League Against Rheumatism collaborative initiative. *Arthritis Rheum.* 2010;62(9):2569-2581. [CrossRef]
18. Redisch W, Messina EJ, Hughes G, McEwen C. Capillaroscopic observations in rheumatic diseases. *Ann Rheum Dis.* 1970;29(3):244-253. [CrossRef]
19. Wendling D, Risold JC. Nailfold capillaroscopy and ankylosing spondylarthritis: incidence of anomalies, but absence of diagnostic and prognostic value. *Rev Med Interne.* 1994;15(7):448-451. [CrossRef]

ABCResearch

Arch Basic Clin Res 2026;8(2):164-170
DOI: 10.4274/ABCR.2026.26416

Research Article

Clinical Characteristics of Geriatric Patients Admitted to the Emergency Department and Evaluation According to Age Groups

Orhan Tanrıverdi, Fatih Mehmet Sarı, Yasin Bilgin, Erdem Yakup Çimen, Yusuf Kantar, Abdullah Emre Yurttutan

Department of Emergency Medicine, Erzincan Binali Yıldırım University Faculty of Medicine, Erzincan, Türkiye

Cite this article as: Tanrıverdi O, Sarı FM, Bilgin Y, Çimen EY, Kantar Y, Yurttutan AE. Clinical characteristics of geriatric patients admitted to the emergency department and evaluation according to age groups. *Arch Basic Clin Res.* 2026;8(2):164-170.

ORCID IDs of the authors: O.T. 0000-0002-4677-0946, F.M.S. 0009-0007-7022-3751, Y.B. 0000-0002-1582-223X, E.Y.Ç., 0000-0003-1912-5308, Y.K. 0000-0001-8358-5312, A.E.Y. 0000-0001-6421-0371.

ABSTRACT

Objective: To evaluate the demographic and clinical characteristics, reasons for admission, triage distribution, consultation requests, and hospitalization rates of geriatric patients presenting to a tertiary emergency department, and to examine the associations between age groups and emergency department utilization patterns and outcomes.

Materials and Methods: This retrospective and descriptive study was conducted among patients aged 65 years and older who presented to the emergency department of Mengücek Gazi Training and Research Hospital between July 1, 2024, and June 30, 2025. Data on demographic characteristics, triage categories, reasons for admission, consultation requests, hospitalization status, emergency department outcomes, and repeat visits were obtained from the hospital information management system. The data were analyzed using descriptive statistical methods.

Results: A total of 18,269 geriatric patients were included in the study. The mean age was 74.0 ± 7.2 years, and 54.5% of the patients were female. The highest proportion of admissions was observed in the 65-74 age group. Hospitalization occurred in 11.4% of cases. As age increased, ambulance admissions, repeat emergency department visits, and hospitalization rates increased significantly ($P < 0.05$). The most common reasons for admission were musculoskeletal, respiratory, and cardiovascular diseases.

Conclusion: This study demonstrates that geriatric patients presenting to the emergency department exhibit distinct clinical and utilization characteristics by age group. The findings indicate that patients in older age groups require more complex clinical evaluation and tailored care during management in the emergency department.

Keywords: Geriatric assessment, emergency services, age groups

INTRODUCTION

According to projections by the World Health Organization (WHO), the global elderly population is expected to increase markedly in the coming years, accompanied by a substantial rise in the utilization of health care services.[1] Similarly, population projections by the Turkish Statistical Institute estimate that the proportion of the elderly population in Türkiye will reach 13.5% in 2030, 17.9% in 2040, 27.0% in 2060, and 33.4% in 2080.[2] The rapid growth of the elderly population at global and national levels is anticipated to increasingly affect the provision of health care services.

In previous studies conducted at different centers, individuals aged 65 years and older have been reported to constitute between 10.1% and 17.4% of all emergency department admissions.[3,4] With the expansion of the elderly population, the growing number of emergency department visits has led to increased patient turnover and resource utilization, resulting in

Corresponding author: Orhan Tanrıverdi, **E-mail:** orhan.tanriverdi@erzincan.edu.tr

Received: February 10, 2026
Revision Requested: March 9, 2026 **Accepted:** May 25, 2026 **Publication Date:** July, 14, 2026

a greater workload for emergency services.[5] Moreover, discharge rates from the emergency department among geriatric patients have been reported to range from 79.4% to 92.4% in various studies.[3-5] These findings suggest potential inappropriate use of emergency departments and highlight the need for new strategies regarding the care, follow-up, and management of elderly patients.[5]

As the proportion of elderly individuals in the community continues to rise, it has become essential to address in greater detail the health-care needs specific to this age group and to reorganize health-care services accordingly. Age-related declines in physiological and psychosocial reserves increase vulnerability to diseases and impair older adults' ability to adapt to changes in daily life. The presence of multiple comorbidities and chronic health conditions is a major contributor to increased health-care utilization among elderly individuals. In particular, the higher incidence of emergency conditions and more frequent atypical clinical presentations in this population lead to higher rates of emergency department visits and hospital observation compared with younger adults. These characteristics complicate the evaluation of geriatric patients in emergency settings and necessitate considering this group as a distinct patient population.[6]

The aim of this study was to evaluate the demographic characteristics, modes of presentation, reasons for admission, and clinical outcomes (referral, discharge, hospitalization, and death) of patients aged 65 years and older presenting to the Emergency Department of Mengücek Gazi Training and Research Hospital. The study sought to identify key features of emergency department utilization among geriatric patients and to contribute to geriatric patient management and health care resource planning. Ultimately, this approach aims to promote more effective emergency care delivery while reducing unnecessary crowding, costs, and workload in emergency departments.

MAIN POINTS

- Geriatric patients constitute a substantial proportion of emergency department visits, and the high rate of repeated presentations highlights the ongoing and complex healthcare needs of this population.
- Musculoskeletal disorders were the most common diagnoses in the overall geriatric population; however, with advancing age, non-specific complaints, urinary system diseases, and general condition disorders became more prominent.
- Advancing age was associated with significant increases in yellow-triage classifications and ambulance arrivals, and with a decrease in green-triage admissions, reflecting greater clinical complexity.
- Among patients aged 85 years and older, discharge rates declined markedly, while the proportions of visits resulting in hospitalization, referral, or death increased, indicating the need for heightened clinical attention in this age group.

MATERIALS AND METHODS

This study was designed as a retrospective, observational, and single-center investigation. Ethical approval for this study was obtained from the Erzincan Binali Yıldırım University Non-Interventional Clinical Research Ethics Committee (session no: 16, decision no: 2024-16/05, date: 21.11.2024 The study was conducted among patients who presented to the adult emergency department of Mengücek Gazi Training and Research Hospital between July 1, 2024, and June 30, 2025. Demographic data and clinical characteristics (triage, diagnosis, outcome) were analyzed based on patients' initial visits; however, the total number of visits and repeat visit rates were also recorded throughout the study period. During the study period, the total numbers of patients and emergency department visits were determined, and patients aged 65 years and older were selected for analysis.

Data were obtained from the hospital's electronic information management system. Demographic variables, including age and sex, were collected from patient records. Clinical variables included triage category assigned in the emergency department (green, yellow, red), mode of arrival (ambulatory or by ambulance), time of admission, and seasonal distribution of visits. Diagnoses were classified under system-based categories according to the International Classification of Diseases, 10th Revision (ICD-10). Accordingly, diagnoses were grouped into cardiovascular diseases, respiratory diseases, musculoskeletal diseases, urinary diseases, neurological/neurovascular diseases, gastrointestinal system diseases, general condition disorders, and other diseases. Consultation data included the number of consultation requests and the departments consulted. Outcome variables were categorized as discharge, referral to another center, hospitalization, and death. Patients were divided into three age groups according to the WHO classification: 65-74 years (early old age), 75-84 years (old age), and ≥ 85 years (advanced old age). Demographic characteristics, triage status, mode of arrival, outcomes, and number of repeat visits were statistically analyzed across these three age groups. Patients younger than 65 years and those with missing data were excluded from the study.

Statistical Analysis

Statistical analyses were performed using IBM SPSS Statistics for Windows version 20.0. Armonk, NY: IBM Corp.. Continuous variables were presented as mean ± standard deviation or, when appropriate, as median (minimum-maximum). Categorical variables were expressed as number (n) and percentage (%). For categorical variables, overall comparisons between age groups were performed using the chi-square test. A P value of < 0.05 was considered statistically significant.

Due to the retrospective design of the study, informed consent was not required, and all data were analyzed after anonymization.

RESULTS

Between July 1, 2024, and June 30, 2025, 183,453 patients presented to the adult emergency department of Mengücek

Gazi Training and Research Hospital, accounting for 272,103 visits. Of these visits, 18,269 (14.7%) involved patients aged 65 years or older who constituted the study cohort.

During the study period, 9.931 (54.4%) of patients aged 65 years and older presented to the emergency department only once, whereas 8.338 (45.6%) had multiple visits (range: 2-58). Among included patients, 9,960 (54.5%) were women and 8.309 (45.5%) were men. The mean age was 74.0 ± 7.2 years (range: 65-113). By age group, 10,855 patients (59.4%) were aged 65-74 years, 5,612 (30.7%) were aged 75-84 years, and 1,802 (9.9%) were aged 85 years and older. The demographic and clinical characteristics of the study population are presented in Table 1. A statistically significant difference in sex distribution was observed among age groups, with the proportion of female patients increasing with advancing age (51.7% in the 65-74 age group vs. 61.7% in the ≥ 85 age group; $P < 0.05$). Demographic and clinical characteristics, modes of presentation, triage distributions, outcomes, and diagnostic distributions by age group are summarized in Table 2.

Overall, 8.395 patients (46.0%) were triaged to the green category, 9.746 (53.3%) to the yellow category, and 128 (0.7%) to the red category. Analysis of triage categories demonstrated that the proportion of yellow-category admissions increased with age, whereas the proportion of green-category admissions decreased ($P < 0.05$). A total of 16,120 visits (88.2%) were ambulatory presentations, while 2.149 (11.8%) occurred via ambulance transport. The rate of ambulance arrival increased significantly with age (8.3% in the 65-74 age group vs. 25.1% in the ≥ 85 age group; *P < 0.05). Emergency* department visits most frequently occurred between 08:00 and 15:59 (54.8%). With respect to seasonal distribution, visits were most common during the summer months (7,312 patients, 40.0%).

When diagnoses were evaluated according to system-based categories, musculoskeletal system diseases were the most frequent diagnoses in the overall population (22.3%), followed by respiratory system diseases (17.9%) and cardiovascular system diseases (11.4%) (Table 1). The prevalence of musculoskeletal and respiratory system diseases decreased with advancing age, whereas general-condition disorders (non-specific complaints), urinary system diseases, and other diagnostic categories were more frequent in older age groups; these differences were statistically significant ($P < 0.05$).

Among the study population, 4.386 patients (24.0%) required a total of 8.590 consultation requests. Cardiology, chest diseases, internal medicine, orthopedics, and neurology were the most frequently consulted departments, listed in descending order. Overall, 16.114 patients (88.2%) were discharged from the emergency department, whereas 2.088 (11.4%) were hospitalized. As age increased, the proportion of patients discharged decreased, whereas the proportion of visits resulting in hospitalization, referral, or death increased significantly ($P < 0.05$; Table 2). The most common admission units were the coronary intensive care unit, the orthopedics unit,

Table 1. Baseline Demographic and Clinical Characteristics of the Study Population

Variable	n (%)
Sex	
Female	9.960 (54.5)
Male	8.309 (45.5)
Age (years), mean ± SD (74.0 ± 7.2)	
65-74	10.855 (59.4)
75-84	5.612 (30.7)
≥ 85	1.802 (9.9)
Mode of arrival	
Ambulatory	16.120 (88.2)
Ambulance	2.149 (11.8)
Triage category	
Green	8.395 (46.0)
Yellow	9.746 (53.3)
Red	128 (0.7)
Outcome	
Discharged	16.114 (88.2)
Hospitalized	2.088 (11.4)
Referred	34 (0.2)
Death	33 (0.2)
Time of admission	
08.00-15.59	10.021 (54.8)
16.00-23.59	6.582 (36.0)
00.00-07.59	1.666 (9.1)
Season	
Spring	3.503 (19.2)
Summer	6.276 (34.4)
Autumn	5.261 (28.8)
Winter	3.229 (17.7)
Top 5 diagnoses (grouped ICD-10)	
Musculoskeletal system diseases	4.066 (22.3)
Respiratory system diseases	3.269 (17.9)
Cardiovascular system diseases	2.085 (11.4)
General condition disorder and non-specific complaints	2.019 (11.1)
Urinary system diseases	2.073 (11.3)
Number of visits	
Single visit	9.931 (54.35)
Repeated visits (≥2)	8.338 (45.65)

Values are presented as n (%).SD, standard deviation; ICD, International Classification of Diseases.

Table 2. Demographic and Clinical Characteristics of Emergency Department Visits According to Age Groups

Variable	65-74, n (%)	75-84, n (%)	≥ 85, n (%)	*P* value
Sex				**< 0.001**
Female	5616 (51.7)	3232 (57.6)	1112 (61.7)	
Male	5239 (48.3)	2380 (42.4)	690 (38.3)	
Triage category				**< 0.001**
Green	5894 (54.3)	2150 (38.3)	351 (19.5)	
Yellow	4914 (45.3)	3412 (60.8)	1420 (78.8)	
Red	47 (0.4)	50 (0.9)	31 (1.7)	
Mode of arrival				**< 0.001**
Ambulatory	9950 (91.7)	4820 (85.9)	1350 (74.9)	
Ambulance	905 (8.3)	792 (14.1)	452 (25.1)	
Outcome				**< 0.001**
Discharged	9814 (90.4)	4854 (86.5)	1446 (80.2)	
Others (hospitalization, referral, or death)	1041 (9.6)	758 (13.5)	356 (19.8)	
Number of visits				**< 0.001**
Single	6070 (55.9)	2928 (52.2)	933 (51.8)	
Repeated (≥2)	4785 (44.1)	2684 (47.8)	869 (48.2)	
Top five diagnoses (grouped ICD-10)				**< 0.001**
Musculoskeletal system diseases	2591 (23.9)	1177 (21.0)	298 (16.5)	
Respiratory system diseases	2017 (18.6)	976 (17.4)	276 (15.3)	
Cardiovascular system diseases	1203 (11.1)	670 (11.9)	212 (11.8)	
General condition disorder and non-specific complaints	1121 (10.3)	647 (11.5)	251 (13.9)	
Urinary system diseases	1048 (9.7)	604 (10.8)	421 (23.4)	

Values are presented as n (%). Patients were categorized according to their age at the first emergency department visit. Comparisons between age groups were performed using the chi-square test. *P* value of < 0.05 was considered statistically significant.

Table 3. Distribution of Consultation and Admission Departments

Department	n (%)
Consultation departments	
Cardiology	2055 (23.9)
Chest diseases	1177 (13.7)
Internal medicine	728 (8.5)
Orthopedics	716 (8.3)
Neurology	673 (7.8)
Others	3241 (37.7)
Admission departments	
Coronary intensive care unit	286 (13.7)
Orthopedics service	284 (13.6)
Internal medicine service	209 (10.0)
Neurology service	150 (7.2)
General surgery service	145 (6.9)
Others	1014 (48.6)

Values are presented as n (%).

the internal medicine unit, the general/adult intensive care unit, and the general surgery unit. The distribution of consultation and admission departments is presented in Table 3.

DISCUSSION

In previous studies, Çığşar et al.[7] and Kekeç et al.[8] reported that geriatric patients accounted for 19.6% and 14.3% of emergency department admissions, respectively. Other studies conducted in Türkiye have reported that this proportion ranges between 9% and 23%.[3,4,9] In the present study, patients aged 65 years and older constituted 14.7% of all adult emergency department visits. This variability across studies may be attributed to differences in geographic regions and sociocultural factors. Previous reports have generally indicated a female predominance, with female proportions ranging between 51% and 59%, although some studies have reported higher proportions of male patients.[3,5,10-12] In our study, female patients accounted for 54.5% of the cohort, which is consistent with the literature. Furthermore, the proportion of female patients increased with advancing age, reaching 61.7% in the ≥ 85 age group, suggesting that women constitute a more prominent patient population among the oldest-old presenting to emergency departments.

Aydemir et al.[5] reported that the proportions of patients aged 65-74 years, 75-84 years, and ≥ 85 years presenting to the emergency department were 56.4%, 34.5%, and 9.1%, respectively. Similarly, Nur et al.[13] found that 55.1% of patients aged 65 years and older belonged to the 65-74 age group. In line with these findings, our study demonstrated that 59.4% of geriatric patients were aged 65-74 years, 30.7% were aged 75-84 years, and 9.9% were aged ≥ 85 years. These results indicate that the geriatric population presenting to emergency departments is predominantly composed of younger-old adults. The higher rates of discharge and ambulatory presentation observed among younger-old patients suggest a relatively stable clinical status, whereas increasing age appears to be associated with greater frailty and vulnerability.

In the study by Bedel and Tomruk[14], the rate of ambulance arrivals was reported as 40.6%, whereas another study reported a much lower rate of 2.5%.[5] In the present study, most emergency department visits occurred via ambulatory presentation (88.2%), while ambulance arrivals accounted for 11.8% of visits. Notably, the proportion of ambulance arrivals increased substantially with age, rising from 8.3% in the 65-74 age group to 25.1% in the ≥ 85 age group. This finding suggests that older patients, particularly those in oldest age groups, are more likely to present with severe clinical conditions that require ambulance transport. Variations in ambulance utilization across studies may be influenced by regional socioeconomic characteristics, urban infrastructure, and access to emergency medical services.

According to the findings of Aydemir et al.[5], yellow triage constituted 69.4% of emergency department visits, followed by green and red triage categories. In our study, the yellow triage category was the most common (53.3%), followed by green (46.0%) and red (0.7%). Age-stratified analysis revealed a marked increase in yellow triage assignments with advancing age, from 45.3% in the 65-74 age group to 78.8% in the ≥85 age group. Although red triage accounted for a small proportion of visits overall, its frequency increased with age, rising from 0.4% to 1.7%. These findings are consistent with previous studies and likely reflect the cumulative effects of increasing comorbidity burden, polypharmacy, and frailty associated with aging.

Öktem and Üzer[3] reported that musculoskeletal, respiratory, and circulatory system diseases were the most common reasons for emergency department admission. In another study, general condition disorders, respiratory diseases, and urinary system disorders were reported as the most frequent reasons for admission.[5] In the present study, the most common reasons for emergency department visits were musculoskeletal, respiratory, and cardiovascular system diseases. When diagnostic distributions were examined by age group, the prevalence of musculoskeletal and respiratory system diseases decreased with advancing age, whereas general condition disorders/non-specific complaints, urinary system diseases, and other diagnostic categories increased significantly in older age groups. The marked increase in urinary system diseases among patients aged ≥ 85 years may be related to age-associated declines in physiological reserve, a higher burden of comorbidities, and the predominance of atypical clinical presentations. These findings underscore the growing diagnostic complexity observed in advanced age groups.

Previous studies have reported that emergency department visits are more frequent during daytime hours (08:00-16:00).[4,9,15] Consistent with these reports, more than half of emergency department visits in our study occurred between 08:00 and 15:59, while visits during nighttime hours (00:00-07:59) were least frequent. This pattern may reflect the need for caregiver support, greater daytime activity levels, and avoidance of nighttime emergency department visits among elderly patients.

Aydemir et al.[5] reported that emergency department visits were most frequent during the winter months, although this pattern may have been influenced by the COVID-19 pandemic. In contrast, other studies have reported a higher frequency of visits during summer months.[3] In the present study, emergency department visits were most common in summer (34.4%) and least common in winter (17.7%). Seasonal variations in emergency department utilization among elderly individuals may be influenced by environmental factors (including temperature) and daily activity levels. These findings highlight the importance of incorporating seasonal and temporal patterns into emergency department staffing and resource planning.

Reported discharge, hospitalization, and mortality rates among geriatric emergency department patients vary widely in the literature, with discharge rates of 46.3%-92.4%, hospitalization rates of 3.6%-53.3%, and mortality rates of 0.3%-0.4%.[3,5,16,17] In our study, 88.2% of patients were discharged from the emergency department, 11.4% were hospitalized, and 0.2% died. When evaluated by age groups, the proportion of non-discharge outcomes (hospitalization, referral, or death) increased from 9.6% in the 65-74 age group to 19.8% in the ≥ 85 age group. These outcome distributions are consistent with previously reported ranges and emphasize the increasing need for inpatient care among older age groups.

Previous studies have reported repeat emergency department visit rates of 37%-50% within the first year.[18-21] In accordance with these findings, 45.6% of patients in our study had more than one emergency department visit within the same year. Repeat visit rates increased from 44.1% in the 65-74 age group to 48.2% in the ≥ 85 age group, suggesting that health care needs and utilization intensity increase with advancing age.

Öktem and Üzer[3] reported that 30.1% of geriatric patients required consultation, with cardiology being the most frequently consulted internal medicine specialty and orthopedics the most common surgical specialty. In our study, consultation was required in 24.0% of patients. Cardiology was the most frequently consulted department (23.9%), and orthopedics was the most frequently consulted surgical specialty (8.3%). This distribution suggests that cardiac conditions and trauma-related complaints play a substantial role in emergency department utilization among elderly patients.

In a study by Kılınç et al.[22] conducted in 2012, the most common admission departments following emergency department visits were internal medicine, chest diseases, neurology, and orthopedics. Bedel and Tomruk[14] reported that

15.8% of patients aged 65 years and older were hospitalized, with 28.7% of hospitalized patients requiring intensive care. The most common admission departments in their study were internal medicine, cardiology, chest diseases, and neurology.[14] In our study, 11.4% of patients were hospitalized, and the most common admitting unit was the coronary intensive care unit (13.7%), followed by orthopedics, internal medicine, neurology, and general surgery units. These findings indicate that hospitalizations among elderly patients are driven by traumatic injuries, cardiovascular conditions, and internal medical conditions, and that the diversity of admission diagnoses increases with advancing age, resulting in a broad spectrum of inpatient care needs.

Study Limitations

This study has several limitations. First, due to its retrospective design, the data were obtained from the hospital information management system, which may have led to missing or inaccurate information. Second, the study was conducted in a single center, which may limit the generalizability of the findings to other emergency departments. In addition, geriatric-specific triage tools, such as the Geriatric Emergency Department Triage system, were not used during triage evaluation. The absence of such geriatric-specific triage systems may have negatively affected the observed triage distribution, particularly among patients in the older age groups.

CONCLUSION

In this study, the demographic characteristics, modes of presentation, triage distributions, diagnostic profiles, clinical outcomes, repeat visit patterns, and consultation and hospitalization requirements of patients aged 65 years and older presenting to the emergency department were comprehensively evaluated. The findings indicate that the geriatric population presenting to the emergency department is predominantly composed of younger-old adults; however, with advancing age, ambulance utilization, triage priority, hospitalization rates, diagnostic diversity, and repeat-visit tendencies increase markedly.

Furthermore, the predominance of cardiopulmonary complaints and the involvement of multiple medical specialties highlight the need for a multidisciplinary approach in the emergency department management of elderly patients. Effective management of emergency department visits among geriatric patients requires developing age-specific triage strategies, strengthening multidisciplinary assessment processes, and integrating geriatric care principles into emergency department practice. Such an approach is expected to enhance patient safety and contribute to reductions in both workload and health care costs in emergency departments.

Ethics

Ethics Committee Approval: This study was approved by the Erzincan Binali Yıldırım University Non-Interventional Clinical Research Ethics Committee (session no: 16, decision no: 2024-16/05, date: 21.11.2024).

Informed Consent: Retrospective study. Permission was obtained from hospital management to collect study data from the Information Management System.

Acknowledgments

The authors would like to thank the hospital administration for their support in providing access to the study data.

Footnotes

Author Contributions

Concept Design – O.T., F.M.S.; Data Collection or Processing – O.T., Y.B.; Analysis or Interpretation – O.T., Y.K.; Literature Review - O.T., F.M.S., A.E.Y.; Writing, Reviewing and Editing – O.T., F.M.S., Y.B., E.Y.Ç., A.E.Y.

Declaration of Interests: The authors declare no conflicts of interest.

Funding: The authors declare no financial support or funding.

REFERENCES

1. World Health Organization. Ageing and health [Internet]. Geneva: World Health Organization; 2023 [cited 2025 Jan 1]. [CrossRef]
2. Turkiye Istatistik Kurumu. Istatistiklerle Yaslilar, 2024 [Internet]. Ankara: TUIK; 2025 [cited 2025 Dec 30]. [CrossRef]
3. Oktem B, Uzer F. Acil servise başvuran geriatrik hasta popülasyonun genel özellikleri. *Kocatepe Med J*. 2022;23:283-287. [CrossRef]
4. Bilgili MA, Oncu MR. Acil servise başvuran geriyatrik hastaların değerlendirilmesi. *Van Med J*. 2021;28(3):180-186. [CrossRef]
5. Aydemir A, Karakus O, Ayyildiz M. Acil servise başvuran geriatrik hasta ozelliklerinin ve triyaj uygulamasinin retrospektif olarak incelenmesi: kırsal bolge hastanesi ornegi. *J Nat Life Med*. 2024;6(1):31-38. [CrossRef]
6. Celik P, Celik S, Hastaoglu F. Acil servise basvuran geriatrik hasta profilinin belirlenmesi. *J Acad Emerg Med*. 2015;14(3):117-121. [CrossRef]
7. Cigsar G, Akkus Y, Elnare G, Erdemir-Ozturk E, Palas MB. Yaşlıların acil servise başvurma nedenleri: Kars'ta retrospektif bir calisma. *Turk J Geriatr*. 2016;19(1):19-26. [CrossRef]
8. Kekec Z, Koc F, Buyuk S. Acil serviste yaşlı hasta yatislarinin gözden gecirilmesi. *Akad Acil Tip Derg*. 2009;8(3):21-24. [CrossRef]
9. Mert E. Geriatrik hastalarin acil servis kullanımı. *Turk J Geriatr*. 2006;9(2):70-74. [CrossRef]
10. Gulalp B, Aldinc H, Karagun O, Cetinel Y, Benli S. The complaint and outcome of geriatric patients in the emergency department. *Turk J Emerg Med*. 2009;9(2):73-77. [CrossRef]
11. Yildirim H, Kaya M. Acil servis başvurusu sonrasi hastaneye yatirilan yaşlı hasta grubunun analizi. *Turk J Emerg Med*. 2018;18(4):170-176. [CrossRef]
12. Oztok Tekten B, Celik K, Colak T. Investigation of the reasons and frequency of geriatric patients applying to the emergency department. *Eurasian J Emerg Med*. 2019;18(2):79-84. [CrossRef]
13. Nur N, Demir OF, Cetinkaya S, Tirek N. Evaluation of the 112 emergency service use by older people. *Turk J Geriatr*. 2008;11(1):7-11. [CrossRef]
14. Bedel C, Tomruk O. Bir üniversite acil servisine basvuran geriatrik hastalarin ozellikleri. *SDU Tip Fak Derg*. 2018;25(4):393-399. [CrossRef]

15. Alpaslan M, Oktay M, Baykan N. Acil servise basvuran 90 yas ve ustundeki hastalarin degerlendirilmesi. *Turk J Geriatr*. 2017;20(3):215-221. [CrossRef]

16. Varisli B. Acil servise basvuran geriatrik yas grubu hastalarin klinik, demografik ve maliyet acisindan incelenmesi. *Anatol J Emerg Med*. 2018;1(2):18-24. [CrossRef]

17. Tortum F, Tekin E, Gur A. Predictive value of the Hemoglobin, Albumin, Lymphocyte and Platelet score for mortality in geriatric patients presenting to the emergency department. *Geriatr Gerontol Int*. 2025;25:387–391. [CrossRef]

18. Demircan A, Aygencel Bikmaz SG, Kadi G, et al. Evaluation of the general characteristics of patients aged 85 years and above admitted to a university hospital emergency department. *Turk J Med Sci*. 2017;47(5):1393-1400. [CrossRef]

19. Vilpert S, Ruedin HJ, Trueb L, et al. Emergency department use by oldest-old patients from 2005 to 2010 in a Swiss university hospital. *BMC Health Serv Res*. 2013;13:344. [CrossRef]

20. Kennelly SP, Drumm B, Coughlan T, et al. Characteristics and outcomes of older persons attending the emergency department: a retrospective cohort study. *QJM*. 2014;107(12):977-987. [CrossRef]

21. Graf E, Gianelli SV, Hermann FR, et al. Identification of older patients at risk of unplanned readmission after discharge from the emergency department: comparison of two screening tools. *Swiss Med Wkly*. 2012;141:w13327. [CrossRef]

22. Kilinc AS, Catak B, Badillioglu O. Causes and consequences of admission to the emergency department in elderly. *Suleyman Demirel Univ Tip Fak Derg*. 2012;19(4):139-143. [CrossRef]

ABCResearch

Arch Basic Clin Res 2026;8(2):171-182
DOI: 10.4274/ABCR.2026.25401

Research Article

Bibliometric Analysis of Articles Investigating Hematologic Malignancy Patients Admitted to the Intensive Care Unit

Özlem Öner[1], Sinem Namdaroğlu[2]

[1]Clinic of Anesthesiology and Reanimation Subdivision of Critical Care Medicine, İzmir Buca Seyfi Demirsoy Training and Research Hospital, İzmir, Türkiye

[2]Department of Internal Medicine, Subdivision of Hematology, Dokuz Eylül University Faculty of Medicine, İzmir, Türkiye

Cite this article as: Öner Ö, Namdaroğlu S. Bibliometric analysis of articles investigating hematologic malignancy patients admitted to the intensive care unit. *Arch Basic Clin Res*. 2026;8(2):171-182.

ORCID IDs of the authors: Ö.Ö. 0000-0001-6171-2114, S.N. 0000-0002-8074-7301.

ABSTRACT

Objective: To evaluate the citation trends and scientific landscape of studies investigating critically ill patients with hematological malignancies (HM) admitted to intensive care units (ICUs) using bibliometric analysis.

Methods: The Web of Science Core Collection database was searched on March 14, 2026, for original articles published between 2000 and 2025. Publications related to HM requiring ICU admission were analyzed for citation counts, authorship, journals, countries of origin, international collaborations, and keyword trends.

Results: A total of 290 publications were included in the final analysis. These studies received 5,576 citations, of which 5,003 remained after excluding self-citations. The mean number of citations per publication was 19.23. A total of 3,649 citing articles were identified (3,487 excluding self-citations). The most frequent keywords were mortality (n=44), intensive care (n=42), and critical care (n=34), reflecting the primary research focus of the field.

Conclusion: Research on critically ill patients with HM has primarily focused on mortality and prognostic evaluation, with a growing emphasis on intensive care management strategies. The increasing number of publications and strong international collaboration networks indicate a rapidly evolving field. Future research should focus on multicenter collaborations and standardized clinical approaches to enhance the generalizability and clinical impact of findings.

Keywords: Adult, bibliometric, education, hematological malignancy, hematopoietic stem cell transplantation, intensive care unit

INTRODUCTION

Hematologic malignancies are tumors of myeloid or lymphoid origin that result from disturbances in normal hematopoietic processes.[1] These disorders are generally grouped into major categories such as leukemia, multiple myeloma (MM), non-Hodgkin lymphoma (NHL), and Hodgkin lymphoma (HL).[2] On a global scale, data regarding the incidence, prevalence, and overall disease burden of hematological cancers remain limited, and scientific investigation in this field is progressing. Conventional therapeutic strategies remain insufficient for this cluster of diseases; thus, novel treatment modalities continue to be actively pursued.[3] Although advances in emerging therapies have improved survival among patients with hematological malignancies (HMs), outcomes for patients with HMs requiring intensive care unit (ICU) admission remain unclear. Reported ICU mortality rates among HM patients vary between 46% and 90%, far exceeding those observed in general medical ICU populations.[4] Mortality during ICU management and its

Corresponding author: Özlem Öner, **E-mail:** namdaroner@gmail.com

Received: December 18, 2025
Revision Requested: February 20, 2026 **Accepted:** May 25, 2026 **Publication Date:** July, 14, 2026

associated determinants constitute additional major research interests, alongside therapeutic approaches for HM patients.[5]

Health systems around the world face growing challenges due to an expanding elderly population, a factor that further escalates the clinical and economic impact of HM.[6] Determining morbidity and mortality data for hematological malignancies within ICU settings is crucial not only for shaping and optimizing clinical strategies but also for guiding the allocation of scientific research resources. Bibliometric analysis is one methodological tool capable of evaluating such developments.[7]

Bibliometric analysis constitutes a quantitative approach that uses statistical methods and analytic instruments to assess multiple dimensions of scholarly output.[8] This methodology facilitates the identification of research patterns, visualization of scientific networks, and assessment of scholarly influence. It offers extensive insight into a research discipline through comprehensive statistical and quantitative analyses.[9]

With the increasing number of publications on HM requiring ICU admission, evidence and knowledge in this domain have expanded steadily each year. In the current study, bibliometric techniques were applied to explore publication trends, highly cited authors, contributing countries, international cooperation patterns, frequently employed keywords, and associated visual analytic metrics. The objective of this investigation is to pinpoint current research focal points at the interface between ICU care and HM, characterize citation trends and emerging themes, and provide direction for future scientific efforts in this field.

MATERIALS AND METHODS

Data Sources and Search Strategies

For this bibliometric analysis, we selected the Thomson Reuters' Web of Science Core Collection (WoSCC) as our database. The selection of the Web of Science (WoS; Clarivate Analytics, USA) platform was justified by its inclusion of diverse bibliometric indicators and its extensive coverage of multidisciplinary literature.[10]

The following template was created as the search strategy: TS= "hematologic* malignan*" OR leukemia* OR lymphoma * OR "MM" OR "hematopoietic stem cell transplant*" OR HSCT OR "Bone marrow transplant" AND "intensive care" OR "intensive care unit" OR ICU OR "critical care" OR "critically ill".

Articles were selected under the 'Document Types' category. The search time range was set to 2000-2025 (publication years). Critical Care Medicine and Hematology were selected as WoS categories. The topic 'Intensive care' was selected for the Citation Topics Micro search. The Science Citation Index Expanded (SCI-EXPANDED) was selected in the WoS Index, and English was selected as the language option. Hematology and Anesthesiology were selected as research areas for the search plan. The search strategy is shown in detail in Figure 1.

All records (including titles, authors, sources, and abstracts) and references in our search results were exported in plain text format. Data collection was carried out in 1 day (March 14, 2026) to prevent variations due to daily updates in the database. All data are publicly available and do not contain any personal information; therefore, informed consent was not required. While ethical committee approval is not required for bibliometric studies involving publicly available data, approval was obtained for our study from Dokuz Eylül University with approval no: 2023/41-16, date: 20.12.2023). Publications concerning "HMs admitted to the intensive care unit" were evaluated based on citation counts, contributing authors, publishing journals, national origins, international collaborations, and research hotspots. Details regarding data acquisition and analytical procedures are described below.

Performance Analysis

Excel 2019 (Redmond, WA) and VOSviewer (version 1.6.11, Leiden University, van Eck, NJ) were used for bibliometric analysis. Excel 2019 was used to present the number of articles published each year and trends in journal distribution.[11,12] VOSviewer was used to perform co-citation analysis of references, journals, and authors and to create relevant knowledge maps. Co-citation maps contain nodes representing cited references, journals, and authors, and node size reflects citation frequency. The connections between nodes represent co-citation relationships. The Fractional counting method was used in VOSviewer, and the threshold was set to select publications. Performance analysis was used to quantify core indicators of scientific activity by evaluating publication growth, leading institutions and countries, highly cited journals, and keyword mappings. Citation analysis was performed during this stage. The Journal Citation Reports dataset was employed to determine the 2023 impact factors (IFs). Both the h-index and the IF were used to describe publication impact. The h-index serves as a key measure of scholarly productivity.[13] It can also be applied to institutions, countries, journals, and research groups. The IF reflects a journal's scientific influence based on the citation performance of its published articles.[13] Finally, the 15 most-cited sources, journals, authors, and articles were identified. Additionally, a table containing the top 50 articles is included as Appendix 1 in the publication.

Keywords Strategy

Bibliometric analysis was performed using VOSviewer (version 1.6.15) and the R package Bibliometrix. Fractional counting

MAIN POINTS

- Comprehensive bibliometric mapping of hematologic malignancies in intensive care units (ICUs) revealed 156 original studies published between 1970 and 2024, with an h-index of 39 and an average of 28.4 citations per article.
- Research hotspots identified include "mortality," "prognostic factors," "outcomes," and "survival," indicating the predominant focus on patient prognosis and outcome improvement in ICU settings.
- Global analysis showed that France, Belgium, and Austria lead in publication impact, while emerging countries such as Brazil, Türkiye, and China demonstrate increasing but lower research influence, underscoring regional disparities in scientific contribution.

was applied to reduce bias from multi-authored publications. No additional normalization method was applied beyond the default normalization implemented in VOSviewer. For keyword co-occurrence analysis, a minimum occurrence threshold of 5 was used. Both Author Keywords and Keywords Plus were included in the analysis. Preprocessing steps included the removal of non-informative stop words and the merging of synonymous terms (e.g., ICU, intensive care unit, intensive care) to improve consistency. The most frequent terms were identified based on their frequency after preprocessing.

Scientific Mapping

Scientific mapping provides a structural representation of relationships among disciplines, subfields, individual works, or researchers. In this study, highly cited authors, collaboration networks, and co-word analyses were visualized using VOSviewer. Mapping outputs depicting these relationships were generated using VOSviewer version 1.6.15 (https://www.vosviewer.com/).

RESULTS

Analysis of Performance

Records were identified through the WoS database (n=1,283,318). After applying the document type filter (Article), 835,905 records remained. Subsequently, restricting the publication years to 2000-2025 resulted in 695,680 records. During the screening phase, records were filtered using WoS categories (Hematology OR Critical Care Medicine), yielding 129,725 records. Further refinement using the citation topic (micro), "Intensive Care", reduced the number of records to 4,666. After limiting the dataset to the SCI-EXPANDED, 4,021 records were retained. Applying the language filter (English) resulted in 3,918 records. During the eligibility phase, records were further restricted based on research areas (Hematology or Anesthesiology), resulting in 290 studies. A total of 290 studies were included in the bibliometric analysis (Figure 1).

A total of 290 publications were included in the final bibliometric analysis. These publications spanned 2000-2025, reflecting the long-term development of research activity in the field. The included studies collectively received 5,576 citations, of which 5,003 remained after excluding self-citations, indicating substantial external scientific impact. The mean number of citations per publication was 19.23, indicating moderate citation performance across the dataset. In total, the publications were cited by 3,649 articles, of which 3,487 remained after the exclusion of self-citations, further supporting the robustness and dissemination of the scientific output. The calculated h-index was 38, indicating that 38 publications have each received at least 38 citations, reflecting a consistent and influential body of work within the analyzed domain.

Analysis of Articles

A total of 15 highly cited articles were identified in the WoSCC, focusing on ICU outcomes, prognostic factors, and management strategies for critically ill patients. Citation counts ranged from 67 to 143, indicating a strong representation of influential studies within the field (Table 1).

The most-cited article in this group reported that delayed ICU admission was associated with significantly increased mortality among cancer patients with acute respiratory failure (n=143 citations). The second most-cited article is "Transport of critically ill patients: Complications and difficulties," published in the journal Anaesthesia And Intensive Care, with 114 citations. The third most-cited article is "Prognostic factors for ICU admission, intensive care outcome, and post-intensive care survival in patients with de novo acute myeloid leukemia: a single center experience," published in Haematologica-The Hematology Journal, and has 108 citations (Table 2).

Analysis of Sources (Journals)

A total of 290 publications appeared in multiple scientific journals, reflecting the interdisciplinary nature of the field, which spans anesthesiology, critical care, and hematology.

The most productive journal was Anaesthesia and Intensive Care (74 publications), followed by Minerva Anestesiologica (41 publications) and Bone Marrow Transplantation (21 publications).

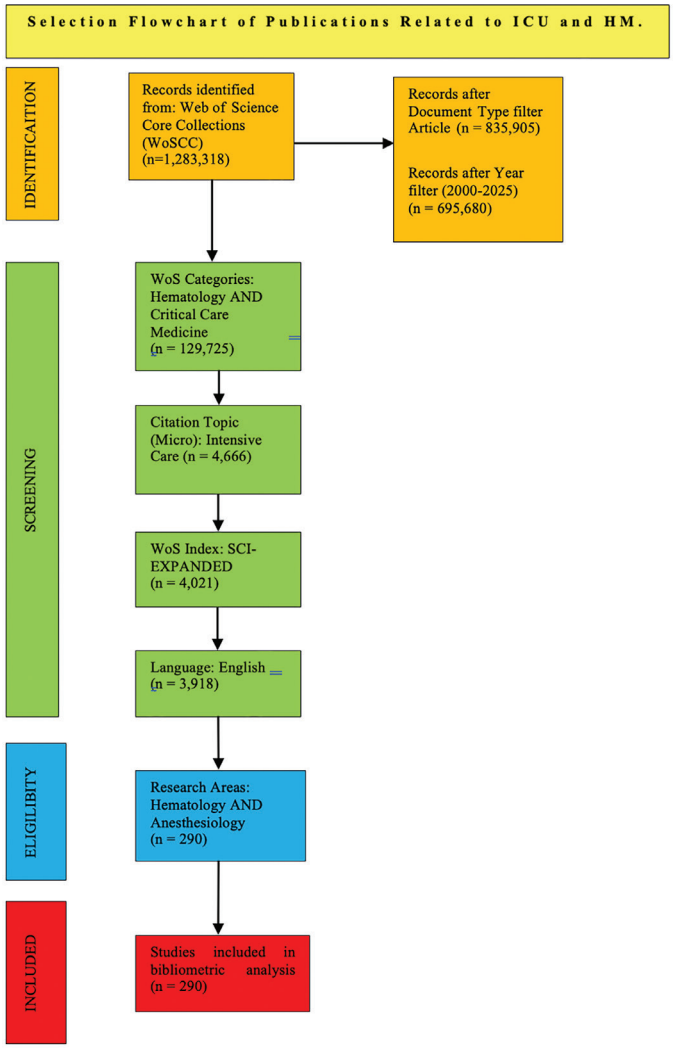

Figure 1. PRISMA 2020 flow diagram illustrating the selection process of studies included in the bibliometric analysis.

Table 1. Bibliometric Analysis of the 15 Most Highly Cited Publications in ICU and Hematological Malignancies Research, Including Citation Counts, Network-Based Total Link Strength, and Journal Distribution

Article title	Source title	Times cited, Wos Core	Total link strength
Delayed intensive care unit admission is associated with increased mortality in patients with cancer with acute respiratory failure	Leukemia & Lymphoma	143	23
Intrahospital transport of critically ill patients: complications and difficulties	Anaesthesia and intensive care	114	20
Prognostic factors for care unit admission, intensive care outcome, and post-intensive care survival in patients with de novo acute myeloid leukemia: a single center experience	Haematologica-The Hematology Journal	108	19
Postoperative complications after craniotomy for brain tumor surgery	Anaesthesia Critical Care & Pain Medicine	95	18
Incidence and prognostic value of respiratory events in acute leukemia	Leukemia	94	16
Intensive care unit management of patients with newly diagnosed acute myeloid leukemia with no organ failure	Leukemia & Lymphoma	91	16
Efficacy of the APACHE Ii Score at ICU discharge in predicting post-ICU Mortality and ICU readmission in critically ill surgical patients	Anaesthesia and Intensive Care	87	16
Identification of poor prognostic features among patients requiring mechanical ventilation after hematopoietic stem cell transplantation	Blood	85	15
The epidemiology of adult rapid response team patients in Australia	Anaesthesia and Intensive Care	84	15
Prognosis of patients with acute Myeloid Leukaemia admitted to intensive care	British Journal of Haematology	82	15
Outcomes in critically Ill cancer patients with septic shock of pulmonary origin	Shock	71	15
Changes in intensive care for allogeneic hematopoietic stem cell transplant recipients	Bone Marrow Transplantation	69	15
After-Hours discharge from intensive care increases the risk of readmission and death	Anaesthesia and Intensive Care	68	14
Night-shift discharge from intensive care unit increases the mortality-risk of ICU survivors	Anaesthesia and Intensive Care	68	14
Combining Sequential Organ Failure Assessment (SOFA) Score with Acute Physiology and Chronic Health Evaluation (APACHE) Ii score to predict hospital mortality of critically ill patients	Anaesthesia and Intensive Care	67	14

Other notable contributors included Journal of Pediatric Hematology/Oncology (20 publications) and Anaesthesia Critical Care & Pain Medicine (19 publications). In terms of citation impact, Anaesthesia and Intensive Care ranked first with 1,510 citations, followed by Minerva Anestesiologica (620 citations) and Bone Marrow Transplantation (557 citations) (Table 3).

Network analysis revealed that Bone Marrow Transplantation had the highest total link strength (131), indicating strong interconnections with other journals in the citation network. This was followed by Annals of Hematology (90) and Leukemia & Lymphoma (79).

Analysis of Institutions

Multiple leading institutions contributing to the field of intensive care and to outcomes for critically ill patients were identified based on publication output, citation counts, and total link strength.

The Medical University of Vienna emerged as the most productive institution, with 12 publications, followed by Monash University (n=10). Several Australian centers, including Alfred Hospital and Royal Perth Hospital (each n=8), as well as Royal Adelaide Hospital and Royal Brisbane and Women's Hospital (each n=7), demonstrated substantial research output. Institutions such as the University Medical Center Utrecht and the University of Queensland (each n=7) also contributed significantly.

In terms of citation counts, Medical University of Vienna ranked first with 298 citations, indicating both high productivity and strong academic impact. Monash University followed with 196 citations, while European institutions such as Hôpital Hôtel-Dieu (176 citations) and CHU Angers (164 citations) also demonstrated high citation performance. Other notable contributors included Institut Paoli-Calmettes (154 citations) and University of Western Australia (152 citations).

Network analysis revealed that Medical University of Vienna had the highest total link strength (156), reflecting its central role in international research collaboration. Nino Jesus Children's Hospital (130) and University Medical Center Utrecht (108) also exhibited strong collaborative connections. Additional key institutions within the collaboration network included Leiden University (100), CHU Angers (99), and University of California San Francisco (89) (Table 4).

Table 2. Bibliometric Evaluation of Leading Journals Contributing to ICU and Hematological Malignancies Literature, Including Productivity, Citation Impact, and Collaboration Network Strength

Source	Documents	Source	Citations	Source	Total link strength
Anaesthesia and Intensive Care	74	Anaesthesia and Intensive Care	1510	Bone Marrow Transplantation	131
Minerva Anestesiologica	41	Minerva Anestesiologica	620	Annals of Hematology	90
Bone Marrow Transplantation	21	Bone Marrow Transplantation	557	Leukemia & Lymphoma	79
Journal of Pediatric Hematology Oncology	20	Leukemia & Lymphoma	471	Biology of Blood and Marrow Transplantation	75
Anaesthesia Critical Care & Pain Medicine	19	Journal of Pediatric Hematology Oncology	358	British Journal of Haematology	65
Leukemia & Lymphoma	19	Annals of Hematology	313	Journal of Pediatric Hematology Oncology	59
Annals of Hematology	16	Anaesthesia Critical Care & Pain Medicine	243	Hematology	43
Shock	13	Biology of Blood and Marrow Transplantation	225	European Journal of Haematology	36
Biology of Blood and Marrow Transplantation	11	British Journal of Haematology	225	Pediatric Blood & Cancer	25
Pediatric Blood & Cancer	11	Shock	155	Haematologica-The Hematology Journal	18
Hematology	8	Pediatric Blood & Cancer	122	Anaesthesia and Intensive Care	17
European Journal of Haematology	7	Haematologica-The Hematology Journal	108	Minerva Anestesiologica	17
British Journal of Haematology	6	Hematology	107	Haematologica	16
Transplantation and Cellular Therapy	3	European Journal of Haematology	94	Acta Haematologica	15
Acta Haematologica	2	Leukemia	94	Transplantation and Cellular Therapy	14

Analysis of Countries

Multiple countries contributed to the literature on intensive care and outcomes of critically ill patients, with notable variability in research productivity, citation impact, and strength of collaboration (Table 5).

Australia was the most productive country, with 58 publications, followed by the United States (n=48) and France (n=40). Germany (n=29) and Italy (n=24) also demonstrated substantial contributions. Other countries with moderate output included the Netherlands (n=16), Spain (n=15), and England (n=13). Contributions from Austria (n=12), Belgium (n=11), and Canada (n=11) were also noteworthy (Figure 2).

In terms of total citations, Australia again led with 1,246, indicating both high productivity and strong academic influence. France ranked second with 1,001 citations, followed by the United States (782 citations). Germany (406 citations) and Italy (331 citations) maintained a consistent presence in both productivity and citation impact. The Netherlands (290 citations) and England (257 citations) also exerted considerable influence.

Network analysis revealed that France had the highest total link strength (156), indicating a central role in international research collaboration. The United States closely followed, with 154 collaborations, while Germany (106) and the Netherlands (83) also showed strong collaborative connectivity. Spain (74) and England (67) contributed meaningfully to the global collaboration network.

Analysis of Authors

Leading authors contributing to the field of intensive care and outcomes of critically ill patients were identified based on publication productivity, citation impact, and collaboration strength.

Among the authors, Azoulay E. was the most productive with 11 publications, followed by Lemiale V. (n=9) and Mokart D. (n=7). Several authors, including Canet E., Lengline E., Pilcher D.V., and Staudinger T., contributed six publications each (Figure 3). Additional contributors, such as Dobb G.J., Ho K.M., Kouatchet A., and Schellongowski P., demonstrated moderate productivity, each with five publications (Figure 3).

Table 3. Institutional Contribution And Collaboration Network Analysis in ICU and Hematological Malignancies Research

Organization	Documents	Organization	Citations	Organization	Total link strength
Med Univ Vienna	12	Med Univ Vienna	298	Med Univ Vienna	156
Monash Univ	10	Monash Univ	196	Nino Jesus Childrens Hosp	130
Alfred Hosp	8	Hop Hotel Dieu	176	Univ Med Ctr Utrecht	108
Royal Perth Hosp	8	Chu Angers	164	Leiden Univ	100
Royal Adelaide Hosp	7	Inst J Paoli I Calmettes	154	Chu Angers	99
Royal Brisbane & Womens Hosp	7	Univ Western Australia	152	Univ Calif San Francisco	89
Univ Med Ctr Utrecht	7	Alfred Hosp	150	Univ Groningen	85
Univ Queensland	7	Univ Paris 07	148	Karolinska Univ Hosp	82
Univ Western Australia	6	Ch Versailles	143	Ghent Univ Hosp	76
Leiden Univ	5	Chu Avicenne	143	British Soc Blood & Marrow Transplantat	71
Univ Calif San Francisco	5	Chu Cochin	143	Royal Free London Nhs Fdn Trust	71
Univ Groningen	5	Chu Hotel Dieu	143	Ucl Med Sch	71
Univ Melbourne	5	Chu St Louis	143	Univ Coll London Hosp Nhs Fdn Trust	71
Ghent Univ Hosp	4	No Hosp	136	Univ Padua	70
Harvard Univ	4	Royal Brisbane & Womens Hosp	131	Univ Hosp Padua	70

Table 4. Country-Based Bibliometric Analysis of ICU and Hematological Malignancies Research Productivity, Impact, and Collaboration Networks

Country	Documents	Country	Citations	Country	Total link strength
Australia	58	Australia	1246	France	156
USA	48	France	1001	USA	154
France	40	USA	782	Germany	106
Germany	29	Germany	406	Netherlands	83
Italy	24	Italy	331	Spain	74
Netherlands	16	Austria	298	England	67
Spain	15	Netherlands	290	Italy	65
England	13	England	257	Canada	52
Austria	12	Spain	231	Austria	48
Belgium	11	Canada	200	Turkey	38
Canada	11	South Korea	181	Sweden	38
People's Republic of China	9	Belgium	151	Belgium	37
South Korea	8	Brazil	99	Australia	32
New Zealand	7	Turkey	97	South Korea	29
Brazil	6	Sweden	90	Israel	27

ICU, intensive care unit.

Table 5. Author-level Bibliometric Analysis Highlighting the Most Productive, Cited, and Collaborative Researchers in ICU and Hematological Malignancies Research

Author	Documents	Author	Citations	Author	Total link strength
Azoulay E	11	Azoulay E	405	Schellongowski P	438
Lemiale V	9	Lemiale V	395	Azoulay E	413
Mokart D	7	Lengline E	306	Lemiale V	374
Canet E	6	Kouatchet A	252	Kouatchet A	356
Lengline E	6	Mokart D	243	Staudinger T	352
Pilcher DV	6	Pène F	240	Bojic A	338
Staudinger T	6	Bruneel F	231	Sperr WR	338
Dobb GJ	5	Vincent F	231	Lengline E	334
Ho KM	5	Chevret S	214	Wohlfarth P	316
Kouatchet A	5	Lambert J	214	Mokart D	283
Schellongowski P	5	Staudinger T	197	Jaeger U	277
Williams TA	5	Schellongowski P	193	Valent P	277
Pène F	4	Bojic A	182	Diaz M	271
Wohlfarth P	4	Sperr WR	182	Madero L	271
Amigoni A	3	Chaoui D	176	Sevilla J	271

ICU, intensive care unit.

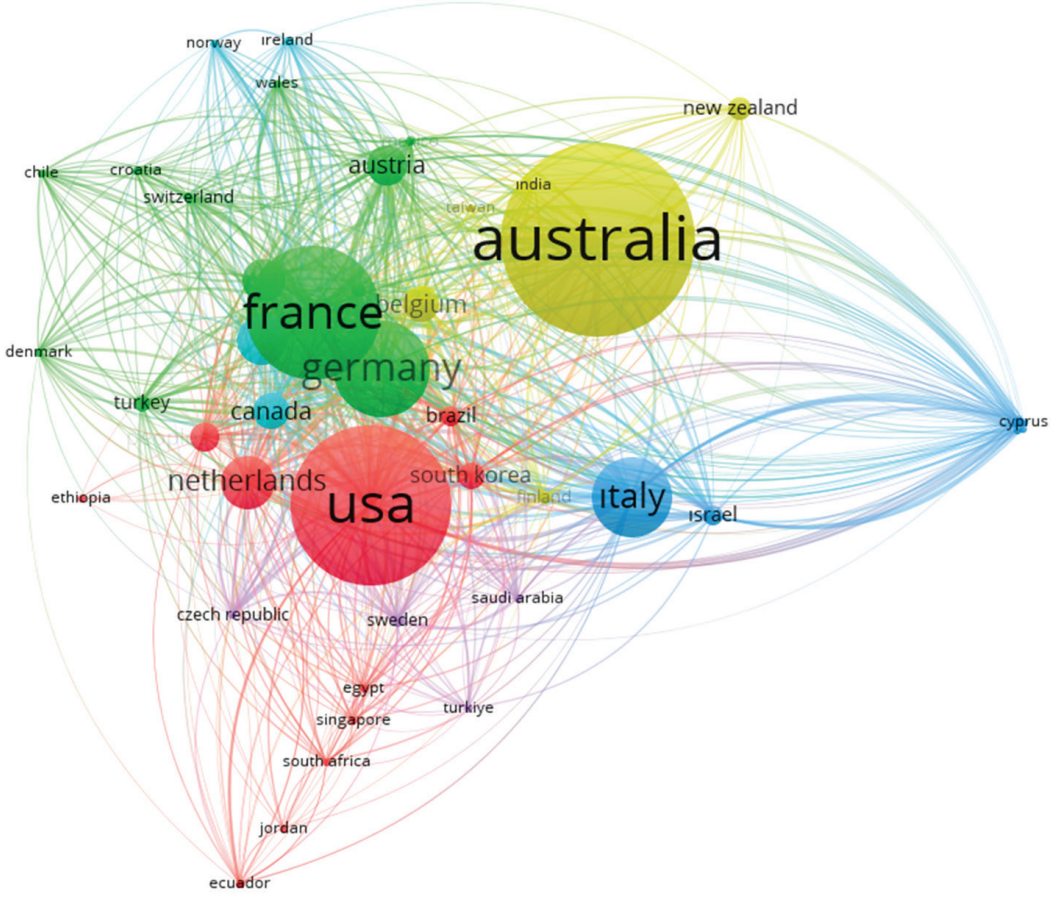

Figure 2. Network visualization of international collaboration among countries based on co-authorship analysis.

Node size reflects publication productivity, while edge thickness corresponds to the total link strength between countries. Different colors denote distinct collaboration clusters, highlighting regional and international research partnerships. Prominent nodes such as Australia, the USA, France, Germany, and Italy represent leading contributors and key connectors in the global research network.

In terms of citation counts, Azoulay E. ranked first with 405 citations, followed closely by Lemiale V. with 395 citations. Lengline E. (306 citations) and Kouatchet A. (252 citations) were also among the most influential authors. Other notable contributors included Mokart D. (243 citations), Pène F. (240 citations), and Bruneel F. (231 citations), indicating a consistent overlap between productivity and citation impact among leading researchers.

Network analysis revealed that Schellongowski P. had the highest total link (Figure 4) (438), indicating a central role in collaborative research networks. Azoulay E. (413) and Lemiale V. (374) also demonstrated strong collaborative connectivity. Additional key contributors included Kouatchet A.(356)and Staudinger T. (352), highlighting a dense, interconnected author network.

Analysis of Keywords

Bibliometric analysis was performed using VOSviewer (version 1.6.15) and Bibliometrix (R package). Fractional counting was applied to reduce bias from multi-authored publications (Figure 5).

No additional normalization method was applied beyond the default normalization implemented in VOSviewer (Table 6). For keyword co-occurrence analysis, a minimum occurrence threshold of 5 was used. Both Author Keywords and Keywords Plus were included in the analysis. Preprocessing steps included the removal of non-informative stop-words and the merging of synonymous terms (e.g., ICU, intensive care unit, intensive care) to improve consistency. The most frequently occurring terms were identified based on their frequency of occurrence after preprocessing (Figure 6).

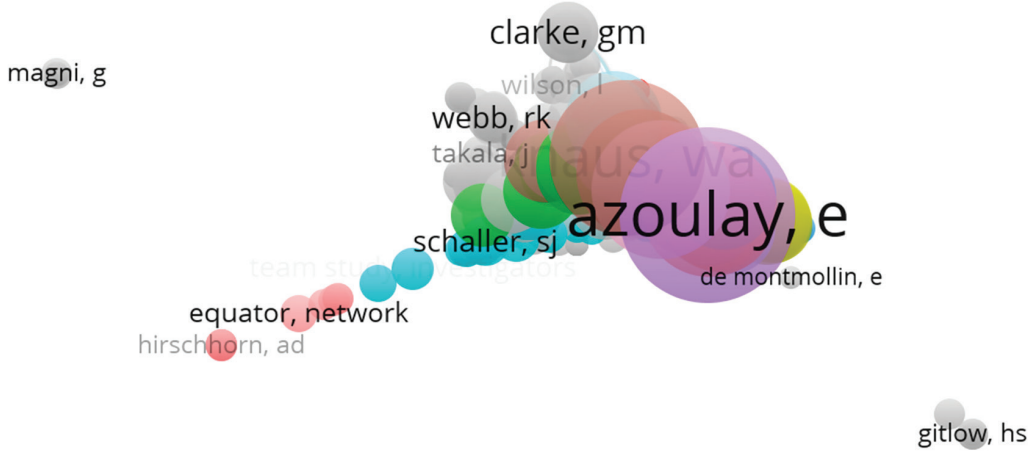

Figure 3. Co-authorship network of authors showing collaborative relationships and publication clusters.

Node size represents the number of publications contributed by each author, while the thickness of connecting lines indicates the strength of collaboration between authors.

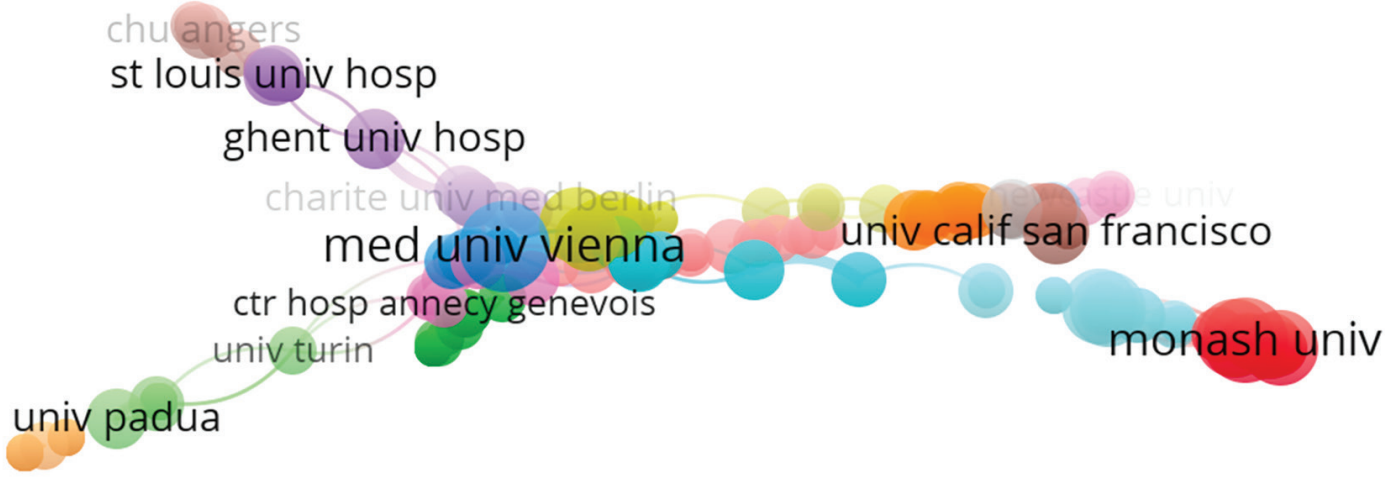

Figure 4. Institutional collaboration network highlighting the most productive research centers.

The size of each node represents the number of publications produced by the institution it represents, while link strength reflects collaborative relationships between institutions.

A number of frequently occurring keywords were identified to characterize the main research themes within the field of intensive care and outcomes of critically ill patients. The most common keyword was mortality (n=44), followed closely by intensive care (n=42) and critical care (n=34). Other high-frequency terms included intensive care unit (n=29; n=26 for variant forms), prognosis (n=24), and mechanical ventilation (n=21). Multiple variations of similar terms were observed, including intensive care, intensive care unit, intensive care units, and ICU, reflecting differences in indexing and authors' keyword preferences. Despite these variations, all terms consistently pointed toward the same core research domain.

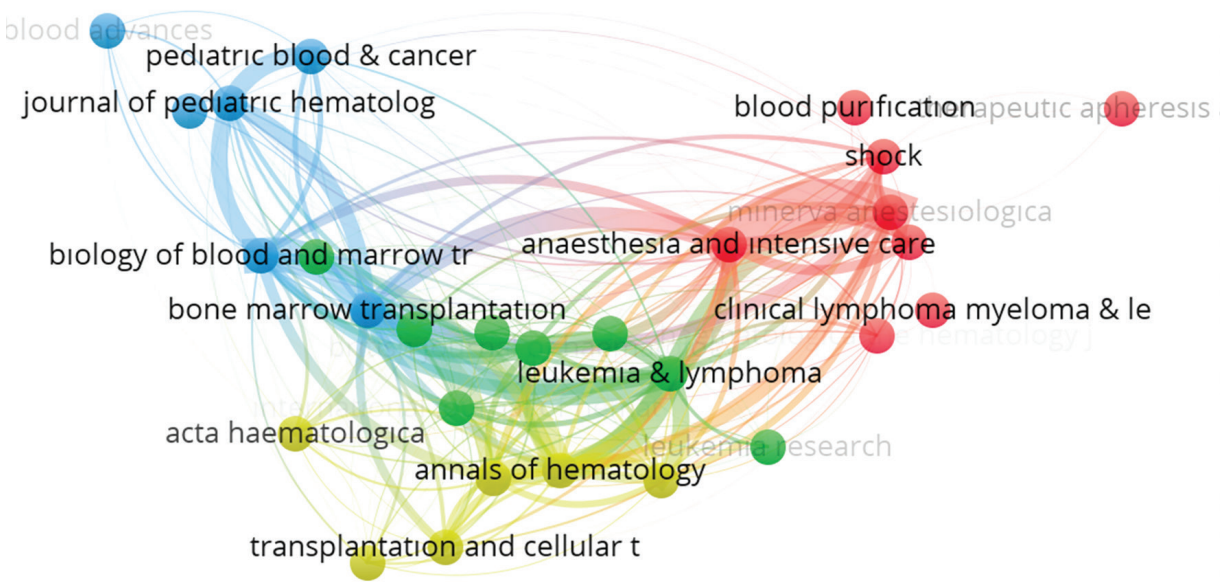

Figure 5. Journal co-citation network representing relationships among leading journals.

The size of each word reflects its frequency of occurrence within the dataset. malignancies in intensive care units.

Table 6. Co-occurrence Analysis of Keywords in ICU and Hematological Malignancies Research, Including Frequency of Occurrence and Total Link Strength

Keyword	Occurrences	Keyword	Total link strength
Mortality	44	Intensive care	169
Intensive care	42	Mortality	167
Critical care	34	Critical care	138
Intensive care unit	29	Intensive care unit	122
Intensive care unit	26	Intensive care unit	94
Prognosis	24	Mechanical ventilation	92
Mechanical ventilation	21	Prognosis	91
Cancer	19	Cancer	81
Intensive care units	17	Sepsis	68
Sepsis	16	Hematopoietic stem cell transplantation	61
Critical illness	14	Critical illness	59
Outcome	14	Outcome	57
Hematopoietic stem cell transplantation	13	Intensive care units	54
ICU	12	ICU	41
Children	11	Pediatric	41

ICU, intensive care unit.

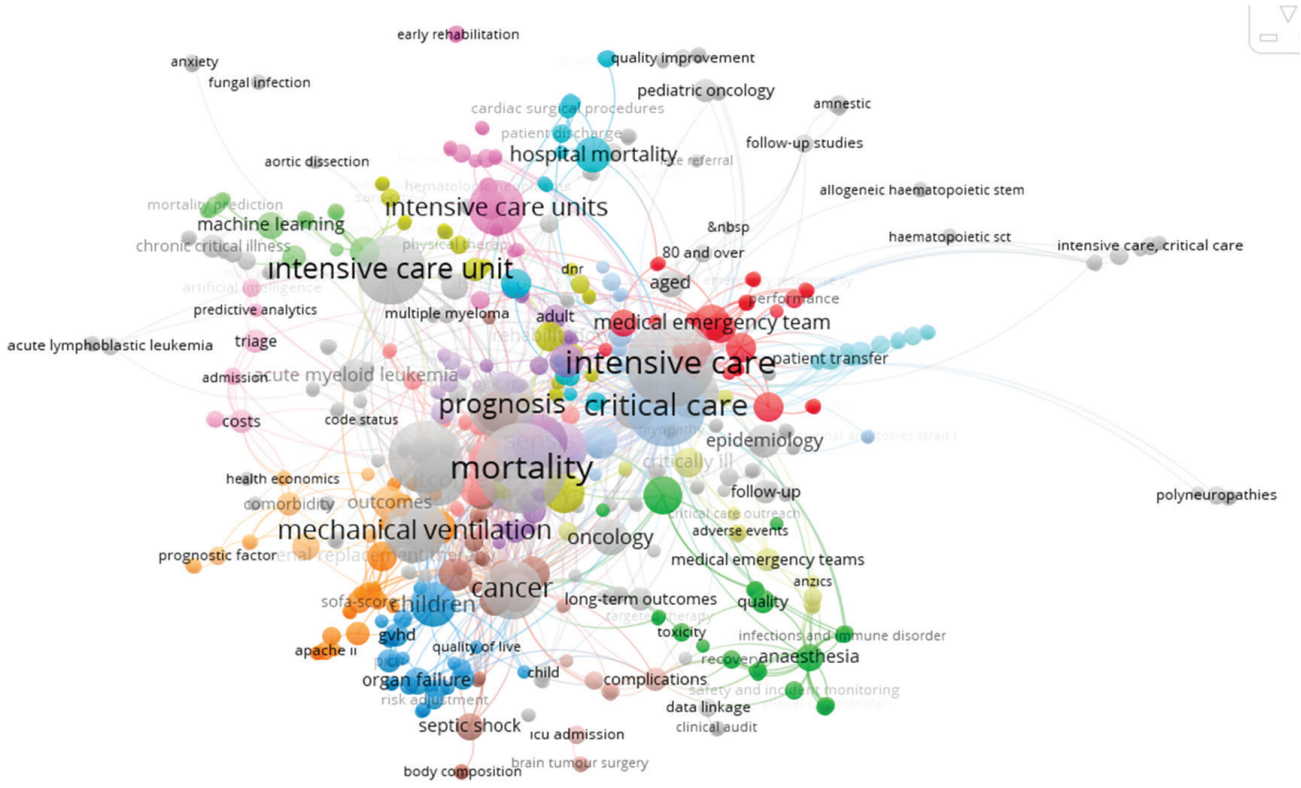

Figure 6. Keyword co-occurrence network illustrating major research themes and their interconnections.

Node size indicates keyword frequency, while link strength represents co-occurrence relationships between terms.

DISCUSSION

This bibliometric analysis provides a comprehensive overview of the scientific landscape concerning critically ill patients with HMs admitted to ICUs. A total of 290 publications were included in the final bibliometric analysis. These publications spanned a broad temporal range from 2000 to 2025, reflecting the long-term development of research activity in the field. The included studies collectively received 5,576 citations, of which 5,003 citations remained after excluding self-citations, indicating a substantial level of external scientific impact. The overall average number of citations per publication was 19.23, demonstrating a moderate citation performance across the dataset. In total, the publications were cited by 3,649 citing articles, with 3,487 citing articles remaining after the exclusion of self-citations, further supporting the robustness and dissemination of the scientific output.

Globally, 1.28 million newly diagnosed hematological malignancy cases were reported in 2020 (7.6%), accompanied by 711,840 cancer-related deaths (7.1%).[14] Despite recent improvements in survival associated with targeted therapies and innovative treatment modalities, a considerable proportion of patients with unfavorable prognoses continue to experience relapse and resistance to therapy.[15] Assessing the quality of care provided to this patient population is a crucial performance measure that assists policymakers and healthcare providers in monitoring clinical processes and enhancing the standards of care.[16] Quality indicators offer insight into areas of strong performance as well as deficiencies, thereby informing future research directions.[16] Bibliometric approaches designed for such purposes enable both qualitative and quantitative characterization of knowledge structures and the identification of evolving trends within specific research domains through mathematical and statistical analyses.[17,18] This methodological strategy enables comparison of contributions and collaborative interactions among authors, countries, and journals.[19] A total of frequently occurring keywords were identified to characterize the main research themes within the field of intensive care and critically ill patient outcomes.

Within this review, the article receiving the highest number of citations was "Delayed intensive care unit admission is associated with increased mortality in patients with cancer with acute respiratory failure''.[20] The analysis of highly cited articles underscores the clinical orientation of the field. The most influential studies addressed critical issues, including delayed ICU admission, prognostic determinants, and the application of severity scoring systems (e.g., APACHE II and SOFA). Notably, delayed ICU admission was consistently associated with increased mortality, highlighting the importance of timely critical care intervention in this vulnerable patient population. The second most cited article, "Intrahospital transport of critically ill patients:complications and difficulties", was published in Anaesthesia and Intensive Care Medicine. Similarly, studies focusing on mechanical ventilation, post-transplant complications, and septic shock in oncologic patients further emphasize the complexity and severity of clinical presentations

encountered in this setting.[21] These findings indicate that the literature is strongly aligned with real-world clinical challenges and decision-making processes.

These findings indicate that the majority of research output is concentrated in journals focused on anesthesiology and intensive care, with a significant contribution from hematology-oriented journals. The most productive journal was Anaesthesia and Intensive Care, with 74 publications, followed by Minerva Anestesiologica (41 publications) and Bone Marrow Transplantation (21 publications). Other notable contributors included Journal of Pediatric Hematology/Oncology (20 publications) and Anaesthesia Critical Care & Pain Medicine (19 publications).

Institutional analysis further corroborates this concentration of scientific output. The Medical University of Vienna was identified as the leading institution in both publication count and citation impact, highlighting its central role in advancing the field. Similarly, institutions such as Monash University and several major Australian hospitals exhibited high levels of productivity, while European centers—including University Medical Center Utrecht and leading French academic hospitals—demonstrated stronger integration within collaborative networks. These findings suggest that research on critically ill hematological patients is predominantly conducted in high-volume, specialized tertiary care centers with established expertise in both intensive care and hematology.[22]

From a productivity perspective, the literature seems to be dominated by a small number of geographically clustered research hubs. Australia (documents, n=58) emerged as the most prolific country in terms of publication output and total citations, highlighting its leading role in producing high-impact research in this field. Despite its high productivity, Australia showed comparatively low total link strength (n=32), indicating that its research efforts might be more focused at the national level. In contrast, European countries, especially France (n=156) and the United States (n=154), demonstrated stronger positions within international collaboration networks, as reflected by their higher total link strength values.

Furthermore, beyond publication volume, total citations and average citations per article are also important metrics for assessing scientific impact.[23] Australia leads in this area with 58 publications, 1,246 citations, and an average of 21.48 citations per article, demonstrating a significant research impact. France received a total of 1001 citations for fewer publications (n=40), whereas the USA received 782 citations for 48 publications. Furthermore, developing countries, such as Brazil and Turkey, had lower numbers of publications and citations.

The bibliometric results indicated that European countries and the USA were the predominant contributors within this research area. These regions produced the largest number of publications, likely because they are supported by robust research funding environments. Both governmental agencies and biotechnology companies in these countries allocate significant financial resources for scientific advancement, fostering progress in innovative therapeutics for the management of HMS.[3]

Institutions generating large volumes of publications also tend to possess highly developed research infrastructures, expert clinical teams, extensive experience, and strong scientific traditions.[3] Collectively, these elements create fertile conditions for the development of novel approaches in the care of patients with HMs.

At the author level, the analysis revealed a clear dominance by a significant number of highly influential researchers. In particular, Azoulay and collaborators constitute a central intellectual hub in the field and lead both in publication output and citation impact.

The high total link strength associated with this group further indicates that it plays a pivotal role in fostering international collaborations and shaping the research agenda. Other key contributors, including Lemiale, Mokart, Lengline, and Kouatchet, also demonstrated substantial influence, reflecting a tightly interconnected authorship network. This concentration suggests that scientific advancement in this area is largely driven by a core group of expert investigators and collaborative consortia.

Keyword analysis provides additional insight into the thematic structure of the field. The predominance of terms such as mortality, intensive care, critical care, and prognosis reflects a primary focus on outcome prediction and survival. The frequent occurrence of keywords such as sepsis, mechanical ventilation, and hematopoietic stem cell-transplantation indicates an emphasis on high-risk subgroups and critical complications. Furthermore, the presence of multiple terminological variants (e.g., ICU, intensive care unit, intensive care units) suggests heterogeneity in indexing practices, although these variations converge on the same core research domain.

Taken together, these findings demonstrate that research on critically ill patients with HMs is highly centralized, both geographically and intellectually, and is predominantly oriented toward clinically relevant outcomes such as mortality and prognostic stratification. The strong representation of collaborative European networks, alongside highly productive yet relatively-interconnected research systems, such as Australia, highlights important differences in research structure and knowledge dissemination.

Future research efforts should aim to enhance global collaboration, particularly by increasing contributions from underrepresented regions, to improve the generalizability of findings. Further integration of multicenter, prospective studies may help address existing gaps and advance evidence-based management strategies for this complex and high-risk patient population.

Limitations and Strengths

This bibliometric assessment is confined to original articles indexed within the Web of Science (WOS) database. Furthermore, only English-language publications were included, which may limit the global representativeness of the dataset. Relying solely on citation counts as an indicator of article quality may restrict the depth of evaluation. Additionally, distinctions among types of HMs could not be made from the analyzed publications, nor could staging or disease severity be assessed. Conversely, analyzing publications by country using multiple bibliometric indicators is a notable strength of this study.

CONCLUSION

This bibliometric analysis demonstrates that research on critically ill patients with HMs is increasingly centered on mortality, prognostic evaluation, and intensive care management strategies. The field is characterized by a concentrated yet highly collaborative research structure, with significant contributions from specific countries, institutions, and leading authors. Despite moderate citation performance, the steady growth in publication output reflects rising scientific interest. Future research should emphasize multicenter collaboration, standardized clinical approaches, and broader global participation to enhance the generalizability and clinical applicability of findings.

Ethics

Ethics Committee Approval: Approval for the study was obtained from the Dokuz Eylül University (approval no:2023/41-16, date: 20.12.2023).

Informed Consent: Due to the nature of the retrospective study, written informed consent form was waived.

Footnotes

Author Contributions

Concept Design – Ö.Ö., S.N.; Data Collection or Processing – Ö.Ö., S.N.; Analysis or Interpretation – Ö.Ö.; Literature Review – Ö.Ö.; Writing, Reviewing and Editing – Ö.Ö., S.N.

Declaration of Interest: The authors declared no conflicts of interest.

Funding: The authors declare that this study has received no financial support.

Appendix 1 Link: https://d2v96fxpocvxx.cloudfront.net/beb8919b-f013-4ea1-b1c8-40332e840fe1/content-images/6c051784-db98-42ef-bf18-c54da1f530f2.pdf

REFERENCES

1. Tseng YD, Ng AK. Hematologic malignancies. *Hematol Oncol Clin North Am*. 2020;34(1):127-142. [CrossRef]
2. Sant M, Allemani C, Tereanu C, et al. Incidence of hematologic malignancies in Europe by morphologic subtype: results of the HAEMACARE project. *Blood*. 2010;116(19):3724-3734. [CrossRef]
3. Huang Q, Li H, Zhang Y. A bibliometric and knowledge-map study on the treatment of hematologic malignancies with CAR-T cells from 2012 to 2023. *Hum Vaccin Immunother*. 2024;20(1):2371664. [CrossRef]
4. Biard L, Darmon M, Lemiale V, et al. Center effects in hospital mortality of critically ill patients with hematologic malignancies. *Crit Care Med*. 2019;47(6):809-816. [CrossRef]
5. Azoulay E, Mokart D, Pène F, et al. Outcomes of critically ill patients with hematologic malignancies: prospective multicenter data from France and Belgium. *J Clin Oncol*. 2013;31(22):2810-2818. [CrossRef]
6. El-Jawahri A, Nelson AM, Gray TF, Lee SJ, LeBlanc TW. Palliative and end-of-life care for patients with hematologic malignancies. *J Clin Oncol*. 2020;38(9):944-953. [CrossRef]
7. Gao Y, Wu Z, Chen Y, Shang G, Zeng Y, Gao Y. A global bibliometric and visualized analysis of the links between autophagy and acute myeloid leukemia. *Front Pharmacol*. 2023;14:1291195. [CrossRef]
8. Shahzad M, Chaudhary SG, Anwar I, et al. Top 100 cited articles on clinical hematopoietic stem cell transplantation: a bibliometric analysis. *Front Med(Lausanne)*. 2022;9:872692. [CrossRef]
9. Cui Z, Luo F, Zhang Y, Diao J, Pan Y. Bibliometric analysis of worldwide research on polycythemia vera in the 21st century. *Ann Hematol*. 2024;103(10):3905-3920. [CrossRef]
10. Leydesdorff L, Carley S, Rafols I. Global maps of science based on the new Web of Science categories. *Scientometrics*. 2013;94(2):589-593. [CrossRef]
11. Synnestvedt MB, Chen C, Holmes JH. CiteSpace II: visualization and knowledge discovery in bibliographic databases. *AMIA Annu Symp Proc*. 2005;2005:724-728. [CrossRef]
12. van Eck NJ, Waltman L. Software survey: VOSviewer, a computer program for bibliometric mapping. *Scientometrics*. 2010;84:523-538. [CrossRef]
13. Pagel PS, Hudetz JA. An analysis of scholarly productivity in United States academic anesthesiologists by citation bibliometrics. *Anaesthesia*. 2011;66(10):873-878. [CrossRef]
14. Staudinger T, Stoiser B, Müllner M, et al. Outcome and prognostic factors in critically ill cancer patients admitted to the intensive care unit. *Crit Care Med*. 2000;28(5):1322-1328. [CrossRef]
15. Zhang N, Wu J, Wang Q, et al. Global burden of hematologic malignancies and evolution patterns over the past 30 years. *Blood Cancer J*. 2023;13(1):82. [CrossRef]
16. Ou L, Su C, Liang L, et al. Current status and future prospects of chimeric antigen receptor T-cell therapy in lymphoma research: a bibliometric analysis. *Hum Vaccin Immunother*. 2023;19(3):2267865. [CrossRef]
17. Zhang G, Deng L, Lu H, Zhang W. Bibliometric analysis of research trends and active research areas in chimeric antigen receptor T-cell therapy for hematologic malignancies. *Int J Clin Pharm*. 2024;46(1):186-194. [CrossRef]
18. Chen P, Du Z, Wang J, Liu Y, Zhang J, Liu D. A bibliometric analysis of research on hematological tumor microenvironment. *Ann Transl Med*. 2021;9(16):1337. [CrossRef]
19. Wei N, Xu Y, Li Y, et al. A bibliometric analysis of T cells and atherosclerosis. *Front Immunol*. 2022;13:948314. [CrossRef]
20. Mokart D, Lambert J, Schnell D, et al. Delayed intensive care unit admission is associated with increased mortality in patients with cancer with acute respiratory failure. *Leuk Lymphoma*. 2013;54(8):1724-1729. [CrossRef]
21. Lovell MA, Mudaliar MY, Klineberg PL. Intrahospital transport of critically ill patients: complications and difficulties. *Anaesth Intensive Care*. 2001;29(4):400-405. [CrossRef]
22. Wang Y, Yang C, Wan J, et al. Bone marrow adipocyte: origin, biology and relationship with hematologic malignancy. *Int J Lab Hematol*. 2024;46(1):10-19. [CrossRef]
23. Öner Ö, Ecevit MC, Gökmen AN. A bibliometric analysis of obstructive sleep apnea and anesthesia. *Medicine(Baltimore)*. 2023;102(17):e32993. [CrossRef]

ABCResearch

Arch Basic Clin Res 2026;8(2):183-188
DOI: 10.4274/ABCR.2026.26411

Research Article

Parturients' Anesthesia Preferences For Caesarean Section Delivery: A Prospective Observational Study

Duygu Karaköse Çalışkan[1], Halide Aydın Sakar[2], Nihan Yaman Mammadov[3]

[1]Clinic of Intensive Care, Muş State Hospital, Muş, Türkiye
[2]Clinic of Anesthesiology and Reanimation Department, University of Health Sciences Türkiye, Van Training and Research Hospital, Van, Türkiye
[3]Clinic of Anesthesiology and Reanimation, University of Health Sciences Türkiye, Kartal Dr. Lütfi Kırdar Training and Research Hospital, İstanbul, Türkiye

Cite this article as: Karaköse Çalışkan D, Aydın Sakar H, Yaman Mammadov N. Parturients' anesthesia preferences for caesarean section delivery: a prospective observational study. *Arch Basic Clin Res*. 2026;8(2):183-188.

ORCID IDs of the authors: D.K.Ç. 0000-0003-0025-1478, H.A.S. 0000-0002-7091-3505, N.Y.M. 0000-0002-4159-8788.

ABSTRACT

Objective: As cesarean section (CS) rates continue to rise, the choice of anesthesia has become increasingly important. Two main anesthetic approaches are commonly used: general anesthesia (GA) and regional anesthesia (RA), the latter comprising spinal anesthesia (SA), epidural anesthesia (EA), and CS-EA. The aim of this study was to evaluate the influence of educational status, prior anesthesia experience, and procedure-related concerns on parturients' choice of anesthesia for elective CS.

Methods: Between January 2019 and December 2019, 275 pregnant women classified as American Society of Anesthesiologists II and scheduled for elective cesarean delivery at a tertiary care hospital were included in this study. Parturients were questioned in the preoperative room about age, educational level, previous birth experiences, knowledge of and concerns about SA. Subsequently, they were transferred to the operating room, where the choice of anesthesia modality was determined according to each parturient's preference.

Results: The study population primarily consisted of women with a low educational level; however, no significant association was found between the type of anesthesia used for the current CS delivery and educational level (P = 0.26). Parturients' knowledge about SA was limited, and the predominant source of information was friends and relatives. Only 19% of those who have knowledge mentioned "doctor" as the source. A statistically significant relationship was observed between the current anesthesia modality and prior anesthesia experience (P = 0.015). Fear of experiencing pain during the operation was the principal concern expressed by 37.45% of parturients.

Conclusion: Parturients preferred SA to GA across all education levels. Prior anesthesia experience led parturients to choose SA. Parturients who had experienced either general or SA prefer SA for the current operation.

Keywords: Anesthesia experience, anesthesia preference, caesarean section delivery, education level, spinal anesthesia

INTRODUCTION

The increasing prevalence of cesarean section (CS) deliveries has underscored the importance of understanding maternal preferences regarding anesthesia modalities. Two anesthetic modalities are used in procedures: general anesthesia (GA) and regional anesthesia (RA), the latter of which includes spinal anesthesia (SA), epidural anesthesia (EA), and combined SA-EA anesthesia. According to the National Anesthesia Clinical Outcomes Registry RA accounts for approximately 94.2% of anesthetic techniques used for CS in the United States.[1] The most frequently used anesthetic modality for CS delivery is single-shot SA, which is easy to apply, is associated with fewer maternal and fetal complications, and provides adequate operating conditions and patient comfort.[2-4] Despite clinical guidelines and recommendations, the choice of anesthesia often depends on a combination of surgical urgency, institutional practices, anesthesiologist experience, and, critically, the preferences of the parturient.[4,5] Parturients' preferences should receive priority consideration in elective cases.[6]

Corresponding author: Duygu Karaköse Çalışkan, **E-mail:** duygukarakosecaliskan@gmail.com

Received: February 10, 2026
Revision Requested: February 19, 2026
Accepted: March 12, 2026
Epub: May 22, 2026
Publication Date: July, 14, 2026

Although RA is widely recommended and increasingly utilized for elective CS, the factors shaping maternal anesthesia preference remain complex and context-dependent. Previous studies have explored demographic and clinical determinants; however, the interaction between prior anesthesia experience, educational level, sources of information, and procedure-related concerns has not been sufficiently examined, particularly in populations with predominantly low educational attainment. Moreover, the role of misinformation and non-medical information sources in influencing maternal perceptions and fears continues to be underreported.

Therefore, this prospective observational study aimed to investigate the determinants of anesthesia preference among parturients undergoing elective CS, with particular emphasis on demographic characteristics, educational status, prior anesthesia exposure (including experience with both general and SA), and specific maternal concerns regarding the procedure. By evaluating these variables within a real-world tertiary care setting, our study seeks to provide further insight into maternal decision-making processes and to highlight the potential importance of structured preoperative counseling in supporting informed and patient-centered anesthesia choice.

MATERIAL AND METHODS

This prospective observational study was conducted at a tertiary care hospital between January and December 2019. Of the 363 eligible parturients, 275 consented to participate and were enrolled in the study, while 88 declined participation. A total of 275 pregnant women, classified as American Society of Anesthesiologists (ASA) II and scheduled for elective CS, were enrolled. Ethical approval was obtained from the institutional review board of Van, University of Health Sciences Türkiye, Training and Research Hospital (approval no: 2019/17, date: 12.09.2019), and all participants provided written informed consent in accordance with the Declaration of Helsinki.

Exclusion criteria included requirement for emergency CS delivery; classification as ASA status ≥ III; patients who refused to participate; multiple gestations; possibility of intraoperative hemorrhage, such as cases of placenta previa or coagulation defects; premature membrane rupture; preterm delivery (defined as before the 37th week of pregnancy); pregnancies with obstetric problems such as fetal abnormality.

Parturients were evaluated in the preoperative room by an anesthesiologist. The questions about the parturients' ages, education level, and previous births (for CS deliveries: anesthesia type and postoperative complaints) were asked of the parturients who agreed to participate, and their answers were recorded. She was also asked whether she had any knowledge of SA and where she had obtained that information. Each participant was also asked about her anesthesia preference for the upcoming CS; if SA was chosen, her specific concerns about the procedure were recorded. The recorded anesthesia modality reflected the patient's self-reported preference prior to anesthetic administration, and no institutional or clinician-driven coercion influenced the choice in elective cases. After the interview, the parturients were transferred to the operating room.

To minimize selection bias, all eligible parturients meeting the inclusion criteria were invited consecutively to participate, regardless of their demographic or clinical background. A standardized, structured questionnaire was used to ensure consistent data collection across participants; to reduce interviewer bias, the anesthesiologist followed this questionnaire and was blinded to participants' medical histories beyond the study requirements. The questionnaire was pilot-tested on 10 patients to ensure clarity and comprehensibility, and necessary modifications were made prior to the main study. Participation was voluntary, and informed consent was obtained from all participants without coercion. Additionally, we recorded the basic characteristics of non-responders to assess potential non-response bias.

Statistical Analysis

Data pertaining to the study were entered into spreadsheet software (Microsoft Excel 16.43). Statistical analyses were performed using R (version 4.0.3, R Core Team (2020). R: A language and environment for statistical computing. R Foundation for Statistical Computing, Vienna, Austria. (URL:https://www.R-project.org/). The Wilcoxon rank-sum test was used to compare continuous variables, and chi-square tests were applied for categorical variables. A P value < 0.05 was considered statistically significant.

A post-hoc power calculation, based on the observed effect size for the association between prior anesthesia exposure and current anesthesia preference, was conducted using a chi-square test framework. With a total sample size of 275 participants and a two-sided alpha of 0.05, the study achieved a statistical power greater than 80% to detect a medium effect size (Cramér's V ≈ 0.20). This suggests that the study was adequately powered to detect clinically relevant differences in anesthesia preferences in the study population.

RESULTS

A total of 275 parturient patients were enrolled in the study. Patient characteristics are summarized in Table 1. The median age of the parturients was 29 years (range = 19-44). Educational attainment were distributed as follows: non-literate (32%), primary school (31.27%), middle school (14.55%), high school (12.73%), and higher education (9.45%).

Of the current CS deliveries, 90 (32.73%) were primary, whereas 185 (67.27%) were recurrent CS deliveries. Among all parturients, 58 (21.09%) preferred GA for the current CS delivery, while 217 (78.91%) preferred SA. The median age (as shown in Figure 1) and education level (as shown in Table 2) did not differ significantly between anesthesia modalities (P = 0.17 and P = 0.26, respectively). Education level was not directly associated with anesthesia preference (P = 0.26); however, lower education levels were linked to reduced knowledge about SA, which may influence preference formation.

There was a statistically significant relationship between the current anesthesia modality and prior anesthesia experience (χ^2 test P = 0.015). As shown in Table 3, all parturients with prior experience of both GA and SA preferred SA.

Table 1. Values are presented as median (range) for continuous variables and n (%) for categorical variables. Educational status was classified as non-literate, primary school, middle school, high school, and higher education. Prior birth history includes the number and type of previous deliveries (vaginal, CS under GA, CS under SA). Current CS delivery was categorized as primary or recurrent. Current anesthesia modality reflects the patient's preference for GA or SA.

Variable	
Age [median (range)]	29 (19-44)
Education n(%)	
Non-literate	88 (32%)
Primary school	86 (31.27%)
Middle school	40 (14.55%)
High school	35 (12.73%)
Higher education	26 (9.45%)
Prior births [median (range)]	
Total number of prior births	1 (0-8)
Number of vaginal births	0 (0-8)
Number of CS births with GA	1 (0-4)
Number of CS births with SA	0 (0-2)
Current CS delivery [n(%)]	
Primary	90 (32.73%)
Recurrent	185 (67.27%)
Current anesthesia modality [n(%)]	
GA	58 (21.09%)
SA	217 (78.91%)

CS, cesarean section; GA, general anesthesia; SA, spinal anesthesia.

MAIN POINTS

- Spinal anesthesia was the preferred anesthetic technique for elective cesarean section across all educational levels.
- Prior anesthesia experience significantly influenced current anesthesia preference, with parturients previously exposed to spinal anesthesia showing a strong tendency to choose it again.
- Educational level alone was not directly associated with anesthesia preference; however, lower educational levels were linked to reduced knowledge about spinal anesthesia.
- Most parturients obtained information about spinal anesthesia from non-medical sources, whereas physician-based counseling was limited but strongly associated with a preference for it.
- Fear of intraoperative pain was the most common concern affecting the choice of anesthesia, highlighting the need for structured prenatal education and effective preoperative counseling.

Among parturients with a previous CS delivery, 78 (42.62%) experienced postoperative complaints. The most common complaint was pain at the wound site, followed by nausea, headache, shivering, vomiting, motor deficit, and other complaints (as shown in Figure 2). The other postoperative complaints included back pain (4.37%), dyspnea (1.64%), throat ache (1.09%), treatment in the intensive care unit (0.55%), hypertension (0.55%), urinary catheter pain (0.55%), and wound infection (0.55%). When parturients

Table 2. Values are presented as n (%). The table demonstrates the frequencies of GA and SA preferences across different education levels, from non-literate to higher education. No statistically significant association was observed between education level and anesthesia preference(χ^2 test, $P = 0.26$)

	GA	SA
Non-literate (n(%))	17 (19.32%)	71 (80.68%)
Primary school (n(%))	23 (26.74%)	63 (73.26%)
Middle school(n(%))	10 (25%)	30 (75%)
High school (n(%))	6 (17.14%)	29 (82.86%)
Higher education (n(%))	2 (7.69%)	24 (92.31%)
χ^2 *test P = 0.26*		

GA, general anesthesia; SA, spinal anesthesia.

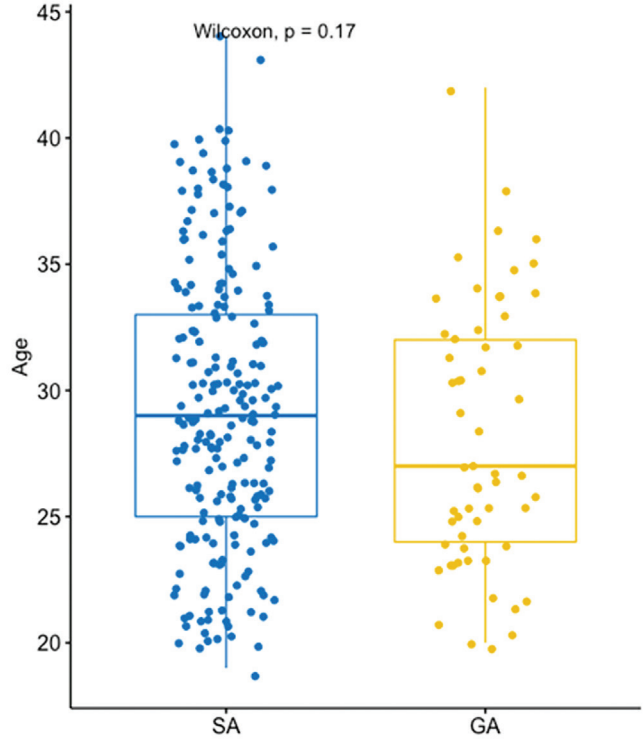

Figure 1. Boxplots illustrate the age distribution of parturients who preferred GA versus SA for their current CS delivery. Median values, interquartile ranges, and outliers are displayed. The Wilcoxon rank-sum test was used to compare groups; *P* values are indicated above the plots.

SA,spinal anesthesia; GA, general anesthesia.

Table 3. Values are presented as n (%). The table compares anesthesia preferences in patients with no prior anesthesia experience, those with previous GA, previous SA, or both GA and SA. A statistically significant relationship was observed between prior anesthesia experience and current anesthesia choice (χ^2 test, P = 0.015).

	GA	SA
No anesthesia experience [n(%)]	14 (15.22%)	78 (84.78%)
GA [n(%)]	40 (27.78%)	104 (72.22%)
SA [n(%)]	4 (18.18%)	18 (81.82%)
GA + SA [n(%)]	0 (0%)	17 (100%)
χ^2 *test* ***P = 0.015***		

GA, general anesthesia; SA, spinal anesthesia.

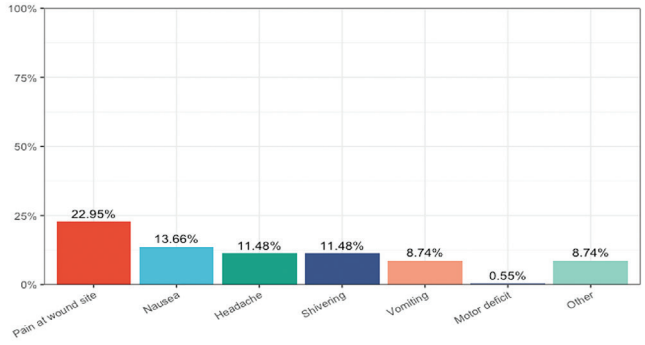

Figure 2. Bar plot showing the percentages of parturients reporting specific postoperative complaints following previous CS. The most common complaint was wound site pain, followed by nausea, headache, shivering, vomiting, motor deficit, and other complications (back pain, dyspnea, throat pain, ICU admission, hypertension, urinary catheter pain, wound infection).

CS, cesarean section; ICU, intensive care unit.

were questioned about their knowledge of SA 97 (35.4%) of parturients reported that SA was "useful", 70 (25.55%) reported that it was "harmful", and 107 (39.05%) responded "don't know". When asked about the source of this information, 39.27% of parturients responded "friends, relatives", 19.27% responded "doctor", 11.27% responded "own experience" and 4% responded "internet, television".

Before performing SA, parturients who preferred this modality for CS delivery were asked about their concerns regarding the procedure. Fear of experiencing pain during operation was the principal concern expressed by 37.45% of parturients. Seeing/hearing the operation, permanent backache, fear of paralysis (which is a common misconception rather than an evidence-based concern and reported to be less than 0.01% after SA),[7] nausea were other concerns in 27.64%, 23.64%, 8% and 3.27% of parturients, respectively. In our experience with these 275 patients—both the general and SA groups— no irreversible complications were observed.

DISCUSSION

In this study, we described parturients' anesthesia preferences for CS delivery in 2019 at a tertiary care hospital. Compared with GA, RA is associated with fewer respiratory complications, superior pain control, earlier mother–newborn interaction, and shorter mobilization time; therefore, SA remains the preferred technique.[8-10] Our study aligns with other studies showing that SA is generally favored because it has minimal impact on neonatal outcomes, is associated with better postoperative recovery, and results in greater maternal satisfaction.[11-13]

Obstetric anesthesia differs from other surgical procedures due to additional concerns regarding neonatal well-being, breastfeeding, and newborn care. This process could be seriously impeded by postoperative nausea and vomiting.[14] In our cohort, wound site pain and nausea were the most frequently reported postoperative complaints. Although nausea has been cited as a potential barrier to maternal comfort and early bonding, its frequency in our study was comparable to previously reported ranges.[15] These findings suggest that concerns about postoperative discomfort may influence perception of anesthesia more strongly than the actual complication rates.

Previous experiences appear to play a guiding role for current preferences. We observed a statistically significant relationship between current anesthesia modality and prior anesthesia experience (P = 0.015), with parturients previously exposed to either GA or SA showing a preference for SA in subsequent procedures. This finding aligns with previous studies where 80% of parturients with prior SA experience reported they would choose it again for a subsequent delivery.[9] Similarly, maternal satisfaction after CS under SA has been reported as high as 97% in other studies.[16] In a 160-patient cohort study, parturients with previous SA experience opted for SA more often than the GA-experienced group.[17] On the contrary, in a systematic review Afolabi and Lesi[18] compared the neuraxial vs GA in CS delivery and more parturients in the GA group declared they would use the same technique for anensuing CS delivery. Taken together, these findings suggest that prior personal experience may outweigh abstract risk-benefit information when parturients make anesthesia decisions. Familiarity appears to function as a psychological anchor, potentially increasing perceived safety and predictability.

Although the majority of our study population had low educational attainment, no direct association was observed between education level and anesthesia preference (χ^2 test, P = 0.26). SA was favored across all educational categories. This suggests that even in populations with limited formal education, parturients tend to prefer SA if they have had a positive prior experience with it. Our results differ from those reported by Carvalho et al.[14], who identified education level as a significant determinant of anesthesia preference. However, in our cohort, lower educational status was associated with reduced knowledge regarding SA, indicating that knowledge gaps — rather than educational attainment per se— may influence uncertainty or anxiety during decision-making.[19] In this context, misinformation or an insufficient understanding of the safety

profile and benefits of SA may contribute to a preference for GA despite its comparatively less favorable maternal profile.

In a prospective observational study conducted by Şahin et al.[20], both maternal and partner educational levels were found to be significantly associated with anesthesia choice for elective CS, with higher educational attainment favoring SA. In that cohort, anesthesia preference was assessed after structured preoperative counseling in the anesthesia clinic, which may have enhanced patients' understanding of anesthesia techniques, unlike in our study. This methodological difference suggests that education level alone may not directly determine anesthesia preference; rather, its effect may be mediated through access to accurate information and effective preoperative counseling. Our findings are further supported by a recent cross-sectional study from Pakistan, in which, despite a remarkably high acceptance of SA (93.7%), nearly half of the parturients reported significant fears, which were predominantly misconceptions such as paralysis, intraoperative pain, and postoperative backache. Importantly, fear was significantly more common among younger, nulliparous women with lower knowledge scores, and was frequently associated with information obtained from non-medical sources such as friends or relatives.[21] Collectively, these findings indicate that misinformation and inadequate counseling may constitute more influential barriers than formal education itself. From a clinical perspective, this underscores the importance of structured prenatal education and standardized preoperative counseling in promoting informed, patient-centered anesthesia decision-making.

A according to our study, parturients' knowledge about SA remains limited, with 39% indicating that they "don't know" enough about it. Among those who reported having knowledge, only 19% cited a doctor as the source of information, while the majority relied on information from friends and relatives. There are many studies in the literature in which parturients were referred to SA by clinicians in proper cases[22-24] and this is especially evident in obstetric-specialized anesthesiologists.[25,26] Similarly, in our study, we determined that 100% of the parturients who were informed by their doctors preferred SA. Even though Tekin et al.[23] emphasized the opposite; social environment and relatives had principal effect in the choice of anesthesia on parturients according to our findings. This condition may cause concerns that have no medical basis. Patients generally feel uncomfortable in the operating theatre. Fears of sensing pain and of seeing or hearing the operation were main concerns, and these may result in a strong inclination for GA.[15,16,23,27]

Study Limitations

The main limitation of our study was the generally low levels of education among participants, which may limit the generalizability of the findings to the broader obstetric population. Our hospital does not provide prenatal classes for labor or CS delivery, and we therefore lack the opportunity to inform parturients in advance about available anesthesia options and their advantages. This study demonstrated that most parturients had insufficient knowledge regarding CS delivery and SA. Therefore, implementing prenatal classes and structured preoperative anesthesia consultations is necessary to improve maternal satisfaction and promote neonatal well-being.

CONCLUSION

Although parturients' knowledge about SA remains limited, the findings of this study suggest that structured prenatal education could enhance informed decision-making about anesthesia preferences for cesarean delivery. The observed association between prior anesthesia experience and current preference underscores the importance of providing comprehensive information on the benefits and potential risks of different anesthesia modalities. Targeted prenatal education programs that address common misconceptions—such as fear of paralysis or intraoperative pain during SA—may empower parturients to make more confident and informed choices, ultimately leading to improved maternal satisfaction and better clinical outcomes.

Ethics

Ethics Committee Approval: Ethical approval was obtained from the institutional review board of Van, University of Health Sciences Türkiye, Training and Research Hospital (approval no: 2019/17, date: 12.09.2019), and all participants provided written informed consent in accordance with the Declaration of Helsinki.

Author Contributions

Concept Design – D.K.Ç.; Data Collection or Processing – D.K.Ç., H.A.S.; Analysis or Interpretation – D.K.Ç., H.A.S., N.Y.M.; Literature Review – D.K.Ç., H.A.S., N.Y.M.; Writing, Reviewing and Editing – D.K.Ç., N.Y.M.

Informed Consent: All participants provided written informed consent in accordance with the Declaration of Helsinki.

Footnotes

Declaration of Interest: The authors declared no conflicts of interest.

Funding: The authors declare that this study has received no financial support.

REFERENCES

1. Juang J, Gabriel RA, Dutton RP, Palanisamy A, Urman RD. Choice of anesthesia for cesarean delivery: an analysis of the National Anesthesia Clinical Outcomes Registry. *Anesth Analg*. 2017;124(6):1914-1917. [CrossRef]
2. Ranasinghe JS, Birnbach D. Current status of obstetric anaesthesia: improving satisfaction and safety. *Indian J Anaesth*. 2009;53(5):608-617. [CrossRef]
3. Bucklin BA, Hawkins JL, Anderson JR, Ullrich FA. Obstetric anesthesia workforce survey: twenty-year update. *Anesthesiology*. 2005;103(3):645-653. [CrossRef]
4. Staikou C, Makris A, Theodoraki K, et al. Current practice in obstetric anesthesia and analgesia in public hospitals of Greece: a 2016 National Survey. *Balkan Med J*. 2018;35(5):394-397. [CrossRef]

5. Saygı Aİ, Özdamar Ö, Gün İ, Emirkadı H, Müngen E, Akpak YK. Comparison of maternal and fetal outcomes among patients undergoing cesarean section under general and spinal anesthesia: a randomized clinical trial. *Sao Paulo Med J*. 2015;133(3):227-234. [CrossRef]
6. Kan RK, Lew E, Yeo SW, Thomas E. General anesthesia for cesarean section in a Singapore maternity hospital: a retrospective survey. Int J Obstet Anesth. 2004;13(4):221-226. [CrossRef]
7. Horlocker TT. Complications of regional anesthesia and acute pain management. *Anesthesiol Clin*. 2011; 29(2):257-278. [CrossRef]
8. Aksoy M, Aksoy AN, Dostbil A, Çelik MG, Ahıskalıoğlu A. Anaesthesia techniques for caesarean operations: retrospective analysis of last decade. *Turk J Anaesthesiol Reanim*. 2014;42(3):128-132. [CrossRef]
9. Fassoulaki A, Staikou C, Melemeni A, Kottis G, Petropoulos G. Anaesthesia preference, neuraxial vs general, and outcome after caesarean section. *J Obstet Gynaecol*. 2010;30(8):818-821. [CrossRef]
10. Gandhi KA, Jain K. Management of anaesthesia for elective, low-risk (category 4) caesarean section. *Indian J Anaesth*. 2018;62(9):667-674. [CrossRef]
11. Eroglu S, Eroglu A, Aziz V, Simar S, Mutlu S. The relationship between anxiety and satisfaction level in women who had cesarean section with spinal or general anesthesia:anxiety and satisfaction level in cesarean section. *Med Sci Discov*. 2020;7:560-565. [CrossRef]
12. Ring L, Landau R, Delgado C. The current role of general anesthesia for cesarean delivery. *Curr Anesthesiol Rep*. 2021;11(1):18-27. [CrossRef]
13. Cocchi E, Pini R, Gallipoli A, et al. Impact of general vs. neuraxial anesthesia on neonatal outcomes in non-elective cesarean sections. *Front Pediatr*. 2025;13:1518456. [CrossRef]
14. Carvalho B, Cohen SE, Lipman SS, Fuller A, Mathusamy AD, Macario A. Patient preferences for anesthesia outcomes associated with cesarean delivery. *Anesth Analg*. 2005;101(4):1182-1187. [CrossRef]
15. Idris IM, Weldegiorgis GG, Tesfamariam EH. Maternal satisfaction and its associated factors towards spinal anesthesia for caesarean section: a cross-sectional study in two Eritrean Hospitals. *Anesthesiol Res Pract*. 2020;2020:5025309. [CrossRef]
16. Dharmalingam TK, Ahmad Zainuddin NA. Survey on maternal satisfaction in receiving spinal anaesthesia for caesarean section. *Malays J Med Sci*. 2013;20(3):51-54. [CrossRef]
17. Ghaffari S, Dehghanpisheh L, Tavakkoli F, Mahmoudi H. The effect of spinal versus general anesthesia on quality of life in women undergoing cesarean delivery on maternal request. *Cureus*. 2018;10(12):e3715. [CrossRef]
18. Afolabi BB, Lesi FE. Regional versus general anaesthesia for caesarean section. *Cochrane Database Syst Rev*. 2012;10(10):CD004350. [CrossRef]
19. Erturk E, Akdogan A, Arslan A. Comparison of anesthesia professionals' preferences of delivery method with other health professionals. *J Clin Med Kaz*. 2021;18(2):44-48. [CrossRef]
20. Şahin M, Uluç K, Ayık MB, Kına S. The impact of educational level on anesthesia preference in caesarean section surgeries. *Dicle Med J*. 2025; 52(4):783-789. [CrossRef]
21. Shahid N, Rashid AM. Knowledge, fear and acceptance rate of spinal anesthesia among pregnant women scheduled for cesarean section: a cross-sectional study from a tertiary care hospital in Karachi. *BMC Anesthesiol*. 2024;24(1):408. [CrossRef]
22. Dağlı R, Dağlı SS. Anaesthetic method preference of obstetricians for caesarean section. *Turk J Anaesthesiol Reanim*. 2015;43(1):41-46. [CrossRef]
23. Tekin İ, Laçin S, Arıcan İ, Ok G. Factors influencing patients preference of anesthesia type for caesarean section. *Turk J Anaesthesiol Reanim*. 2005; 3:1-6. [CrossRef]
24. Ikeda T, Kato A, Bougaki M, et al. A retrospective review of 10-year trends in general anesthesia for cesarean delivery at a university hospital: the impact of a newly launched team on obstetric anesthesia practice. *BMC Health Serv Res*. 2020;20(1):421. [CrossRef]
25. Cobb BT, Lane-Fall MB, Month RC, Onuoha OC, Srinivas SK, Neuman MD. Anesthesiologist specialization and use of general anesthesia for cesarean delivery. *Anesthesiology*. 2019;130(2):237-246. [CrossRef]
26. Wagner JL, White RS, Mauer EA, Pryor KO, Kjaer K. Impact of anesthesiologist's fellowship status on the risk of general anesthesia for unplanned cesarean delivery. *Acta Anaesthesiol Scand*. 2019;63(6):769-774. [CrossRef]
27. Akıcı ÖÇ, Bakı ED, Büyükerkmen E, Sıvacı RG. Evaluation of the satisfaction from general and spinal anesthesia in cesarean applied pregnant. *Kocatepe Med J*. 2019; 20:217-224. [CrossRef]

ABCResearch

Arch Basic Clin Res 2026;8(2):189-193
DOI: 10.4274/ABCR.2026.24285

Research Article

Comparison of the Syringe Preparation Time for Ranibizumab Prefilled Syringe versus Bevacizumab, Ranibizumab, and Aflibercept Vials

Ahmet Mehmet Somuncu[1], Adem Uğurlu[2], Nurdan Gamze Taşlı[1], Yücel Karakurt[2], İbrahim Çiçek[2]

[1]Clinic of Ophthalmology, University of Health Sciences Türkiye, Kanuni Training and Research Hospital, Trabzon, Türkiye
[2]Deparment of Ophthalmology, Erzincan Binali Yıldırım University Faculty of Medicine, Erzincan, Türkiye

Cite this article as: Somuncu AM, Uğurlu A, Taşlı NG, Karakurt Y, Çiçek İ. Comparison of the syringe preparation time for ranibizumab prefilled syringe versus bevacizumab, ranibizumab, and aflibercept vials. *Arch Basic Clin Res*. 2026;8(2):189-193.

ORCID IDs of the authors: A.M.S. 0009-0008-0304-5278, A.U. 0000-0002-8900-7043, N.G.T. 0000-0001-8587-3430, Y.K. 0000-0001-8104-3819, İ.Ç. 0000-0003-3297-1568.

ABSTRACT

Objective: To compare the syringe preparation time for ranibizumab prefilled syringe versus bevacizumab, ranibizumab, and aflibercept vials in routine retinal practice.

Methods: The study was conducted retrospectively between July 2019 and February 2021 at the Ophthalmology Department of the Erzincan Binali Yıldırım University Faculty of Medicine, Türkiye. Syringe preparation times for 157 eyes were collected for the study. For each injection, one independent observer recorded the duration of each step required to prepare the syringe, starting with the removal of the ranibizumab prefilled syringe or bevacizumab, ranibizumab, and aflibercept vials from their respective packaging, and ending at the moment the dose was ready for injection. Injections were excluded if disruptions during the drug administration process were due to external factors or if other errors occurred in measuring preparation time. In addition to preparation time, formation of air bubbles during syringe preparation was qualitatively observed.

Results: Forty-five eyes were treated with the ranibizumab prefilled syringe, while bevacizumab, ranibizumab, and aflibercept vials were used to treat 40, 36, and 36 eyes, respectively. The mean injection preparation time was 46.5±4.8 s for the syringe and 66.1±7.2 s, 64.2±5.1 s, and 74.7±8.5 s for the bevacizumab, ranibizumab, and aflibercept vials, respectively. Air bubble formation was more frequently observed in the vial groups, particularly in the aflibercept group, than in the prefilled syringe group.

Conclusion: The ranibizumab-prefilled syringe required fewer preparation steps and had a lower incidence of bubble formation compared with other vials. Specifically, when preparing the aflibercept vial for injection, dose adjustment took longer than for the bevacizumab and ranibizumab vials, primarily due to air bubbles.

Keywords: Ranibizumab, prefilled syringe, preparation time, vial

INTRODUCTION

Anti-vascular endothelial growth factor (VEGF) drugs are developed to bind to and inhibit VEGF, which is believed to play a key role in the formation of new blood vessels. Randomised clinical trials have shown that intravitreal administration of these drugs is effective in the treatment of retinal diseases such as diabetic retinopathy, retinal vein occlusion and exudative age-related macular degeneration.[1] It has been shown that the intravitreal injection of anti-VEGF is effective in treating some retinal diseases and improving their prognosis. In addition, research indicates that anti-VEGF therapy helps prevent visual loss and improve vision.[2-4]

Anti-VEGF treatment is becoming increasingly widespread and includes the administration of intravitreal injections.[5,6]

Corresponding author: Ahmet Mehmet Somuncu, **E-mail:** mehmetsomuncu89@hotmail.com

Received: July 10, 2024
Revision Requested: March 11, 2025 **Accepted:** June 22, 2026 **Publication Date:** July, 14, 2026

The number of patients receiving intravitreal injections in the USA increased from over 4 million in 2013 to nearly 6 million in 2016.[7] However, this therapy requires frequent follow-up examinations. In addition, more patients are becoming eligible for this treatment compared to previous surgical procedures, resulting in an additional workload.[8-11] To accommodate the growing patient population requiring anti-VEGF therapy and to reduce the risk of complications, pre-injection preparation time should be minimized. Nevertheless, some diseases, such as endophthalmitis, still pose certain safety risks due to the invasive nature of the treatment.[12]

In 2013, the EU granted approval for the use of ranibizumab solution in pre-filled syringe injections (PFSs) for the treatment of visual impairment caused by neovascular age-related macular degeneration , diabetic macular edema, retinal vein occlusion, pathological myopia. The use of intravitreal Ranibizumab 0.3 mg PFS for the treatment of diabetic retinopathy and diabetic macular edema was approved by the US Food and Drug Administration in March 2018.[13,14]

PFS solutions have the same formulation as their vial counterparts (a single intravitreal injection of 0.5 mg delivered in a 0.05 mL volume). They have a latex-free, non-retractable plunger and a small, minimally siliconised barrel with a low void volume. Additionally, PFSs are packaged in sterile, disposable trays.

We aimed to compare intravitreal injection preparation times between the ranibizumab PFS and the vials of ranibizumab, bevacizumab, and aflibercept in routine clinical practice.

MATERIALS AND METHODS

The study was an observational, cross-sectional study conducted in the Department of Ophthalmology, Erzincan Binali Yıldırım University Faculty of Medicine, between July 2019 and February 2021. Ethical approval was obtained from the ethics committee of Erzincan Binali Yıldırım University Faculty of Medicine (E-21142744-804.99-138855**;** date: 17.01.2022) and the principles stated in the Declaration of Helsinki were followed in the study. Since the study involved only observation of clinical practices without collecting identifiable patient data, informed consent for participation was not obtained.

In addition to preparation time, the occurrence of air bubble formation during syringe preparation was qualitatively observed by the same independent observer.

MAIN POINTS

- The frequency of anti-vascular endothelial growth factor (VEGF) injections has been increasing, and they are being evaluated as treatment options for numerous diseases.
- However, anti-VEGF injections require a preparation time, and as this time increases, the risk of contamination and, consequently, of endophthalmitis increases.
- Therefore, we believe that determining the biological agent with the shortest preparation time and comparing the preparation time of the Ranibizumab Prefilled Syringe with those of other anti-VEGF agents used in clinical practice will contribute to the literature.

Data on syringe preparation time were gathered from 157 eyes. For each injection, one independent observer recorded the duration of each step required to prepare the syringe, starting with the removal of the ranibizumab-prefilled syringe or vials of bevacizumab, ranibizumab, and aflibercept from their respective packaging and ending when the dose was ready for injection.

Six injection-preparation steps were identified when using vials of bevacizumab, ranibizumab, and aflibercept: 1) removal of the contents from the external box and internal packaging; 2) donning gloves; 3) attaching a filter needle; 4) extracting the solution from the vial using the filter needle; 5) removing the filter needle and attaching the injection needle; and 6) adjusting the dose. In contrast, four injection-preparation steps were identified when using the ranibizumab-prefilled syringe: 1) the removal of contents from the external box and internal packaging, 2) the donning of gloves, 3) the removal of the syringe cap and the attachment of the injection needle, and 4) the adjustment of the dose.

Exclusion Criteria

Injections were excluded if disruptions occurred during the drug administration process due to external factors or if other errors occurred in measuring preparation time.

Statistical Analysis

The data were analysed using the Statistical Package for the Social Sciences (IBM SPSS) version 22.0. Descriptive statistics are presented using means and standard deviations for measured data. The Shapiro-Wilk test was used to assess whether the measured data were normally distributed. The Mann-Whitney U test was used to compare the measured data. The level of significance was set at $P < 0.05$.

RESULTS

No cases of endophthalmitis were observed in any group.

Forty-five eyes were treated with the ranibizumab prefilled syringe, while bevacizumab, ranibizumab, and aflibercept vials were used to treat 40, 36, and 36 eyes, respectively. The mean injection preparation time was 46.5 ± 4.8 s for the ranibizumab prefilled syringe and 66.1 ± 7.2 s, 64.2 ± 5.1 s, and 74.7 ± 8.5 s for the bevacizumab, ranibizumab, and aflibercept vials, respectively. The injection preparation time was significantly lower in the ranibizumab prefilled syringe group. The preparation time for the aflibercept vial was significantly longer than that for the other intravitreal drugs under investigation (Table 1). No findings of endophthalmitis were encountered in any patient who received the injection (Table 2).

DISCUSSION

A limitation of this study is that silicone-induced symptoms were not evaluated, and future studies may investigate these symptoms.

This study demonstrated a significant reduction in syringe preparation time and bubble formation when using the ranibizumab PFS vial compared to other vials. In particular,

when preparing the aflibercept vial for injection, the dose-adjustment process took longer than that for the bevacizumab and ranibizumab vials, primarily due to bubble formation. With the PFS form, the administering physician was less dependent on a nurse's continuous presence during injection preparation.

Drugs in the form of PFS have been used for many years in various medical treatments. Similar to previous studies on insulin and heparin PFSs, PFSs have been shown to be beneficial in terms of speed of delivery, reducing the complexity of syringe preparation, time efficiency and user satisfaction.[15,16] Kasi et al.[17] reported that PFSs also increased safety in vaccination versus traditional vials, as they involved fewer handling errors.

Ranibizumab PFS is a novel intravitreal anti-VEGF agent used to treat retinal diseases, including diabetic retinopathy, retinal vein occlusion, and exudative macular degeneration. The use of PFS requires less time and eliminates several procedural steps, including attachment and removal of the aspiration needle and aspiration of the drug from the vial. Consequently, the user needs only to insert the injection needle into the PFS and adjust the dose.

Consistent with our study, Souied et al.[18] reported that the preparation time for intravitreal ranibizumab syringes using PFS was significantly shorter than with the vial. The authors found that the PFS resulted in a 17-29 s reduction in preparation time, similar to our findings (18-28 s). They also noted that the staff perceived a reduction in time spent addressing bubbles when using the PFS.[18]

Although air bubbles can form in the eye during intravitreal anti-VEGF injections, these bubbles are usually expected to be absorbed spontaneously within 3 days.[19-21] However, sometimes these bubbles can increase intraocular pressure when travelling at high altitudes, causing unexpected uncomfortable symptoms and even sudden loss of vision.[22] Similar to our findings, Sassalos and Paulus[23] demonstrated that the syringe design offers improved dose assurance and reduces injection time, the formation of air or silicone oil droplets and the risk of endophthalmitis by eliminating many steps in injection preparation. It has been observed that a solution of aflibercept has a higher viscosity than that of ranibizumab, which results in a greater propensity for the formation of bubbles and increased difficulty in their elimination.[24] The presence of bubbles poses a challenge since their injection into the vitreous can cause visual disturbances, leading to discomfort, fear of falling, and a reduced dose of the drug administered.[19]

According to our results, when preparing the aflibercept vial for injection, the dose adjustment process took longer than for the bevacizumab and ranibizumab vials because of bubble formation. Ranibizumab PFS features a Luer Lock design, which allows the needle to be gripped securely. The design of the PFS uses a siliconization process, called ''baked silicone'', in which an oil-in-water emulsion is spray-coated onto the inner surface of the syringe barrel and heat-fixed. This process minimises oil migration into the ranibizumab absolution and is expected to reduce the incidence of silicone-induced symptoms that may develop due to repeated intravitreal injections.[18] In addition to intraocular air bubbles, silicone oil droplets, which are thought to be associated with intravitreal anti-VEGF drug injections, have been detected in recent studies. Khurana et al. [25] showed that 1.7% of patients receiving bevacizumab prepared by an insulin syringe experienced silicone oil drip complications. This was attributed to dimethicone, a lubricant employed to reduce friction between the syringe body and the piston. Silicone oil droplets are assumed to resemble air bubbles in the eye and to cause floaters associated with water droplets. Although there are not enough studies on this subject in the literature, it is theoretically thought that these oil droplets may lead to the development of glaucoma.[26]

In a recent publication, Thompson highlighted the importance of utilizing silicone-free syringes for intravitreal injections, particularly in cases involving multiple regular anti-VEGF injections.[27] Melo et al.[28] reported that syringes without silicone oil performed best, in addition, the needles also contained silicone and this silicon oil may increase injection into the vitreous.

Lode et al.[29] described a novel method of pharmaceutical compounding using silicone-free syringes and an injection

Table 1. Preparation Times of Drugs

	Number of patients	Time (mean ± SD[1]) (s[2])	Min[3]	Max[4]
Ranibizumab prefilled syringe	45	46.5 ± 4.8	**41.7**	**51.3**
Bevacizumab vial	40	66.1 ± 7.2	**58.9**	**73.3**
Ranibizumab vial	36	64.2 ± 5.1	**59.1**	**69.3**
Aflibercept vial	36	74.7 ± 8.5	**66.2**	**83.2**

SD, standard deviation; s, second Min, minimum; Max, maximum

Table 2. The Development of Endophthalmitis In Patients Receiving Injections

	Number of patients	Endophthalmitis +	Endophthalmitis -
Ranibizumab prefilled syringe	45	0	45
Bevacizumab vial	40	0	40
Ranibizumab vial	36	0	36
Aflibercept vial	36	0	36

needle with a 33 G × 9 mm needle hub and low-dead-space. This method was evaluated for three widely used anti-VEGF biologics in ophthalmology: aflibercept (Eylea), bevacizumab (Avastin), and ranibizumab (Lucentis). Building on their previous work, which detailed a compounding method for the repackaging and storage of aflibercept in silicone-oil-coated plastic syringes while maintaining drug stability and potency, the authors reported benefits, including enhanced safety and reduced time per patient. Combining anti-VEGF biologics allows single-dose vials to be divided into multiple syringes, considerably reducing waste and drug costs. These results suggest that compounding and storage of biologics for one week do not affect their functional activity. This allows safe and cost-effective compounding of anti-VEGF biologics into prefilled silicone oil-free syringes for intravitreal injection.

The proposed approach involves compounding anti-VEGF biologics and storing them in prefilled plastic syringes for intravitreal use. Additionally, bevacizumab is repackaged for ophthalmic use into small glass vials rather than plastic syringes. This innovative method aims to enhance safety and efficacy. Peterson et al.[30] reported that bevacizumab can be successfully packaged in small, single-dose glass vials for intravitreal injections. It was also stated that the properties of the product, including anti-VEGF bioactivity, would remain similar for 21 months under refrigerator storage conditions.[30] This approach warrants consideration as an alternative to plastic syringes for repackaging ophthalmic bevacizumab in small glass vials.

Endophthalmitis, a serious complication of intravitreal treatment that results in permanent vision loss, remains a significant concern in ophthalmic care. The utilisation of PFSs effectively eliminates numerous steps in the preparation of injections, thereby reducing the risk of iatrogenic contamination resulting from suboptimal drug or device handling.[18,31] Although no comparative study in the literature has proven this hypothesis, Storey's ongoing multicentre study suggests that the odds of endophthalmitis are lower with ranibizumab PFS than with conventional intravitreal injections. A large, multi-centered, retrospective study revealed that the use of PFS during intravitreal ranibizumab administration reduced the incidence of culture-positive endophthalmitis, and improved visual outcomes.[32]

In their multi-centre study, Souied et al.[18] demonstrated that the use of PFS resulted in a 25.5 second reduction in preparation time compared to the use of conventional syringes.[18] In our study, the mean injection preparation time was 46.5 ± 4.8 s for the ranibizumab prefilled syringe versus 66.1 ± 7.2 s, 64.2 ± 5.1 s, and 74.7 ± 8.5 s for the bevacizumab, ranibizumab, and aflibercept vials, respectively. Accordingly, injection preparation time was significantly lower in the ranibizumab prefilled syringe group and significantly higher for the aflibercept vial compared with the other intravitreal drugs.

Our findings, along with those from similar studies, reflect the common goal of shortening the preparation stages for intravitreal injections, thus reducing the total drug preparation time and, most importantly, minimizing the risk of infection. In the current study, the ranibizumab prefilled syringe required fewer preparation steps, enhancing ophthalmologists' work efficiency. This allows clinicians to see more patients per session, to reduce the total time required to see the same number of patients, to provide additional time for consultations when needed. In a busy retinal practice where several injections are performed per day, the use of PFSs could be a significant time-saver compared with vials. Although it is encouraging that no patient developed endophthalmitis in our study, we think that this finding may reflect the small sample size. Larger studies are needed on this subject.

Ethics

Ethics Committee Approval: Ethical approval was obtained from the ethics committee of Erzincan Binali Yıldırım University Faculty of Medicine (E-21142744-804.99-138855, date: 17.01.2022)

Informed Consent: Since the study involved only observation of clinical practices without collecting identifiable patient data, informed consent for participation was not obtained.

Footnotes

Author Contributions

Concept Design – A.U., İ.Ç.; Data Collection or Processing – A.U., N.G.T, Y.K.; Analysis or Interpretation – A.U., İ.Ç. Literature Review – N.G.T, Y.K.; Writing, Reviewing and Editing – A.M.S.

Declaration of Interests: The authors declare that they have no conflicts of interest.

Funding: The authors declare that this study has received no financial support.

REFERENCES

1. Ferrara N, Damico N, Shams M, et al. Development of ranibizumab, an anti-vascular endothelial growth factor antigen binding fragment, as therapy for neovascular age-related macular degeneration. *Retina*. 2006;26(8):859–870. [CrossRef]
2. Rosenfeld PJ, Brown DM, Heier JS, et al. Ranibizumab for neovascular agerelated macular degeneration. *N Engl J Med.* 2006;355:1419-1431. [CrossRef]
3. Krüger falk M, Kemp H, Sørensen TL. Four-year treatment results of neovascular age- related macular degeneration with ranibizumab and causes for discontinuation of treatment. *AMJ Ophthalmol.* 2013;155:89-95. [CrossRef]
4. Holz FG, Bandello F, Gillies M, et al. Safety of ranibizumab in routine clinical practice: 1-year retrospective pooled analysis of four european neovascular amd registries within the luminous programme. *BR J Ophthalmol*. 2013;97(9):1161–1167. [CrossRef]
5. Rein DB, Wittenborn JS, Zhang X, et al. Forecasting age-related macular degeneration through the year 2050: the potential impact of new treatments. *Arch Ophthalmol.* 2009;127:533-540. [CrossRef]
6. Lindekleiv H, Erke MG. Projected prevalence of age-related macular degeneration in scandinavia 2012-2040. *Acta Ophthalmol*. 2013;91:307-311. [CrossRef]

7. Grzybowski A, Told R, Sacu S, et al. 2018 update on intravitreal injections: euretina expert consensus recommendations. *Ophthalmologica*. 2018;239(4):181–193. [CrossRef]
8. Menon G, Walters G. New paradigms in the treatment of wet AMD: the impact of anti- vegf therapy. *Eye*. 2009;23:1-7. [CrossRef]
9. Brown DM, Michels M, Kaiser PK, et al. Ranibizumab versus verteporfin photodynamic therapy for neovascular age-related macular degeneration: two-year results of the anchor study. *Ophthalmology*. 2009;116:57-65. [CrossRef]
10. Wolf S, Balciuniene VJ, Laganovska G, et al. Radiance: a randomized controlled study of ranibizumab in patients with choroidal neovascularization secondary to pathologic myopia. *Ophthalmology*. 2014;121:682-692.
11. Han DP. Age-related macular degeneration, anti-vegf therapy, and ophthalmic imaging: is there a best practice? *Jama Ophthalmol*. 2013;131:1124. [CrossRef]
12. Mccannel CA. Meta-analysis of endophthalmitis after intravitreal injection of anti-vascular endothelial growth factor agents: causative organisms and possible prevention strategies. *Retina*. 2011;31:654-661. [CrossRef]
13. Fda approves lucentis (ranibizumab injection) prefilled syringe. [october 14, 2016]. available from: https://www.gene.com/media/press-releases/14640/2016-10-14/fda-approves-genentechs-lucentis-ranibiz. accessed september 14, 2018. [CrossRef]
14. Fda approves genentech's lucentis (ranibizumab injection) 0.3 mg prefilled syringe for diabetic macular edema and diabetic retinopathy. [march 21, 2018]. available from: https://www.gene.com/media/press-releases/14708/2018-03-21/fda-approves-genentechs-lucentis-ranibiz. accessed september 10, 2018. [CrossRef]
15. Plevin S, Sadur C. Use of a prefilled insulin syringe (novolin prefilled) by patients with diabetes. *Clin ther*. 1993;15: 423-431. [CrossRef]
16. Barber ND. Heparin administration using prefilled syringes or ampoules: a comparative cost-effectiveness study. *Int J Pharm Pract*. 1993;2:15-27. [CrossRef]
17. Kasi GS, Prabhu SV, Sanjay S, et al. Prefilled syringes versus vials: impact on vaccination efficiency and patient safety in indian private market. *Pediatr infect dis*. 2013;5:181-186[CrossRef]
18. Eric S, Sylvia NB , Claudia L , et al. Ranibizumab prefilled syringes: benefits of reduced syringe preparation times and less complex preparation procedures. *Eur J Ophthalmol*. 2015;25(6):529-534. [CrossRef]
19. Subhi Y, Kjer B, Munch IC. Prefilled syringes for intravitreal injection reduce preparation time. *Dan Med J*. 2016;63(4). [CrossRef]
20. Somner JE, Mansfield D. Inadvertent injection of intravitreal air during intravitreal lucentis injection for wet age-related macular degeneration: an undescribed complication. *Eye*. 2009;23(8):1744. [CrossRef]
21. Sukgen EA, Gunay M, Kocluk Y. Occurrence of intraocular air bubbles during intravitreal injections for retinopathy of prematurity. *Int ophthalmol*. 2017;37(1):215–219. [CrossRef]
22. Mills MD, Devenyi RG, Lam WC, et al. An assessment of intraocular pressure rise in patients with gas-filled eyes during simulated air flight. *Ophthalmology*. 2001;108(1):40–44. [CrossRef]
23. Thérèse MS , Yannis MP. Prefilled syringes for intravitreal drug delivery. *Clin Ophthalmol*.2019;13:701-706. [CrossRef]
24. Rojas-juárez S, Sánchez-ramos JA, Saucedo-castillo A, et al. Intravitreal anti-vascular endothelial growth factor complications. *Int J Ophthal Clin Res*. 2015;2:022. [CrossRef]
25. Khurana RN, Chang LK, Porco TC. Incidence of presumed silicone oil droplets in the vitreous cavity after intravitreal bevacizumab injection with insulin syringes. *Jama Ophthalmol* .2017;135(7):800–803. [CrossRef]
26. Yu JH, Gallemore E, Kim JK, et al. Silicone oil droplets following intravitreal bevacizumab injections. *Am J Ophthalmol Case Rep*. 2018;10:142–144. [CrossRef]
27. John TT. 2021 prospective study of silicone oil microdroplets in eyes receiving intravitreal anti-vascular endothelial growth factor therapy in 3 different syring. *Ophthalmol Retina*. 2021 ;5(3):234-240. [CrossRef]
28. Melo GB, da Cruz NFS, do Monte Agra LL, et al.Silicone oil-free syringes, siliconized syringes and needles: quantitative assessment of silicone oil release with drugs used for intravitreal injection. *Acta Ophthalmol* . 2021; 99:1366-1374. [CrossRef]
29. Lode HE, Gjølberg TT, Foss S, et al. A new method for pharmaceutical compounding and storage of anti-vegf biologics for intravitreal use in silicone oil-free prefilled plastic syringes. *Sci Rep*. 2019;9(1):18021. [CrossRef]
30. Jan SP, Kenneth R, Ingrid US, et al. Long-term physical stability, sterility, and anti-vegf bioactivity of repackaged bevacizumab in 2-ml glass vials. *Retina*. 2019;39(9):1802-1809. [CrossRef]
31. Jean-Eric M, Juergen S, Lina B, et al. Ranibizumab pre-filled syringe approved in the European Union: innovation to improve dose accuracy, reduce potential infection risk, and offer more efficient treatment administration. *Invest Ophthalmol Vis Sci* .2014;55(13):1949. [CrossRef]
32. Philip P, Zujaja T, Yoshihiro Y, et al. The impact of prefilled syringes on endophthalmitis following intravitreal injection of ranibizumab. *American Journal of Ophthalmology*. 2019 Mar:199:200-208. [CrossRef]

ABCResearch

Arch Basic Clin Res 2026;8(2):194-200
DOI: 10.4274/ABCR.2026.26448

Research Article

Diagnostic Performance of the BioFire® Joint Infection Panel in Native Septic Arthritis and Periprosthetic Joint Infection: A Retrospective Diagnostic Accuracy Study

Mehmet Burak Gökgöz[1], Volkan Gür[1], Akın Öztürk[1], İbrahim Doğan[1], Nedim Batuhan Toğaluğurlu[1], Harun Dündar[1], Barış Gülhan[2], Sümeyye Akyüz[2], Furkan Yapıcı[1]

[1]Department of Orthopedics and Traumatology, Erzincan Binali Yıldırım University Faculty of Medicine, Erzincan, Türkiye
[2]Department of Medical Microbiology, Erzincan Binali Yıldırım University Faculty of Medicine, Erzincan, Türkiye

Cite this article as: Gökgöz MB, Gür V, Öztürk A, et al. Diagnostic performance of the BioFire® joint infection panel in native septic arthritis and periprosthetic joint infection: a retrospective diagnostic accuracy study. *Arch Basic Clin Res*. 2026;8(2):194-200.

ORCID IDs of the authors: M.B.G., 0000-0003-0758-5382, V.G., 0000-0003-4736-6555, A.Ö., 0000-0001-6195-9475, İ.D., 0000-0003-4183-7993, N.B.T., 0009-0005-3835-3607, H.D., 0009-0005-1743-0183, B.G., 0000-0002-2605-1282, S.A., 0000-0003-1999-7827, F.Y., 0000-0002-5349-4580.

ABSTRACT

Objective: Rapid identification of causative microorganisms is essential in suspected native septic arthritis and periprosthetic joint infection. This study evaluated the diagnostic performance of the BioFire® Joint Infection Panel and assessed its agreement with conventional culture and systemic inflammatory biomarkers.

Methods: Hospital records from January 2025 to April 2026 were retrospectively reviewed. Of 115 screened patients with suspected joint infection, nine were excluded because BioFire® testing had not been performed and only culture results were available. The final analysis included 106 synovial fluid samples. All samples were tested using conventional culture and the BioFire® Joint Infection Panel during the same clinical episode. Demographic data, infection category, localization, C-reactive protein, erythrocyte sedimentation rate, procalcitonin, and white blood cell count were recorded. Agreement was assessed using Cohen's kappa, discordance using the McNemar test, and diagnostic performance using culture as the reference method.

Results: Sixty-five samples (61.3%) were classified as suspected native septic arthritis and 41 (38.7%) as periprosthetic joint infection. BioFire® was positive in 22 samples (20.8%) and culture was positive in 32 (30.2%). Overall agreement was 86.8%, with substantial agreement according to Cohen's kappa (0.656). Discordance was significant, predominantly due to culture-positive/BioFire®-negative samples (P = 0.013). BioFire® showed 62.5% sensitivity [95% confidence interval (CI): 43.7-78.9), 97.3% specificity (95% CI: 90.6-99.7), 90.9% positive predictive value, 85.7% negative predictive value, and 86.8% accuracy. C-reactive protein, procalcitonin, and white blood cell counts were significantly higher in patients with suspected native septic arthritis.

Conclusion: The BioFire® Joint Infection Panel provides rapid and highly specific microbiological support in suspected joint infection. However, its moderate sensitivity and inability to detect off-panel organisms indicate that it should complement rather than replace conventional culture.

Keywords: Septic arthritis, periprosthetic joint infection, polymerase chain reaction, microbiological techniques, synovial fluid

Corresponding author: Furkan Yapıcı, **E-mail:** furkanyapici@hotmail.com

Received: June 9, 2026
Revision Requested: June 15, 2026 **Accepted:** June 23, 2026 **Publication Date:** July, 14, 2026

INTRODUCTION

Septic arthritis and periprosthetic joint infection (PJI) are serious orthopedic infections that may lead to irreversible joint damage, systemic sepsis, repeated surgery, increased morbidity, and mortality when diagnosis and treatment are delayed.[1,2] Rapid and accurate pathogen identification is therefore central to targeted antimicrobial therapy, surgical planning, and risk stratification.[3] Conventional microbiological culture of synovial fluid and tissue specimens remains the cornerstone of microbiological diagnosis, but pathogen recovery is time-dependent and may be affected by sample volume, bacterial burden, previous antibiotic exposure, biofilm formation, and the presence of slow-growing or low-virulence microorganisms.[4-7]

These limitations are particularly relevant in PJI, where biofilm-associated pathogens may be difficult to recover by standard culture methods, and in native septic arthritis, where empirical antibiotic treatment before aspiration may reduce culture positivity. As a result, molecular diagnostic approaches, including syndromic multiplex polymerase chain reaction (PCR) panels, have attracted increasing interest because they can provide standardized pathogen detection in a substantially shorter time frame.[8]

The BioFire® FilmArray® Joint Infection Panel (bioMérieux, Marcy-l'Étoile, France) is a closed, automated, multiplex molecular diagnostic system developed for the analysis of synovial fluid. The panel can detect, directly from synovial fluid, a predefined set of bacterial and fungal targets and selected antimicrobial resistance genes in approximately one hour.[9,10] Recent studies have suggested that the panel may improve early microbiological documentation, contribute to the management of culture-negative cases, and support timely antimicrobial stewardship.[11-16]

Nevertheless, the clinical usefulness of the panel depends on the target spectrum, organism burden, the biology of biofilm-related disease, and the presence of off-panel microorganisms. Moreover, the relationship between molecular positivity and systemic inflammatory response may differ between suspected native septic arthritis and PJI. This study aimed to evaluate the diagnostic performance of the BioFire® Joint Infection Panel, its agreement with conventional culture, and its association with systemic inflammatory biomarkers in patients evaluated for suspected native or prosthetic joint infection.

MAIN POINTS

- The BioFire® Joint Infection Panel showed high specificity and positive predictive value in suspected joint infection.
- Moderate sensitivity and discordance between culture-positive and BioFire-negative results indicate that negative BioFire results cannot exclude infection.
- The panel may provide rapid microbiological guidance when urgent organism-directed treatment decisions are required.
- Suspected native septic arthritis showed a stronger systemic inflammatory response than in periprosthetic joint infection.
- BioFire testing should be interpreted as an adjunct to, rather than a replacement for, conventional culture.

MATERIALS AND METHODS

Study Design and Population

This retrospective diagnostic accuracy study included synovial fluid samples obtained from patients evaluated in our clinic for suspected joint infection. The study was prepared in accordance with the standards for reporting of diagnostic accuracy (STARD) principles for diagnostic accuracy research and the Declaration of Helsinki. Ethics committee approval was obtained from the Erzincan University Faculty of Medicine Ethics Committee (approval no: 2025-18/03, date: 16.10.2025).

In this retrospective study, hospital records from January 2025 to April 2026 were reviewed, and 115 patients with suspected joint infection were initially screened. The cohort comprised patients who presented to the emergency department or the orthopedic outpatient clinic with suspected septic arthritis, and patients with prosthetic joints who developed acute clinical findings suggestive of infection, such as periarticular effusion, increased local temperature, and pain. PJI was classified according to institutional diagnostic practice based on clinical findings, serum inflammatory markers, synovial fluid analysis, microbiological results, and intraoperative findings when available. Nine patients were excluded because BioFire® Joint Infection Panel testing had not been performed, and only conventional culture results were available for these patients. Accordingly, the final analysis included 106 synovial fluid samples, each assessed concurrently by conventional culture and the BioFire® Joint Infection Panel during the same clinical episode. Samples with invalid or non-evaluable molecular results were excluded. Clinical and demographic variables, including age, sex, prosthesis status, infection category, and anatomical localization, were extracted from the hospital information management system. After clinical evaluation, cases were categorized as suspected native septic arthritis or suspected PJI. The unit of analysis was the synovial fluid sample. The patient selection process and final study cohort are summarized in the STARD flow diagram (Figure 1).

Laboratory Parameters

C-reactive protein (CRP, mg/L), erythrocyte sedimentation rate (ESR, mm/h), procalcitonin (PCT, ng/mL), and white blood cell count (WBC, 10^3/μL) were recorded from venous blood samples collected on the day of joint aspiration. Biochemical and hematological analyses were performed in the central laboratory of our hospital according to standardized procedures. The exact timing of biomarker sampling relative to antibiotic administration was not consistently available in the retrospective records; therefore, biomarker values were defined as those obtained on the day of aspiration.

Conventional Microbiology

Synovial fluid samples were aspirated under sterile conditions and immediately transferred to the microbiology laboratory. For conventional microbiological assessment, samples were

inoculated onto blood agar, MacConkey agar, and chocolate agar plates and also introduced into aerobic and anaerobic blood culture bottles for enrichment, according to the laboratory protocol. In suspected native joint infection, culture plates were incubated for 5-7 days; in suspected PJI, incubation was extended to 14 days to improve detection of low-virulence or biofilm-forming organisms, including Cutibacterium acnes. Colony identification and antimicrobial susceptibility testing were performed using the laboratory's routine matrix-assisted laser desorption/ionization time-of-flight mass spectrometry and automated systems.

BioFire Joint Infection Panel

In parallel with culture, approximately 0.2 mL of synovial fluid was analyzed using the BioFire Joint Infection Panel. In accordance with the manufacturer's instructions, the sample was mixed with the designated hydration solution, loaded into the cartridge, and placed in the BioFire FilmArray system. The closed cartridge performs cell lysis, nucleic acid extraction, reverse transcription (when required), multiplex PCR amplification, and fluorescent probe-based detection. Results were reported by the software as Detected, Not Detected, or Invalid. The target spectrum of the panel is summarized in Table 1.

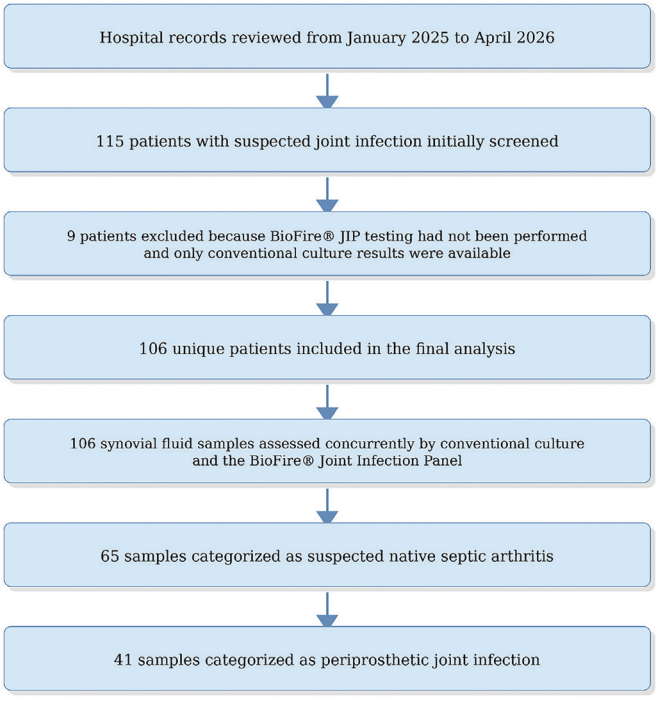

Figure 1. STARD flow diagram of patient selection and inclusion process. Hospital records from January 2025 to April 2026 were retrospectively reviewed. Among 115 initially screened patients with suspected joint infection, nine were excluded because BioFire® Joint Infection Panel testing had not been performed and only conventional culture results were available. The final analysis included 106 synovial fluid samples obtained from 106 unique patients, including 65 samples categorized as suspected native septic arthritis and 41 samples categorized as periprosthetic joint infection.

Statistical Analysis

Statistical analyses were performed using the Statistical Package for the Social Sciences, version 26.0 (IBM Corp., Armonk, NY, USA). The distribution of continuous variables was evaluated using the Shapiro-Wilk test and visual methods. Non-normally distributed continuous variables were reported as median [interquartile range (IQR)]; categorical variables were reported as frequencies and percentages. Either the chi-square test or Fisher's exact test was used for categorical variables, and the Mann-Whitney U test was used for continuous variables. Agreement between BioFire and culture was evaluated using Cohen's kappa coefficient, and directional discordance was assessed using the McNemar test. Sensitivity, specificity, positive predictive value (PPV), negative predictive value (NPV), and accuracy were calculated using conventional culture as the reference method. A P value of < 0.05 was considered statistically significant. Exact 95% confidence intervals were calculated for sensitivity, specificity, PPV, negative predictive value, and overall diagnostic accuracy using the binomial method.

RESULTS

The study included 106 synovial fluid samples. Female and male patients were equally represented, with 53 patients (50.0%) from each sex. The overall mean age was 65.6 ± 15.5 years, and the median age was 66.5 years (IQR: 59.5-77.0). According to clinical categorization, 65 samples (61.3%) were classified as suspected native septic arthritis and 41 (38.7%) as PJI. The most common anatomical site was the knee (n=73, 68.9%), followed by the hip (n=21, 19.8%), the ankle (n=5, 4.7%), the elbow (n=5, 4.7%), and the shoulder (n=2, 1.9%) (Table 2).

Sex distribution did not differ significantly between the suspected native septic arthritis and PJI groups (P = 0.231). Age distributions were also similar between the groups, with median ages of 67 years in the suspected native septic arthritis group and 66 years in the PJI group (P = 0.763). In contrast, localization differed significantly between groups ($P < 0.001$). The knee was the predominant site in suspected native septic arthritis, whereas involvement of the knee and hip was equally represented in PJI (Table 2).

The BioFire panel was negative in 84 samples (79.2%) and positive in 22 samples (20.8%). Conventional culture was negative in 74 samples (69.8%) and positive in 32 samples (30.2%). When both methods were evaluated together, 20 samples were positive by both methods, and 72 were negative by both. Overall observed agreement was 86.8%, and Cohen's kappa was 0.656, indicating substantial agreement. Discordance was asymmetric, with significantly more culture-positive/BioFire-negative samples than BioFire-positive/culture-negative samples (McNemar P = 0.013) (Table 3).

Using conventional culture as the reference method, the BioFire® Joint Infection Panel demonstrated a sensitivity of 62.5% (95% CI: 43.7-78.9), specificity of 97.3% (95% CI: 90.6-99.7), PPV of 90.9% (95% CI: 70.8-98.9), negative predictive value of 85.7% (95% CI: 76.4-92.4), and overall diagnostic accuracy of 86.8% (95% CI: 78.8-92.6) (Table 4). BioFire positivity was observed

Table 1. Targets Detected by the BioFire® Joint Infection Panel

Category	Microorganisms/Resistance Genes
Gram-positive bacteria	*Enterococcus faecalis*; *Enterococcus faecium*; *Listeria monocytogenes*; *Staphylococcus aureus*; *Staphylococcus lugdunensis*; *Streptococcus agalactiae* (Group B); *Streptococcus pneumoniae*; *Streptococcus pyogenes* (Group A); *Streptococcus anginosus* group (S. *anginosus*, S. *intermedius*, S. *constellatus*); *Streptococcus dysgalactiae*
Gram-negative bacteria	*Bacteroides fragilis*; *Citrobacter* spp. (*C. freundii, C. koseri, C. amalonaticus*); *Enterobacter* cloacae complex; *Escherichia coli*; *Haemophilus* influenzae; *Kingella kingae*; *Klebsiella aerogenes*; *Klebsiella pneumoniae* group; *Klebsiella oxytoca*; *Morganella morganii*; *Neisseria gonorrhoeae*; *Proteus* spp.; *Pseudomonas aeruginosa*; *Salmonella* spp.; *Serratia marcescens*
Yeast	*Candida albicans*; *Candida glabrata*
Antimicrobial resistance genes	Carbapenemases: blaIMP, blaKPC, blaNDM, blaOXA-48-like, blaVIM; extended-spectrum beta-lactamase: blaCTX-M; methicillin resistance: mecA/C and mecA/C with MREJ; vancomycin resistance: vanA/B

Target list is presented for interpretation of potential on-panel and off-panel discordance. BioFire JIP: BioFire® Joint Infection Panel; MREJ: *Staphylococcal* cassette chromosome mec right-extremity junction.

Table 2. Demographic and Clinical Characteristics of the Study Population

Parameters	Total (n=106)	Suspected Native Septic Arthritis (n=65)	PJI (n=41)	P value
Gender, n (%)				0.231
Female	53 (50.0)	30 (46.2)	23 (56.1)	
Male	53 (50.0)	35 (53.8)	18 (43.9)	
Age (years)				0.763
Median (IQR)	66.5 (59.5-77.0)	67 (58.0-78.0)	66 (60.0-76.5)	
Localization, n (%)				**<0.001**
Knee	73 (68.9)	55 (84.6)	18 (43.9)	
Hip	21 (19.8)	3 (4.6)	18 (43.9)	
Ankle	5 (4.7)	4 (6.2)	1 (2.4)	
Elbow	5 (4.7)	2 (3.1)	3 (7.3)	
Shoulder	2 (1.9)	1 (1.5)	1 (2.4)	

IQR: interquartile range; PJI: periprosthetic joint infection.

Table 3. Comparison of BioFire Joint Infection Panel and Conventional Culture Results

	Culture (+)	Culture (-)	Total
BioFire JIP (+)	20	2	22
BioFire JIP (-)	12	72	84
Total	32	74	106

BioFire JIP: BioFire® Joint Infection Panel. Overall agreement: 86.8%; Cohen's kappa: 0.656; McNemar P = 0.013.

Table 4. Diagnostic Performance of the BioFire® Joint Infection Panel Using Conventional Culture as the Reference Method

Parameter	Value	95% CI
Sensitivity	62.5%	43.7-78.9
Specificity	97.3%	90.6-99.7
Positive predictive value	90.9%	70.8-98.9
Negative predictive value	85.7%	76.4-92.4
Accuracy	86.8%	78.8-92.6

CI: confidence interval.

in 13 of 65 samples (20.0%) in the suspected native septic arthritis group and in 9 of 41 samples (22.0%) in the PJI group, with no statistically significant difference between groups (P = 0.811). Culture positivity was observed in 16 of 65 samples (24.6%) from the suspected native septic arthritis group and in 16 of 41 samples (39.0%) from the PJI group; however, this difference did not reach statistical significance (P = 0.132).

Discordant results were observed in 14 samples. Two samples were BioFire-positive/culture-negative, whereas 12 samples were culture-positive/BioFire-negative. Because conventional culture is an imperfect reference standard in joint infection, particularly in patients with prior antibiotic exposure or biofilm-associated infection, BioFire-positive/culture-negative results were interpreted as discordant findings rather than definitive false-positive results. Conversely, culture-positive/BioFire-negative discordance may have been related to off-panel microorganisms, a low organism burden below the analytical detection threshold of the molecular panel, or low-inoculum organisms commonly encountered in indolent or biofilm-associated infections. Table 5 summarizes the microorganisms or molecular targets identified in the 14 discordant samples. The two BioFire-positive/culture-negative samples were *Streptococcus* spp. (from a PJI knee sample) and Klebsiella aerogenes (from a suspected native septic arthritis knee sample). The 12 culture-positive/BioFire-negative samples

Table 5. Microorganisms or Molecular Targets Identified in Discordant Cases

Case	Study sample no.	Infection category	Location	Discordance pattern	BioFire® JIP result	Culture result	Interpretation
1	15	Periprosthetic joint infection	Knee	BioFire® positive / culture negative	*Streptococcus* spp., no resistance marker	Negative	BioFire® target detected despite negative culture; possible culture limitation, prior antibiotics, low viable burden, or nonviable DNA.
2	16	Suspected native septic arthritis	Knee	BioFire® positive / culture negative	*Klebsiella aerogenes;* no resistance marker	Negative	BioFire® target detected despite negative culture; possible culture limitation, prior antibiotics, low viable burden, or nonviable DNA.
3	2	Suspected native septic arthritis	Hip	Culture positive / BioFire® negative	Not detected	*Staphylococcus aureus*	On-panel organism; possible low organism burden, sampling variation, or inhibition.
4	5	Suspected native septic arthritis	Knee	Culture positive / BioFire® negative	Not detected	*Achromobacter denitrificans*	Off-panel organism.
5	29	Suspected native septic arthritis	Knee	Culture positive / BioFire® negative	Not detected	*Brucella spp.*	Off-panel organism.
6	45	Periprosthetic joint infection	Knee	Culture positive / BioFire® negative	Not detected	*Staphylococcus epidermidis*	Off-panel low-virulence skin flora organism.
7	48	Periprosthetic joint infection	Knee	Culture positive / BioFire® negative	Not detected	*Staphylococcus lugdunensis*	On-panel organism; possible low organism burden, sampling variation, or inhibition.
8	55	Periprosthetic joint infection	Knee	Culture positive / BioFire® negative	Not detected	*Staphylococcus hominis and Staphylococcus epidermidis*	Off-panel low-virulence skin flora organisms.
9	68	Periprosthetic joint infection	Hip	Culture positive / BioFire® negative	Not detected	*Staphylococcus hominis*	Off-panel low-virulence skin flora organism.
10	69	Periprosthetic joint infection	Hip	Culture positive / BioFire® negative	Not detected	*Corynebacterium simulans*	Off-panel low-virulence skin flora organism.
11	72	Periprosthetic joint infection	Hip	Culture positive / BioFire® negative	Not detected	*Staphylococcus epidermidis*	Off-panel low-virulence skin flora organism.
12	82	Suspected native septic arthritis	Knee	Culture positive / BioFire® negative	Not detected	*Brucella* spp.	Off-panel organism.
13	86	Periprosthetic joint infection	Knee	Culture positive / BioFire® negative	Not detected	*Staphylococcus haemolyticus*	Off-panel low-virulence skin flora organism.
14	88	Periprosthetic joint infection	Knee	Culture positive / BioFire® negative	Not detected	*Staphylococcus epidermidis*	Off-panel low-virulence skin flora organism.

BioFire® JIP, BioFire® Joint Infection Panel; PJI, periprosthetic joint infection. Independent molecular confirmation, such as broad-range 16S rRNA sequencing, was not performed.

included *Staphylococcus* aureus (n=1), *Achromobacter* denitrificans (n=1), *Brucella* spp. (n=2), *Staphylococcus epidermidis* (n=3), *Staphylococcus lugdunensis* (n=1), mixed *Staphylococcus hominis* and *Staphylococcus epidermidis* (n=1), *Staphylococcus hominis* (n=1), *Corynebacterium simulans* (n=1), and *Staphylococcus haemolyticus* (n=1). Most culture-positive/BioFire-negative discordant samples involved organisms outside the panel's target spectrum or low-virulence skin flora, whereas Staphylococcus aureus and Staphylococcus lugdunensis were on-panel organisms.

Among positive samples, *Staphylococcus aureus* was the most frequently identified organism by both BioFire and culture. The BioFire panel also detected Candida albicans and Streptococcus species. Conventional culture also identified *Streptococcus agalactiae*, *Staphylococcus epidermidis*, and other organisms. BioFire detected the mecA/C and MREJ resistance markers compatible with methicillin-resistant *Staphylococcus aureus* in three samples, and CTX-M in one sample.

In the overall cohort, the median CRP, ESR, PCT, and WBC were 66.2 mg/L, 31 mm/h, 0.075 ng/mL, and 9.61 × 10^3/μL, respectively. The systemic inflammatory response was more prominent in suspected native septic arthritis. Median CRP was 80.4 mg/L in suspected native septic arthritis and 18.9 mg/L in PJI (P = 0.004). Median PCT (P = 0.005) and WBC (P = 0.009)

values were also significantly higher in patients with suspected native septic arthritis. ESR did not differ significantly between groups (P = 0.842). When biomarkers were compared by BioFire positivity, CRP, ESR, PCT, and WBC values were numerically higher in BioFire-positive samples, but most differences were not statistically significant.

DISCUSSION

This study demonstrated that the BioFire Joint Infection Panel had high specificity, high PPV, and substantial agreement with conventional culture in patients evaluated for suspected native septic arthritis or PJI. The overall agreement rate of 86.8% and a kappa value of 0.656 indicate that the panel can provide clinically useful microbiological information. However, the moderate sensitivity and the predominance of culture-positive/BioFire-negative discordance support its use as a rapid adjunct to culture.

The high specificity of 97.3% and the PPV of 90.9% are clinically important. In practice, a positive molecular result can rapidly support organism-directed antimicrobial treatment, particularly when urgent therapeutic decisions are required in acute septic arthritis. The approximately one-hour turnaround time of the panel may also facilitate early antimicrobial stewardship by allowing earlier narrowing or escalation of empirical regimens when a target organism or resistance marker is detected.[9-16]

The sensitivity of 62.5% observed in our cohort requires careful interpretation. Culture-positive/BioFire-negative samples may reflect a low bacterial burden below the analytical detection threshold, organisms not included in the panel, or pathogens associated with indolent biofilm-related infection. Conventional culture was used as the reference method, but it may also be affected by prior antibiotic exposure, sample volume, transport conditions, organism burden, incubation requirements, and slow-growing or biofilm-forming microorganisms. Accordingly, discordant results should be interpreted together with clinical, laboratory, and intraoperative findings rather than in isolation.

The distribution of organisms in our study was consistent with the established microbiology of joint infections, with Staphylococcus aureus being the most frequently detected pathogen. The ability of the panel to detect mecA/C and MREJ directly from synovial fluid may be valuable in cases of suspected methicillin-resistant Staphylococcus aureus infection, because early recognition of resistance can influence empirical treatment. Nevertheless, the panel does not include all potentially relevant bacteria, fungi, or resistance mechanisms; this restricted target range explains the need for culture, prolonged incubation when indicated, and clinical correlation

A notable finding was that suspected native septic arthritis and PJI exhibited different inflammatory biomarker profiles. CRP, PCT, and WBC were significantly higher in patients with suspected native septic arthritis, whereas ESR did not differ significantly. This pattern suggests that suspected native septic arthritis is more often associated with an acute systemic inflammatory response, whereas PJI may present with a more indolent biomarker profile because of biofilm formation and lower-virulence pathogens. Consequently, reliance on systemic biomarkers alone may be insufficient in suspected PJI, and microbiological tests should be interpreted within the broader clinical context.

The relationship between BioFire positivity and systemic inflammatory biomarkers was limited. Although median biomarker values were numerically higher in BioFire-positive samples, most differences were not statistically significant. Molecular positivity reflects the presence of a target nucleic acid, whereas systemic biomarker concentrations are influenced by infection duration, organism virulence, host immune response, comorbidities, and previous treatment. These findings suggest that molecular testing and systemic inflammatory markers provide different diagnostic information.

Study Limitations

This study has several limitations. First, its retrospective design may have introduced selection bias and limited the availability of some clinically relevant variables. Second, conventional culture was used as the reference method, although it is not a perfect gold standard for diagnosing joint infection, particularly in patients who received antibiotics before aspiration or in infections involving low-virulence or biofilm-forming organisms. Third, prior antibiotic exposure the exact timing of biomarker sampling relative to antibiotic administration, synovial fluid leukocyte count, polymorphonuclear cell percentage, intraoperative findings, histopathological data, and treatment modifications based on BioFire® results were not uniformly available. Fourth, because the analysis was conducted at the synovial-fluid sample level, potential within-patient correlation could not be fully addressed. Fifth, the sample size limited the ability to perform detailed subgroup analyses, particularly within the PJI group and for individual pathogens. Sixth, this was a single-center study reflecting local patient selection and microbiological epidemiology; therefore, the generalizability of the findings to other institutions may be limited. Finally, off-panel organisms and discordant results were not further evaluated using an independent molecular reference method, such as broad-range 16S rRNA sequencing. Prospective multicenter studies using composite diagnostic standards are needed to better define the diagnostic and clinical impact of BioFire® testing in native and prosthetic joint infections.

CONCLUSION

The BioFire® Joint Infection Panel is a rapid, highly specific microbiological diagnostic tool for cases of suspected joint infection. A positive result may guide early organism-directed management; however, moderate sensitivity and off-panel limitations mean a negative result does not exclude infection. The panel should therefore be interpreted in conjunction with conventional culture and clinical findings. Prospective studies using composite diagnostic standards are needed to define its clinical and economic impact on native septic arthritis and PJI.

Ethics

Ethics Committee Approval: The ethics committee approval and permission for the study were obtained from the Erzincan Binali Yıldırım University Clinical Research Ethics Committee with the decision number 2025-18/03, date 16.10.2025.

Informed Consent: The requirement for informed consent was waived because the study used a retrospective design with anonymized patient data.

Footnotes

Author Contributions

Concept Design – M.B.G., V.G., A.Ö., F.Y.; Data Collection or Processing – M.B.G., N.B.T., H.D., B.G., S.A.; Analysis or Interpretation – M.B.G., F.Y.; Literature Review – M.B.G., V.G., A.Ö., İ.D., N.B.T., H.D., S.A.; Writing, Reviewing and Editing – M.B.G., F.Y.

Declaration of Interest: The authors declared no conflicts of interest.

Funding: The authors declare that this study has received no financial support.

REFERENCES

1. Weston VC, Jones AC, Bradbury N, Fawthrop F, Doherty M. Clinical features and outcome of septic arthritis in a single UK Health District 1982-1991. *Ann Rheum Dis*. 1999;58(4):214-219. [CrossRef]
2. Mathews CJ, Weston VC, Jones A, Field M, Coakley G. Bacterial septic arthritis in adults. *Lancet*. 2010;375(9717):846-855. [CrossRef]
3. Ravn C, Neyt J, Benito N, et al. Guideline for management of septic arthritis in native joints (SANJO). *J Bone Jt Infect*. 2023;8(1):29-37. [CrossRef]
4. Kalbian I, Park JW, Goswami K, Lee YK, Parvizi J, Koo KH. Culture-negative periprosthetic joint infection: prevalence, aetiology, evaluation, recommendations, and treatment. *Int Orthop*. 2020;44(7):1255-1261. [CrossRef]
5. Lenguerrand E, Whitehouse MR, Beswick AD, Kunutsor SK, Burston B, Porter M, Blom AW.Risk factors associated with revision for prosthetic joint infection after hip replacement: a prospective observational cohort study. *Lancet Infect Dis*. 2018;18(9):1004-1014. [CrossRef]
6. Tande AJ, Patel R. Prosthetic joint infection. *Clin Microbiol Rev*. 2014;27(2):302-345. [CrossRef]
7. Tkadlec J, Peckova M, Sramkova L, et al. The use of broad-range bacterial PCR in the diagnosis of infectious diseases: a prospective cohort study. *Clin Microbiol Infect*. 2019;25(6):747-752. [CrossRef]
8. Berneking L, Haas M, Frielinghaus L, et al. Evaluation of a syndromic panel polymerase chain reaction assay for the diagnosis of device-associated bone and joint infections. *Int J Infect Dis*. 2022;116:283-288. [CrossRef]
9. Berinson B, Spenke L, Krivec L, et al. Performance and hypothetical impact on joint infection management of the BioFire Joint Infection Panel: a retrospective analysis. *J Clin Microbiol*. 2023;61(8):e0059223. [CrossRef]
10. Gaillard T, Dupieux-Chabert C, Roux AL, et al. A prospective multicentre evaluation of BioFire Joint Infection Panel for the rapid microbiological documentation of acute arthritis. *Clin Microbiol Infect*. 2024;30(7):905-910. [CrossRef]
11. Pascual S, Noble B, Ahmad-Saeed N, et al. Potential value of a rapid syndromic multiplex PCR for the diagnosis of native and prosthetic joint infections: a real-world evidence study. *J Bone Jt Infect*. 2024;9(1):87-97. [CrossRef]
12. Lund-Andersen J, Petersen MLH, Kostadinov K, Friis-Hansen L, Calum H, Overgaard S. Clinical evaluation of a multiplex PCR-based test for joint infection: a prospective diagnostic accuracy study of forty-nine patients. *Eur J Orthop Surg Traumatol*. 2024;34(8):4105-4111. [CrossRef]
13. Hoffman T, Kriger O, Cohen S, Gefen-Halevi S, Yahav D, Amit S. Real-life experience and diagnostic utility of the BioFire Joint Infection PCR Panel in bone and joint infections: analysis of a prospective validation study. *Infect Dis Ther*. 2023;12(5):1437-1443. [CrossRef]
14. Berinson B, Tanida K, Spenke L, et al. Prospective evaluation of real-world performance and clinical impact of the BioFire FilmArray Joint Infection Panel. *Microbiol Spectr*. 2025;13(4):e0223924. [CrossRef]
15. Balada-Llasat JM, Stamas N, Vincent T, et al. Epidemiology and economic outcomes associated with timely versus delayed receipt of appropriate antibiotic therapy among US patients hospitalized for native septic arthritis: a retrospective cohort study. *Antibiotics* (Basel). 2022;11(12):1732. [CrossRef]
16. Gardete-Hartmann S, Mitterer JA, Sebastian S, et al. The role of BioFire Joint Infection Panel in diagnosing periprosthetic hip and knee joint infections in patients with unclear conventional microbiological results. *Bone Joint Res*. 2024;13(7):353-361. [CrossRef]

ABCResearch

Arch Basic Clin Res 2026;8(2):201-205
DOI: 10.4274/ABCR.2026.26404

Research Article

Gender-Based Variations and Bilateral Symmetry of the Distal Tibiofibular Syndesmosis: A 3D Computed Tomography Study

Oğuzhan Tanoğlu

Department of Orthopaedics and Traumatology, İzmir Democracy University Faculty of Medicine, İzmir, Türkiye

Cite this article as: Tanoğlu O. Gender-based variations and bilateral symmetry of the distal tibiofibular syndesmosis: a 3D computed tomography study. *Arch Basic Clin Res*. 2026;8(2):201-205.

ORCID IDs of the author: O.T. 0000-0001-8984-9008.

ABSTRACT

Objective: This study aimed to investigate the influence of gender and bilateral asymmetry on the complex anatomical features of the distal tibiofibular syndesmosis using computed tomography (CT)-generated 3D anatomical models in the Turkish population.

Methods: Bilateral non-weight-bearing CT scans of 80 adults (40 females, 40 males), totaling 160 ankles, were analyzed. 3D anatomical models of the tibia and fibula were created using Materialise Mimics. Key morphological parameters were measured, including incisura width, depth, angle, and version; anterior and posterior tibiofibular widths; and tibiofibular overlap.

Results: In the male group, all measured parameters in the right ankle and most in the left ankle were significantly higher than those in the female group. Specifically, incisura width, anterior tibiofibular width, posterior tibiofibular width, and incisura version were significantly higher in males. Despite these gender differences, intraclass correlation coefficient analysis demonstrated strong correlations between the right and left ankles across the majority of parameters in both gender groups, including incisura depth and incisura angle.

Conclusion: Although gender-based dimensional variations exist, there are no clinically significant differences between contralateral ankles within each gender group. The strong bilateral symmetry confirms that the contralateral ankle may serve as a reliable template for determining syndesmotic integrity or assessing intraoperative reduction quality.

Keywords: Tibiofibular syndesmosis, computed tomography, three-dimensional imaging, ankle fractures, bimalleolar fractures, trimalleolar fractures

INTRODUCTION

Malleolar fractures are common injuries with an incidence that has been increasing over the years.[1,2] Distal tibiofibular syndesmosis is an important and a complex structure to maintain the integrity of the ankle joint and the injuries of syndesmosis accompanying malleolar fractures are observed in approximately 20% of cases.[3,4] Accurate reduction and the stabilization of the syndesmosis is essential to obtain better functional outcomes and to avoid post-traumatic osteoarthritis of the ankle joint.[5,6] Therefore, understanding these complex anatomical features of the ankle joint is critical for preventing complications.

Morphological variations of different anatomical parts of the human body according to gender and race have been largely investigated in the literature.[3,6-9] The 3D anatomy of the distal tibiofibular joint is particularly important for detecting syndesmotic subluxation. The congruence of the ankle joint biomechanically affects the motion of the fibula within the tibial notch. Moreover, incongruence of the syndesmosis may cause post-traumatic osteoarthritis on long-term follow-up. Data obtained from these morphological studies have been used to develop new surgical methods and implant designs for orthopaedic interventions.

Corresponding author: Oğuzhan Tanoğlu, **E-mail:** drtanoglu@gmail.com

Received: January 27, 2026
Revision Requested: February 19, 2026
Accepted: February 26, 2026
Epub: May 22, 2026
Publication Date: July, 14, 2026

Radiological modalities are the primary means of detecting distal tibiofibular syndesmosis injuries. Computed tomography (CT) is a common modality that is widely available in many medical centers.[7,10] Although there are many 2D CT studies investigating the syndesmosis anatomy in the current literature, conventional 2D measurements often fail to capture the true rotational geometry of the incisura fibularis.[7-9,11,12] Consequently, studies utilizing 3D CT-based anatomical models to analyze syndesmosis morphology remain limited.[10,13]

The present study aimed to investigate the influence of gender and bilateral asymmetry on complex anatomical features of the distal tibiofibular syndesmosis using CT-generated 3D anatomical models in the Turkish population.

MATERIALS AND METHODS

Institutional review board approval was obtained from Ethics Committee of Ankara City Hospital with, decision no: EI/1309/2020, date: 11.11.2020. prior to the study CT angiography scans of the lower extremities in patients aged 18-60 years who were admitted to İzmir Democracy University Buca Seyfi Demirsoy Training and Research Hospital were reviewed in the medical records. Patients with incomplete CT images; prior surgeries for fractures or deformities of the tibia, fibula, or ankle joint; ankle osteoarthritis; a history of knee or ankle arthroplasty; or oncological interventions were excluded from the study. Data from the adults were anonymized using Mimics Medical 27.0 software (Materialise, Leuven, Belgium). Forty female and forty male adults were randomly selected from adults who met the inclusion criteria. The randomization was made with true random number generator program (www.random.org).

The total sample size was calculated a priori using G Power 3.1 (Dusseldorf University, Dusseldorf, Germany) to be at least 26 adults per group. Therefore, two gender groups were created, each comprising 40 adults. A total of 160 ankles (both right and left sides) were investigated. CT scans were performed on a Siemens SOMATOM Emotion (Siemens) (110 kV- 90 mAs, slice thickness 1.2 mm).

The tibia and fibula bones were segmented using the Advanced Segment option of the software Mimics Medical 27.0 (Materialise, Leuven, Belgium) to create 3D anatomical models. Thresholding limits were determined to be between 180 and 2150 Hounsfield Units to isolate bone tissue from other tissues. The tibia and fibula were segmented separately. The inner articular surface of the medial malleolus was marked, and a mortise plane was created with "Fit to Surface" option, as described previously by Tanoğlu et al.[6] The length of the tibia was measured between the center points of the knee and ankle joint lines. The borders of the proximal and distal 1/3 of the tibial shaft were determined. These borders were marked circumferentially, and two different spheres were created on them using the "Best-Fit to Surface" option. The entire tibial anatomical axis was created using the center points of these two spheres.[14] The ankle plane, perpendicular to the tibial anatomical axis, was created using the "Plane Normal to Curve" option and represents the intersection of the most superior articular surface of the ankle joint and the anatomical axis of the tibia. The ankle plane was aligned 10 millimeters superior to the most superior articular surface of the ankle joint along the Z-axis (Figure 1). At this level of the incisura, the most prominent anterior and posterior points of the tibia and fibula were marked. The positions of these points were adjusted using the "Closest Point" option relative to the ankle plane (Figure 2). Finally, the anterior and posterior points of the tibia were connected to measure the incisura width (IW). By the same method, the deepest point of the incisura was identified.

MAIN POINTS

- No clinically significant differences were observed between contralateral ankles within each gender group.
- Strong correlations in the majority of measurement parameters observed between bilateral ankles.
- The contralateral ankle may serve as a reliable template for determining syndesmotic integrity.

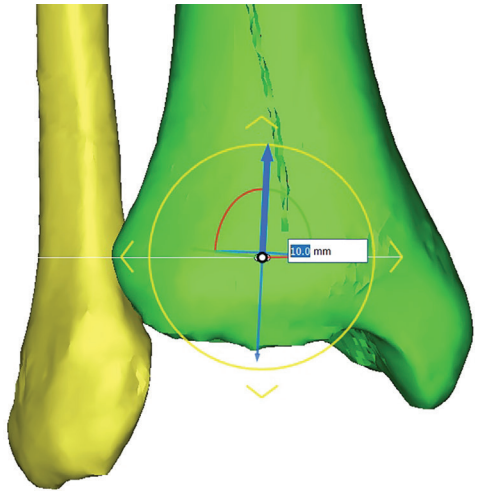

Figure 1. The ankle plane was aligned 10 millimeters superiorly from the most superior articular surface of ankle joint.

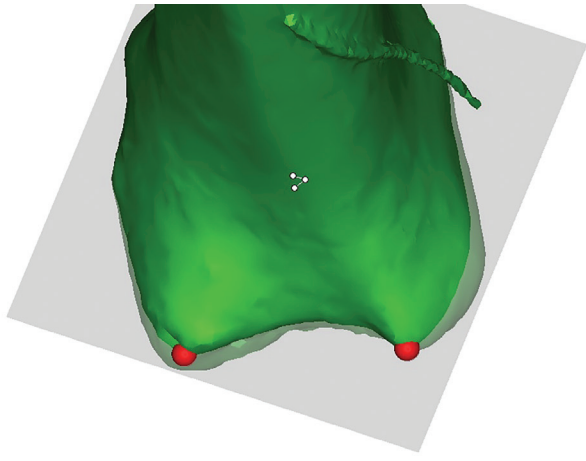

Figure 2. Marking of the most prominent anterior and posterior tibial points according to the ankle plane on 3D anatomical model.

The tibia and fibula were osteotomized using the "Cut" option according to the ankle plane. The cortical borders of distal parts of the tibia and fibula were marked separately to create splines. The center points of these splines were connected to create the ankle-version line. All anatomical data were transferred to 3-Matic 19 (Materialise, Leuven, Belgium). The depth of the incisura was measured between its deepest point and the anteroposterior tubercular line. The incisura angle (IA) was determined as the angle between the line drawn from the anterior point of the tibia to the deepest point of the notch and the line drawn from the deepest point of the notch to the posterior point of the tibia. The widths of the anterior and posterior points on the tibia and fibula were calculated. The angle between the ankle line and the anteroposterior tubercular line was measured to calculate the incisura version (IV). The tibia and fibula were positioned perpendicular to the mortise and ankle planes, and the tibiofibular overlap was measured using the program's ruler (Figure 3).

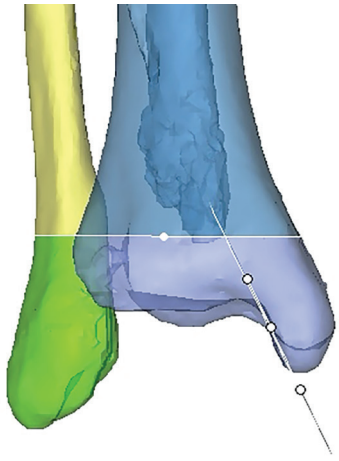

Figure 3. Determining the tibiofibular overlap according to the mortise plane on 3D anatomical model.

Statistical Analysis

Statistical analysis was performed with JASP 95.4 (University of Amsterdam, Amsterdam, Netherlands). The Shapiro-Wilk test indicated that the data were normally distributed. Therefore, the Student's t-test was used to compare data between gender groups. Reliability between right and left ankle measurements within gender groups was assessed using the intraclass correlation coefficient (ICC) analysis.

RESULTS

This study investigated bilateral ankle measurements in 80 adults, comprising 40 females (mean age: 42.8 ± 13.4 years) and 40 males (mean age: 42.5 ± 11.3 years). Descriptive statistics and comparisons of the right- and left-ankle measurements between gender groups are presented in Table 1.

All measurement parameters of the right ankle were higher in the male group than in the female group. Specifically, IW, anterior tibiofibular width (ATW), posterior tibiofibular width (PTW), and IV measurements were significantly higher in the right ankles of males than in those of females (Table 1).

Similarly, left-ankle measurements were higher in the male group, except for the mean ATW. Statistically significant gender differences were observed for IW, incisura depth (ID), and tibiofibular overlap (TO) in left ankle measurements.

The reliability of measurements between the right and left ankles within gender groups was evaluated using ICC analysis. In the male group, measurements revealed strong correlations between the bilateral ankles for IW, ID, IA, and TO (Table 2). In the female group, strong correlations were observed among ID, IA, ATW, PTW, IV, and TO (Table 3).

Table 1. Descriptives and the Comparisons of Right and Left Ankle Measurements Between Gender Groups

	Group	Right ankle Mean ± SD	*P*	Left ankle Mean ± SD	*P*
Incisura width	Female	17.8 ± 1.5	< 0.001*	17.8 ± 2	< 0.001*
	Male	22.8 ± 2.9		20.2 ± 2.7	
Incisura depth	Female	2.9 ± 1	0.051	2.8 ± 1	< 0.001*
	Male	3.4 ± 1.2		2.9 ± 1.1	
Incisura angle	Female	141.5 ± 11.9	0.256	141.5 ± 11	0.138
	Male	144.4 ± 10.2		145.1 ± 10.7	
Anterior tibiofibular width	Female	2.8 ± 0.9	< 0.001*	3 ± 1	0.576
	Male	3.4 ± 1		2.9 ± 1	
Posterior tibiofibular width	Female	2.8 ± 0.9	< 0.001*	2.9 ± 0.8	0.054
	Male	4.2 ± 1.5		3.3 ± 0.9	
Incisura version	Female	-7.1 ± 1.6	< 0.001*	-7.6 ± 5	0.054
	Male	-8.4 ± 1.6		-8.5 ± 4.7	
Tibiofibular overlap	Female	6.1 ± 4.7	0.931	7.3 ± 1.4	< 0.001*
	Male	6.2 ± 4.9		8.6 ± 1.6	

*Statistically significant.
SD: Standard deviation.

Table 2. Reliability Between Right and Left Ankle Measurements of Male Group Using the Interclass Correlation Coefficient (ICC) Analysis

	ICC	Confidence Interval
Incisura width	0.783	0.591-0.885
Incisura depth	0.808	0.636-0.898
Incisura angle	0.814	0.648-0.901
Anterior tibiofibular width	0.661	0.359-0.821
Posterior tibiofibular width	0.577	0.201-0.776
Incisura version	0.471	-0.004-0.72
Tibiofibular overlap	0.782	0.587-0.885

Table 3. Reliability Between Right and Left Ankle Measurements of Female Group using the Interclass Correlation Coefficient (ICC) Analysis

	ICC	Confidence Interval
Incisura weight	0.709	0.449-0.846
Incisura depth	0.793	0.608-0.890
Incisura angle	0.847	0.710-0.919
Anterior tibiofibular weight	0.799	0.620-0.894
Posterior tibiofibular weight	0.801	0.624-0.895
Incisura version	0.891	0.795-0.943
Tibiofibular overlap	0.797	0.617-0.893

DISCUSSION

The primary finding of this study is the strong bilateral correlation between syndesmotic measurements for both gender groups, as assessed with 3D anatomical models.

Gender-based comparisons of the right ankle revealed that all investigated parameters were significantly greater in the male group. Statistically significant differences were observed in IW, ATW, PTW, and IV. Similarly, left ankle measurements showed that all parameters, with the exception of ATW, were higher in the male group. Statistically significant differences in the left ankle were noted for IW, ID, and TO. Despite these statistical differences, the variations in mean values were minimal and likely lacked clinical importance.

ICC analysis of IW demonstrated a strong correlation (ICC=0.78) between the right and left ankles in the male group, whereas a moderate correlation (ICC=0.7) was observed in the female group. A study by Yüzügüldü et al.[12] reported mean 2D IW measurements across gender groups that were higher than those observed in the present study. Despite the common Turkish origin of the sample populations in both studies, this disparity may be attributable to the use of 3D measurement methods in this study. Furthermore, Huysse et al.[10] also reported mean 3D IW measurements that were elevated relative to the results of this study. This divergence may stem from underlying racial differences between Western and Eastern Caucasians.

The ICC analysis of bilateral ankles revealed a strong correlation (ICC=0.8) for ID in both gender groups. In a 2D CT study by Misir et al.,[8] incisura morphology was classified into three categories based on depth: Type C (> 4 mm), Type I (< 4 mm) and Type R (=4 mm).[8] Applying the criteria established by Misir et al.[8], the following were observed: the right ankles of 31 males (77%), the left ankles of 34 males (85%), and bilateral involvement in 35 females (87%). The discrepancies in incisura-type distribution between studies may result from the application of 2D measurement definitions to 3D anatomical models. Defining a novel 3D measurement method that incorporates both ID and angle could yield different results. Although mean ID measurements showed minimal differences between 2D and 3D studies, the clinical importance of these findings remains controversial.[7,8,10,12] Unlike 2D CT images, which can be affected by leg positioning, 3D modeling allows for the acquisition of accurate ankle positioning; thus, spatial positioning may contribute to these observed differences.[11,13] Huysse et al.[10] determined a threshold of 4 mm for ID in a 3D CT study comparing patients with high ankle sprains to a control group, noting that the control group exhibited deeper incisura compared to unstable patients. The control group in this study has a deeper incisura compared with patients with unstable high ankle sprain. The mean ID of the control group in their study was higher than the mean presented here, potentially due to racial variation or differences in measurement methodology.

Bilateral comparison revealed a strong correlation in both the male (ICC=0.80) and female (ICC=0.84) groups. In the 3D study by Huysse et al.[10], the mean IA in the control group was measured lower than the findings of the current study. Although similar methods were used to determine the ankle reference plane for the prominent anterior and posterior tibial points, different results were obtained in the study.

ICC analysis of bilateral ankles showed a moderate correlation (ICC=0.66) in the male group and a strong correlation (ICC= 0.79) in the female group. In a 3D study, Peiffer et al.[13] found no significant differences in ATW weight-bearing and non-weight-bearing CT scans of bilateral ankles, and their mean ATW measurements were similar to the results of this study. The means of ATW measurements in the gender groups were similar to our study results. Conversely, compared to the 3D results of Chen et al.[11], the mean ATW measurements in the present study were similar for the male group but higher for the female group.

ICC analysis indicated a moderate correlation (ICC=0.57) in the male group and a strong correlation (ICC=0.80) in the female group. While the 3D study by Chen et al.[11] reported approximate results, Peiffer et al.[13] reported higher mean PTW measurements using non-weight-bearing CT-based 3D models compared to the current findings. Additionally, 2D studies by Misir et al.[8] and Yüzügüldü et al.[12], both conducted on Turkish populations, reported higher mean PTW measurements. Additionally, 2D studies by Misir et al.[8] and Yüzügüldü et al.[12], both conducted in Turkish populations, reported higher mean PTW measurements. These differences may be attributable to racial characteristics or to the distinct measurement methods used in 2D CT, although they are likely of minimal clinical significance.

An ankle line was established linking the centers of the tibia and the fibula across the ankle plane. The IV was calculated as the angle between this ankle line and the anteroposterior

tubercular line. Most adults exhibited a retroverted incisura, present in 87% of right ankles and 90% of left ankles, with no statistically significant differences between right and left ankles. ICC analysis revealed a moderate correlation in the male group (ICC=0.47) and a strong correlation in the female group (ICC=0.89). To the best of the author's knowledge, this is the first study to evaluate IV using 3D anatomical models.

TO, a critical clinical parameter for evaluating syndesmosis injury, was measured with the tibia and fibula positioned perpendicular to the mortise and ankle planes. The mean TO results showed no significant difference for right ankles, but showed a statistically significant difference for left ankles (7.3 vs. 8.6 degrees) between gender groups. Nevertheless, the ICC analysis demonstrated strong correlations for TO in both gender groups. Higher mean TO results were obtained in the present study using the mortise plane, which may be attributable to the use of a 2D measurement method and a different reference axis in the study of Yüzügüldü et al.[12], despite both studies examining Turkish populations. This is the first, based on a review of current literature, to measure TO using 3D anatomical models.

Study Limitations

This study has certain limitations. First, the sample size, comprising the bilateral ankles of 80 adults, may appear limited; however, a post-hoc power analysis indicated 94% power. Second, while a single investigator performed the 3D analysis, reliance on automated computer-aided protocols ensured that measurement errors were minimized. Finally, this study utilized non-weight-bearing CT images. Different measurements may be obtained using weight-bearing CT imaging.

CONCLUSION

The results of this study corroborate the existing literature by demonstrating no clinically significant differences between contralateral ankles within gender groups. ICC analysis revealed strong correlations for the majority of measurement parameters between the bilateral ankles. Consequently, based on the 3D anatomical data, the contralateral ankle may serve as a reliable template for determining syndesmotic integrity or assessing intraoperative reduction quality.

Ethics

Ethics Committee Approval: Institutional review board approval was obtained from Ethics Committee of Ankara City Hospital with, decision no: EI/1309/2020, date: 11.11.2020.

Informed Consent: There is no need for informed consent due to the retrospective design of the study.

Footnotes

Funding: The author declare that this study has received no financial support.

Declaration of Interests: The author declare no conflict of interest regarding the publication of this paper.

REFERENCES

1. Tanoğlu O, Gökgöz MB, Özmeriç A, Alemdaroğlu KB. Two-stage surgery for the malleolar fracture-dislocation with severe soft tissue injuries does not affect the functional results. *J Foot Ankle Surg*. 2019;58(4):702-705. [CrossRef]
2. Lee KM, Chung CY, Kwon SS, et al. Ankle fractures have features of an osteoporotic fracture. *Osteoporos Int*. 2013;24(11):2819-2825. [CrossRef]
3. Yaradılmış YU, Polat Y, Uslu MB, Ateş A, Demirkale İ, Altay M. The evaluation of radiological measurements used in diagnosis and treatment of syndesmosis injury: a regional study in Turkey. *Jt Dis Relat Surg*. 2020;31(1):123-129. [CrossRef]
4. Egol KA, Pahk B, Walsh M, Tejwani NC, Davidovitch RI, Koval KJ. Outcome after unstable ankle fracture: effect of syndesmotic stabilization. *J Orthop Trauma*. 2010;24(1):7-11. [CrossRef]
5. Hunt KJ, Phisitkul P, Pirolo J, Amendola A. High ankle sprains and syndesmotic ınjuries in athletes. *J Am Acad Orthop Surg*. 2015;23(11):661-673. [CrossRef]
6. Tanoğlu O, Subaşı İÖ, Gökgöz MB. Determination of the optimal syndesmosis fixation angle using the mortise view of the ankle joint. *J Am Podiatr Med Assoc*. 2023;113(2):21-34. [CrossRef]
7. Tonogai I, Hamada D, Sairyo K. Morphology of the Incisura Fibularis at the Distal Tibiofibular Syndesmosis in the Japanese population. *J Foot Ankle Surg*. 2017;56(6):1147-1150. [CrossRef]
8. Misir A, Uzun E, Tokmak T. Morphology of the incisura fibularis in the Turkish population. *Ann Med Res*. 2021;28(3):464-470. [CrossRef]
9. Liu GT, Ryan E, Gustafson E, et al. Three-dimensional computed tomographic characterization of normal anatomic morphology and variations of the distal tibiofibular syndesmosis. *J Foot Ankle Surg*. 2018;57(6):1130-1136. Epub 2018 Sep 7. Erratum in: J *Foot Ankle Surg*. 2019;58(2):407. [CrossRef]
10. Huysse W, Burssens A, Peiffer M, et al. Morphometric analysis of the incisura fibularis in patients with unstable high ankle sprains. *Skeletal Radiol*. 2021;50(6):1141-1150. [CrossRef]
11. Chen Y, Qiang M, Zhang K, Li H, Dai H. A reliable radiographic measurement for evaluation of normal distal tibiofibular syndesmosis: a multi-detector computed tomography study in adults. *J Foot Ankle Res*. 2015;8:32. [CrossRef]
12. Yüzügüldü U, Ramazanlı L, Tüzün HY, et al. Tibiofibular relationships of the normal syndesmosis on axial computed tomography in the Turkish Population. *J Am Podiatr Med Assoc*. 2024;114(4):23-145. [CrossRef]
13. Peiffer M, Van Den Borre I, Segers T, et al. Implementing automated 3D measurements to quantify reference values and side-to-side differences in the ankle syndesmosis. *Sci Rep*. 2023;13(1):13774. [CrossRef]
14. Tanoğlu O, Subaşı İÖ, Gökgöz MB, Arıcan G. Is proximal tibia sufficient for accurate measurement of tibial slope angles on three-dimensional tomography-based anatomical models? *Curr Med Imaging*. 2021;17(12):1419-1424. [CrossRef]

ABCResearch

Arch Basic Clin Res 2026;8(2):206-211
DOI: 10.4274/ABCR.2026.26444

Research Article

Balancing Function and Cost: Kirschner Wire Fixation Versus Volar Plating in Intra-Articular Distal Radius Fractures

Eyüp Şenocak[1], Muhammet Çelik[1], İbrahim Dağ[1], Bilal Karabak[2], Kamber Kaşali[1]

[1]Department of Orthopaedics and Traumatology, Atatürk University Faculty of Medicine, Erzurum, Türkiye
[2]Clinic of Orthopaedics and Traumatology, Erzurum City Hospital, Erzurum, Türkiye

Cite this article as: Şenocak E, Çelik M, Dağ İ, Karabak B, Kaşali K. Balancing function and cost: Kirschner wire fixation versus volar plating in ıntra-articular distal radius fractures. *Arch Basic Clin Res.* 2026;8(2):206-211.

ORCID IDs of the authors: E.Ş., 0000-0002-9804-9309, M.Ç., 0009-0000-2751-0172, İ.D., 0009-0009-1184-4325, B.K., 0000-0003-3134-8731, K.K. 0000-0002-2851-5263.

ABSTRACT

Objective: To comparatively evaluate the clinical, functional, radiological, and cost related outcomes of Kirschner wire fixation versus volar locking plate osteosynthesis in the management of intra-articular distal radius fractures.

Methods: A retrospective comparative study was conducted in 133 patients who had Arbeitsgemeinschaft für Osteosynthesefragen/Orthopaedic Trauma Association type C distal radius fractures and who underwent surgical treatment between 2017 and 2023. Patients were allocated to two groups based on fixation technique: Kirschner wire fixation (n=67) and volar locking plate fixation (n=66). Functional outcomes were assessed using the disabilities of the arm, shoulder and hand (DASH) questionnaire and the Mayo Wrist Score at the 1st, 3rd, and 6th postoperative months. Additionally, Wrist range of motion, perioperative variables, and total treatment costs were analyzed. Longitudinal and intergroup comparisons were performed to determine temporal recovery patterns and treatment-related differences.

Results: Kirschner wire fixation was associated with significantly shorter operative duration, reduced intraoperative blood loss, shorter hospitalization, and substantially lower overall treatment cost compared with volar plating (all $P < 0.001$). Conversely, patients treated with volar plate osteosynthesis demonstrated significantly superior functional recovery and greater wrist range of motion during the early postoperative period ($P < 0.001$). Although both groups exhibited progressive and significant improvement over time ($P < 0.001$), intergroup differences diminished by the sixth postoperative month. Notably, DASH scores at 6 months indicated slightly better patient-reported outcomes, suggesting comparable mid-term patient-reported functional outcomes with the less invasive technique despite inferior early recovery.

Conclusion: Volar locking plate fixation provides enhanced early postoperative functional recovery and wrist mobility in intra-articular distal radius fractures. However, Kirschner wire fixation remains a cost-effective and surgically efficient alternative with comparable mid-term clinical outcomes. These findings support an individualized treatment strategy based on fracture characteristics, patient expectations, surgeon experience, and healthcare resource considerations.

Keywords: Distal radius fracture, Kirschner wire fixation, volar locking plate, ORIF, functional outcomes, cost-effectiveness analysis

Corresponding author: Eyüp Şenocak, **E-mail:** eyupsenocakmd@gmail.com

Received: May 21, 2026
Revision Requested: June 26, 2026 **Accepted:** June 29, 2026 **Publication Date:** July, 14, 2026

INTRODUCTION

Distal radius fractures (DRFs) are among the most common reasons for emergency department visits, accounting for approximately 1.5% of all such visits in the United States.[1] Furthermore, they constitute nearly 18% of orthopedic trauma admissions.[2] DRFs demonstrate a bimodal age distribution, with increasing incidence in two distinct age groups. Their frequency increases secondary to high-energy trauma among young males whereas in elderly women the incidence increases primarily due to osteoporosis.[3] As average life expectancy increases, the incidence of osteoporotic DRFs is expected to rise further.[4]

Current treatment strategies for DRFs encompass a wide range of modalities, including nonoperative management with closed reduction and casting and surgical options such as volar and dorsal plate-and-screw fixation, external fixation, and closed reduction with percutaneous Kirschner wire fixation.[5] The primary objective of all treatment methods is to restore fracture alignment and joint congruity, thereby enabling early mobilization and recovery of wrist function. Failure to achieve proper alignment may result in wrist osteoarthritis, restricted range of motion, and diminished grip strength.[6]

In this retrospective study, we aimed to comparatively evaluate the clinical, functional, radiological, and cost-related outcomes of Kirschner wire fixation versus volar locking plate osteosynthesis in the management of intra-articular DRFs.

MATERIALS and METHODS

This retrospective comparative study was approved by the Institutional Ethics Committee of Atatürk University Faculty of Medicine (decision no: B.30.2.ATA.0.01.00/292, date: 29.04.2026). Between January 2017 and January 2023, patients admitted to our clinic with a diagnosis of DRF were retrospectively reviewed. The study included patients who met the inclusion criteria and underwent either volar plate (VP)-and-screw fixation or Kirschner-wire fixation.

The inclusion criteria were as follows: patients with Arbeitsgemeinschaft für Osteosynthesefragen/Orthopaedic Trauma Association type C DRFs involving the articular surface; patients with closed fractures or Gustilo-Anderson type I open fractures; patients aged 18-80 years; and patients presenting within 10 days of injury.

MAIN POINTS

- Volar locking plate fixation provided superior early postoperative functional recovery and greater wrist range of motion compared with Kirschner wire fixation in intra-articular distal radius fractures.
- Despite the early functional advantages of volar plating, both fixation methods achieved comparable functional outcomes by the sixth postoperative month.
- Treatment selection for intra-articular distal radius fractures should be individualized by considering functional expectations, surgical burden, fracture characteristics, and healthcare resource utilization.

The exclusion criteria included patients with Gustilo-Anderson type II and III open fractures; those younger than 18 years or older than 80 years; those with pathological fractures; those with less than one year of follow-up; and those with a history of DRF.

A retrospective evaluation of the hospital automation system identified 247 patients who underwent surgery for DRFs. Of these, 32 patients with type A fractures were excluded. In addition, routine follow-up was considered inadequate in 33 patients treated with Kirschner wire fixation and 41 patients treated with plate-and-screw fixation. In the plate-and-screw fixation group, 5 patients required implant removal and revision to external fixation due to infection. In the Kirschner wire fixation group, fixation failure occurred in 3 patients, necessitating revision surgery with plate-and-screw fixation. Ultimately, 67 patients treated with Kirschner wire fixation and 66 patients treated with plate-and-screw osteosynthesis, all of whom met the inclusion criteria and had a minimum follow-up of one year, were included in the study.

According to patients' records, disabilities of the arm, shoulder and hand (DASH) scores obtained at postoperative months 1, 3, and 6, Mayo Wrist Scores, wrist flexion-extension range of motion, and forearm pronation-supination range of motion were evaluated and compared between the two surgical groups.

Fracture union time, operative duration, intraoperative blood loss, and length of hospital stay were assessed. A comprehensive cost analysis was performed using data obtained from the hospital billing and administrative records. The total treatment cost included implant costs, operating room costs, costs related to operative duration, hospitalization costs, perioperative medication costs, laboratory and radiological examination costs, postoperative follow-up costs, and costs associated with additional interventions when required. All costs were initially calculated in Turkish Lira (TRY) according to the hospital reimbursement system in effect during the study period and subsequently converted to U.S. Dollars (USD) using the official exchange rates for the period when the treatment was performed. The total treatment costs were then recorded and analyzed statistically.

Surgical Technique

All surgical procedures were performed under standard regional or general anesthesia by a surgical team with at least five years' operative experience, with the patient in the supine position on a radiolucent hand table and with C-arm fluoroscopic guidance.

In the Kirschner wire fixation group, following gentle reduction, percutaneous fixation was achieved under fluoroscopic guidance with two or three 2-mm Kirschner wires inserted in a crossed configuration from the distal radius toward the proximal radial shaft. Perioperative blood loss, operative time, and intraoperative complications were recorded during the procedure.

In the VP group, the affected extremity was approached through a longitudinal volar incision under pneumatic tourniquet control. After dissection through the tissue planes, the fracture site was exposed, while the radial artery and median nerve

were carefully protected. Fixation was subsequently performed using an anatomically contoured VP and an appropriate number of screws. Operative time, intraoperative blood loss, and perioperative complications were recorded during surgery.

Statistical Analysis

Statistical analyses were performed using IBM SPSS Statistics v20. Data were presented as mean and standard deviation, median (minimum-maximum), and as percentages and frequencies. The normality of continuous variables was assessed using the Shapiro-Wilk test.

For comparisons between two independent groups, the Independent samples t-test was used when the assumption of normality was met, and the Mann-Whitney U test when it was not. For comparisons of more than two dependent groups, Repeated Measures ANOVA was used when normality was met, and the Friedman test when it was not; post-hoc comparisons were performed using the Tukey test or Tamhane's T2 test according to the homogeneity of variances.

For categorical variables, the Pearson chi-square test, Yates' continuity correction chi-square test, Fisher's exact test, or the Fisher-Freeman-Halton test were used depending on expected frequencies. A P value < 0.05 was considered statistically significant.

RESULTS

A total of 133 patients were included in the study. Analysis of the age distribution demonstrated that the study population had a mean age of 41 ± 18 years, with a median age of 39 years (range: 17-77 years), indicating a broad age spectrum. In terms of sex distribution, males constituted the majority of the cohort (80.5%, n=107), while females represented 19.5% (n=26). This distribution is consistent with the known sex-related epidemiology of DRFs. Clinical variables were compared (Table 1).

Fracture union time, operative duration, blood loss, length of hospital stay, and costs differed significantly between the Kirschner wire (KIRSC) and open reduction and internal fixation (ORIF) groups (P < 0.001). No statistically significant difference was observed between the two groups with respect to age (Z = -1.045, P = 0.296).

In the intergroup comparison, a statistically significant difference favoring the KIRSC group was observed for the DASH score at postoperative month 6 (Z = -3.564, P < 0.001) and for the Mayo score at postoperative months 1 and 3 (Z = -9.882 and Z = -6.260, respectively; P < 0.001). However, no significant intergroup differences were found in DASH scores at postoperative months 1 and 3 or in the Mayo score at postoperative month 6.

Wrist flexion-extension values were consistently higher in the ORIF group across all follow-up periods, and these differences were statistically significant (P < 0.001). Forearm supination-pronation demonstrated a significant between-group difference only at postoperative month 1 (Z = -7.354, P < 0.001), whereas no significant intergroup differences were detected at postoperative months 3 and 6 (P > 0.05).

In the intragroup repeated-measures analysis, DASH and Mayo scores, wrist flexion-extension, and forearm supination-pronation values showed statistically significant changes across postoperative months 1, 3, and 6 in both groups (Friedman test, P < 0.001). Post-hoc analyses revealed statistically significant differences between all pairwise time periods. Table 2 compares demographic and clinical characteristics.

No statistically significant differences were observed between the KIRSC and ORIF groups with respect to sex, side involvement, hand dominance, mechanism of trauma, or associated injuries (P > 0.05). These findings indicate that the two groups had similar distributions of the evaluated demographic and clinical characteristics and were therefore comparable.

Functional scores and range of motion parameters improved significantly over time in both treatment groups (Friedman test, P < 0.001). Intergroup comparisons demonstrated significantly higher Mayo Wrist Scores at postoperative months 1 and 3 and greater wrist flexion-extension values at all follow-up periods in the ORIF group. In contrast, DASH scores at postoperative month 6 were significantly lower in the KIRSC group. No significant differences were observed between groups regarding forearm supination-pronation at postoperative months 3 and 6. Detailed results are presented in Figure 1 and Table 2.

Table 1. Comparison of the KIRSC and ORIF Groups According to Clinical Variables

	KIRSC		ORIF			
Variable	**Mean ± SD**	**Med (min-max)**	**Mean ± SD**	**Med (min-max)**	**Z**	***P***
Age (year)	42 ± 19	41 (17-77)	39 ± 18	35 (18-74)	-1.045	0.296
Union time (week)	6 ± 2	5 (4-11)	9 ± 2	9 (5-13)	- 7.019	**< 0.001**
Surgery duration (minute)	19 ± 8	16 (10-45)	56 ± 12	55 (35-80)	-9.701	**< 0.001**
Blood loss (mL)	8 ± 7	5 (5-50)	96 ± 27	90 (45-200)	-10.189	**< 0.001**
Hospitalisation time (day)	1 ± 1	1 (0-6)	3 ± 2	3 (1-7)	-8.387	**< 0.001**
Cost (USD)	221 ± 116	210 (100-720)	1321 ± 1206	1075 (600-10000)	-9.857	**< 0.001**

Table 2. Comparison of the KIRSC and ORIF Groups in Terms of Demographic and Clinical Characteristics

		KIRSC	ORIF		*P*
		n (%)	n (%)	Test ist.	
Sex	Male	54 (80.6%)	53 (80.3%)	0.002	0.966[a]
	Female	13 (19.4%)	13 (19.7%)		
Side	Right	45 (67.2%)	45 (68.2%)	0.016	0.900[a]
	Left	22 (32.8%)	21 (31.8%)		
Dominence	Right	62 (92.5%)	63 (95.5%)		0.718[b]
	Left	5 (7.5%)	3 (4.5%)		
Etiology	Simple fall	50 (74.6%)	44 (66.7%)	6.651	0.132[c]
	Out-of-vehicle traffic accident	7 (10.4%)	4 (6.1%)		
	Fall from height	2 (3.0%)	0 (0.0%)		
	Skiing accident	6 (9.0%)	12 (18.2%)		
	Motorcycle accident	2 (3.0%)	6 (9.1%)		
Concomitant injury	No concomitant injury	56 (83.6%)	56 (84.8%)	0.040	0.841[a]
	Presence of concomitant injury	11 (16.4%)	10 (15.2%)		

[a]chi-square test, [b]Fisher exact test, [c]Fisher freman halton test

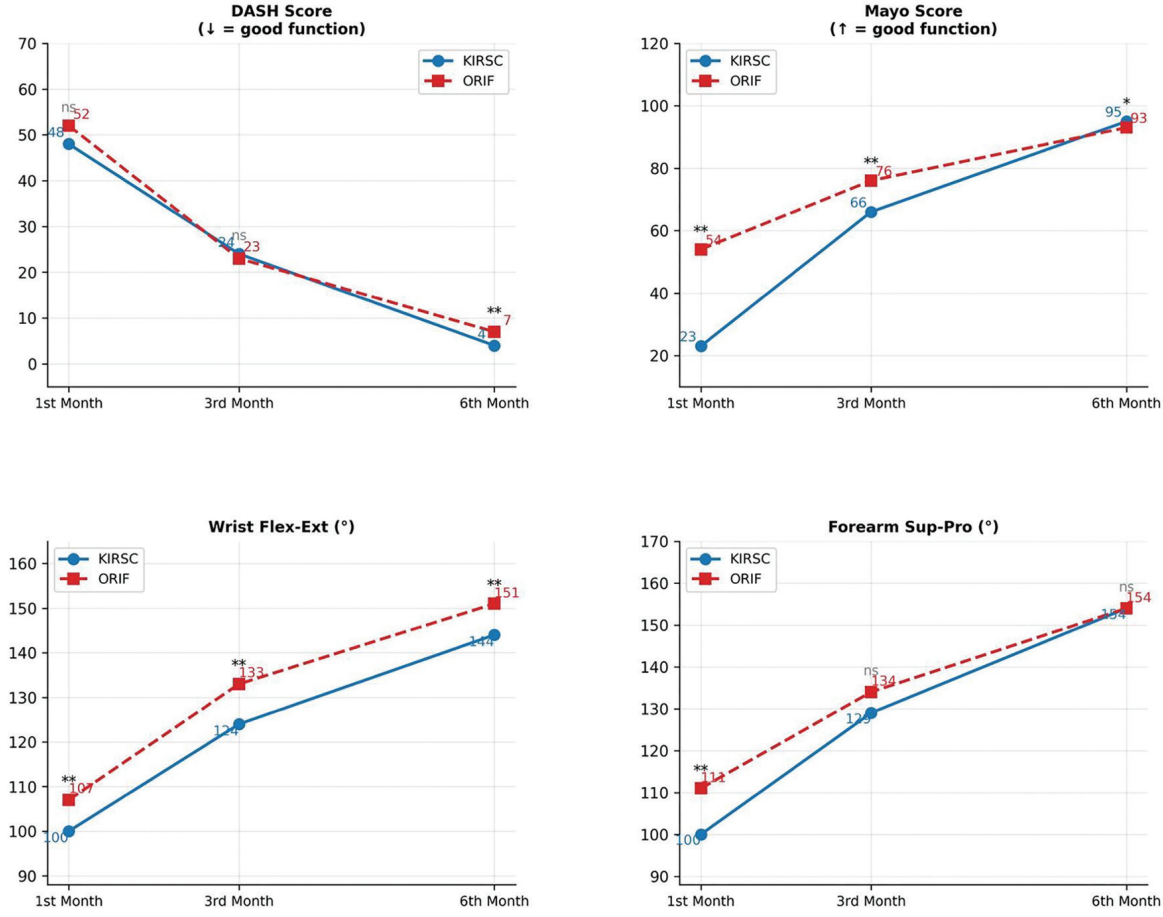

Figure 1. Changes in functional scores and range of motion over time. The lines represent median values at postoperative months 1, 3, and 6. Inter-period *P* values are indicated as follows: **$P < 0.001$, *$P < 0.05$, ns = not significant. Within-group changes in both groups were statistically significant according to the Friedman test ($P < 0.001$).

DISCUSSION

In the present study, we performed a comprehensive comparison of Kirschner wire fixation and VP osteosynthesis for intra-articular DRFs and demonstrated that, whereas volar plating provides superior early functional recovery and range of motion, Kirschner wire fixation offers significant advantages in operative efficiency and cost while achieving comparable mid-term functional outcomes.

DRFs represent a substantial proportion of orthopedic trauma, with a well-established bimodal distribution and increasing incidence due to aging populations and osteoporosis.[1-4] Despite advances in surgical techniques, the optimal treatment strategy for intra-articular fractures remains controversial, particularly regarding the balance between anatomical restoration and minimally invasive approaches.[5-7]

The significantly shorter operative time, reduced blood loss, and shorter hospitalization, observed in the Kirschner wire group in our study, are consistent with the minimally invasive nature of percutaneous fixation techniques. Ribeiro et al.[7] emphasized that less invasive methods may reduce perioperative morbidity, although functional superiority remains uncertain. Similarly, Wei et al.[8] reported that external fixation and less invasive approaches are associated with lower surgical burden compared to plate fixation. In contrast to some studies in the literature, Yılmaz found no clinical or radiological differences between VP fixation and EF fixation in the surgical treatment of intra-articular DRFs.[9]

In contrast, the superior early functional outcomes and greater wrist range of motion observed in the ORIF group can be attributed to the biomechanical stability provided by volar locking plates. Malisorn[10] highlighted the advantages of volar fixation in maintaining reduction and enabling early mobilization. Furthermore, Che Daud et al.,[11] in a multicenter prospective study, demonstrated that locking plate fixation provides stable construct integrity, facilitating early rehabilitation and improved early functional outcomes. Our findings are in strong agreement with these reports, particularly regarding early postoperative recovery.

A key finding of our study is that the early advantages of ORIF diminish over time, with both techniques yielding comparable functional outcomes at six months. This observation is consistent with the randomized trial by Wei et al.[11] and the meta-analysis by Margaliot et al.,[12] both of which reported no significant long-term functional superiority of plate fixation over alternative methods. Importantly, our finding that DASH scores favored the Kirschner group at mid-term follow-up supports the notion proposed by Samal et al.[13] that patient-reported outcomes may not directly correlate with radiological or biomechanical parameters.

From a biomechanical perspective, the persistent superiority of ORIF in wrist flexion-extension range of motion throughout the follow-up period may be explained by improved anatomical restoration and stable fixation, which allow for controlled early mobilization.[14] However, in our study the absence of long-term differences in forearm rotation suggests that rotational recovery is primarily dependent on fracture healing rather than fixation method.

A key strength and novel aspect of this study is the simultaneous and integrated evaluation of functional outcomes, range of motion parameters, and costs in patients with intra-articular DRFs treated with two commonly used fixation techniques. While previous studies have predominantly focused on either radiological or functional outcomes, cost-effectiveness has rarely been evaluated in conjunction with longitudinal functional recovery.[15] Our study provides a more comprehensive perspective by combining clinical efficacy and economic burden, which is particularly relevant for healthcare systems with constrained resources. Furthermore, the demonstration that mid-term functional outcomes converge despite the early biomechanical advantages of ORIF provides important evidence in the ongoing debate over optimal treatment selection.

The strengths of this study include a relatively large and homogeneous patient cohort, standardized follow-up intervals, and the simultaneous assessment of multiple clinically relevant outcome measures. Moreover, the comparable baseline characteristics between groups enhance the internal validity of the findings. However, several limitations should be acknowledged. First, the retrospective single-center design may limit the generalizability of our findings and introduce the potential for selection bias. Second, treatment allocation was based on surgeon preference and clinical judgment rather than on randomization, and this may have influenced the observed outcomes. Third, postoperative rehabilitation protocols were not fully standardized across patients, and variations in these protocols may have affected functional recovery. Fourth, radiological parameters were not comprehensively analyzed, limiting the ability to assess the correlation between anatomical and functional outcomes. Fifth, the absence of multivariate regression analysis precludes adjustment for potential confounders. Although all patients were followed for a minimum of one year, the relatively short follow-up period limits the assessment of long-term functional outcomes, late complications, and treatment durability.

In conclusion, both volar locking plate fixation and Kirschner wire fixation are effective treatment options for intra-articular DRFs. Volar locking plate fixation provides enhanced early postoperative functional recovery and improved wrist mobility, likely due to its superior biomechanical stability and facilitation of early mobilization. However, these advantages diminish over time, as Kirschner wire fixation demonstrates comparable mid-term clinical outcomes while offering significant benefits in terms of operative efficiency, reduced surgical burden, and cost-effectiveness. These findings support an individualized treatment strategy that considers not only fracture characteristics and patient expectations but also surgeon experience and healthcare resource utilization. Prospective, randomized, multicenter studies with standardized rehabilitation protocols and longer follow-up periods are warranted to further optimize treatment selection for intra-articular DRFs.

Ethics

Ethics Committee Approval: This retrospective comparative study was approved by the Institutional Ethics Committee of Atatürk University Faculty of Medicine (decision no.: B.30.2.ATA.0.01.00/292, date: 29.04.2026).

Informed Consent: Retrospective study.

Footnotes

Author Contributions

Concept Design – E.Ş., M.Ç.; Data Collection or Processing – E.Ş., M.Ç., İ.D., B.K., K.K.; Analysis or Interpretation – E.Ş., İ.D., B.K., K.K.; Literature Review – E.Ş., M.Ç.; Writing, Reviewing and üEditing – E.Ş., M.Ç., İ.D., B.K., K.K.

Declaration of Interests: The authors declared no conflicts of interest.

Funding: The authors declare that this study has received no financial support.

REFERENCES

1. Azad A, Kang HP, Alluri RK, Vakhshori V, Kay HF, Ghiassi A. Epidemiological and treatment trends of distal radius fractures across multiple age groups. *J Wrist Surg*. 2019;8(4):305-311. [CrossRef]
2. Court-Brown CM, Caesar B. Epidemiology of adult fractures: a review. *Injury*. 2006;37(8):691-697. [CrossRef]
3. Gencer B, Ender İbaç S, Teoman Yeni B, Sezer T, Doğan Ö. Surgical treatment of bilateral distal radius fractures: an analysis of epidemiological variables and outcome parameters. *Arch Basic Clin Res*. 2024;6(3):202-208. [CrossRef]
4. Sagerfors M, Jakobsson H, Thórdardóttir Á, Wretenberg P, Möller M. Distal radius fractures in the superelderly: an observational study of 8486 cases from the Swedish fracture register. *BMC Geriatr*. 2022;22(1):140. [CrossRef]
5. Koval KJ, Harrast JJ, Anglen JO, Weinstein JN. Fractures of the distal part of the radius. The evolution of practice over time. Where's the evidence? *J Bone Joint Surg Am*. 2008;90(9):1855-1861. [CrossRef]
6. Arora R, Gabl M, Gschwentner M, Deml C, Krappinger D, Lutz M. A comparative study of clinical and radiologic outcomes of unstable colles type distal radius fractures in patients older than 70 years: nonoperative treatment versus volar locking plating. *J Orthop Trauma*. 2009;23(4):237-242. [CrossRef]
7. Ribeiro E, Campanholi G, Acherboim M, Ruggiero GM. Mini-invasive surgery for distal radius fractures: a double incision under 12 mm. *J Wrist Surg*. 2021;10(2):136-143. [CrossRef]
8. Wei XM, Sun ZZ, Rui YJ, Song XJ, Jiang WM. Minimally invasive percutaneous plate osteosynthesis for distal radius fractures with long-segment metadiaphyseal comminution. *Orthop Traumatol Surg Res*. 2016;102(3):333-338. [CrossRef]
9. Yılmaz M. Comparison of the clinical and radiological results of volar locking plate and external fixation treatment of intra-articular fractures of the distal radius. *Arch Basic Clin Res*. 2023;5(3):378-385. [CrossRef]
10. Malisorn S. Functional outcomes and early complications following volar locking plate fixation of unstable distal radius fractures: a minimum two-year follow-up study. *Cureus*. 2026;18(2):e103133. [CrossRef]
11. Che Daud AZ, Mohd Nayan NA, Ahmad A, Alrashdi M, Kadar M, Mohd Poot EF. Distal radius fracture rehabilitation: a bibliometric and scoping review. *J Hand Ther*. 2026;39(1):120-132. [CrossRef] Epub 2025 Jul 4. Erratum in: *J Hand Ther*. 2025:S0894-1130(25)0019019-5. [CrossRef]
12. Margaliot Z, Haase SC, Kotsis SV, Kim HM, Chung KC. A meta-analysis of outcomes of external fixation versus plate osteosynthesis for unstable distal radius fractures. *J Hand Surg Am*. 2005;30(6):1185-11899. [CrossRef]
13. Samal BP, Pradhan S, Mohanty RR, Chatterjee G, Acharya T, Sahoo BS. Volar plate versus Kirschner-wire fixation in intra-articular fracture of distal radius. *J Pharm Bioallied Sci*. 2025;17(Suppl 3):S2320-S2322. [CrossRef]
14. Kong L, Li C, Bai J, Lu J. Surgical treatment of distal radius fractures: impact on forearm rotation in non-elderly patients. *Sci Rep*. 2024;14(1):2876. [CrossRef]
15. Kumar J, Rahul K, Niraj NK, Mane A, Navaneethan P, Pandey P. An economically feasible solution for distal radius fractures treated with column-specific fixation. *J Orthop Case Rep*. 2026;16(3):338-344. [CrossRef]

ABCResearch

Arch Basic Clin Res 2026;8(2):212-221
DOI: 10.4274/ABCR.2026.26417

Review

Pharmacological Modulation of Mitochondrial Dysfunction in Experimental Models of Hepatic Injury

Aslı Özbek Bilgin

Department of Pharmacology, Erzincan Binali Yıldırım University Faculty of Medicine, Erzincan Türkiye

Cite this article as: Özbek Bilgin A. Pharmacological modulation of mitochondrial dysfunction in experimental models of hepatic injury. *Arch Basic Clin Res*. 2026;8(2):212-221.

ORCID IDs of the authors: A.Ö.B. 0000-0001-9027-4299.

ABSTRACT

Mitochondrial dysfunction plays a central role in the pathogenesis of various liver diseases, ranging from drug-induced liver damage to steatotic liver disease associated with metabolic dysfunction. This review synthesizes recent advances in pharmacological strategies targeting mitochondrial quality control mechanisms. The shift from non-specific antioxidants to mitochondria-targeted agents is highlighted, as are the emerging roles of cardiolipin stabilizers (SS-31), next-generation cyclophilin inhibitors (Rencofilstat, C105SR), and modulation of immunometabolic pathways such as cGAS-STING and NLRP3. The transition of these promising experimental agents to clinical applications is also presented.

Keywords: Hepatic injury, mitochondria, mitochondrial dysfunction, mitochondrial permeability transition pore, pharmacological modulation

INTRODUCTION

Hepatic injury is a major global health problem contributing to acute liver failure, chronic liver disease, and liver-related mortality. Diverse insults, including drug toxicity, ischemia-reperfusion, alcohol, viral infections, and metabolic stress, disrupt hepatocellular homeostasis and promote progressive liver damage. Despite advances in supportive care and transplantation, effective pharmacological strategies targeting the core cellular mechanisms of hepatic injury remain limited.

In recent years, increasing evidence has identified mitochondrial dysfunction as a central and unifying event in both acute and chronic liver injury. Hepatocytes are highly dependent on mitochondrial oxidative phosphorylation (OXPHOS) to meet their substantial energy demands, rendering them particularly vulnerable to mitochondrial insults. Experimental models of hepatic injury consistently demonstrate that mitochondrial abnormalities, including excessive reactive oxygen species (ROS) production, impairment of the electron transport chain (ETC), loss of mitochondrial membrane potential ($\Delta\Psi m$), mitochondrial DNA (mtDNA) damage, and dysregulated mitochondrial quality control, precede and drive hepatocellular death.[1-5] Importantly, mitochondria are no longer regarded as passive victims of cellular stress but rather as active regulators of cell fate decisions, inflammation, and tissue repair. This conceptual shift has transformed the therapeutic paradigm from merely counteracting downstream oxidative injury to directly targeting mitochondrial signaling, permeability transition, biogenesis, and quality-control pathways.

Among the various pathogenic mechanisms, mitochondrial oxidative stress has emerged as a key trigger of hepatocellular injury.[6] Excessive generation of mitochondrial ROS and reactive nitrogen species (RNS) disrupts redox homeostasis, promotes lipid peroxidation, and impairs mitochondrial enzymes critical for energy production. These mitochondrial disturbances converge on oxidative stress, permeability transition, bioenergetic failure, and defective quality control, all of which contribute to hepatocyte death and impaired tissue recovery.

Experimental models such as CCl_4, TAA, APAP, methotrexate (MTX), and ischemia-reperfusion injury have been instrumental in defining how mitochondrial dysfunction initiates and amplifies hepatic damage and have enabled the evaluation of mitochondria-targeted pharmacological interventions.[7,8]

Corresponding author: Aslı Özbek Bilgin, **E-mail:** asli.bilgin@erzincan.edu.tr

Received: February 19, 2026
Revision Requested: March 27, 2026 **Accepted:** May 25, 2026 **Publication Date:** July, 14, 2026

In addition to acute mitochondrial injury, adaptive responses such as mitochondrial biogenesis and mitophagy have emerged as critical determinants of hepatocyte survival and recovery. Accordingly, this review examines mitochondrial dysfunction as a central pathogenic driver in experimental hepatic injury and discusses current pharmacological strategies targeting oxidative stress, modulators of the mitochondrial permeability transition pore (mPTP) regulation, mitochondrial biogenesis, mitophagy, and organelle crosstalk.

MATERIALS AND METHODS

This review was conducted in accordance with the Preferred Reporting Items for Systematic Reviews and Meta-Analyses guidelines. PubMed, Scopus, and Web of Science were searched for studies published between 2020 and 2025 using combinations of the terms "hepatic injury," "mitochondrial dysfunction," "oxidative stress," "mPTP," "mitophagy," and "experimental model." Titles and abstracts were screened for relevance, followed by full-text evaluation of potentially eligible articles. The primary focus was on peer-reviewed original experimental studies that used in vivo or in vitro models of hepatic injury and addressed mitochondrial pathways and their pharmacological modulation. To provide mechanistic context and clinical perspective, selected review articles and a limited number of foundational studies published before 2020 were also included, where directly relevant.

Molecular Mechanisms and Pharmacological Modulation of Mitochondrial Dysfunction in Hepatic Injury

An overview of mitochondria-targeted pharmacological agents and their mechanisms of action is presented in this chapter and summarized in Table 1.

Oxidative/Nitrosative Stress and Antioxidants-ROS Scavengers

Mitochondria, while essential for OXPHOS, are also a major intracellular source of ROS and RNS. Under physiological conditions, low levels of ROS are involved in redox signaling and cellular homeostasis. However, excessive ROS/RNS generation during hepatic injury leads to oxidative modification of lipids, proteins, and mtDNA, culminating in mitochondrial dysfunction and bioenergetic collapse.

MAIN POINTS

- Mitochondrial dysfunction is a key driver of hepatic injury across experimental models, integrating oxidative stress, energy failure, and cell death.
- Experimental evidence shows that mitochondria actively shape liver injury outcomes, rather than serving as passive targets of damage.
- Mitochondria-targeted pharmacological interventions provide mechanistic advantages over conventional antioxidant strategies in hepatoprotection.
- Restoring mitochondrial quality control and adaptive responses represents a promising translational approach to the treatment of liver injury.

Mitochondrial oxidative stress in hepatocytes is primarily driven by the activation of cytochrome P450 2E1, NADPH oxidase, and nitric oxide synthase isoforms, which together amplify the redox imbalance. ROS overproduction induces lipid peroxidation and membrane depolarization, while RNS, particularly peroxynitrite, promote tyrosine nitration and S-nitrosylation of mitochondrial proteins such as ATP synthase, aconitase, and complex I subunits. These post-translational modifications impair electron transfer efficiency, reduce adenosine triphosphate (ATP) production, and activate redox-sensitive signaling pathways, including NF-κB, JNK, and Nrf2.

In hepatic IR models, characterized by 60 min of ischemia followed by reperfusion of 120 min or longer, increased levels of 3-nitrotyrosine and 4-hydroxynonenal are consistently reported, accompanied by mitochondrial depolarization and enhanced expression of thioredoxin-1, indicating a compensatory redox response to nitrosative stress.[9] Similarly, in APAP-induced hepatotoxicity, typically produced by single oral doses ranging from 200 mg/kg to 3 g/kg, the generation of mitochondrial ROS and peroxynitrite triggers mtDNA fragmentation, ATP depletion, and mPTP opening. The ensuing collapse of the ΔΨm leads to the release of cytochrome c and the activation of caspase-dependent cell death cascades. Recent studies emphasize that nitro-oxidative stress is not merely a byproduct of hepatic injury but a primary initiator of mitochondrial dysfunction. Persistent oxidation of cardiolipin, an inner mitochondrial membrane phospholipid, disrupts the integrity of the ETC and sensitizes mitochondria to permeability transition. Moreover, chronic redox imbalance activates nuclear transcriptional responses mediated by p53, SIRT3, and proliferator-activated receptor gamma coactivator-1α (PGC-1α), which link mitochondrial stress to inflammation and apoptosis.[10]

Based on these mechanisms, pharmacological approaches that directly target mitochondrial oxidative stress have been explored to prevent or reverse hepatic injury. These include both conventional antioxidants (e.g., N-acetylcysteine) and mitochondria-targeted molecules such as MitoQ, SkQ1, and MitoTEMPO, which neutralize ROS within the mitochondrial matrix.

Conventional antioxidants, including N-acetylcysteine (NAC), vitamin E, and silymarin, have been shown to protect hepatocytes by replenishing glutathione (GSH) pools and neutralizing cytosolic ROS. However, their limited ability to penetrate mitochondria restricts their efficacy against mitochondrial oxidative damage. NAC remains the standard treatment for APAP-induced hepatotoxicity, but incomplete protection underscores the need for mitochondria-targeted strategies.

The development of mitochondria-targeted antioxidants represents a major advancement in the pharmacological management of oxidative stress–related liver injury. Unlike conventional antioxidants, which often fail to reach sufficient intramitochondrial concentrations, these agents are chemically engineered to accumulate specifically within the mitochondrial matrix using lipophilic cationic carriers, typically triphenylphosphonium (TPP^+). Because the mitochondrial inner

Table 1. Mitochondria-targeted pharmacological agents and their mechanisms of action

Agent/strategy	Main mitochondrial target	Mechanism of action	Outcomes
MitoQ	Mitochondrial ROS	TPP^+-mediated accumulation in mitochondria; scavenges mitochondrial ROS and prevents lipid peroxidation	Reduced oxidative stress, preserved ΔΨm, decreased hepatocyte necrosis
Mito-TEMPO	Mitochondrial superoxide	SOD mimetic nitroxide conjugated to TPP^+; selectively dismutates mitochondrial superoxide	Reduced mitochondrial ROS, improved ATP levels, attenuated liver injury
SS-31 (elamipretide)	Cardiolipin-ETC interaction	Stabilizes cardiolipin and ETC complexes, improves electron transfer efficiency	Preserved mitochondrial respiration, reduced necrosis
Cyclosporin A	Cyclophilin D/mPTP	Inhibits cyclophilin D, preventing sustained mPTP opening	Reduced mitochondrial swelling, decreased necrotic cell death
NIM811/alisporivir	Cyclophilin D/mPTP	Non-immunosuppressive inhibition of mPTP opening	Preserved ΔΨm, reduced oxidative stress
Metformin	AMPK pathway	Activates AMPK, enhances mitochondrial biogenesis and energy homeostasis	Improved mitochondrial biogenesis, reduced oxidative stress
Resveratrol	SIRT1-PGC-1α axis	Activates SIRT1, promotes mitochondrial biogenesis and antioxidant defense	Enhanced mitochondrial adaptation, hepatoprotection
Urolithin A	Mitophagy machinery	Induces mitophagy, improves mitochondrial quality control	Reduced accumulation of dysfunctional mitochondria
Spermidine	Autophagy/mitophagy pathways	Enhances autophagic flux and mitochondrial turnover	Improved mitochondrial quality, reduced injury
YAQ-005 (TAK-242)	TLR4-mitochondrial necroptosis axis	Inhibits TLR4 signaling, reduces RIPK1/RIPK3-mediated mitochondrial damage and hyperammonemia	Preserved mitochondrial integrity, reduced cell death
Mitochondrial transplantation	Mitochondrial bioenergetics	Delivery of functional mitochondria to injured liver tissue	Increased ATP production, reduced necrosis
Nanoparticle-based delivery systems	Mitochondrial matrix	Targeted delivery of drugs via biomimetic or TPP^+-modified nanoparticles	Enhanced mitochondrial targeting, reduced off-target toxicity

TPP^+: Triphenylphosphonium, ΔΨm: Mitochondrial membrane potential, ATP: Adenosine triphosphate, ETC: Electron transport chain, mPTP: Mitochondrial permeability transition pore, AMPK: Adenosine monophosphate-activated protein kinase, SIRT1: Sirtuin 1.

membrane is highly negatively charged, the positively charged TPP^+ fragment drives these molecules into mitochondria via electrophoretic accumulation, reaching concentrations up to 1000-fold higher in mitochondria than in the cytosol.

MitoQ is obtained by conjugating ubiquinone (the active part of Coenzyme Q10), an endogenous antioxidant, with TPP^+, a lipophilic cation. Thanks to its TPP^+ charge, it is attracted to the negative membrane potential and accumulates in the mitochondrial matrix at concentrations hundreds of times higher than in the cytosol.[11] MitoQ is reduced to ubiquinol by the ETC complex II and detoxifies lipid peroxyl radicals and peroxynitrite. In studies, MitoQ has generally been administered at 10 mg/kg by oral or intraperitoneal routes and is the most extensively studied mitochondria-targeted antioxidant in hepatic models. Experimental studies of CCl_4, TAA-, and APAP-induced hepatotoxicity have shown that MitoQ reduces lipid peroxidation, restores ATP production, and inhibits mPTP opening, thereby attenuating hepatocellular necrosis.[12]

In APAP hepatotoxicity, MitoQ inhibits JNK activation and subsequent activation of mPTP by scavenging mitochondrial ROS. A key finding is that MitoQ prevents necrosis despite not preventing GSH depletion; this suggests that the main driver of damage is mitochondrial redox collapse rather than GSH deficiency. However, MitoQ has a narrow therapeutic window, as it can suppress respiration at high doses and can exhibit a "pro-oxidant" effect.[13]

In CCl_4-induced fibrosis models, MitoQ has been shown to suppress pro-fibrotic TGF-β /smad signaling and reduce hepatic stellate cell activation. It also enhances mitophagy (the clearance of damaged mitochondria) by stabilizing the PINK1/Parkin pathway, thereby inhibiting NLRP3 activation.[14] In high-fat diet (HFD) models, MitoQ reduces hepatic steatosis and insulin resistance. Mechanistically, it increases fatty acid oxidation while and alleviates ER stress associated with lipotoxicity.[13] In a Phase II study (NCT00433108) in patients with chronic hepatitis C, MitoQ was shown to reduce alanin aminotransferaz levels (indicating a reduction in necrosis) but not to alter viral load. Ongoing research is exploring its potential to improve endothelial function in metabolic dysfunction-associated steatohepatitis (MASH) and in diabetic liver damage.

Mito-TEMPO, a mitochondria-targeted antioxidant, is a hybrid molecule composed of two functional moieties. TEMPO, a piperidine nitroxide that acts as a superoxide dismutase mimetic, and TPP^+, a lipophilic cation that enables selective accumulation within mitochondria driven by the negative ΔΨm, are two compounds. TEMPO catalyzes the dismutation of superoxide anions (O_2-) into less reactive species, thereby limiting mitochondrial oxidative stress. Conjugation with TPP^+ allows Mito-TEMPO to accumulate in the mitochondrial

matrix to concentrations several hundred-fold higher than in the cytosol, making it markedly more effective than non-targeted antioxidants at scavenging mitochondrial superoxide. Mito-TEMPO has demonstrated protective effects in multiple experimental models characterized by mitochondrial oxidative stress, including endotoxin-induced liver injury**,** sepsis-associated acute kidney injury**,** hypertension**,** and experimental colitis. These studies consistently show reductions in mitochondrial ROS production, preservation of ΔΨm, and attenuation of tissue injury. Mito-TEMPO has been evaluated as a potential hepatoprotective agent in APAP overdose models. Experimental findings indicate that Mito-TEMPO alleviates mitochondrial oxidative stress and dysfunction, thereby limiting liver injury. Its therapeutic efficacy has also been compared with NAC, highlighting the potential of mitochondria-targeted antioxidants as complementary or alternative strategies.[15] The evidence supporting hepatoprotection remains preclinical, and further standardized dose–response studies are required to define its translational relevance.

SkQ1 (visomitin) is a TPP^+ derivative of plastoquinone that effectively modulates ROS production in mitochondria (particularly during reverse electron transport at Complex I). Adding SkQ1 to the cold storage solutions used for the organ during liver transplantation has been shown to minimize damage during reperfusion. SkQ1 improves sinusoidal microcirculation by protecting endothelial cells and preserves ATP stores in hepatocytes. In hemorrhagic shock models, SkQ1 prevents the release of mtDNA from the liver into the systemic circulation, thereby preventing the spread of liver damage to distant organs, such as the lungs and kidneys.[16] SkQ1 (visomitin) preserves the ΔΨm and limits cytochrome c release during hepatic IR injury.[17]

The mitochondria-targeted peptide SS-31 (elamipretide) binds to cardiolipin, stabilizes the inner mitochondrial membrane, and reduces ROS generation and fibrotic activation in CCl_4-induced fibrosis. SS-31 is a potent agent that may treat liver fibrosis by blocking mitochondrial ROS and suppressing the NLRP3 pathway.[18]

Loss of ΔΨm and Modulators of the mPTP Opening

As discussed in the oxidative stress section, mitochondrial ROS generation and calcium overload are major upstream triggers of mPTP opening. The ΔΨm is a critical electrochemical gradient that drives ATP synthesis and maintains ion homeostasis. Loss of ΔΨm typically results from oxidative damage to mitochondrial membranes, calcium overload, and the opening of the mPTP. The mPTP is a multiprotein complex composed primarily of ANT, the voltage-dependent anion channel, and cyclophilin D (CypD). Under oxidative or calcium overload conditions, conformational changes in these proteins trigger pore opening, leading to ΔΨm dissipation and cytochrome c release.[3] Under physiological conditions, transient pore flickering may serve adaptive roles; however, sustained mPTP opening results in irreversible mitochondrial dysfunction characterized by loss of ΔΨm, cessation of ATP synthesis, osmotic swelling of the mitochondrial matrix, and rupture of the outer mitochondrial membrane, ultimately leading to necrotic cell death.

In CCl_4-induced acute liver injury, reactive trichloromethyl radicals (CCl_3) are formed that attack cardiolipin, a phospholipid essential for maintaining ΔΨm. Six-12 hours after dosing, mitochondria display significant depolarization, decreased ATP levels, and increased expression of CypD and Bax, indicating mPTP-mediated apoptotic priming.[19]

In APAP-induced hepatotoxicity, overdoses (250-500 mg/kg) cause formation of mitochondrial protein adducts, oxidative and nitrosative stress, and opening of the mitochondrial mPTP, leading to ATP depletion and necrosis.[20]

IR injury represents another prototypical model in which ΔΨm collapse plays a central role. During the reperfusion phase, a burst of ROS at Complex I sites triggers mPTP opening via CypD activation. Hepatocytes display massive mitochondrial swelling, loss of cristae, and rapid ATP depletion within 30 minutes of reperfusion onset.[21]

Chronic models, such as TAA-induced fibrosis (200 mg/kg i.p., three times weekly for 8-12 weeks), also exhibit a progressive reduction in ΔΨm, albeit in a slower, cumulative fashion. Long-term oxidative stress and depletion of cardiolipin result in sustained low-grade mPTP opening, driving hepatocyte apoptosis and fibrogenic signaling through TGF-β/Smad.[22] Similarly, during chronic CCl_4 exposure (0.5 mL/kg i.p., twice weekly for 6–8 weeks), prolonged mPTP activation leads to mitochondrial fragmentation and impaired autophagic clearance of damaged organelles, resulting in persistent hepatocyte injury.[23]

Among the regulatory components of the mPTP, CypD is the best-characterized and most widely accepted molecular modulator. Genetic ablation of CypD or its pharmacological inhibition has been shown to confer significant protection against mitochondrial dysfunction and hepatocellular necrosis in experimental liver injury models. Advances in this field have been accelerated by the discovery of new-generation, non-immunosuppressive cyclophilin inhibitors (targeting CypD, A, and B, known as "pan-cyclophilin" inhibitors).

Cyclosporin A (CsA) is the prototypical mPTP inhibitor that binds to CypD and prevents pore opening. Experimental studies have demonstrated that CsA attenuates mitochondrial swelling, preserves ΔΨm, and reduces hepatocellular necrosis in hepatic IR and APAP-induced liver injury models. However, its clinical use is limited by calcineurin inhibition mediated by cytosolic cyclophilin A (CypA) and by immunosuppressive effects that increase the risk of infection.[24] To circumvent these limitations, non-immunosuppressive CypD inhibitors have been developed.

Alisporivir (Debio-025) is a clinically advanced non-immunosuppressive cyclophilin inhibitor. It has been shown to prevent mPTP activation and cell death by inhibiting CypD, and to inhibit Hepatitis C virus replication by inhibiting CypA (an antiviral effect). Recent studies report that Alisporivir reduces mitochondrial fission (Drp1-mediated) and stabilizes mitochondrial fusion (Mfn2-mediated) in diabetic conditions and metabolic liver damage.[25]

Although the majority of evidence regarding CypD inhibition originates from hepatic models, supportive data from

extrahepatic tissues further underscore the central role of mPTP modulation under metabolic stress. In a HFD/streptozotocin-induced diabetes model, alisporivir (Debio-025) significantly alleviated mitochondrial dysfunction in skeletal muscle by preserving ΔΨm, restoring OXPHOS, and reducing mitochondrial ROS production.[25] These findings demonstrate that CypD-dependent mPTP opening represents a common pathogenic mechanism across metabolically active tissues. Given the shared susceptibility of hepatocytes to oxidative stress and mitochondrial calcium overload, inhibition of CypD by alisporivir may represent a translationally relevant strategy for mitigating mitochondrial dysfunction in liver injury, particularly in metabolic and IR contexts.

Rencofilstat is a macrocyclic pan-cyclophilin inhibitor with activity against CypD, A, and B, thereby linking mitochondrial protection to anti-inflammatory and antifibrotic effects. CypD inhibition prevents mitochondrial swelling and necrotic cell death (hepatoprotection); CypA inhibition suppresses inflammatory signaling. CypB, located in the ER, is a chaperone (a prolyl isomerase) necessary for collagen synthesis. Rencofilstat inhibits CypB, thereby disrupting the correct folding and secretion of procollagen. This not only prevents cell death but also directly halts fibrotic scar formation.[26] It has been investigated in preclinical liver fibrosis and NASH-related models, and clinical evaluations in Phase IIa and IIb (AMBITION, ALTITUDE) studies have also been reported in patients with F2/F3 NASH.[27] While these findings suggest that rencofilstat is a promising candidate for liver diseases, it is not yet an established mitochondria-targeted therapy.

Similarly**,** Sanglifehrin A, another CypD ligand, stabilizes mitochondrial integrity and limits necrotic hepatocyte death by preventing prolonged mPTP opening. Sanglifehrin A is a cyclophilin inhibitor that is structurally distinct from CsA. Its derivative, NV556, is particularly effective in liver fibrosis models.[28] Its mechanism of action, similar to that of rencofilstat, focuses on reducing collagen cross-linking and secretion via inhibition of CypB.[29]

The newly identified C105SR is smaller than large macrocyclic structures (CsA, alisporivir). It exhibits nanomolar-level affinity by binding to both the catalytic pocket (S1) and the "gatekeeper" pocket (S2) of

CypD. It has been reported to reduce liver necrosis and apoptosis more effectively than other inhibitors when administered via osmotic pump in mouse ischemia-reperfusion models.[24]

Modulators of Mitochondrial Biogenesis and Energy-Sensing Pathways (AMPK–SIRT–PGC-1α)

Beyond acute oxidative and permeability-related injury, hepatocytes activate adaptive pathways aimed at restoring mitochondrial mass and function. Mitochondrial ETC complexes (I-V) are responsible for the transfer of electrons from NADH and $FADH_2$ to molecular oxygen, generating ATP through OXPHOS. Under physiological conditions, this process is tightly regulated to ensure efficient ATP production and minimal ROS leakage. However, in hepatocellular injury, disruption of ETC activity is a key mechanism contributing to mitochondrial dysfunction and cellular energy failure. Experimental and clinical studies consistently demonstrate that hepatic toxins such as CCl_4, TAA, and APAP inhibit ETC activity, particularly at complex I (NADH: ubiquinone oxidoreductase) and complex III (cytochrome bc_1 complex). This inhibition results in excessive electron leakage and O_2- formation, leading to secondary oxidative stress and lipid peroxidation of mitochondrial membranes.

In CCl_4-induced hepatotoxicity, reactive CCl_3 and trichloromethyl peroxy radicals directly attack mitochondrial membranes and ETC proteins. Within 24 hours of exposure to a single intraperitoneal dose (1-1.5 mL/kg, 1:1 in olive oil), the activities of complexes I and III are markedly reduced, whereas the activity of complex II remains partially preserved. This imbalance increases superoxide release and diminishes the respiratory control ratio, reflecting uncoupling between electron transport and ATP synthesis.[19] In the TAA-induced chronic fibrosis model, mitochondrial respiration is progressively impaired by thioacetamide S-oxide and its reactive intermediates. Animals receiving TAA (200 mg/kg, i.p., three times per week for 8-12 weeks) show a significant reduction in the enzymatic activities of complexes I-III, coupled with a 50-60% decline in the ATP/ADP ratio. The ensuing redox imbalance triggers the accumulation of NADH and reduced coenzyme Q and the subsequent production of ROS at the Q_0 site of complex III. This defective electron transfer promotes hepatocyte apoptosis and the progression of fibrosis.[22]

Similarly, APAP-induced hepatotoxicity, resulting from single oral doses ranging from 200 mg/kg to 3 g/kg, causes accumulation of N-acetyl-p-benzoquinone imine (NAPQI), which binds to mitochondrial proteins, particularly complexes I and IV. This adduct formation interferes with electron flow, resulting in ATP depletion, membrane depolarization, and mitochondrial swelling. A reduced oxygen consumption rate and an elevated NADH/NAD^+ ratio indicate a shift from oxidative to anaerobic metabolism, which is characteristic of mitochondrial bioenergetic collapse. In the MTX-induced hepatotoxicity model, a single intraperitoneal dose of 20 mg/kg MTX results in transcriptional repression of mtDNA-encoded subunits such as ND1, ND6, and COX1, which encode essential components of complexes I and IV. This downregulation correlates with decreases in the oxygen consumption rate and ATP generation, and is accompanied by upregulation of apoptotic markers (Bax, cytochrome c).[30]

In hepatic IR injury**,** transient oxygen deprivation followed by reperfusion results in reverse electron transport at complex I, driven by succinate oxidation. This generates a burst of superoxide at the flavin mononucleotide site, causing damage to complex I, opening of the mPTP, and subsequent ATP depletion.[31]

mtDNA encodes 13 essential subunits of the ETC and components of the OXPHOS machinery. Owing to its close proximity to the inner mitochondrial membrane and the absence of protective histones, mtDNA is highly vulnerable to oxidative and nitrosative damage. In hepatic injury, sustained exposure to ROS/RNS leads to oxidative base modifications (particularly 8-hydroxy-2′-deoxyguanosine, 8-OHdG), strand breaks, and deletions, compromising ETC integrity and mitochondrial gene expression.[19]

In APAP-induced acute hepatotoxicity, single oral doses (300-500 mg/kg) induce mtDNA adduct formation due to NAPQI binding to mitochondrial proteins and nucleic acids. APAP-induced hepatotoxicity results in extensive mtDNA oxidation and fragmentation. This leads to decreased transcription of key OXPHOS genes such as ND1, ND6, and COX1, impairing the activities of complexes I and IV and exacerbating ATP depletion. These events have been confirmed in experimental contexts.[1] Simultaneously, depletion of mitochondrial transcription factor A (TFAM) and POLG (DNA polymerase gamma) limits mtDNA repair, leading to further bioenergetic failure.

TAA-induced fibrosis (200 mg/kg, i.p., 8-12 weeks) and chronic CCl_4 exposure (0.5 mL/kg, twice weekly, 6-8 weeks) lead to cumulative mtDNA damage and repression of biogenic transcriptional regulators. Persistent oxidative stress reduces PGC-1α, SIRT3, and NRF1 levels, impairing mitochondrial replication and turnover. This sustained biogenic failure is associated with increased collagen deposition and hepatocyte apoptosis.[22,23]

In hepatic IR injury, mtDNA degradation occurs rapidly after reperfusion due to enhanced oxidative stress and mitochondrial permeability transition. The cytosolic release of mtDNA activates the cGAS-STING-TBK1-IRF3 signaling cascade, promoting pro-inflammatory cytokine production and amplifying hepatocellular injury.[32]

Hepatocytes require adaptive responses to restore mitochondrial mass and function under toxic, metabolic, and ischemic stress. Central to these adaptive processes is the AMPK-SIRT-PGC-1α signaling axis, which coordinates cellular energy status with mitochondrial biogenesis and oxidative metabolism.[8] AMP-activated protein kinase (AMPK) is the primary cellular energy sensor activated by increases in the AMP/ATP ratio during mitochondrial dysfunction, ischemia, and toxic liver injury. When the ATP/AMP ratio decreases, it is activated and triggers energy-producing pathways. Downstream of AMPK, sirtuins, particularly sirtuin 1 (SIRT1) and SIRT3, play critical roles in regulating mitochondrial function through NAD^+-dependent deacetylation. SIRT1 activates peroxisome PGC-1α, the master transcriptional regulator of mitochondrial biogenesis. Activation of the AMPK–SIRT1–PGC-1α axis enhances transcription of nuclear-encoded mitochondrial genes, improves OXPHOS efficiency, and strengthens antioxidant defenses in hepatocytes.[8]

AMPK Activators

Metformin is the most commonly used antidiabetic drug. It activates AMPK in the liver, increasing insulin sensitivity and reducing fat accumulation (steatosis). In mouse models, 4 weeks of metformin treatment has been shown to improve liver function by restoring contact points between mitochondria and the endoplasmic reticulum (ER).[33]

Berberine is a naturally occurring isoquinoline alkaloid. In experimental models, it promotes fatty acid oxidation by increasing activation of peroxisome PGC-1α. It has also been shown to regulate liver microfibers and to alleviate fibrosis by acting through the gut flora.[34]

SIRT1 and PGC-1α Modulators

SIRT1 is an NAD+-dependent deacetylase that activates PGC-1α, the main regulator of mitochondrial biogenesis.

Resveratrol is a potent SIRT1 activator. It reduces oxidative stress in liver damage models while stimulating mitochondrial biogenesis via PGC-1α.[35]

In APAP-induced liver damage models, MI administration has been shown to significantly increase expression of SIRT1, PGC-1beta, NRF-1, and TFAM, promoting biogenesis and preventing hepatocyte necrosis.[36]

Formoterol is a beta2-adrenergic agonist. In mouse models of liver resection and sepsis, PGC-1α levels have been observed to increase mitochondrial ATP production capacity and to accelerate liver regeneration.[37]

Other Compounds Affecting Energy Pathways

Resmetirom (THR-beta agonist) stimulates thyroid hormone receptor-beta in a liver-specific manner. It reduces liver steatosis and inflammation by directly increasing mitochondrial fatty acid beta-oxidation. While Phase 3 clinical trials, such as MAESTRO-NASH, have shown clinically significant benefit in steatotic liver disease,[38] this review primarily evaluates it within the context of mitochondrial metabolic modulation; further research is still needed to consider it a widely accepted hepatoprotective treatment in all experimental liver damage models.

Astaxanthin coordinates the Nrf2–PGC-1α axis in stressed cells, increasing both antioxidant defense and mitochondrial content.[39]

Quercetin has been shown in animal models to alleviate HFD-induced liver damage by enhancing PINK1/Parkin-dependent mitophagy.[40]

Modulators of Mitophagy and Mitochondrial Quality Control

In addition to antioxidant defense and mPTP modulation, mitochondrial quality control through mitophagy is a major determinant of hepatocyte survival. Mitophagy, a specialized form of autophagy, is a key mitochondrial quality control mechanism that eliminates damaged or dysfunctional mitochondria to preserve cellular homeostasis. In hepatocytes, this process plays a critical role in limiting oxidative stress, preventing excessive inflammation, and maintaining ATP production (Figure 1). The mitophagy pathway is mainly regulated by the PINK1/Parkin, BNIP3/NIX, and FUNDC1 signaling axes, which target depolarized mitochondria for lysosomal degradation.[2] Under physiological conditions, PINK1 is rapidly degraded in healthy mitochondria. However, loss of ΔΨm leads to PINK1 stabilization on the outer mitochondrial membrane, recruitment of the E3 ubiquitin ligase Parkin, and ubiquitination of mitochondrial proteins, thereby initiating mitophagic clearance. Experimental studies in drug-induced and ischemic liver injury models have demonstrated that activation of the PINK1/Parkin pathway limits mitochondrial ROS accumulation, preserves ATP production, and attenuates hepatocellular injury. In contrast, defective or excessive mitophagy may become

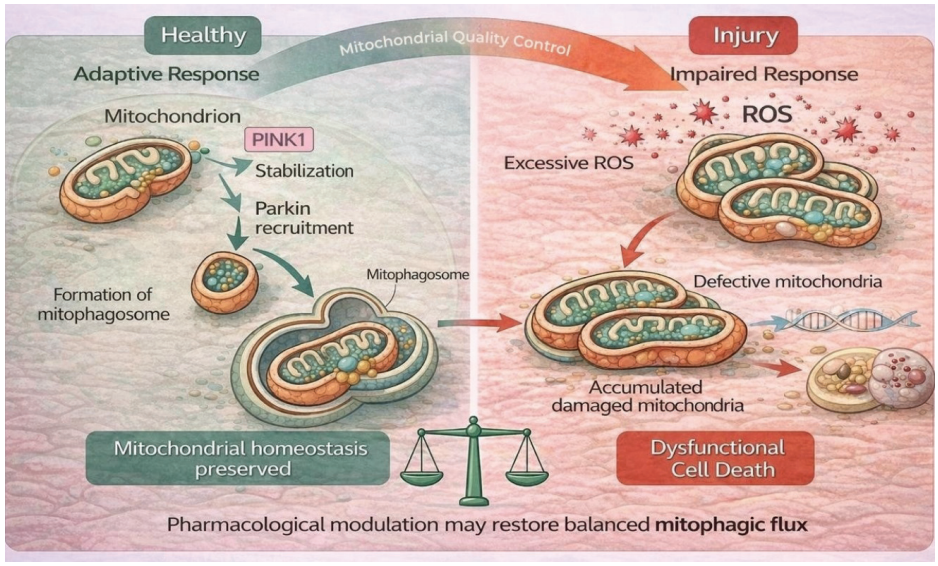

Figure 1. Mitophagy and mitochondrial quality control in experimental hepatic injury.

maladaptive. Insufficient mitophagy promotes accumulation of dysfunctional mitochondria, amplifying oxidative stress and inflammatory signaling, whereas excessive mitophagy can lead to mitochondrial depletion and bioenergetic failure. This dual role highlights the necessity for tightly regulated mitophagic flux in hepatocytes. In hepatic injury, disruption of this process aggravates the accumulation of dysfunctional mitochondria and ROS, exacerbates ATP depletion, and promotes hepatocyte death.

Experimental evidence supports the view that the PINK1/Parkin-mediated mitophagy pathway is a central mechanism of mitochondrial turnover in both acute and chronic liver injury. In APAP-induced hepatotoxicity, excessive mitochondrial ROS production leads to depolarization of ΔΨm, accumulation of PINK1 on the outer mitochondrial membrane, and recruitment of Parkin to initiate mitophagy. Experimental inhibition of PINK1 or Parkin amplifies APAP-induced hepatocellular necrosis, confirming the cytoprotective role of mitophagy.[2,7]

Similarly, during IR injury, transient activation of mitophagy limits mitochondrial ROS buildup, while prolonged or defective mitophagy exacerbates inflammation and necrosis. Enhancing mitophagic flux via AMPK or SIRT3 activation has been shown to protect against IR-induced oxidative damage.[4] In hepatic IR models, PINK1/Parkin-mediated mitophagy is transiently activated during early reperfusion, coinciding with mild restoration of ΔΨm. However, prolonged ischemia leads to suppression of mitophagy through mPTP opening and ATP depletion, resulting in accumulation of damaged mitochondria and exacerbation of oxidative injury.[2,4]

In chronic liver injury models, including non-alcoholic fatty liver disease and CCl_4- and TAA-induced fibrosis, persistent oxidative stress suppresses Parkin translocation, leading to mitophagy failure and contributing to hepatocyte apoptosis and fibrogenesis. The impaired mitophagy, resulting in mitochondrial accumulation, aggravates lipid peroxidation, stellate cell activation, and fibrogenesis. Experimental activation of PINK1/Parkin or SIRT1–SIRT3 pathways restores mitophagy and reduces fibrotic progression.[41] Similarly, decreased expression of PINK1, Parkin, and FUNDC1, along with elevated p62/SQSTM1 accumulation, indicates disrupted autophagic flux. This failure in mitochondrial turnover promotes NLRP3 inflammasome activation and TGF-β1/Smad3-driven fibrosis.[4]

Pharmacological modulation of mitophagy has therefore emerged as a promising therapeutic strategy. Urolithin A, a gut microbiota–derived metabolite, has been shown to enhance mitophagy and improve mitochondrial function in experimental liver injury models by restoring mitochondrial quality control and reducing oxidative stress.[42] These mitochondrial effects are associated with improvement in hepatocellular resilience and attenuation of liver injury. However, its evidence base in hepatic disease remains largely experimental, and its translational potential requires further validation. Similarly, spermidine, a natural polyamine, induces mitophagy through autophagy-related pathways and confers hepatoprotection in models of toxic and metabolic liver injury.[43] It is known to support mitochondrial turnover and preserve mitochondrial quality, thereby limiting the accumulation of dysfunctional organelles in these experimental models. These actions are associated with reduced tissue injury and improved hepatocellular adaptation. Its role should be considered supportive and preclinical, rather than clinically established.

In addition, modulation of mitochondrial dynamics, such as fusion and fission, plays an integral role in the regulation of mitophagy. Excessive mitochondrial fission mediated by dynamin-related protein 1 (Drp1) has been associated with aggravated liver injury, whereas pharmacological inhibition of Drp1 preserves mitochondrial morphology and limits hepatocellular damage.[44] Together, these findings indicate that targeting mitophagy and mitochondrial quality control represents a complementary approach to preserve mitochondrial integrity beyond acute injury prevention.

Mitochondria-Nucleus Crosstalk and Inflammatory Signaling

Inter-organelle communication among mitochondria, the ER, and the nucleus is a key determinant of cellular homeostasis, particularly under hepatic stress conditions, such as toxic injury and IR. The ER and mitochondria are physically connected at specialized regions known as mitochondria-ER contact sites or mitochondria-associated ER membranes (MAMs), which regulate calcium signaling, lipid transfer, and stress responses. Malfunction of these contact sites contributes to mitochondrial dysfunction, ER stress, and aberrant gene expression in liver diseases.[5]

Mitochondria-ER Contacts and Calcium Transfer: Mitochondria and the ER interact at MAMs, facilitating Ca_2^+ transfer between the two organelles. These contact sites help coordinate metabolic and signaling responses. Disruption of MAMs can impair calcium homeostasis and promote mitochondrial calcium overload, which worsens oxidative stress and triggers mPTP opening, a key event in hepatocellular injury.[5] Recent studies show that MAMs not only mediate calcium exchange but also regulate lipid and glucose homeostasis. In hepatocytes, MAMs contribute to neutral lipid metabolism and may influence lipid droplet dynamics and steatosis in fatty liver disease.[45]

ER Stress and the Unfolded Protein Response (UPR): Accumulation of unfolded or misfolded proteins in the ER lumen activates the UPR, a highly conserved stress pathway. UPR initially aims to restore protein folding capacity by upregulating chaperones (e.g., GRP78/BiP) and decreasing general protein translation. However, when ER stress persists, UPR signaling can shift toward pro-apoptotic pathways involving factors such as CHOP and JNK, which also impact mitochondrial function and can exacerbate liver injury.[5] Importantly, prolonged ER stress promotes mitochondrial dysfunction by enhancing ROS production and calcium imbalance, thereby amplifying hepatocellular damage.[46]

cGAS-STING Pathway and mtDNA Signaling: In models of hepatic IR injury, mitochondrial damage leads to the release of mtDNA into the cytosol. Cytosolic mtDNA, which acts as a danger-associated molecular pattern**,** can activate the cGAS-STING cytosolic DNA-sensing pathway, linking mitochondrial dysfunction to innate immune activation and inflammation. Targeting this pathway has been proposed to mitigate sterile inflammation in IRI.[47] Although most studies on the cGAS-STING pathway have been performed in models of systemic inflammation or organ transplantation, similar mechanisms are now recognized in hepatic injury. The resulting inflammatory response exacerbates oxidative stress and further impairs the function of mitochondria and the ER, ultimately promoting hepatocyte death.[47] Recent studies indicate that Dimethyl Fumarate directly targets STING, preventing recruitment of TBK1 and IRF3 and thereby suppressing production of pro-inflammatory cytokines in models of hepatic ischemia-reperfusion.

Modulation of Organelle Crosstalk: Understanding organelle crosstalk reveals therapeutic opportunities. Agents that stabilize MAMs and improve calcium handling or modulators that attenuate ER stress (e.g., chemical chaperones targeting UPR) may help preserve mitochondria and restore homeostasis. Similarly, interventions that dampen cGAS–STING signaling could reduce inflammation triggered by organellar danger-associated molecular patterns. These strategies are being explored in preclinical models of hepatic injury and represent promising directions for translational research.[47]

Emerging Therapeutic Strategies

Ammonia-Targeted Mitoprotection YAQ-005: Data published in 2025 showed that hyperammonemia causes mitochondrial damage and cell death by increasing RIPK1 and RIPK3 protein levels. The drug YAQ-005 (TAK-242) protects mitochondria by blocking the TLR4 pathway and facilitating ammonia removal via the urea cycle. The drug has been proposed for further clinical evaluation in mid-2025.[48]

Mitochondrial transplantation, the transfer of healthy mitochondria (usually isolated from skeletal muscle) directly via the portal vein or spleen, has emerged as an experimental and highly innovative approach in MASH and ischemia-reperfusion injury. Transplanted mitochondria are rapidly internalized by Kupffer cells and can reduce necrosis by more than 20% through increasing ATP production. Ethical and genetic risks, such as immune rejection and incompatibility between the nuclear and mitochondrial genomes in allogeneic transplants, remain under investigation.[49]

Nanomedicine as a Future Perspective: Nanotechnology enables the delivery of drugs to the liver and directly to the mitochondrial matrix. Biomimetic (cell membrane-coated) nanoparticles optimize the targeted distribution of the drug to the space of Disse and to hepatocytes by evading the immune system.[50]

CONCLUSION

Mitochondrial dysfunction has emerged as a central pathogenic hub in experimental models of hepatic injury, integrating oxidative stress, bioenergetic failure, dysregulated cell death, and impaired cellular adaptation. Accumulating experimental evidence demonstrates that mitochondria are not merely secondary targets of hepatocellular damage but active regulators of injury severity and disease progression. Accordingly, pharmacological strategies that directly target mitochondrial pathways, ranging from mitochondria-targeted antioxidants and mPTP modulators to regulators of energy sensing, biogenesis, and mitophagy, offer mechanistically grounded advantages over conventional, non-specific hepatoprotective approaches. In addition to established mitochondria-targeted pharmacological approaches, emerging therapeutic strategies further expand the translational potential of mitochondrial modulation in hepatic injury. Novel concepts such as ammonia-targeted mitoprotection, mitochondrial transplantation, and nanotechnology-based drug delivery highlight innovative directions aimed at preserving mitochondrial integrity and improving hepatocellular resilience. Although these approaches remain at early experimental or clinical stages, they underscore the growing recognition of mitochondria as dynamic and druggable targets in liver disease prevention and therapy. Nevertheless, the current evidence

remains predominantly preclinical, and important uncertainties persist regarding optimal dosing, tissue selectivity, long-term safety, and translatability to human liver disease. Future therapeutic success will likely depend on integrated strategies that combine acute mitochondrial protection with restoration of mitochondrial quality control and adaptive recovery mechanisms. In this context, targeting mitochondrial dysfunction is a promising and evolving avenue for developing more effective treatments for drug-induced liver injury, IR damage, and chronic liver disease.

Ethics

Informed Consent: N/A.

Footnotes

Funding: The author declare that this study has received no financial support.

Declaration of Interests: The author declare no conflict of interest regarding the publication of this paper.

REFERENCES

1. Fromenty B. Alteration of mitochondrial DNA homeostasis in drug-induced liver injury. *Food and Chemical Toxicology*. 2020;135: 110916 [CrossRef]
2. Ma X, McKeen T, Zhang J, Ding WX. Role and mechanisms of mitophagy in liver diseases. *Cells*. 2020;9(4):837. [CrossRef]
3. Baburina Y, Odinokova I, Krestinina O. The effects of pk11195 and protoporphyrin ix can modulate chronic alcohol intoxication in rat liver mitochondria under the opening of the mitochondrial permeability transition pore. *Cells*. 2020;9(8):1774. [CrossRef]
4. Liu S, Wang L, Zhu L, et al. Mechanism and regulation of mitophagy in liver diseases: a review. *Front Cell Dev Biol*. 2025;13:1-18. [CrossRef]
5. Guo M, Liu R, Zhang F, Qu J, Yang Y, Li X. A new perspective on liver diseases: focusing on the mitochondria-associated endoplasmic reticulum membranes. *Pharmacol Res*. 2024;208: 107409. [CrossRef]
6. Şenbil DC, Aydın S. Coronavirus disease 2019-related liver ınjury: ımaging aspects. *Arch Basic Clin Res*. 2024;6(1):69-72. [CrossRef]
7. Wang H, Ni HM, Chao X, et al. Double deletion of PINK1 and Parkin impairs hepatic mitophagy and exacerbates acetaminophen-induced liver injury in mice. *Redox Biol*. 2019;22:101148. [CrossRef]
8. Chen J, Liu B, Yao X, et al. AMPK/SIRT1/PGC-1α Signaling pathway: molecular mechanisms and targeted strategies from energy homeostasis regulation to disease therapy. *CNS Neurosci Ther*. 2025;31(11):1-23. [CrossRef]
9. Samuvel DJ, Krishnasamy Y, Li L, Lemasters JJ, Chou CJ, Zhong Z. LP342, a novel histone deacetylase inhibitor, decreases nitro-oxidative stress, mitochondrial dysfunction and hepatic ischaemia/reperfusion injury in mice. *RPS Pharm Pharmacol Rep*. 2023;2(2):1-13. [CrossRef]
10. LeFort KR, Rungratanawanich W, Song BJ. Contributing roles of mitochondrial dysfunction and hepatocyte apoptosis in liver diseases through oxidative stress, post-translational modifications, inflammation, and intestinal barrier dysfunction. *Cellular and Mol Life Sci*. 2024;81(1):34. [CrossRef]
11. Franczyk B, Bojdo K, Chłądzyński J, et al. Rational design of mitochondria-targeted antioxidants: from molecular determinants to clinical perspectives. *Drugs and Drug Candidates*. 2026;5(1):9. [CrossRef]
12. Dhiman A, Shah Y, Chaudhary U, Garkhal K. Reactive oxygen species-mediated mitochondrial-targeted therapeutics in hepatic disorders: current progress and future opportunities. *Mol Pharm*. 2025;22(10):5715-5737. [CrossRef]
13. Pang M, Wang S, Shi T, Chen J. Overview of MitoQ on prevention and management of cardiometabolic diseases: a scoping review. *Front Cardiovasc Med*. 2025;12:1506460. [CrossRef]
14. Dou SD, Zhang JN, Xie XL, et al. MitoQ inhibits hepatic stellate cell activation and liver fibrosis by enhancing PINK1/parkin-mediated mitophagy. *Open Medicine* (*Poland*). 2021;16(1):1718-1727. [CrossRef]
15. Jamshidi HR, Saadati M, Saghafi F. The protective effects of Mito-TEMPO on acetaminophen-induced hepatotoxicity: a systematic review. journal of current toxicology and venomics. 2024;04: E26661217306815. [CrossRef]
16. Rogov AG, Goleva TN, Aliverdieva DA, Zvyagilskaya RA. SkQ3 Exhibits the most pronounced antioxidant effect on ısolated rat liver mitochondria and yeast cells. *Int J Mol Sci*. 2024;25(2):1107. [CrossRef]
17. Teodoro JS, Da Silva RT, Machado IF, et al. Shaping of hepatic ıschemia/reperfusion events: the crucial role of mitochondria. *Cells*. 2022;11(4):688. [CrossRef]
18. Liu L, Wei YF, Xie NS, Cai H, Lin Y. Mitochondria-targeted reactive oxygen species blockor SS-31 blocks hepatic stellate cell activation and alleviates hepatic fibrosis by regulating NLRP3 inflammasomes. *Cell Mol Biol*. 2024;70(2):183-188. [CrossRef]
19. Chen P, Yao L, Yuan M, et al. Mitochondrial dysfunction: a promising therapeutic target for liver diseases. *Genes Dis*. 2024;11(3):101115. [CrossRef]
20. Ramachandran A, Jaeschke H. A mitochondrial journey through acetaminophen hepatotoxicity. *Food and Chemical Toxicology*. 2020;140:111282. [CrossRef]
21. Shi S, Wang L, Van der Laan LJW, Pan Q, Verstegen MMA. Mitochondrial dysfunction and oxidative stress in liver transplantation and underlying diseases: new insights and therapeutics. *Transplantation*. 2021;105(11):2362-2373. [CrossRef]
22. Ezhilarasan D. Molecular mechanisms in thioacetamide-induced acute and chronic liver injury models. *Environ Toxicol Pharmacol*. 2023;99:104093. [CrossRef]
23. Grabeklis SA, Mikhaleva LM, Dygai AM, Kozlova MA, Chernikov VP, Areshidze DA. Effect of exogenous melatonin on the ultrastructure of hepatocytes in rats with experimental toxic liver injury. *Morphology*. 2025;163(3):210-219. [CrossRef]
24. Kheyar A, Ahnou N, Ahmed-Belkacem A, et al. The novel cyclophilin inhibitor C105SR reduces hepatic ischaemia–reperfusion injury via mitoprotection. *JHEP Reports*. 2023;5(11):100876. [CrossRef]
25. Belosludtsev KN, Starinets VS, Talanov EY, Mikheeva IB, Dubinin M V., Belosludtseva N V. Alisporivir treatment alleviates mitochondrial dysfunction in the skeletal muscles of C57BL/6NCrl mice with high-fat diet/streptozotocin-induced diabetes mellitus. *Int J Mol Sci*. 2021;22(17):9524. [CrossRef]
26. Ure D, Stauffer W, Variya B, et al. Cyclophilin inhibition with rencofilstat shifts the liver transcriptome and lipidome in preclinical models toward resolution of non-alcoholic steatohepatitis. J Hepatol. 2023;78:770. [CrossRef]

27. Harrison SA, Mayo PR, Hobbs TM, et al. Rencofilstat, a cyclophilin inhibitor: a phase 2a, multicenter, single-blind, placebo-controlled study in F2/F3 NASH. *Hepatol Commun*. 2022;6(12):3379-3392. [CrossRef]

28. Serrano SS, Grönberg A, Longato L, et al. Evaluation of NV556, a novel cyclophilin inhibitor, as a potential antifibrotic compound for liver fibrosis. Cells. 2019;8(11):1409. [CrossRef]

29. Flaxman HA, Chrysovergi MA, Han H, et al. Sanglifehrin a mitigates multi-organ fibrosis in vivo by inducing secretion of the collagen chaperone cyclophilin B. *bioRxiv*. Published online 2023;03: 531890. [CrossRef]

30. Schmidt S, Messner CJ, Gaiser C, Hämmerli C, Suter-Dick L. Methotrexate-ınduced liver ınjury ıs associated with oxidative stress, impaired mitochondrial respiration, and endoplasmic reticulum stress ın vitro. *Int J Mol Sci*. 2022;23(23):15116. [CrossRef]

31. Zhou M, Lv J, Chen X, Shi Y, Chao G, Zhang S. From gut to liver: Exploring the crosstalk between gut-liver axis and oxidative stress in metabolic dysfunction-associated steatotic liver disease. *Ann Hepatol*. 2025;30(1):101777. [CrossRef]

32. Xiong Y, Chen J, Liang W, et al. Blockade of the mitochondrial DNA release ameliorates hepatic ischemia-reperfusion injury through avoiding the activation of cGAS-Sting pathway. *J Transl Med*. 2024;22(1):796. [CrossRef]

33. Hasanvand A. The role of AMPK-dependent pathways in cellular and molecular mechanisms of metformin: a new perspective for treatment and prevention of diseases. *Inflammopharmacology*. 2022;30(3:775-788. [CrossRef]

34. Ionita-Radu F, Patoni C, Nancoff AS, et al. Berberine effects in pre-fibrotic stages of non-alcoholic fatty liver disease—clinical and pre-clinical overview and systematic review of the literature. *Int J Mol Sci*. 2024;25(8):4201. [CrossRef]

35. Shamardl HAMA, Ibrahim NA, Merzeban DH, Elamir AM, Golam RM, Elsayed AM. Resveratrol and Dulaglutide ameliorate adiposity and liver dysfunction in rats with diet-induced metabolic syndrome: Role of SIRT-1 / adipokines / PPARγ and IGF-1. Daru. 2023;31(1):13-27. [CrossRef]

36. Xia S, Hu ZY, Cao R, et al. Magnesium isoglycyrrhizinate prevented the liver injury of acetaminophen by promoting mitochondrial biogenesis. *Toxicol Res (Camb)*. 2025;14(2). [CrossRef]

37. Richardson AK. Formoterol promotes mitochondrial biogenesis, improves liver regeneration, and suppresses liver injury and inflammation after liver resection in mice with endotoxemia. *Int J Physiol Pathophysiol Pharmacol*. 2025;17(4):131. [CrossRef]

38. Brennan PN, Kopka CJ, Agirre-Garrido L, et al. Reviewing MAESTRO-NASH and the implications for hepatology and health systems in implementation/accessibility of Resmetirom. npj Gut and Liver. 2025;2(1):3. [CrossRef]

39. Li J, Guo C, Wu J. Astaxanthin in liver health and disease: a potential therapeutic agent. *Drug Des* Devel Ther. 2020;14:2275-2285. [CrossRef]

40. Cao P, Wang Y, Zhang C, et al. Quercetin ameliorates nonalcoholic fatty liver disease (NAFLD) via the promotion of AMPK-mediated hepatic mitophagy. Journal of Nutritional Biochemistry. 2023;120: 109414. [CrossRef]

41. He H, Tang Y, Zhuang L, Zheng Y, Huang X. PINK1/Park2-mediated mitophagy relieve non-alcoholic fatty liver disease. Physiol Res. 2024;73(2):934925. [CrossRef]

42. Alrawili HM, Elshal M, Serrya MS, El-Agamy DS. The gut microbiota metabolite urolithin b mitigates cholestatic liver ınjury in mice via modulating the crosstalk between PPARα, Nrf2, and NF-κB signaling pathways. *J Xenobiot*. 2025;15(4):128. [CrossRef]

43. Liu H, Dong J, Song S, et al. Spermidine ameliorates liver ischaemia-reperfusion injury through the regulation of autophagy by the AMPK-mTOR-ULK1 signalling pathway. *Biochem Biophys Res Commun*. 2019;519(2):227-233. [CrossRef]

44. Zhou H, Zhu P, Wang J, Toan S, Ren J. DNA-PKcs promotes alcohol-related liver disease by activating drp1-related mitochondrial fission and repressing FUNDC1-required mitophagy. *Signal Transduct Target Ther*. 2019;4(1):56. [CrossRef]

45. Dong J, Chen L, Ye F, et al. Mic19 depletion impairs endoplasmic reticulum-mitochondrial contacts and mitochondrial lipid metabolism and triggers liver disease. *Nat Commun*. 2024;15(1):168. [CrossRef]

46. Pu S, Pan Y, Zhang Q, et al. Endoplasmic reticulum stress and mitochondrial stress in drug-ınduced liver ınjury. *Molecules*. 2023;28(7):3160. [CrossRef]

47. Chen Z, Liu Y, Lin Z, Huang W. cGAS–STING pathway in ischemia-reperfusion injury: a potential target to improve transplantation outcomes. *Front Immunol*. 2023;14:1231057. [CrossRef]

48. Kerbert AJC, Engelmann C, Habtesion A, et al. Hyperammonemia induces programmed liver cell death. *Science Advances*. 2025;11(10):1648. [CrossRef]

49. Chen Y, Yang F, Chu Y, Yun Z, Yan Y, Jin J. Mitochondrial transplantation: opportunities and challenges in the treatment of obesity, diabetes, and nonalcoholic fatty liver disease. *J Transl Med*. 2022;20(1):483. [CrossRef]

50. Peng M, Fang F, Wang B. Nanoparticle technologies for liver targeting and their applications in liver diseases. *Front Bioeng Biotechnol*. 2025;13:1661872. [CrossRef]

ABCResearch

Arch Basic Clin Res 2026;8(2):222
DOI: 10.4274/ABCR.2026.e001

Erratum

Article corrected: Alkan H, Veizi E, Erdoğan Y, Fırat A, Özay Subaşı İ, Şahin A, et al. A combination therapy for osteonecrosis of the femoral head and short-term results. Arch Basic Clin Res. 2023;5(3):310-319. **http://dx.doi.org/10.5152/ABCR.2023.23153**

In the article titled "A Combination Therapy for Osteonecrosis of the Femoral Head and Short-Term Results," published in Archives of Basic and Clinical Research, an error was identified in the study period stated under the "Patient Selection" subsection of the Methods section.

The sentence originally read as follows:

"Patients who were treated for osteonecrosis of the femoral head at our medical center between January 2016 and January 2019 were eligible for this study."

The corrected sentence should read as follows:

"Patients who were treated for osteonecrosis of the femoral head at our medical center between January 2018 and December 2020 were eligible for this study."

Accordingly, the study period has been corrected from "January 2016 to January 2019" to "January 2018 to December 2020" in the Methods section, under the "Patient Selection" subsection. This correction does not alter the scientific content, results, interpretation, or conclusions of the article.